U. PORTO
FEUP FACULDADE DE ENGENHARIA
UNIVERSIDADE DO PORTO

STRUCTURAL HEALTH MONITORING OF BRIDGES: PHYSICS-BASED ASSESSMENT AND DATA-DRIVEN DAMAGE IDENTIFICATION

A thesis submitted for the degree of Doctor of Philosophy in Civil Engineering
at the Faculty of Engineering of the University of Porto

by

Filipe José Moreira Guerra dos Santos Cavadas

Supervisor
Prof. Joaquim de Azevedo Figueiras
(Full Professor)

April 2016

To my parents

“You give your children enough money to do
something but not enough
to do nothing."

in The Descendants
(a film by Alexander Payne)

Abstract

Bridges are critical components of the transportation network that ensure economic prosperity and quality of life. However, they are susceptible to structural damage that may lead to their collapse. Therefore, maintaining safe and reliable structures is paramount. In this context, in the last three decades, structural health monitoring (SHM) of bridges has arisen as a powerful tool to support management and maintenance activities of bridges. The main purpose of a typical SHM system is to provide timely and objective information about the health of a structure as well as warnings regarding any damage that has been detected. However, despite the growing body of research that has been devoted to the subject, this is still a challenge.

In this context, this thesis comprises two main goals. The first is to emphasise the need of using field results together with physics-based behavioural models in order to attain a sound and reliable assessment of the structural condition of the bridge. The second is to propose an alternative data-driven approach for damage detection in bridges. Both objectives are addressed using the quasi-static component of moving-loads responses, which provides a valuable insight as regards the structural behaviour.

First, this thesis provides a brief overview on the SHM of bridges as a powerful tool for the management of bridges, in which the structural analysis and the early damage detection are emphasised. Then, an alternative approach for early damage detection, entirely data-driven, is proposed for latter application and validation along the thesis. The methodology involves, firstly, building time-series of moving-loads data and, secondly, processing data by using adequate statistical algorithms, namely the robust regression analysis (RRA), the moving principal component analysis (MPCA) and the influence-line assurance criterion (ILAC).

As regards the assessment of the structural condition of bridges, two different case studies are considered. The first is a centenary steel truss bridge, the Eiffel Bridge, which was subjected to a load test to characterize the structural behaviour after major rehabilitation works. An appropriate numerical analysis supports the discussion of the field results and the assessment of the most relevant aspects of the structural behaviour, such as the main girders bending and the nodes rotations.

The second case study regards the analysis of the in-service behaviour of reinforced and prestressed concrete bridges. The results of tests carried out in a laboratorial model resembling a typical frame bridge have shown that, due to the existence of small-width cracks, the structural response under moving-loads is not linear. The reasons for this behaviour are assessed with the aid of a dedicated finite-element model.

Then, the performance of the alternative approach for early damage detection proposed herein is firstly assessed by using numerically-simulated data, in which a stiffness reduction replicating a crack was selected as a damage scenario. Thereafter, this methodology is evaluated by using experimental data collected in a reinforced and prestressed concrete laboratorial model. Two typical damage scenarios are addressed: a prestress loss and a partial restraint for the longitudinal rotation of a support bearing. In addition, different measurement systems are assessed regarding the ability and time required for damage detection.

Finally, a centenary steel truss bridge, the Luiz I Bridge, was selected as the case study to evaluate the performance of the approach for early damage detection in full-scale bridges. With the objective of collecting influence-lines of in-service vehicles, a bridge weigh-in-motion (B-WIM) system was implemented. This system enables, in addition, to characterize the traffic by estimating vehicle parameters such as crossing direction, speed and vehicles loads.

The proposed approach is then assessed by using both numerically-simulated data and field results. Firstly, a restraint for the longitudinal displacement of the support bearings installed in a critical pillar of the bridge identified in field measurements is evaluated through adequate numerical simulations. Additionally, a similar restraint in the support bearings installed in a quite stiffer pillar is simulated. At last, both field measurements and numerically-simulated data replicating the former are analysed with the objective of detecting changes in the structural response.

Resumo

As pontes são componentes críticos da rede de transportes que asseguram prosperidade económica e qualidade de vida. Contudo, são suscetíveis a dano estrural que pode levar ao seu colapso. Assim, é fundamental manter as estruturas seguras e fiáveis. Neste contexto, nas três últimas décadas, a monitorização da integridade estrutural (SHM) de pontes tem vindo a tornar-se uma ferramenta essencial para as atividades de gestão e manutenção de pontes. O principal propósito de um sistema SHM é proporcionar informação objetiva e em tempo útil acerca do estado da estrutura e fornecer avisos no caso da ocorrência de dano. No entanto, apesar da crescente investigação nesta área, este objetivo continua a constituir-se como um desafio.

Neste contexto, esta tese compreende dois objetivos principais. O primeiro é enfatizar a necessidade de usar resultados experimentais associados a modelos baseados no comportamento físico para conseguir uma avaliação sólida e fiável da condição estrutural da ponte. O segundo é propor uma nova metodologia assente na análise estatística de dados para a deteção de danos em pontes. Ambos os objetivos são abordados usando a componente quasi-estática da resposta de cargas móveis, a qual fornece informação relevante sobre o comportamento estrutural.

Inicialmente, esta tese apresenta, num breve enquadramento, a SHM de pontes como uma ferramenta poderosa para a gestão de pontes, focando-se na análise estrutural e na deteção precoce de dano. Subsequentemente, é proposta uma nova metodologia de deteção de dano, assente na análise estatística dos dados, para posterior aplicação e validação ao longo da tese. A metodologia envolve, primeiro, a construção de séries temporais de dados de cargas móveis e, segundo, o processamento de dados usando algoritmos adequados, nomeadamente a análise de regressão robusta (RRA), a análise das componentes principais móveis (MPCA) e o critério de garantia da linha de influência (ILAC).

No que concerne à avaliação da condição estrutural de pontes, foram considerados dois casos de estudo. O primeiro é uma ponte metálica centenária em treliça, a Ponte Eiffel, que foi sujeita a um ensaio de carga para caracterizar o seu comportamento após a profunda reabilitação a que foi submetida. A análise dos resultados experimentais assim como de aspetos relevantes do comportamento estrutural, como a flexão das vigas principais e as rotações dos nós, apoiou-se nos resultados de um modelo numérico desenvolvido para o efeito.

O segundo caso de estudo diz respeito à análise do comportamento em serviço de pontes de betão armado e pré-esforçado. Os resultados de testes realizados num modelo laboratorial replicando uma ponte em pórtico mostraram que, devido à existência de fendas com abertura reduzida, a resposta estrutural sob cargas móveis não é linear. As razões para este comportamento são avaliadas através de um modelo de elementos finitos apropriado.

De seguida, o desempenho da metodologia aqui apresentada para deteção de dano é inicialmente avaliado usando dados simulados numericamente, tendo como cenário de dano uma redução de rigidez localizada. Posteriormente, esta metodologia é avaliada usando dados experimentais recolhidos num modelo laboratorial de betão, sendo tratados dois cenários de dano típicos: uma perda de pré-esforço e uma restrição parcial da rotação longitudinal de um aparelho de apoio. Adicionalmente, são avaliados diferentes sistemas de medição do ponto de vista da capacidade e tempo necessário para a deteção de dano.

Finalmente, uma ponte metálica centenária em treliça, a Ponte Luiz I, foi selecionada como caso de estudo para avaliar o desempenho da metodologia de deteção precoce de dano em pontes à escala real. Foi implementado um sistema de medição de cargas em movimento (B-WIM) com o objetivo de recolher linhas de influência de veículos em serviço a atravessar o tabuleiro superior. Este sistema permite, adicionalmente, caracterizar o tráfego estimando parâmetros do veículo como o sentido da passagem, a velocidade e as cargas.

A abordagem proposta é depois avaliada usando quer dados simulados numericamente quer resultados experimentais. Primeiro, uma restrição do deslocamento longitudinal dos aparelhos de apoio instalados num pilar crítico da ponte identificada em ensaios periódicos é avaliada através de simulações numéricas adequadas. Adicionalmente, simula-se uma restrição similar nos aparelhos de apoio instalados num pilar bastante mais rígido. Por fim, quer os resultados experimentais, quer os dados simulados numericamente replicando aqueles, são analisados com o objetivo de detetar alterações na resposta estrutural.

Acknowledgements

To all accompanying me through this journey, for their support, friendship and understanding, contributing to the completion of this thesis, I herein present my sincerest gratitude. Nonetheless, I would like to emphasize the contribution of the following.

First of all, I would like to express my gratitude to my supervisor, Prof. Joaquim Figueiras, for the opportunity of working in a challenging topic such as structural health monitoring, for the support given throughout, the fruitful discussions and valuable comments. The working conditions provided at the Laboratory for the Concrete Technology and Structural Behaviour (LABEST) at the Faculty of Engineering of University of Porto (FEUP) as well as the opportunity to develop work in outstanding landmarks such as the Eiffel and the Luiz I Bridges are also deeply appreciated.

I would also like to thank Prof. Ian Smith for receiving me during a six-month stay at the Applied Computing and Mechanics Laboratory (IMAC) at the *École Polytechnique Fédérale de Lausanne* (EPFL). As a result of our fruitful discussions I gained a new and valuable insight on damage identification approaches.

I would like to thank the construction company *Soares da Costa, SGPS, SA*, in charge of the rehabilitation works of the Eiffel Bridge, for the assistance provided in the installation of the monitoring system, as well as the cooperation of the bridge owner *REFER – Rede Ferroviária Nacional, EPE*. The opportunity conceded by *Metro do Porto, SA*, the Luiz I Bridge owner, for the research works carried out in the structure as well as all the support and information provided are also acknowledged.

I would like to express my gratitude to Carlos Rodrigues for his cooperation in the research concerning the Eiffel Bridge and to Carlos Sousa for his support in the analysis of the nonlinear behaviour of the concrete laboratorial model. I would also like to express special thanks to

Bruno Costa for his support in both the finite-element analysis of the Luiz I Bridge and the text revision, as well as for his encouragement, fruitful discussions and continuous support.

I would like to acknowledge all the IMAC researchers, for welcoming me and sharing experiences. James Goulet, for sharing all the knowledge concerning system identification, Irwanda Laory, for the support in the application of data-driven techniques and Thanh Trinh for the fruitful discussions are especially acknowledged. I would also like to thank Mrs. Josiane Reichenbach for her administrative support prior and during my stay at the EPFL.

I would like to acknowledge Prof. Carlos Félix for his support on my arrival at LABEST in the instrumentation field, Américo Dimande for his support in the deployment of the measurement system in the laboratorial model, especially the acquisition system, as well as Helder Sousa for his encouragement in processing data obtained in SHM systems. I would also like to thank Prof. Adriano Carvalho, from the Department of Electrical and Computer Engineering for his support in solving electrical issues in the measurement systems.

The dedication, commitment and work experience of Amândio Pinto were fundamental for the successful installation of the monitoring system in the Eiffel Bridge and, thus, are gratefully appreciated. I would also like to thank Rogério Pinheiro for the support in the installation of the monitoring system and Cláudio Ferraz for the continued presence both in the field and laboratorial works. Mr. Alberto Monteiro is also acknowledged for his support in the experimental works. I would like to particularly thank Paula Silva for her patience and help. Cláudia Correia and Marta Poínhas are also acknowledged for their administrative support during the last years.

For the good work environment, wise opinions and cheerful conversations, my thanks to my colleagues at FEUP, especially Helena Figueiras, Leonel Ramos, Miguel Azenha, Cláudia Lemos, Pedro Ferreira, Joana Maia, Emanuel Tomé, José Matos, José Carvalhal and José Conceição. The support of Rémy Faria and confidence of Diogo Ribeiro are deeply acknowledged.

I would like to express my gratitude to Francisco Natário for his partnership and to Patrick Bishop for the conversations and shared experiences during my stay at EPFL.

I would also like to express my gratitude to everyone in *GEG – Gabinete de Estruturas e Geotecnia*, for the understanding during last year and particularly to Eng. José Luís Barbosa, Director of the Structures and Bridges Department, and to the administration in the person of Prof. António Campos e Matos, for releasing me in the final preparation of this thesis.

A special thank to my closest friends for the encouragement and patience through these years.

Last, but not least, a special word of appreciation and affection for the unlimited and unconditional love, sacrifice and support throughout my entire life from my parents and my brother, Vitor, and loving care of my sister-in-law, Susana, and my nieces Inês and Margarida.

The financial support given by the Portuguese Foundation for Science and Technology (FCT) through the PHD grant SFRH/BD/42315/2007 is also gratefully acknowledged.

Contents

4. Analysis of the in-service behaviour of concrete bridges using a laboratorial model 71

5. Damage identification based on moving-loads responses using numerically-simulated data 105

List of Figures

List of Tables

List of Symbols and Abbreviations

Symbols and abbreviations are defined upon their first appearance in the text. The following list is presented in alphabetic order and does not include some symbols and notations of a secondary significance (whose concern is limited to specific applications). Moreover, although some symbols denote more than one signification, their meaning should be clear when read in context.

Roman letters

A	Area of a given cross-section
ADC	Analogue-to-digital converter
BIL	Bogie influence-line
d	Distance between de rotation axis and the steel bars
d_{ij}	Displacement at coordinate i due to a unit force acting at j
d_{ji}	Displacement at coordinate j due to a unit force acting at i
DOF	Degree of freedom
E	Young's modulus
e_i	Error in the fit of the model to the i^{th} observation (residual)
F_k	Load of the k^{th} axle for a multi-axles vehicle
FBG	Fibre Brag grating
FE	Finite-element
FEM	Finite-element model
I_2	Moment of inertia of a given cross-section about 2-2 axis
I_3	Moment of inertia of a given cross-section about 3-3 axis
ILAC	Influence-line assurance criterion
$ILAC(r_A, q_B)$	Influence-line assurance criterion between the r^{th} influence-line of a dataset A, $\Upsilon_{r,A}$, and the q^{th} influence-line of a dataset B, $\Upsilon_{q,B}$

k_L	Axial stiffness
k_{R}	Rotational stiffness
L	Expansion length between the fixed support and the movable joint or bearing
LVDT	Linear variable differential transformer
M	Bending moment
M_2	Bending moment about 2-2 axis
M_3	Bending moment about 3-3 axis
MAC	Modal assurance criterion
$MAC(r_A, q_B)$	Modal assurance criterion between the r^{th} modal vector of a dataset A, $\psi_{r,A}$, and the q^{th} modal vector of a dataset B, $\psi_{q,B}$
MPCA	Moving principal component analysis
MS	Measurement system
n	Number of observations of a dataset
n_c	Number of crossings collected during a the monitoring period
n_m	Number of measurements
n_p	Number of load positions in which the structural response is collected
n_S	Number of sensors included in the monitoring system
NDE	Non-destructive evaluation
NDT	Non-destructive techniques
p	Number of features
P	Axial force
PC	Principal component
PCA	Principal component analysis
POD	Proper orthogonal decomposition
PTFE	Polytetrafluoroethylene
r	Number of principal components that retain most of the variation present in all of the original variables
RRA	Robust regression analysis
s	Slip values at the interface between the longitudinal reinforcement and the surrounding concrete
S	Covariance matrix $\epsilon\ \Re^{p \times p}$
SHM	Structural Health Monitoring
T	Temperature

U	Loadings matrix $\epsilon\ \mathfrak{R}^{p\times p}$
$\bar{U}$	r-dimensional matrix of the loadings $\epsilon\ \mathfrak{R}^{p\times r}$
U_k	k^{th} principal component
UIL	Unit influence-line
USA	United States of America
VIL	Vehicle influence-line
w	Crack opening
x_2	Coordinate of a point along 2-2 axis
x_3	Coordinate of a point along 3-3 axis
x_i	i^{th} observation of the variable X; Position occupied by a multi-axles vehicle
$x_{k,i}$	Position occupied by the k^{th} axle for a multi-axles vehicle located at a position i
X	Variable; Features matrix $\epsilon\ \mathfrak{R}^{n\times p}$
X_i	p-dimensional vector containing the i^{th} observation stored in the features matrix X
y_i	i^{th} observation of the variable Y
$\hat{y}_i$	Estimated value for the i^{th} observation of the variable Y
$y_{k,i}$	Ordinate of the UIL at the position occupied by the k^{th} axle for a multi-axles vehicle located at a position i
Y	Variable
z_i	Response of a given quantity z for a multi-axles vehicle located at a position i
Z	Scores matrix $\epsilon\ \mathfrak{R}^{n\times p}$
$\bar{Z}$	r-dimensional matrix of the scores $\epsilon\ \mathfrak{R}^{n\times r}$
Z_i	p-dimensional vector containing the components scores corresponding to the i^{th} observation

Greek letters

α	Coefficient of thermal expansion
β_0	Intercept of the line of the simple linear regression model
β_1	Slope of the line of the simple linear regression model
Δ	Joint displacement
ΔT	Difference of temperature

ε	Strain
μ	Mean
σ	Stress; Standard deviation
σ_c	Concrete stress
τ	Bond stress at the interface between the longitudinal reinforcement and the surrounding concrete
$\Upsilon_{r,A}$	r^{th} influence-line of a dataset A
$\Upsilon_{q,B}$	q^{th} influence-line of a dataset B
$\psi_{r,A}$	r^{th} modal vector of a dataset A
$\psi_{q,B}$	q^{th} modal vector of a dataset B

Chapter 1

Introduction

1.1. General remarks

The society's economic prosperity and quality of life depend on a complex and extensive infrastructure system, of which bridges, serving as node points of the infrastructure transportation system, are critical components. Over the years of civilization, especially in the last decades, the stock of bridges has been accumulating (Bergmeister and Santa, 2001). This accelerating growth led to increasingly complex problems, namely regarding the management and maintenance of the transportation systems, of wide interest to infrastructures authorities (Aktan *et al.*, 2000).

Bridges are susceptible to structural damage over their lives due to many factors, such as, aging, normal wear, operating loads, fatigue and corrosion (Al-Ostaz *et al.*, 2009). Furthermore, these structures are often subjected to excessive live loading and severe environmental conditions or extreme events not anticipated during their design, which may result in long-term structural damage and deterioration (Yanaka and Kitagawa, 2002).

It is quite evident that, as a result of the large expansion of highways built during the post-war boom era of the 1950s to 1970s, the bridge stock all over the world, in particular in developed countries, is aging (Bell, 2004; Davis *et al.*, 2013; Lee, 2012). In addition, these key components of the transportation systems have suffered from decades of neglect and overuse, leading to accelerated deterioration (Bisby, 2004). As a consequence, the performance of these in-service structures has decayed and the inherent level of safety is often inadequate (Bergmeister and Santa, 2001). Undetected damage may result in the failure of the components of the bridge or even of the structure itself, which may be very costly both economically and in human lives terms. In December 15, 1967, the 681 m long Silver Bridge, at Point Pleasant, West Virginia, in the United States of America (USA), collapsed (see Figure 1.1 (a)) killing 46 people (Ryan *et al.*, 2006). More recently, on August 1, 2007, the interstate highway bridge I-35W over the Mississippi River in Minneapolis, Minnesota, in the USA, suddenly collapsed (see Figure 1.1 (b)) resulting in 13 fatalities and 145 injuries, with 111 vehicles involved (Hao, 2010).

In a world where public safety is paramount and the consequences of failure are great, an effective management of civil structures such as bridges has become more and more important (Frangopol *et al.*, 1998). However, available resources are increasingly scarce. Bridge management requires, therefore, in addition to operational and structural conditions, careful evaluation of economical, ecological and social conditions (Catbas *et al.*, 2001). The high costs of building new bridges are only economically justifiable by proving a significantly longer service life together with smaller maintenance costs in relation to old structures. Therefore, corrective maintenance of old structures is increasingly becoming a cost efficient alternative to the building of new structures (Sedlaccek *et al.*, 2007). Furthermore, nowadays, bridge owners and planners tend to include life-cycle cost analyses in their decision processes regarding the overall design trying to optimize structural reliability and durability within financial constraints (Neves and Frangopol, 2005).

Simultaneously, sustainability aspects and a sensitive treatment of energy and material resources are, in a great extent, taken into consideration by designers and financiers and may determine the non-replacement of old structures. Furthermore, especially for steel bridges, historical and social aspects may lead to a cultural value which has to be preserved (Sedlaccek *et al.*, 2007).

As a result of this comprehensive concern on the conservation of existing structures, the

(a) (b)

Figure 1.1 – Collapses of: (a) the Silver Bridge, at Point Pleasant, West Virginia, in the USA; and (b) the interstate highway bridge I-35W over the Mississippi River in Minneapolis, Minnesota, in the USA.

general trend goes towards rehabilitation efforts for increasing the service life of existing structures and reducing the costs of keeping the infrastructure systems safe and operational. Figure 1.2 shows the opposite trends of investments for new structures and for maintenance of existing structures in western countries.

Until a few decades ago, little emphasis was placed on the condition assessment and safety inspection of bridges. This issue has become a priority only after tragic collapses, and presently, particular attention has been given on preventive maintenance, in which structures are maintained before they become susceptible to deterioration. In the USA, for instance, the tragic collapse of the Silver Bridge in 1967 (mentioned above) had lead to the development of the National Bridge Inspection Standards (FHWA, 2009) which, firstly published in 1971, established the national policy regarding: (i) inspection procedures; (ii) frequency of inspections; (iii) qualifications of personnel; (iv) inspection reports; and (v) maintenance of the bridge stock.

Since then, bridge management systems, using mainly the results of visual inspections data, have been implemented by the infrastructures authorities with the goal of determining needed maintenance and repairs, for prioritizing rehabilitations and replacements, and for allocating resources. In this context, the accuracy and consistency of the inspections and the resulting documentation is vital because it not only impacts programming and funding appropriations, but also affects public safety (Ryan *et al.*, 2006). However, based on, in general, biennial visual inspections, the bridges condition is described by relatively global, in nature, and subjective condition ratings, which can lead to variations in the reliability of the overall management process (Casas, 2007).

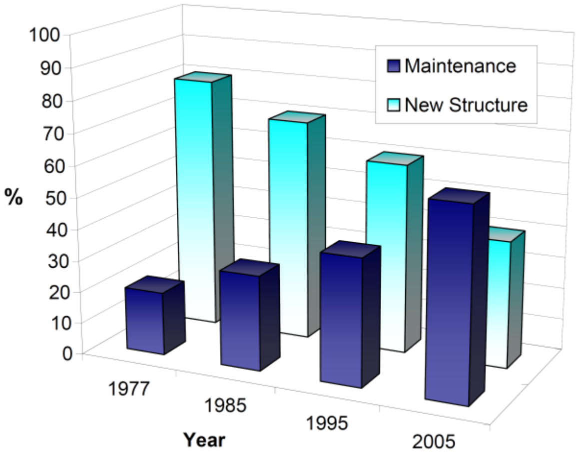

Figure 1.2 – Comparison of the investments in maintenance and in new structures (Sedlaccek *et al.*, 2007).

A recent study (Moore *et al.*, 2001) conducted in the USA has indicated that at least 56% of the average condition ratings from visual inspections were incorrect. The variations are a result of factors such as the inspectors' experience, type of bridge and type of condition of the bridge. Within the European Project *Sustainable Bridges – Assessment for Future Traffic Demands and Longer Lives*, Casas (2007) summarizes the methods applied in different countries and by different infrastructure administrations in the condition assessment of the bridges and highlights the following conclusions. First, today, all administrations use the visual inspection as the main source of relevant data to carry out the condition assessment. Second, all administrations have a systematic inspection procedure but not all use the results of the inspection in a comprehensive and objective way to derive a condition rating, either numerical (in the range of 1 to 10, 1 to 100,...) or grammatical (poor, fair, acceptable, good,...). Finally, each administration is using different condition rating techniques, which may lead that the same bridge, assessed by two engineers from different countries, can be rated with different grades. Therefore, a guideline (Helmerich, 2007) proposing inspection and condition assessment tools to get comparable description of the railway infrastructure condition in different countries of the European Community was delivered.

In spite of these efforts in order to increase their reliability, visual inspections still reveal a set of shortcomings that must be accounted for and should be overcome. Notwithstanding, existing bridge management systems still rely on inspection data for condition assessment and to program maintenance actions for bridges. Often, this results in major repair or replacement of bridges rather than maintenance (Frangopol *et al.*, 1998).

As visual inspection provides little or no quantitative data on the condition of bridges, new methods for condition assessment that can be used in conjunction with traditional visual inspection are needed to assist authorities in management and planning repairs of bridges, and, thus, making the best use of the limited financial resources available. In this context, advanced inspection techniques, such as non-destructive testing or evaluation (NDT or NDE), give inspectors the ability to further evaluate suspected defects found during a visual inspection (Ryan *et al.*, 2006).

Non-destructive testing is a wide group of analysis techniques used in science and industry to evaluate the properties of a material, component or system without causing damage. It can be used to get more detailed information about in-built defects, such as insufficient grouting of tendon ducts, or in-service defects caused by deterioration, such as fatigue in steel bridge details. Depending on the application, certain non-destructive methods yield better than others. A comprehensive overview on available non-destructive testing methods, required equipment and time consumption can be found in (Helmerich, 2007; Ryan *et al.*, 2006). The appropriate non-destructive testing methods for reinforced and prestressed concrete, steel and masonry bridges are also addressed therein.

In general, when compared with other conventional destructive inspection techniques, non-destructive testing techniques have many advantages (Rens *et al.*, 2005): (i) no damage or sacrifice of specimens is required; (ii) these techniques can be applied for in-service inspections; (iii) early detection of flaws and defects is provided; and (iv) very precise characterization of the defect extent can be achieved depending upon the method. However, because of their complexity there are several obstacles to the application of non-destructive testing techniques in bridge management systems, such as: (i) it is often time consuming and expensive, and access is not always possible; (ii) experience is required to handle the equipment; (iii) expertise is necessary for interpretation of results; and (iv) not all tools and techniques can be applied for all bridge materials. Furthermore, the application of non-destructive testing methods needs to address specific problems, in specific locations, in the bridge. In fact, techniques based on radiography, acoustic signals, wave propagation, etc. can be effectively applied to damage detection in a few known locations of the structure. In addition, methods such as ultrasonic guided waves to measure the state of stress, or eddy current techniques to locate cracks, can determine the exact location and extent of the damage. However, all of these local non-destructive techniques require that the vicinity of the damage is known a priori and the portion of the structure being inspected is readily accessible. Therefore, although local monitoring techniques are much more likely to locate and quantify the damage, local monitoring of all infrastructures in a timely manner is not a realistic goal at present (Chang and Liu, 2003; Rens *et al.*, 2005).

Motivated by the shortcomings of traditional inspection techniques (visual inspections and non-destructive testing) on one hand, and the availability of affordable hardware and advances in signal processing techniques on the other, engineers and researchers have turned their attention to instrumented global structural health monitoring (SHM) systems to complement and enhance visual inspection (Mufti, 2002; Sun *et al.*, 2010; Van der Auweraer and Peeters, 2003). Global structural health monitoring (SHM) refers to the use of in-situ, non-destructive sensing and analysis of system characteristics including structural response, for detecting changes in the structure, which may indicate damage or degradation. Measurements of strain, acceleration, velocity, displacement, rotation, and other parameters have always been a primary tool in engineering, so the concept of experimental monitoring is certainly not new to civil engineering. However, recent developments in measurement, communications and computational technology facilitate the application of health monitoring of large structures (Housner *et al.*, 1997).

SHM is, therefore, an alternative approach for identifying damage occurrence at an early stage and for objectively assessing the condition of structures. SHM systems enable to measure the structure's operating and loading environment in order to track and evaluate incidents, anomalies, damage and deterioration that are either in its inception or too small to be detected by human eye (Brownjohn, 2007). Furthermore, these systems are used to capture the critical inputs and responses of a structural system in order to understand the root causes of problems, and to track responses to predict future behaviour (Farrar and Lieven, 2007).

It is noteworthy to mention that the goal of continuous monitoring is not to supersede traditional inspection but to optimize the inspection and the management processes with modern smart tools. Furthermore, although non-destructive testing methods are impractical for search of potential damage through all engineering components, these techniques remain as one important part of the health monitoring of civil infrastructure. Their ability to specifically identify a wide set of types of damage may be viewed as a useful part of damage detection, in that global methods often do not give enough information to determine the exact mode of deterioration (Chang *et al.*, 2003). In this context, both visual inspections and local non-destructive testing methods should be used in conjunction with continuous global monitoring systems, which are typically used to detect the general location of damage. Then, visual inspections and NDT methods may be used to locate the exact location and characteristics of the damage so that the corrective action can be taken (Chang and Liu, 2003). Global SHM systems are used, in addition, to obtain measurable and quantifiable information regarding the existing structural condition, to better determine the structural resistance and to provide information needed in the overall management of bridges. Often, problems perceived by visual inspections do not require repairs when investigated further using quantitative measures. On the other hand, when repairs are needed, this approach may be used to determine the most cost effective approach (DeWolf *et al.*, 2002). Therefore, global structural health monitoring allows for increasing the reliability of the obtained information, reducing the human intervention as far as possible and improving the benefit costs ratio.

1.2. Scope and motivation

The shortage of appropriate information concerning the structural health may result in incorrect decisions as regards the infrastructure management, including maintenance, retrofitting or replacement. For instance, as a result of a poor structural health evaluation a structure may be retrofitted or replaced, while, in fact, is still sound. On the other hand, existing damage in a structure may be identified only when it reaches a severe stage and, therefore, becomes expensive to repair, and, ultimately, a danger to structural integrity (Frangopol *et al.*, 1998).

The effective management of existing bridges requires, therefore, well-informed decision-making processes (Helmerich, 2007). Although a careful visual inspection can provide valuable information, it has limitations. It is not always possible to access all critical areas of the structure, thereby allowing some problems to go unnoticed until they become serious and expensive to repair. Moreover, a visual inspection does not provide information about the actual stress/strain levels. Thus, it does not always provide sufficient information to make anything other than conservative estimates of load carrying capacity, or general estimations on the need for repair or replacement (Catbas *et al.*, 2007).

Even though, so far, the most commonly applied bridge management systems are based on periodical inspections, which generally relies on visual inspections. Therefore, the most current structural maintenance is carried out in a time-based mode. However, the increasing importance of maintaining the existing structures in good operating conditions, on one hand, and the shrinking budgets and scarce resources (Bisby, 2004), on the other, has lead to the introduction of two main conservation strategies and respective tactics based on their reactive or proactive characteristics (fib, 2010). The conservation strategy to be adopted for a given structure depends on factors such as the importance and the function of the structure, the design service life, the impact on third parties, the environmental conditions, the ease of maintenance and the cost.

Reactive conservation approaches, adopted generally for buildings and other common structures, entail corrective measures and interventions, with the goal of stopping currently active processes, which are causing deterioration or damage. Typically, remedial interventions involve some form of treatment or the taking of measures after damage has become apparent, identified on planned periodic inspections only. On the contrary, proactive conservation activities, adopted, in general, for monumental or important structures, such as bridges, are based on preventive measures and interventions with the objective of avoiding and minimizing future deterioration or loss. This is accomplished by applying some form of treatment or taking action before damage becomes visible. Tactics for delivering a proactive conservation strategy involve both planned periodic inspection and the systematic monitoring of critical parameters associated with the durability and the performance of the structure.

As aforementioned, the underlying principle of the proactive conservation approach is taking action before damage becomes visible. Consequently, the detection of structural damage at its onset is paramount. This permits, therefore, early action, which may prevent the structure from having to sustain loads for an extended period of time while in a damaged state. Moreover, repairs made at the onset of damage can drastically decrease the resulting repair costs and prevent further deterioration (Bisby, 2004). Therefore, time-based maintenance philosophies (related with reactive conservation approaches) should evolve into potentially more cost effective condition-based maintenance approaches (related with proactive conservation strategies), which can be achieved by using SHM systems (Chase, 2001). The basis of this strategy consists in installing a sensing system on the structure that will monitor the structural response and notify the operator that damage has been detected (Farrar and Worden, 2007). Changes in the response patterns may indicate modifications in the structural conditions. Sudden changes are the indication of damage in the members whereas modifications that are more gradual would indicate deterioration and wear. Note, in addition, that if monitoring data is transferred remotely from the structure to an offsite location for analysis, additional cost savings may be achieved in that decreased site visits and manual investigations by maintenance workers are needed (Bisby, 2004).

The advantages of using advanced sensing technology, such as electronic inclinometers and fibre-optic sensors, for bridge monitoring have been thoroughly demonstrated (Hou *et al.*, 2005; Vurpillot *et al.*, 1998). Moreover, sensors are becoming more reliable and cheaper while equipments for data acquisition, storage and management are more portable, less expensive and faster. Therefore, today, structures may be endowed with sophisticated measurement systems employing hundreds of sensors, and may be monitored at a high level of automation, versatility and flexibility, and with a good cost effectiveness (Ko and Ni, 2005). However, instrumentation and data acquisition are only the start of an effective structural health monitoring system. Interpretation of the acquired data and consecutive decision-making is equally important (Bergmeister and Santa, 2001; Glaser and Tolman, 2008).

Continuous monitoring has the potential of providing up to date information as it furnishes data about processes that change in time, such as live loads, fatigue damage and temperature (Farrar and Worden, 2007). However, despite these systems generate large amounts of data, it is often difficult to achieve early damage alarming (Zhang and Zhou, 2007). Therefore, so far, the greatest beneficiaries of monitoring data have been academics, who have gained insight into the behaviour and performance of a wide variety of structures (Brownjohn *et al.*, 2005). For bridge managers, the main purpose of a SHM system is, first of all, to detect damage at its onset. Therefore, with the goal of making this technology fully exploited by bridge authorities, one of the major challenges to be overcome is to make sense of the large amounts of data that are continuously produced by SHM systems (Glaser and Tolman, 2008). Structural safety and economic benefits of implementing SHM in the structures can only be attained if the system provides warning so that corrective action can be taken before damage evolves. It is, thus, fundamental to define suitable methodologies to detect changes associated with damage and to apply them in an automatic procedure in order to send an alarming signal to bridge owners when damage occurs (Farrar and Worden, 2007).

The choice and implementation of algorithms to process the collected data aiming at early damage identification is one of the most crucial aspects of an intelligent fault detection strategy. However, before choosing the methodology, it is necessary to choose between two complementary approaches: system identification and pattern recognition (ASCE, 2011; Worden and Dulieu-Barton, 2004). The former, also denoted as inverse problem or model-based approach, uses physics-based behavioural models and tries to relate changes in measured data from the structure with changes in the analytical model, thereby identifying anomalies in the structure. However, although conceptually straightforward, accurate system identification is difficult to perform due to errors in both models and measurements. Furthermore, models can be complex and expensive to create (Catbas *et al.*, 2007). In addition, this approach may be very time consuming, which may prevent effective damage detection at an early state. The latter approach (pattern recognition), also designated as data-driven or model-free approach, is entirely based on statistical analysis of data. It consists in looking for changes in a signature of the structure that is related to its structural response under a certain excitation. The anomalous behaviour is detected without information of physical processes, which makes this method generally faster (Sohn *et al.*, 2001). Nevertheless, although this approach is suitable to swiftly detect changes in the structural response, it is inappropriate to assess the structural condition (Farrar and Lieven, 2007).

Notwithstanding, SHM systems should be ultimately capable of performing autonomously a diagnostic of the state of health of a bridge (Farrar and Worden, 2007). In order to attain this objective, it is essential to understand the relationships between the signal measurements and the real occurred phenomena. Therefore, the comparison of measured and calculated data must be included in the SHM system (Bergmeister and Santa, 2001). In this context, although data-driven methods suffice for effective early damage detection, physics-based approaches are needed for assessing the structural condition. The process of creating a physics-based model of the structure begins by collecting as much initial system information as possible, including testing and analyses that were performed during the design stage, and, where applicable, data from maintenance and repair operations. This information is used not only to develop initial physics-based numerical models of the system, but also to design the sensing system that will be implemented for damage assessment, and to aid in the identification of additional sensors needed to monitor operational and environmental conditions. Then, data delivered from the sensing system are used to validate and update the physics-based models, and, therefore, to evaluate the mechanical and numerical assumptions both before and after damage (Farrar and Lieven, 2007).

The most popular existing techniques for both damage detection and condition assessment may be generically categorized in dynamic or static approaches, depending on the used features and the nature of the collected measurements. The former consists in monitoring the dynamic parameters of the structure, such as natural frequencies and modal shapes, under operating conditions (Doebling *et al.*, 1996). The latter focuses on the evolution of critical structural quantities, such as strains or displacements, under environmental changes, namely temperature variations (Del Grosso *et al.*, 2006). In addition, the measurements pattern obtained by a given sensor as a vehicle moves along the bridge is a signature of the structural response, thereby providing a great insight into the system behaviour (Ghali *et al.*, 2009; Hirachan and Chajes, 2005; Strauss *et al.*, 2012). Therefore, since bridges are permanently monitored, passages of in-service vehicles traversing the structure may be treated as a series of load tests, and, thus, the measurements of critical quantities may be used for both damage identification and structural condition assessment. Therefore, in addition to the typical approaches referred above, methodologies based on the responses originated by moving-loads on bridges, have been also used for both damage identification and structural condition assessment. These techniques may use either the dynamic (Yokoyama and Rafiquzzaman, 2005) or the quasi-static (Zaurin and Catbas, 2011) component of moving-loads responses. However, in spite of the valuable insight that the latter component of moving-loads responses provides into the structural behaviour, this kind of data has been rarely used within SHM problems.

Finally, it must be emphasized that, despite the growing body of research devoted to the implementation of fully automatic structural health monitoring systems in bridges, recovering reliable information in real time as regards both early damage detection and the structural condition remains a challenge (Brownjohn, 2007).

1.3. Objectives

The scope and motivation of this work were carefully framed in the previous section where two aspects that remain a challenge in the field of structural health monitoring were pointed out, which constitute the major goals of this thesis. The first is to emphasize the need of using field results together with physics-based behavioural models in order to understand the relationships between the signal measurements and the real occurred phenomena. This is the only way of evaluating the consequences on the structural behaviour of changes that might be detected in the measured response, and attaining, therefore, a sound and reliable assessment of the structural condition of a bridge. The second major goal is to propose an alternative data-driven approach for damage detection in bridges. Most existing approaches, despite some shortcomings, have shown promising capabilities for damage detection. Therefore, the purpose of the alternative approach presented herein is not to supersede the existing ones but to supplement them, thereby achieving effective detection of damage occurrence at an early state.

In addition, it was highlighted that despite the valuable insight of the quasi-static component of moving-loads responses, this kind of data has been less commonly used for structural health monitoring. In this context, an additional goal of this thesis is to accentuate the strengths of using this type of data for structural health monitoring purposes. Therefore, both the assessment of the structures condition and the approach for early damage detection are mainly based on moving-loads responses, particularly on their quasi-static component.

Within the major goals pointed out above, this thesis comprises a set of smaller objectives listed below. As shown in the previous section, the damage detection problem and the assessment of the structural condition are complementary subjects, in that they cannot be dissociated. However, as the structural health monitoring of bridges is a very comprehensive theme, and each of these topics encompasses also a large scope, for the sake of simplicity, these subjects are addressed separately. Still, the first objective of this thesis encompasses both, as follows:

i. To frame the two main topics aforementioned in the comprehensive discipline of SHM of bridges. First, SHM as a powerful tool for management of bridges shall be addressed. Secondly, a typical SHM system and the main objectives to be attained with its deployment shall be described. Finally, the structural condition assessment by using experimental data together with physics-based behavioural models, and the early damage identification by using data-driven approaches will be emphasized as key components of any SHM system.

Within the topic concerning the condition assessment of bridges by using experimental data together with physics-based behavioural models, four further objectives can be pointed out:

ii. To address the main field-tests available aiming at the characterization of the structural response of bridges. Thereafter, the benefits and shortcomings of the quasi-static component of the structural response obtained during the crossing of vehicles at crawling speed, under controlled conditions, namely in load tests, in order to characterize adequately the bridges' behaviour shall be highlighted.

iii. To emphasize the meaning of using physics-based behavioural models for analysing and interpreting the field results as well as for predictions of future structural behaviour.

iv. To show the importance of combining field tests, as comprehensive as possible regarding both static and quasi-static responses (note that the dynamic responses are out of the scope of this thesis), with adequate numerical modelling in order to establish a baseline condition for future assessments of the structure. Bridges may exhibit a structural behaviour different from the predicted by simplified design models, which do not take into account phenomena detected only through field-testing.

v. To validate the previous points using both laboratorial experiments and tests in full-scale bridges.

As regards the data-driven approaches for early damage identification in bridges, four final objectives can be addressed:

vi. To present and to describe the main damage identification methodologies, highlighting their main advantages and shortcomings. Within the scope of this thesis, data-driven approaches based on static and quasi-static data shall be emphasised.

vii. To propose an alternative approach for early damage identification based on moving-loads responses. This methodology shall be completely data-driven and use the quasi-static component of the structural response of in-service moving-vehicles. A set of algorithms to be applied within this approach shall be selected.

viii. To demonstrate that the proposed approach can identify damage at an early stage by using numerically-simulated data resembling the quasi-static component of the response of vehicles crossing a bridge.

ix. To validate the proposed approach for damage identification by using experimental moving-loads responses obtained in appropriate laboratorial tests as well as in full-scale applications.

1.4. Outline of the thesis

This thesis comprises seven chapters preceded and followed by, respectively, this introductory chapter and the conclusions. A brief description of the contents of each chapter is given in the following paragraphs.

Chapter 1 is the introductory chapter where the framework of this work is presented and the scope and motivation are described. This chapter includes also a section where the objectives to be attained with this research are formulated and the contents of the thesis are outlined.

Chapter 2 provides a brief insight on the structural health monitoring of bridges emphasising the two main topics addressed in this research: the structural condition assessment based on the analysis of field-tests data supported by physics-based behavioural models, and the damage identification process based on exclusively data-driven analysis of the structural response. In this context, it firstly gives an overview of a typical SHM system and of the main objectives to be attained with its deployment. Furthermore, particular emphasis is given for the existing approaches for damage identification, in which physics-based and data-driven approaches are compared, and methodologies based on either dynamic or static responses are briefly addressed. Thereafter, the physics-based assessment of bridges is addressed, where the numerical modelling as a tool to support the interpretation of the field results is emphasised, and the insight provided by moving-loads responses collected during field-tests is demonstrated. Building on this knowledge, this chapter presents an alternative data-driven approach for early damage detection, based on moving-loads responses, which involves building time-series of influence-lines and subsequent data-processing in order to enhance changes in the structural behaviour. Then, a set of algorithms that have shown to be successful in continuous monitoring are presented for later application along the subsequent chapters.

Chapter 3 presents an experimental and numerical analysis regarding the structural assessment of an existing steel bridge – the Eiffel Bridge – after a recent rehabilitation. The Eiffel Bridge, a centenary road-rail truss bridge, comprising two superimposed decks, was subjected to major rehabilitation works involving the replacement of the top concrete deck, the strengthening of the upper chords of the main truss girders and the replacement of the support bearings. In this context a load test and an environmental test were carried out aiming at the assessment of the new structural condition and the evaluation of the effectiveness of the elements strengthening. A numerical analysis, using an adequate numerical model of the bridge, was carried out in order to characterize the most relevant aspects of the structural behaviour and to support the discussion of the field results. Particular aspects concerning the main girders bending, the nature of nodes rotations, and the response under temperature changes are highlighted.

Chapter 4 focuses on the analysis of the in-service behaviour of reinforced and prestressed concrete bridges using a laboratorial model. In prestressed concrete structures small-width cracks may exist, which are, however, usually closed under working loads, i.e. cross-sections remain compressed during the passage of vehicles. Still, the in-service behaviour of these structures may be different from that observed in uncracked structures. In this chapter it is shown that the structural response is not linear, due to the imperfect match of the crack faces and the bond behaviour at the interface between the reinforcement and the surrounding concrete. It is shown that the influence-line for a moving-load crossing the structure depends on the movement direction. The reasons for that dependency are explained with the aid of the laboratorial model (which simulates a bridge structure at a reduced scale) and a dedicated finite-element modelling. It is also shown that the structural response is not proportional to the load crossing the structure, and depends on the applied prestressing force.

Chapter 5 is devoted to the application of the proposed methodology for damage identification based on moving-loads responses by using numerically-simulated data. The approach consists in building time-series and, thereafter in processing data using statistical algorithms that have already been shown to be successful in continuous monitoring: the moving principal component analysis (MPCA) and the robust regression analysis (RRA). Only the quasi-static component of the response is taken into consideration in this approach. A stiffness reduction replicating a crack was selected as the damage scenario to assess the performance of the methodology.

Chapter 6 aims at validating the methodology for damage identification by using experimental data. The reinforced and prestressed concrete laboratorial model analysed in chapter 4 was selected as the case study. The tests were designed with the purpose of replicating as close as possible real case scenarios for later application of these methodologies in full-scale bridges. In this context, two typical damage scenarios were addressed: a prestress loss and a partial restraint for the longitudinal rotation of a support bearing. Firstly, time-series of experimental data concerning both damage scenarios were built following an especially devoted approach. Then, these data were analysed by three selected algorithms for early damage detection: the robust regression analysis (RRA), the moving principal component analysis (MPCA) and the influence-line assurance criterion (ILAC). In addition, taking advantage of the comprehensive monitoring system installed in the laboratorial model, the performance of different measurement systems, combining different number and distinct types of sensors, is also assessed.

Chapter 7 presents a bridge weigh-in-motion (B-WIM) system implemented in a centenary double-deck steel truss bridge, the Luiz I Bridge located in Porto. The objective is to characterize the traffic of the upper deck, which holds a double tram-train railway line. The implemented B-WIM system uses only two fibre-optic strain gauges, applied in two crossbeams, from a very comprehensive monitoring system, installed mainly to monitor the structure's health. The methodologies proposed herein are supported by the analysis of the structural response under metro traffic, through numerical simulations carried out with an adequate finite-element model of the bridge. The system enables to identify the crossing direction, the speed and the vehicles loads, irrespectively of the track in which the metro crosses the bridge. In addition, this system is used to assist the collection of accurate influence-lines of the structural response under in-service metro traffic for later application of damage detection methods.

Chapter 8 is devoted to the application in full-scale bridges of the damage detection methodology based on the vehicle influence-lines acquired under in-service conditions of traffic, in which the Luiz I Bridge was selected as a case study. This structure, an outstanding centenary steel arch double-deck bridge recently rehabilitated and strengthened, which was endowed with a comprehensive fibre-optic based monitoring system, is prone to present bearings malfunctions. Firstly, a restraint for the longitudinal displacement of the support bearings installed in a critical pillar of the bridge identified in field measurements was evaluated through adequate numerical simulations. Additionally, a similar restraint in the support bearings installed in a quite stiffer pillar was simulated using the numerical model. Finally, both field measurements and numerically-simulated data replicating the former were analysed by the two selected algorithms for early damage detection: the moving principal component analysis (MPCA) and the influence-line assurance criterion (ILAC).

Chapter 9 is the final chapter in which the main conclusions drawn are outlined and future research topics within the subjects addressed along this text are briefly pointed out.

As aforementioned, chapter 2 provides a brief insight on the SHM of bridges, constituting, thus, a guiding principle for the issues addressed in the remaining chapters. Notwithstanding, each of these chapters was prepared in order to give rise to a journal paper, thereby allowing to be read separately. Consequently, and occasionally, some subjects are addressed in different chapters and, therefore, some repetition arises. For instance, firstly, the approach for early damage detection proposed in this thesis is addressed in chapters 5, 6 and 8. Furthermore, although different data-processing algorithms are used along these chapters, some of them arise more than once. Secondly, the laboratorial model is addressed in both chapters 4 and 6, as well as in chapter 5 in that the structure used to obtain numerically-simulated data intended to resemble the laboratorial model. Finally, the Luiz I Bridge is the case study of both chapters 7 and 8.

A list of the papers that constitute the basis of the chapters 3 to 8 included in this thesis is given below:

- Chapter 3: Cavadas, F., Rodrigues, C., Félix, C. and Figueiras, J. (2013). *Post-rehabilitation assessment of a centenary steel bridge through numerical and experimental analysis*. Journal of Constructional Steel Research 80(0): pp. 264-277;
- Chapter 4: Cavadas, F., Sousa, C. and Figueiras, J. (xxxx). *Analysis of the in-service behaviour of concrete bridges under moving-loads*. (prepared for submission);
- Chapter 5: Cavadas, F., Smith, I. F. C. and Figueiras, J. (2013). *Damage detection using data-driven methods applied to moving-load responses*. Mechanical Systems and Signal Processing 39(1–2): pp. 409-425;
- Chapter 6: Cavadas, F. and Figueiras, J. (xxxx). *Damage detection using data-driven approaches applied to experimental moving-loads responses*. (prepared for submission);
- Chapter 7: Cavadas, F., Costa, B. and Figueiras, J. (xxxx). *Implementation of a B-WIM system for the characterization of the railway traffic of a centenary steel truss bridge*. (prepared for submission);
- Chapter 8: Cavadas, F., Costa, B. and Figueiras, J. (xxxx). *Damage detection in a centenary steel truss bridge based on moving-loads responses*. (prepared for submission).

As shown above, the papers that originate the chapters included in this thesis had the contribution of co-authors other than the author of this thesis. Still, the later is the first author of each paper and thereby played a major role in the development of the works described therein. However, some key achievements, crucial both to attain the objectives proposed above and for the understanding of the whole text, are due to the contribution of some of the co-authors the author of this thesis had the privilege to work with.

Chapter 2

Structural health monitoring of bridges

2.1. Introduction

In the last years, major advances have been made in the design, modelling and analysis, as well as in the materials and construction techniques, which have led to a transition towards a life-cycle and performance oriented design of civil engineering structures (Yang *et al.*, 2004). This transition process was possible only because of recent progresses in the development of sensing technologies and data-processing techniques (Chong and Kumar, 2003; Farrar *et al.*, 2006; Fraser *et al.*, 2010; Masri *et al.*, 2004). These developments have led to the advent of structural health monitoring (SHM), which is a term increasingly used in the last two decades to describe the process of implementing a system on full-scale civil infrastructures, whose purposes are to assist and inform operators about the structures condition under gradual or sudden changes to their state, and to learn about either or both of the load and response mechanisms (Brownjohn, 2007).

In the context of modern bridge management systems, this is, thus, an effective way to follow the in-service behaviour of existing structures, and to gather quantitative information for planning maintenance and repair works (Orcesi and Frangopol, 2011). In addition, as a complement to the more traditional methods of observation, SHM permits a finer analysis and enables to detect infrastructure deterioration before it becomes critical, and, thus, represents a powerful tool in the ongoing struggle for sustainable infrastructure (Brownjohn, 2007). Therefore, a SHM system should be capable of providing information on demand about the health of a structure as well as warnings regarding any damage that has been detected (Bisby, 2004). For that purpose, the comparison and combination of measured and modelled behaviour are useful to calibrate and tune the mechanical and numerical assumptions. These results are, thus, the basis for the condition assessment and the safety evaluation, thereby supporting the decision-making and enabling an effective management of bridges (Bergmeister and Santa, 2001).

Any monitoring system involves the use of expertise in many disciplines, such as structures, materials, sensors, data management, intelligent processing, and communication (Bisby, 2004). Besides, each of these topics entails a huge amount of knowledge. Therefore, as clearly pointed out in the introductory chapter, this thesis focuses only on two main subjects within the extensive scope of the SHM of bridges. The first regards the structural condition assessment, in which the need of using field results together with physics-based behavioural models in order to understand the real occurred phenomena shall be emphasised. The second is related with the early damage detection problem, in which an approach, exclusively data-driven, is proposed. As aforementioned as well, both topics are addressed herein using the quasi-static component of moving-loads.

In this context, for the sake of clarity and ease of reading, the objective of this chapter is to provide a brief insight on the structural health monitoring of bridges, emphasising the main topics addressed along this thesis. It should be noted that the presentation of a detailed literature review regarding the wide scope subject of SHM of bridges is not a goal of this text. Even though, after this introduction, this chapter includes a section in which an overview of a typical SHM system is given, and the main objectives to be attained with its deployment are outlined. Furthermore, particular emphasis is given for the existing approaches for damage identification. First, physics-based and data-driven approaches are compared. Then, methodologies based on either dynamic or static responses are briefly addressed. In the third section, the condition assessment of bridges by combining field-results with physics-based behavioural models is discussed. The main static-based field-tests available to characterize the structural behaviour are presented, and the numerical modelling as a tool to support the interpretation of the field results is emphasised. Furthermore, the insight provided by the quasi-static component of moving-loads responses, collected during field-tests, for the analysis of the structural behaviour of bridges is carefully addressed. Building on this knowledge, the fourth section is devoted to presenting a data-driven approach for early damage identification based on moving-loads. It, firstly, involves building time-series of influence-lines and, secondly, processing data in order to enhance changes in the structural behaviour. Finally, a set of algorithms that have shown to be successful in continuous monitoring are presented for later application along the subsequent chapters.

2.2. Structural health monitoring systems

2.2.1. General overview

A typical SHM system, depicted in Figure 2.1, consists of six components, namely (Bisby, 2004; Mufti, 2001):

i. Acquisition;
ii. Communication;
iii. Intelligent processing;
iv. Storage;
v. Diagnostics;
vi. Retrieval of information as required.

The first subset in a SHM system involves the acquisition of data, in which the first task is the preparation plan for the installation of various sensing devices that can measure absolute values of strains, deformations, accelerations, temperatures, etc. The sensors should be selected for their ability to provide information about the health of the structure. The volume of acquired data, on one hand, should not be so scarce as to jeopardize its usefulness. On the other hand, it should not be so voluminous as to overwhelm interpretation.

The communication component refers to the conveyance of data from the data acquisition system to the location where the data is processed. Today, collected data is transmitted remotely, either through telephone lines or by a wireless mode.

Data retrieved directly from sensors may contain extraneous information that is both useless and uneconomical to store. Therefore, it is important for interpretation that the collected data be cleansed or intelligently processed, which is done at the third component of the SHM system. A further consideration for processing of data is correction for thermal effects.

The fourth component regards the storage of data in which data that has been cleansed by intelligent processing is stored and is made available for the diagnostics.

The most important subset of a SHM system deals with the interpretation of the collected and cleansed data. In this fifth component, the data are converted into quantities that relate directly to the response of a structure. For example, the deflection measurements might be converted into quantities of flexural stiffness, strains into stresses, etc. It is noteworthy to mention that the conversion of raw data into response indicators always depends upon assumptions, which are rarely perfect. In addition, the level of complexity of the analysis changes based on the needs of the monitoring program and the SHM system components. Still, regardless the level of sophistication of diagnostic activity, an appropriate numerical model of the structure calibrated against baseline field measurements is normally required.

The final component of a SHM system is related with the decision regarding the data that is deemed fit for retrieval. In the cases in which the observed data is not too voluminous, such as that obtained in static field-tests, it can be stored along with the interpreted responses. However, when it is voluminous, such as that regarding dynamic tests, it is considered sufficient to record only the interpreted data. The decision about the storage of data for retrieval should also attend to the confidence of its interpretation.

SHM systems are applicable to all types of civil engineering structures, including bridges, buildings, tunnels, pipes, highways and railways, and are generally deployed to (Kim and Frangopol, 2010; Ko and Ni, 2005):

i. Validate design assumptions and parameters with the potential benefit of improving design specifications and guidelines for future similar structures;

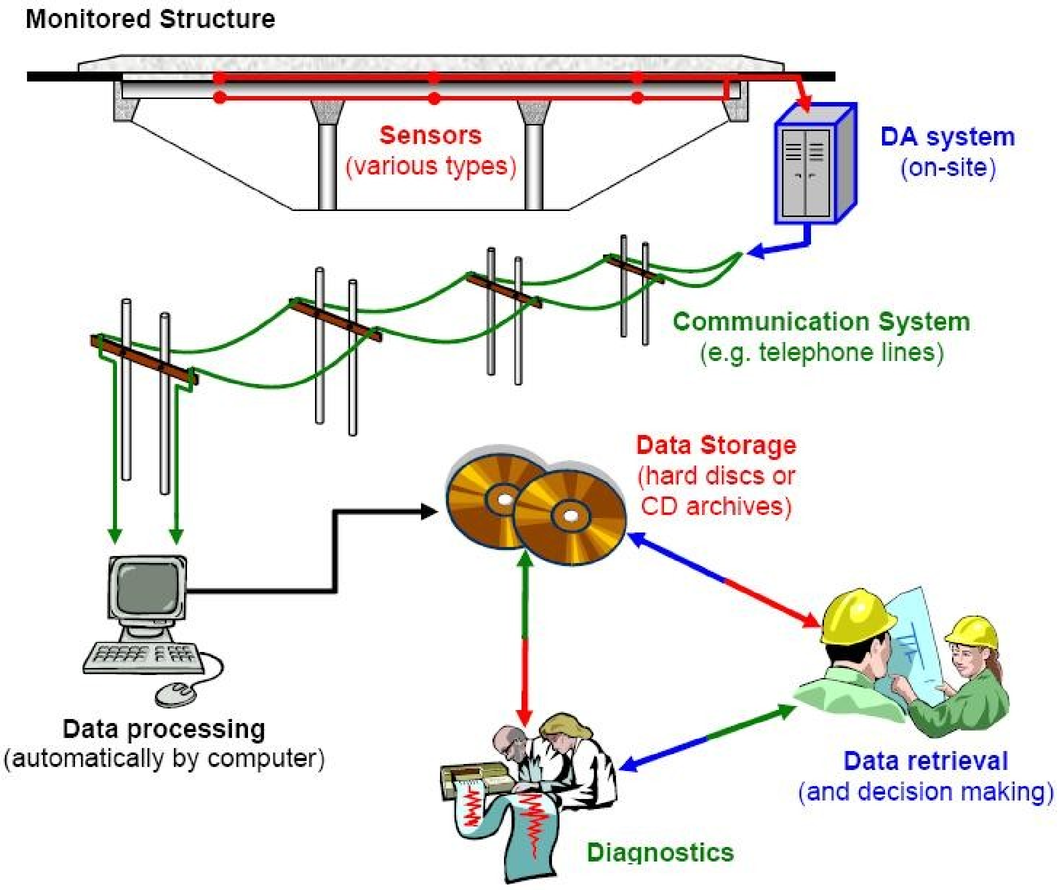

Figure 2.1 – Scheme of a typical SHM system (Bisby, 2004).

ii. Obtain massive amounts of in-situ data for leading-edge research in bridge engineering, such as wind- and earthquake-resistant designs, new structural types and smart material applications.
iii. Detect anomalies in loading and response, and possible damage/deterioration at an early stage to ensure structural and operational safety;
iv. Provide a decision support tool for safety assessment immediately after disasters and extreme events;
v. Provide evidence and instruction for planning and prioritizing bridge inspection, rehabilitation, maintenance and repair;
vi. Monitor repairs and reconstruction with the view of evaluating the effectiveness of maintenance, retrofit and repair works;
vii. Predict the remaining life of a structure.

Nonetheless, nowadays, SHM systems are generally applied for obtaining information about the health of a structure as well as warnings regarding any significant structural change that might have occurred. In order to illustrate the main principle of SHM, Mufti (2001) presented an analogy with the human body. Just as a doctor checks the health of his patients, today’s engineers need to be able to examine the condition of structures. The doctor uses specialized equipment to check the vital signs of a patient, and thereby monitor that patient’s health. The engineer utilizes specialized sensors embedded in a structure to check the structural health of that facility. If a patient’s vital signs are too high, the doctor prescribes corrective medicine. Similarly, in SHM, if the data flowing from the sensors indicate, for instance, excessive stress on the structure, the engineer can act appropriately to correct the situation. In both cases, early detection and immediate action prevents catastrophic consequences.

2.2.2. Damage identification approaches

2.2.2.1. General remarks

The core of any SHM system consists in the ability of automatically identifying damage, which means determining that some type of damage has occurred, localizing it, and finally assessing the extension and severity of damage (Silkorsky, 1999). In the most general terms, damage can be defined as changes introduced into a system that adversely affects its current or future performance (Farrar and Worden, 2007).

Building on the approach proposed by Rytter (1993), the damage detection problem may be described as a five-step process by answering the following questions (Sohn *et al.*, 2004):

i. Is there damage in the system? The method gives a qualitative indication that damage might be present in the structure. This is denoted as the *Detection* level.
ii. Where is the damage in the system? The method gives information about the probable position of the damage. This is referred to as *Localization* level.
iii. What kind of damage is present? The damage gives information about the type of damage. This is denoted as the *Classification* level.
iv. How severe is the damage? The method gives an estimate of the extent of the damage. This is referred to as the *Assessment* level.
v. How much useful life remains? The method offers information about the safety of the structure, estimating, e.g., a residual life. This is denoted as the *Prediction* level.

The vertical structure of the process is clear: each level requires that all lower-level information is available. Comparing to the structure proposed in (Rytter, 1993), this scheme added a new level: *Classification*. This level is important, if not vital, for effective identification as regards the *Assessment* and, possibly, the *Prediction* levels. Herein it is noteworthy to mention that *Prediction* is distinguished from the others in that it cannot be accomplished without an understanding of the physics of the damage. Conversely, *Detection* can be accomplished with no prior knowledge of how the system will behave when damaged (Worden and Dulieu-Barton, 2004).

2.2.2.2. Physics-based and data-driven approaches

The fundamental requirement of a damage detection system is to support decision making using sensor data. Therefore, the choice and implementation of algorithms to process the data and carry out the identification is the most crucial element of an intelligent damage detection strategy. However, even before choosing the algorithm, it is necessary to choose between two complementary approaches: *inverse problem* or *pattern recognition problem* (Worden and Dulieu-Barton, 2004).

The former, also designated as system identification or model-based approach, uses a behavioural model of the structure in order to compare measurements with those predicted by the model with the aim of discovering anomalies in the behaviour of the structure. It requires, thus, the development of a detailed and reliable analytical model of the structure, which is continuously updated in order to follow the mechanical and material properties of the structure. This technique is commonly designated as model updating (Brownjohn *et al.*, 2003; Zabel and Brehm, 2009). In the last years various methods for structural system identification aiming at the detection of damage, using more or less complex strategies, have been developed (Friswell, 2007; Goulet *et al.*, 2010; Xu and Humar, 2006; Zhu and Xiao, 2007). In addition, models may be used for making behavioural predictions such as the reserve capacity or the ability to carry exceptional loads. Nonetheless, although conceptually straightforward, in practice, this model updating approach to infer damage, due to measurement and modelling errors, is an ill-conditioned, even non-unique, inverse problem (Housner *et al.*, 1997), which makes the process of finding an accurate model difficult. These difficulties and uncertainties increase in presence of complex civil structures, so that a well defined and unique behaviour model cannot be clearly identified. Moreover, it should be mentioned that numerical models are expensive to create, requiring extensive tuning labour.

The pattern recognition approach, also denoted as model-free or data-driven, is entirely based on statistical analysis of data. It consists in looking for changes in a “signature” of the structure that is related to its structural response under a certain excitation (Housner *et al.*, 1997). Therefore, this approach is completely data-driven and the evolution of the structural condition is estimated without information of physical processes. It requires only nominal conditions for training. Moreover, these methods are generally faster than model-based methods as they do not require the evaluation of computation intensive numerical models. However, data-driven methodologies are inadequate for estimating reserve capacity or for predicting response to functional changes. In the last years, several data-driven techniques for damage detection have been proposed (Posenato *et al.*, 2010; Reda Taha and Lucero, 2005; Yao and Pakzad, 2012; Yeung and Smith, 2005). It should be mentioned, in addition, that this procedure does not require that measures of the environmental or operational conditions are available. However, it supposes that the reference database obtained when the structure is undamaged spans the various environmental and operational conditions that might influence the response of the structure (Sohn and Farrar, 2001). Another advantage of this approach is that it is applicable for the entire service life of the structure. Once the presence of an anomaly is detected, the methodologies adapt themselves to the new state in order to detect further anomalies (Del Grosso *et al.*, 2006).

As exposed above, both approaches have shown to have strengths and weaknesses. Table 2.1 summarizes the main characteristics of the two classes of methods (ASCE, 2011). It should be noted, however, that the significance of each of the listed items depends upon the specific application. Moreover, the two types of data interpretation methods are complementary.

Table 2.1 – Comparison of strengths and weaknesses between physics-based and data-driven interpretation methods (ASCE, 2011).

Data-driven	Physics-based
Completely data-driven (low cost modelling);	Modelling is complex, expensive and time consuming;
Easy to update;	Difficult to update;
Anomaly detected as variation from original behaviour;	Errors in models and in measurements can lead to identification of the wrong model;
An expert has to define the reference period;	Boundary conditions are not always known;
Requires a learning phase;	Different for each structure;
Difficult to estimate the thresholds for anomaly detection;	Easy interpretation of results;
Diagnosis difficult;	Diagnosis easier;
No support for structural modification;	Can support decisions related to functional changes;
No knowledge of reserve capacity;	Knowledge of reserve capacity;
Cannot be used to justify replacement avoidance;	Can be used to justify replacement avoidance;

Therefore, methodologies combining both may be able to overcome the weaknesses and benefit from the advantages of each other.

Finally, it is noteworthy to mention that answers to the damage detection problem questions presented above represent increasing knowledge of the damage state. In general, data-driven techniques can be used to address the first two questions in either an unsupervised or supervised learning mode. However, analytical models are usually needed to answer the last three questions unless examples of data are available from the system (or a similar system) when it exhibits varying damage levels (Sohn *et al.*, 2004).

2.2.2.3. Supervised and unsupervised learning

Beyond the previous distinction, the algorithms used for damage detection can be divided in two categories. When data are available from both the undamaged and damaged structure, the statistical pattern recognition algorithms fall into the general classification referred to as *supervised learning*. *Unsupervised learning* refers to algorithms that are applied to data not containing examples from the damaged system (Farrar and Doebling, 1999). The ability to perform the damage detection in an unsupervised learning mode is very important because data from damaged structures are typically not available for most real-world structures (Sohn and Farrar, 2001).

2.2.2.4. Dynamic and static responses

In recent years, the damage assessment of structures has drawn wide attention from various engineering fields. Since damage has an important effect on the dynamic as well as static behaviour of the structure, the existing approaches proposed in this area can be divided into two major categories: the dynamic identification methods using dynamic test data and the static identification methods using static test data (Wang *et al.*, 2001). Notwithstanding, compared with the static identification techniques, the dynamic ones have been developed more maturely due to their ease of practical implementation.

During the past two decades, a significant amount of research has been conducted in the area of SHM by utilizing techniques that rely on the changes in the dynamic properties of a structure and the corresponding literature is quite extensive. Further information about dynamic methods for damage detection can be found in (Carden and Fanning, 2004; Doebling *et al.*, 1996).

Depending on the type of excitation that is used to induce a structural response, one may differentiate forced vibration and ambient vibration testing. In the first case, a controlled excitation is obtained by heavy shakers or drop weights (Andreaus and Baragatti, 2012). In the second, which is a method that is less cost intensive, excitation is obtained by wind- or traffic-loads (Magalhães *et al.*, 2012).

The main idea of dynamic-based damage detection is the fact that modal properties (natural frequencies, mode shapes, mode shape curvatures, modal flexibility, modal damping, etc.) are functions of the physical parameters (mass, stiffness and damping) and hence, existence of damage leads to changes in the modal properties of the structure. Therefore, changes in vibration properties can serve as indicators of damage detection.

Although several researchers developed damage assessment techniques using natural frequency, the feasibility of using frequency changes for the purpose of damage localization is limited. Therefore, in an effort to overcome these difficulties, researchers have turned their attention to using changes in the mode shapes. The appealing feature is that changes in mode shapes are much more sensitive to local damage when compared to changes in natural frequencies. However, using mode shapes also has some drawbacks (Kim *et al.*, 2003). One of the most significant shortcoming pointed out is that methods based on modal parameters lack sensitivity in structures where environmental factors also contribute to modal frequency shifts (Doebling *et al.*, 1996). Therefore, currently, significant research is devoted to fully account for the environmental and operational variability of structures (Peeters *et al.*, 2001; Worden *et al.*, 2002).

Despite the majority of the methods for identifying damage have been focused on dynamic-based techniques, in the last few years static-based procedures have also gained increasing importance. Static-based techniques consist in measuring structural quantities such as displacements or strains, at a slow rate, under environmental and applied loads. In the former, both environmental parameters (namely temperature) and the structural response to ambient excitation are collected to produce time-series for later data-processing (Santos *et al.*, 2013). In the latter, the structural response is measured under applied loads, which may comprise either static load cases (Hjelmstad and Shin, 1997) or vehicles moving slowly on the bridge (Orcesi and Frangopol, 2010).

One of the main advantages of long-term static monitoring is that the structure may be monitored under all scenarios, without generating an amount of data that may be difficult to handle. Furthermore, static deflections may be more sensitive to damage than dynamic parameters (Jenkins *et al.*, 1997). In addition, the structural response collected under a vehicle crossing the bridge provides a better understanding of the structural behaviour, as it will be shown below.

2.3. Physics-based assessment

2.3.1. General overview

In general, bridge assessment is conducted to either confirm an existing load rating (if bridge deterioration is observed or suspected) or increase a load rating. Analytical or predictive approaches to determine load ratings are well documented and widely used. However, on one hand, such approaches may be overly conservative leading to the underestimation of the actual load carrying capacity of a bridge, caused by system effects, load redistribution, contribution of non-structural elements and bearings not behaving in an “idealized” manner (Faber *et al.*, 2000). Therefore, even the current best practices for bridge assessment may point out for the retrofitting or replacement of some bridges not requiring any kind of intervention. On the other hand, some structures in need of engineering renewal or replacement may not be identified, which can pose serious safety problems, ultimately resulting in the occurrence of dramatic failure (Chang *et al.*, 2003).

In this context, the use of non-destructive testing tools emerges as a valuable solution to assist the assessment of the existing condition of structures, both in terms of the load-carrying capacity and serviceability. Moreover, data collected through these means are essential for obtaining field-calibrated numerical models, developed for structural identification, in order to understand the real behaviour and performance of actual bridges and to quantify relative contributions of different stiffness and resistance mechanisms (Aktan *et al.*, 1996). On one hand, experimental results are measures of the actual structural behaviour whose usefulness is only completely attained if the associated physical phenomena are understood. On the other hand, numerical models are extremely important to fully analyse the structures behaviour. Yet, their significance is weakened if the modelling assumptions considered are not suitable, particularly when adopting very sophisticated models for replicating complex phenomena. Therefore, only through a combined analysis of experimental results and numerical data it is possible to take full advantage of field testing and structural modelling.

2.3.2. Static-based field testing

2.3.2.1. General remarks

Field-testing is an essential technology in the condition evaluation of bridges. By itself it stands as a useful tool to determine whether restrictions to traffic conditions are imperative, to evaluate the need for repair, retrofit or strengthening, to assist their planning and design, and ultimately to appraise the bridge behaviour in its new condition (Sartor *et al.*, 1999). The results of the field experimentation are used for the calibration of the linear and nonlinear finite-element models of the bridge and structural identification of its as-is condition (Catbas et al., 2001). However, it is important to understand the policies and procedures relating to field-testing and evaluation of bridges.

Static-based field testing is performed by placing loads of constant magnitude on the bridge very slowly, so that dynamic effects are not induced in the structure (Mufti, 2001). In general it comprises three main types of tests: (i) behaviour tests; (ii) diagnostic tests; and (iii) proof tests. The first type, the most common, is usually performed to appraise the load distribution among various elements of the bridge or to validate some analytical method to adopt, in which the loading level is lower than the maximum for service conditions (Boothby and Craig, 1997; DelGrego *et al.*, 2008). The diagnostic test is specifically carried out to identify the effects of component interaction or the causes for a change in the load acting on a component (Chajes *et al.*, 1997; Farhey *et al.*, 2000). A proof load test, as its own designation suggests, aims to determine the safe load-carrying capacity of the bridge by gradually increasing the applied loads, often surpassing the permitted service levels (Saraf and Nowak, 1998). Within this work, and taking into account the objectives previously presented, this research focuses on behaviour tests.

2.3.2.2. Behaviour tests

These tests are performed with the purpose of either verifying the methods adopted in the analysis process or assess the mechanics of bridge behaviour. In general, the bridge loading is accomplished by applying loaded trucks with identified weight at selected locations along the bridge without creating risk of injury or structural damage. For a static evaluation, the trucks are positioned at stationary critical load configurations, predetermined analytically to provide the most critical response of important structural members.

The monitoring of the structural response for several loading cases is carried out by a set of sensors capable of measuring either local or global quantities. Typically, strain data provide the local flexural response of individual members and components. The global behaviour of a bridge may be captured by measuring the vertical deflections at representative points along the span, support displacements, and response distribution between load-carrying members. These measurements provide information on the boundary conditions and constraints. Although most bridge designs are controlled by strength, rather than serviceability, monitoring deflections and displacements is indicative of structural behaviour and performance (Farhey, 2005).

Additionally, the structure can be monitored while a truck moves along a predetermined path (usually, traffic lanes) across the bridge at a low and steady speed (crawling speed), which constitutes a quasi-static load. The monitoring of the structural response induced by the moving truck is also performed through strain, rotation and displacement measurements at key locations of the bridge.

The structural response measured as a vehicle crosses a bridge is presented graphically in the form of influence-lines. These graphs represent, thus, the variation of the monitored response due to the vehicle traversing the structure. Similar results obtained under a point-load are denoted as unit influence-lines (UIL). Therefore, the UIL shows the variation of the response due to a unit load traversing the structure. In order to differentiate the influence-line regarding a point-load from that related to any vehicle, the later is designated as vehicle influence-line (VIL).

UIL may be obtained numerically, by using a finite-element model of the structure, or by the use of Muller-Breslau's principle, which is one of the most effective methods of obtaining analytical UILs. This principle, using the *Betti*'s theorem, states that the ordinates of the UIL for any action in a structure are equal to those of the deflection curve obtained by releasing the restraint corresponding to this action and introducing a corresponding unit displacement. Note that the term displacement is used in its general sense: the displacement corresponding to a force is a linear displacement; that corresponding to a moment is a rotation (Ghali *et al.*, 2009).

UIL are commonly used by structural engineers to determine the critical combination of possible load effects at a particular location. Taking into account the superposition principle, for a linear and elastic structure, the static response due to a known load scenario can be determined by multiplying each one of the loads by the corresponding UIL ordinate, and simply adding the effects. Moreover, UILs may provide further information as regards the structural behaviour. Consider the following equation expressing the Maxwell's reciprocal theorem (Ghali *et al.*, 2009):

$$d_{ij} = d_{ji} \tag{2.1}$$

which states that in a linear and elastic structure, the displacement at coordinate i due to a unit force at coordinate j, d_{ij}, is equal to the displacement at j due to a unit force acting at i, d_{ji}. Therefore, on the assumption that i and j are, respectively, fixed and moving positions, d_{ij} gives the UIL of the displacement at i whereas d_{ji} is the deformed shape due to a unit force at i. In this context influence-lines are very useful since they provide information not only about the response at one point of the structure under a vertical load moving across the structure but also the deflected shape under the corresponding force applied at that point (Yokoyama and Rafiquzzaman, 2005).

As aforementioned, for a linear and elastic structure, the static response due to a known load scenario can be determined using the superposition principle. Thus, the response of a given quantity z for a multi-axles vehicle located at i, denoted, thus, as z_i, may be expressed as follows:

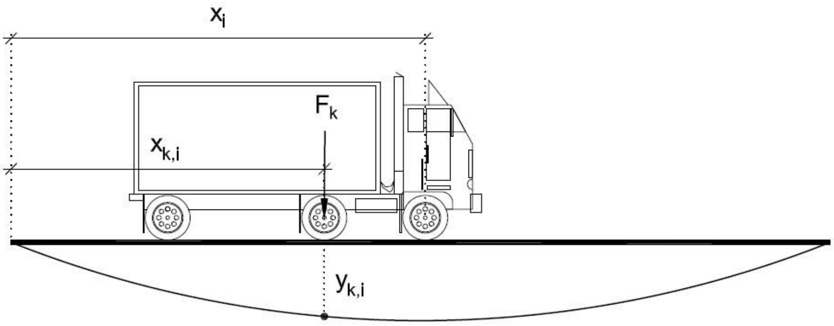

Figure 2.2 – Scheme of the procedure to obtain the VIL.

$$z_i = \sum_{k=1}^{N_{axles}} y_{k,i} \cdot F_k \tag{2.2}$$

where $y_{k,i}$ is the ordinate of the UIL at the position occupied by the k^{th} axle, denoted as $x_{k,i}$, and F_k is the corresponding axle-load (see Figure 2.2). In general, in practical applications, the position of the vehicle, x_i, corresponds to the position of the first axle.

Therefore, building on this knowledge, knowing the weight and the location of each axle of a vehicle crossing a bridge, as well as the structural responses, the UIL may be obtained by means of an inverse problem (O'Brien *et al.*, 2006). While a VIL provides a signature of the bridge response for the vehicle under consideration, the UIL constitutes a normalized signature. This makes UILs particularly suitable for damage detection purposes in that with every vehicle crossing over the bridge, comparison between the previously obtained one and the most recent one can be done (Zaurin and Catbas, 2011).

In the last years, both experimental UILs and VILS have been used for the following purposes: (i) characterization of the structural behaviour (Strauss *et al.*, 2012); (ii) to determine in-situ distribution factors in multi-girders bridges (Orcesi and Frangopol, 2010); (iii) B-WIM systems (Zhao and Uddin, 2010); and (iv) damage detection (Rucker *et al.*, 2006; Zaurin and Catbas, 2011).

2.3.3. Numerical analysis

An important component of the structural health monitoring field is the development of linear and nonlinear finite-element models (FEM), so that field measurements can be compared with numerically-simulated data. In fact, if on one hand, the models are calibrated using the current state characteristics of the bridges as determined from experimental data (Catbas *et al.*, 2001), on the other hand, simulations can contribute significantly for explaining the structural behaviour in a comprehensive way, and serve for the detection of critical elements or regions (Strauss *et al.*, 2012).

In the numerical modelling community, there is a tendency to aim at very high levels of sophistication of models, even in the simulation of the simplest problems. At the same time, there is usually a significant level of uncertainty in experimental data. Therefore, a sound balance between the detail and complexity of the model, the available measurements of the structural response and the objectives of the analysis to accomplish, must be attained. Finding good models of behaviour is important for explaining the performance of structures in service. Engineers often use complex models that require important assumptions which are adopted without adequate justification (Robert-Nicoud *et al.*, 2000). Moreover, for some cases the most relevant variables at stake do not have a physical meaning, thus making difficult the understanding of the results. However, due to the particular nature of certain phenomena their modelling demands an approach of higher level of complexity.

The effort in the simulation and analysis is determined by the complexity of the real structural behaviour that has to be captured under varying loading conditions. In structural engineering, simulation techniques range from efficient simplified static calculation techniques to highly sophisticated nonlinear calculation techniques which are taking into account the overall system deformation and material laws (Strauss *et al.*, 2012). Bathe (1995) suggests a top-down approach starting with the coarsest mesh that will capture the dominant behaviour of the physical model: (i) use the simplest elements that will do the job; and (ii) never use complicated or special elements unless there is perfect confidence in their use.

2.4. A data-driven approach for damage detection based on moving-loads responses

2.4.1. General remarks

In the section above it was shown that the structural response collected as a vehicle moves along a bridge is a signature of the structural behaviour for that vehicle, thereby providing a great insight into the system behaviour. However, little research has been done for the development of methodologies for damage detection based on this kind of data. Even though, a few works based on moving-loads responses may be pointed out.

By comparing undamaged with damaged influence-lines, Choi *et al.* (2004) demonstrated that the variations of the displacement reach the maximum at the damaged location irrespectively of the location at which the load is applied, and the variations of displacement are the largest when the applied load in the actual beam is at the damage location. Rucker *et al.* (2006) referred a proved method for damage identification of beamlike structures using differences of measured inclinations. However, the application of these methods involves periodic static-load tests under controlled conditions, requiring the interruption of regular traffic. Furthermore, they imply knowing precise load levels used in the tests. Thus, in order to detect damage using influence-line data, development of other strategies is necessary.

Since bridges are permanently monitored, passages of in-service vehicles traversing the structure may be treated as a series of load tests, and, thus, the measurements of critical quantities may be used for damage identification. Yokoyama and Rafiquzzaman (2005) used strain data together with the corresponding vehicle data, collected in operating conditions, in order to establish correlations and, thus, detect changes in the structural response. Zaurin and Catbas (2011) described a methodology that uses both video stream and sensor data in conjunction with outlier detection methods to identify changes in the structural behaviour.

In this section, an alternative approach for early damage detection based on the quasi-static component of moving-loads responses is proposed. It consists in collecting vehicle influence-lines (VIL) in operating conditions, building time-series with these data and, thereafter, processing data using suitable algorithms in order to detect the occurrence of damage.

2.4.2. Description of the methodology

The alternative approach proposed herein for early damage detection based on moving-loads responses involves three main steps: (i) data acquisition; (ii) data collection; and (iii) data-processing. The following paragraphs provide a brief description of each step.

The first step, the data acquisition, consists in recording the structural response of the structure for every vehicle that crosses the bridge. For that purpose, a weigh-in-motion (WIM) system should be implemented (O'Brien *et al.*, 2008). This system will serve two main purposes. The first is to shift the data domain from time to space, thereby providing vehicle-influence-lines that will be used for damage detection. The second is to estimate vehicle parameters such as loads, number of axles and axles loads in order to assign it to one of a set of predefined classes.

The data collection consists in building time-series of the VIL recorded in the first step. This step entails, firstly, choosing the vehicle classes that will be considered for analysis. Then, the structural response of a vehicle whose class assigned in the previous step match that selected herein should be added to the time-series. Data regarding the remaining vehicles may be either disregarded or added to additional time-series, thereby enabling to develop analysis in parallel.

The final step regards to the data-processing. It consists in analysing data through suitable data-processing algorithms in order to find changes in the patterns of the VILs and, thus, flag the occurrence of damage. This step involves two phases. The first is the training phase in which the structure is assumed to behave in an undamaged condition. The aim of this first period is to estimate the variability of the control parameters related with the data-processing algorithm and to define the thresholds for detecting anomalies in the monitoring phase. When the established thresholds are exceeded a damage is signalized and further research must be carried out in order to assess the flagged change. The algorithms to be used, which have shown to be successful in continuous monitoring, are described below.

It is noteworthy to mention that, in the second step, the selection of the VILs to be included in the time-series for latter analysis is a key task of this step, in that it enables to prevent the inclusion in the time-series of significantly different VILs. As the data-processing algorithms should seek for dissimilarities in the VILs to flag damage, very different VILs would compromise the ability of the damage detection process.

2.4.3. Data-processing algorithms for data-driven damage detection

2.4.3.1. Regression analysis

Regression analysis is a statistical technique that is very useful for many problems in engineering and science, which involve exploring the relationships between two or more variables. Consider a set of n data points concerning two variables X and Y: (x_1, y_1), (x_2, y_2), ..., (x_n, y_n). Often, the first step of an exploratory data analysis is to draw a graph of the points (x_i, y_i), which is generally called a scatter plot. This plot may give a visual sense of the statistical relationship between the variables. The objective is to assess whether the cloud of points seems to show a linear trend that might fit the cloud of points rather than finding a curve that passes exactly through all the points. In a situation where there is a strong indication that the points lay scattered randomly around a straight line, it is reasonable to assume that the variable Y is related to X by a linear relationship. Therefore, the fitted or estimated regression line is given by:

$$\hat{y} = \beta_0 + \beta_1 \cdot x \tag{2.3}$$

where β_0 and β_1, respectively, the intercept and the slope of the line, are the regression coefficients of the simple linear regression model. Note that each observation i, (x_i, y_i), satisfies the following relationship:

$$y_i = \beta_0 + \beta_1 \cdot x_i + e_i \tag{2.4}$$

where e_i, given by $e_i = y_i - \hat{y}_i$ and denoted as the residual, describes the error in the fit of the model to the i^{th} observation. Montgomery and Runger (2003) show how the residuals are used to provide information about the adequacy of the fitted model.

The regression coefficients are estimated in such a way that the resulting regression line is a "best fit" of the data. In general, the regression coefficients are estimated on the basis of the least squares method, which consists in minimizing the sum of the squares of the vertical deviations, i.e., the residuals.

In the field of structural health monitoring, linear regression analysis may be used to identify changes in the structural behaviour in two ways. The first approach consists in observing the evolution of the coefficients of the linear regression with time (Peterson *et al.*, 2014). The second method is based on monitoring the variation of the residuals in time (Laory *et al.*, 2011). In both cases anomalies are identified when a significant variation is observed.

2.4.3.2. Moving principal component analysis

The principal component analysis (PCA) is one of the methods included in the proper orthogonal decomposition (POD), which is probably the oldest, best known and most used procedure in multivariate analysis (Chatterjee, 2000; Kerschen *et al.*, 2005; Liang *et al.*, 2002). The key idea of PCA is to reduce the dimensionality of a dataset consisting of a large number of interdependent variables to a much smaller number of uncorrelated variables while retaining as much as possible of the variation present in the original dataset. Thus, the original variables are transformed into a new set of uncorrelated variables, the principal components (PCs), which are ordered so that the first few retain most of the variation present in all of the original variables (Jolliffe, 2002). The first principal component corresponds to the direction in which the observations exhibit the largest variance. The second component is orthogonal to the first and maximizes the variance of the data points projected on it. In this way, the remaining principal components are orthogonal to the previous ones and maximize the variance of the data points projected on it (Hubert *et al.*, 2005; Jolliffe, 2002).

Consider a matrix $X \in \Re^{n \times p}$, denoted as features matrix, containing n observations for p features. The row i is a p-dimensional vector representing the i^{th} observation, whereas the column j is a n-dimensional vector representing the j^{th} feature. The i^{th} observation, $X_i = \left(X_{i,1}, X_{i,2}, \dots, X_{i,p}\right)$ can be written as a linear combination of a set of orthogonal vectors $U_j = \left(U_{1,j}, U_{2,j}, \dots, U_{p,j}\right)$ as follows:

$$[X_i]^T = \sum_{j=0}^{p} Z_{ij} U_j \tag{2.5}$$

where Z_{ij} corresponds to the component score for the j^{th} feature at the i^{th} observation. In the matrix form the equation presented above is given by:

$$[X_i] = [Z_i][U]^T \tag{2.6}$$

where $Z_i = \left(Z_{i,1}, Z_{i,2}, \dots, Z_{i,p}\right)$ is a vector containing the components scores corresponding to the i^{th} observation and $U \in \Re^{p \times p}$ is a matrix containing the p orthogonal vectors. Following the same scheme, the features matrix may be computed as follows:

$$[X] = [Z][U]^T \tag{2.7}$$

where $Z \in \Re^{n \times p}$ is the scores matrix and $U \in \Re^{p \times p}$ is the loadings matrix. The scores correspond to the coordinates of the original data in the new coordinate system defined by the orthogonal vectors U_j.

In the classical approach, these orthogonal vectors, denoted as principal components, correspond to the eigenvectors computed from the covariance matrix $S \in \Re^{p \times p}$ of the dataset $X \in \Re^{n \times p}$. The k^{th} principal component is the eigenvector U_k corresponding to the k^{th} largest eigenvalue (Jolliffe, 2002). In order to PCA work properly, the mean of all observations included in each feature of the dataset must be subtracted before the calculation of the covariance matrix S.

As mentioned above, the first few principal components retain most of the variation present in all of the original variables. Thus, for a p-dimensional dataset, it is possible to choose only the first r principal components, where $r < p$, and obtain the original data without significant loss of information. Thus, a good approximation of the features matrix $X \in \Re^{n \times p}$ can be obtained as follows:

$$[X] = [\bar{Z}][\bar{U}]^T \tag{2.8}$$

where $\bar{Z} \in \Re^{n\times r}$ and $\bar{U} \in \Re^{p\times r}$ are, respectively, the r-dimensional matrices of the scores and the loadings.

Figure 2.3 depicts a geometrical interpretation of PCA. Figure 2.3 (a) shows a plot of 50 observations on two highly correlated variables x_1 and x_2. There is considerable variation in both variables, though, rather more in the direction of x_1 than x_2. The plot of the dataset transformed into the principal components z_1 and z_2 is shown in Figure 2.3 (b). It is clear that there is greater variation in the direction of z_1 than in either of the original variables (x_1 and x_2), but very little variation in the direction of z_2. Further details regarding the geometrical interpretation of PCA may be found both in (Jolliffe, 2002) and (Yan *et al.*, 2005a). In addition, it is noteworthy to mention that each principal component is a linear combination of the original variables, which enables to ascribe a meaning to what the components represent.

Because of the large amount of computations required, the POD was virtually unused until the middle of the 20th century. However, with the appearance of powerful computers this technique, and, thus, the PCA, has gained popularity and is being used in numerous applications in the engineering field (Chatterjee, 2000; Kerschen *et al.*, 2005; Liang *et al.*, 2002; Yan *et al.*, 2005a).

In the context of structural health monitoring, PCA has been widely applied in the last years both in structural dynamic (Bandara *et al.*, 2014; Viet Hà and Golinval, 2010) and, although less extended, static (Laory *et al.*, 2011; Posenato *et al.*, 2008) responses. It has been used with three major objectives (Figueiredo *et al.*, 2009): (i) evaluation of patterns in the data; (ii) data cleansing; and (iii) data compression. In the context of damage detection, this technique is generally applied with the objective of reducing the dimensionality and enhancing the

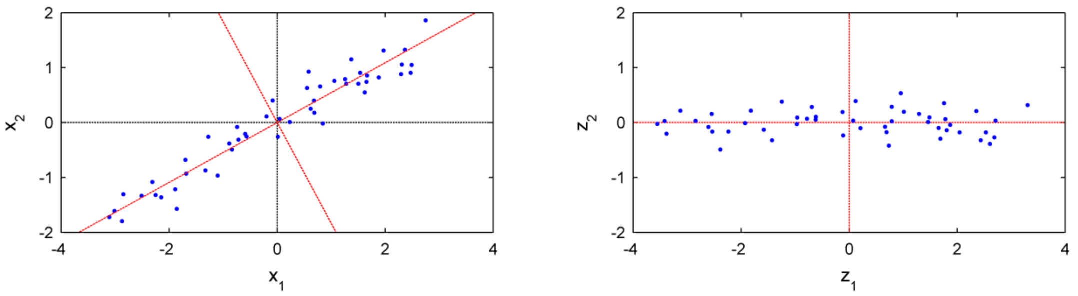

(a) (b)

Figure 2.3 – Geometrical interpretation of PCA based on 50 observations: (a) plot of the observations on two variables x_1 and x_2; and (b) plot of the observations on their principal components z_1 and z_2.

discrimination between features from undamaged and damaged structures. Then, data transformed by PCA are processed by an appropriate damage detection algorithm (Sohn and Farrar, 2000). However, PCA can also be applied straightforwardly for damage detection using either the principal components coordinates (Posenato *et al.*, 2008) or the residuals in relation to the principal components (Yan *et al.*, 2005a; b).

Focusing on the application of PCA for damage detection based on the principal components coordinates, Lanata and Del Grosso (2006) have shown that the analysis of the evolution in terms of eigenvalues and eigenvectors of the covariance matrix of the dataset gives a good indication of the damage initiation. However, a significant time-lag between the identification and the occurrence of damage was found. As the number of measurements is continuously growing during the monitoring process, the fact the algorithm processes all the previous observations, leads to the aforementioned delay. Immediately after damage occurrence, the influence of old measurements (in the undamaged state) is much higher than that of new measurements (in the damaged state). Thus, additional time is required in order to the new measurements may produce changes in the principal components. With the objective of overcoming this drawback, Posenato *et al.* (2008) proposed the moving principal component analysis (MPCA), as an extension of PCA. This approach consists in the calculation of the principal components of the data comprised in a window of constant size moving along the entire dataset. Similarly to the classical approach, a change in the values of the principal components coordinates suggests the occurrence of damage.

2.4.3.3. Influence-line assurance criterion

The influence-line assurance criterion (ILAC) is a statistical indicator that yields the degree of consistency between influence-lines. This parameter is based on the modal assurance criterion (MAC), usually applied to match mode shapes (Allemang, 2003). The MAC gives a measure of consistency between estimates of mode vectors, thereby providing a method of easily comparing estimates of mode vectors originating from different sources. It constitutes a good statistic indicator because it is most sensitive to large differences and relatively insensitive to small differences in the mode shapes (Pastor *et al.*, 2012). The MAC between the r^{th} vector of a dataset A, $\psi_{r,A}$, and the q^{th} vector of a dataset B, $\psi_{q,B}$, is a scalar constant defined as follows (Allemang, 2003):

$$MAC(r_A, q_B) = \frac{\left|\{\psi_{r,A}\}^T\{\psi_{q,B}\}\right|^2}{\left(\{\psi_{r,A}\}^T\{\psi_{r,A}\}\right)\left(\{\psi_{q,B}\}^T\{\psi_{q,B}\}\right)} \tag{2.9}$$

The MAC takes values from zero (representing no consistent correspondence) to one (representing a consistent correspondence). In this manner, if the modal vectors under consideration exhibit a consistent relationship, the modal assurance criterion should approach the unit. The MAC values are presented in a matrix, which is used, in general, for the comparison of mode shapes identified from data obtained experimentally with mode shapes derived from analytical models. Notwithstanding, further potential uses are mentioned by Allemang (2003). For instance, in the last years, the MAC, many times together with other related assurance criteria, has been widely used for damage detection (Doebling *et al.*, 1996; Salgado, 2008; Srinivasan and Kot, 1992; Zhou, 2006).

Building on these results a new statistical indicator, the ILAC, is proposed herein for early damage detection based on moving-loads data. As aforementioned, the influence-line assurance criterion is a measure of consistency between estimates of influence-lines, which may be defined by:

$$ILAC(r_A, q_B) = \frac{\left|\{\Upsilon_{r,A}\}^T\{\Upsilon_{q,B}\}\right|^2}{\left(\{\Upsilon_{r,A}\}^T\{\Upsilon_{r,A}\}\right)\left(\{\Upsilon_{q,B}\}^T\{\Upsilon_{q,B}\}\right)} \tag{2.10}$$

where $ILAC(r_A, q_B)$ is the ILAC between the r^{th} influence-line of a dataset A, $\Upsilon_{r,A}$, and the q^{th} influence-line of a dataset B, $\Upsilon_{q,B}$. On the assumption the datasets A and B are obtained in different time-instants, the diagonal terms of the ILAC matrix may provide a good indication of the occurrence of damage in the structure. An ILAC value of one would show that the two influence-lines are perfectly correlated, or, in this case, identical. The greater the deviation from unit, the less the two modes are correlated, which suggests changes in the structural response, and, thus, the occurrence of damage.

However, preliminary tests have shown that these indicators could hardly provide a reliable damage identification due to the variability of the vehicle influence-lines, which results from the changeability of the vehicle parameters (as thoroughly discussed below). Still, additional tests have shown that the AutoILAC, based on the AutoMAC presented by Pastor *et al.* (2012), allows to overcome this shortcoming. The AutoILAC quantitatively compares all the possible combinations of influence-lines pairs for only one set of influence-lines. The calculation assigns a value of one to influence-lines pairs that exactly match and a value of zero to those pairs that are completely independent or unrelated. In the context of this work, with the goal of early damage detection, instead of discovering the influence-lines included in a given dataset that exactly match, the focus lies on the surveillance of the evolution of the AutoILAC values along a monitoring period. Deviations of the AutoILAC values computed along the monitoring period from those calculated in the training period, in which the structure is assumed to operate under normal conditions, suggest changes in the structural response, and, thus, the occurrence of damage.

2.5. Conclusions

This chapter provides a brief insight on the structural health monitoring of bridges emphasising the two main topics addressed in this research: the structural condition assessment based on the analysis of field-tests data supported by physics-based behavioural models, and the damage identification process based on exclusively data-driven analysis of the structural response.

First, a brief overview of a typical SHM system is given, emphasising the existing damage identification approaches. It was shown that a data-driven approach enables a promptly detection of damage. However, it can hardly provide information at the higher levels of the damage detection hierarchy. Therefore, in order to complete the damage identification process a physics-based approach is also required. It was shown, in addition, that the successful implementation of a damage detection strategy implies the comparison of a given structural state with a reference condition, in which the structure is assumed to be in normal operating conditions. In this context, a thorough analysis of the structural behaviour at the beginning of the monitoring period is paramount for future evaluations.

For a successful physics-based assessment of a bridge both non-destructive field testing and numerical modelling have to equally contribute in the process. If the former provides at the first stage the data of the structural response to validate, calibrate or update the models for simulating the bridge behaviour, in turn, at the second stage, these models must be capable of assisting in the evaluation of the structural condition, either at the serviceability or safety levels. Herein, the valuable insight for the analysis of the structural behaviour provided by moving-loads responses collected in field-tests is demonstrated.

Finally, building on this knowledge, an alternative data-driven approach for early damage detection based on in-service moving-loads responses is presented and the algorithms proposed for subsequent data-processing are described.

Chapter 3

Condition assessment of a centenary steel bridge – The Eiffel Bridge

3.1. Introduction

An important part of the existing steel bridges was built in the later XIX and early XX centuries. In addition to aging, the bridge population has suffered from decades of neglect and overuse, which led to accelerated deterioration. However, the replacement with new structures raises financial, political and environmental problems. The high costs of building new bridges are only economically justifiable by proving a significantly longer service life together with smaller maintenance costs in relation to old ones. Furthermore, due to historical and social aspects, many of the old steel bridges hold a cultural value that has to be preserved. Therefore, the conservation and maintenance of old structures is increasingly becoming an effective alternative to the building of completely new structures (Sedlaccek *et al.*, 2007).

The assessment of the current condition of steel bridges is therefore an issue of increasing interest. Many of the studies performed in order to evaluate the structural safety and the bridges condition combine numerical analysis with field tests. Although calculation methods are well developed, and model and material tests increasingly accurate, it is still to be proven that the finished structures behave according to the predictions. An incorrect evaluation of the bridge behavior may result on the development of damage in the structure that may lead to its collapse, which is not only associated to economical losses but may also result in the loss of human lives (Biezma and Schanack, 2007). In this context, bridge field testing has become a powerful mean of obtaining quantifiable information, complementary to the numerical analysis, for the assessment of the structural behaviour and the identification of its real condition (DeWolf *et al.*, 2002).

During the last few years many field tests on existing steel bridges have been reported. Farhey *et al.* (2000) performed diagnostic truck-load tests and microstructural analysis for structural deterioration assessment of a steel truss bridge and its rehabilitation design. Spyrakos *et al.* (2004) and Ermopoulos and Spyrakos (2006) conducted field measurements to develop validated analytical models to assess the capacity of the bridges to carry heavier train loads. Azizinamini (2002) carried out ultimate load tests on a steel truss bridge to comprehend the behaviour of old truss bridges. DelGrego *et al.* (2008) evaluated the structural behaviour and influence of aging on a century-old steel railroad truss bridge through field monitoring whose results showed that the actual live load distribution was significantly different than expected from conventional analytical approaches.

The studies mentioned above focused only on the live load distribution and on the behaviour of the superstructure components. However, an adequate functioning of the slide bearings is crucial for bridges safety and durability. When the bearings fail to properly accommodate bridge movements due to creep and shrinkage of concrete, temperature fluctuations, traffic loadings, and uneven settlement without imposing significant secondary stress to the superstructure severe damage can occur (Allen and Rens, 2004). In general, the expansion and contraction of the bridge superstructure due to temperature changes are the most important actions to be considered. Therefore, the relation between the movements of the expansion joints and the temperature fluctuations must be adequately taken into account (Ding and Li, 2011; Ni *et al.*, 2007).

This chapter concerns to the post-rehabilitation assessment of the Eiffel Bridge, a centenary double-deck bridge located in the North of Portugal. In 2007 the structure was subjected to rehabilitation works in order to increase the road traffic capacity and to extend its residual service life. The construction works involved the replacement of the top concrete deck and the strengthening of the upper chords of the truss girders, which led to a significant change of the structural system, and the replacement of the support bearings. After the rehabilitation, a load test was carried out and the movements of the expansion joints due to temperature changes were observed. The main objectives were: i) to analyze the bridge behaviour and the live load distribution for the new structural conditions; ii) to evaluate the efficiency of the elements strengthening and; iii) to establish the new baseline condition for future structural assessments. This chapter summarizes the most relevant results and discusses the structural behavior through the comparison of the field results with those obtained with a numerical model. First, a brief description of the Eiffel Bridge and the main tasks carried out during the rehabilitation process are presented. Then, the behaviour of the Eiffel Bridge, emphasizing the most relevant and particular aspects, is discussed through a numerical analysis. Afterwards, the procedures and the measurement systems used during the load test are described and the results are depicted and discussed. Finally, the movements of the expansion joints as well as their relation with temperature changes are presented and evaluated.

3.2. The Eiffel Bridge

3.2.1. General remarks

The Eiffel Bridge crosses the Lima River at the city of Viana do Castelo, in the Northern Portugal (Figure 3.1 (a)). It is structurally divided in three different parts: the main bridge and two viaducts. The main bridge comprises two decks: a road deck, top, and a railroad deck, bottom. In the margins the road traffic travels parallel to the railway being carried to the corresponding deck through the viaducts (Figure 3.1 (b)). The road viaduct is a ramp parallel to the railway and at the top deck level overrides the railway.

The Eiffel Bridge, designed by Gustave Eiffel, is considered a remarkable example of the XIX century iron design. The construction began in 1876 and the bridge was opened to the traffic in 1878. It was built to improve the connection between two important regions in the North of Portugal, by replacing an old road bridge and establishing the crossing of the Minho's railway line over the Lima River. Nowadays, in spite of existing a modern road bridge not far from the old one, the Eiffel Bridge still holds a considerable social and economical importance not only regarding the railway crossing but also the road crossing of the Lima River.

Throughout its history, beyond the regular maintenance works, the bridge has been subjected


(a) (b)

Figure 3.1 – Eiffel Bridge: (a) general view; and (b) southern viaduct.

to depth rehabilitation and strengthening. In 1922, the timber made top deck was replaced by a composite steel and concrete solution. During the 1990's the bridge was strengthened through the application of an external prestressing system to increase its live load carrying capacity. Recently, the bridge was subjected to the replacement and enlargement of the top concrete deck.

3.2.2. Structural characterization of the bridge

The main bridge is a 10-spans continuous truss bridge 561.64 m long (46.98 + 8x58.46 + 46.98) and supported by masonry pillars and abutments. Structurally, it is composed by two parallel truss girders, 5.20 m apart and 7.50 m high, travelling in the north-south direction. The trusses are composed by top and bottom chords, diagonals and verticals, whose elements consist of compound sections made of plates and angles in wrought iron, joined together with rivets. Each member is connected to another by the use of rigid connections, also executed with rivets, transferring transverse forces and bending moments. The bridge is constrained laterally at all the supports and it is fixed to the central pillar longitudinally, while being free with longitudinal movements at the other pillars. The longitudinal rotations are allowed at all the supports.

(a) (b)

Figure 3.2 – Bottom view of the Eiffel Bridge decks: (a) bottom deck; and (b) top deck; before rehabilitation.

Figure 3.3 – View of the Eiffel Bridge highlighting the external prestressing system.

The bottom deck, preserving its initial structural solution, is composed by a set of floor beams and two stringers in the rails' alignment. Its bracing system lies at two levels arranged in "X", at the upper level, and in "V", at the lower level (Figure 3.2 (a)). At the central pillar, the bottom deck is further stiffened with the breaking-acceleration bracing system. Before the rehabilitation carried out in 2007, the top concrete deck, 150 mm thick, was set on a 10 mm steel sheet, lying over a grid of stringers and floor beams aligned with those of the bottom deck (Figure 3.2 (b)).

In 1991, in order to increase the load capacity of the structure, the bridge was strengthened. The solution aimed at compensating the self-weight of the bridge through the application of upwards vertical forces. These forces were applied through an external prestressing system made up by two sets of high-strength steel bars, disposed along a polygonal profile, inflecting on the sections over the pillars and, in each span, at four sections of the bottom chords of the main girders (Figure 3.3). The transmission of the vertical forces to the spans is made through a steel profile set parallel to the main girder and supported at its ends by two stringers placed underneath the bottom chords. The inflections in the spans are made up with deviators that provide the continuity of the steel bars and enable, through a PTFE system, that the deviator slides. The steel bars are anchored to the main girders at the sections over the pillars. However, at the end spans, the steel bars are not anchored at the sections over the abutments. They are anchored at an external steel pillar built next to the masonry abutment and the equilibrium is guaranteed through anchorages to the ground, as shown in Figure 3.3.

3.2.3. Rehabilitation works

In 2007, in order to increase the road traffic capacity and improve the safety and comfort of the users, the bridge was submitted to a rehabilitation program consisting in the replacement and enlargement of the road deck. Moreover, due to the advanced corrosion detected on the top chords flanges, the strengthening of these structural elements was also needed. The main stages of the rehabilitation are shown in Figure 3.4.

The enlargement of the road deck consisted in the installation of a set of precast steel modules over the existing girders (Figure 3.4 (c)). Each module, 3.84 m long and 8.20 m wide, is supported at four neoprene pads and performs individually, bending in both directions. The replacement operation involved the removal of the concrete deck and the secondary stringers, as depicted in Figure 3.4 (a). Additionally, it was installed a bracing system at two distinct levels. A bottom view of the top deck after the recent rehabilitation is shown in Figure 3.5. As the concrete deck contributed for the overall stiffness of the bridge, this rehabilitation led to a significant modification of the load transfer, as was shown through the difference between the strains recorded for the crossing of passenger trains before and after the top deck removal (Rodrigues *et al.*, 2012).

The strengthening of the top chords' flange, due to the advanced deterioration, consisted in its replacement by a set of a HEB300 profile welded to a 420x12 mm^2 steel plate. This set was riveted to the angles connected to the web, enabling that the composite cross-section could perform as a whole. In order to keep not only the structure stability but also the railway in service during the top chord's strengthening, the installation of a temporary structural system was required, as shown in Figure 3.4 (b).

In order to provide reliable information about the actual behavior of the bridge to the agents involved in the process, a set of field measurements was conducted during the most critical stages of the rehabilitation. Further information concerning the corresponding monitoring programs, as well as the several rehabilitation stages, can be found in (Rodrigues *et al.*, 2012).

The rehabilitation of the Eiffel Bridge carried out in 2007 also included the retrofitting of the infrastructure and the restoration of the support bearings. Due to less of conservation and maintenance, the rollers of the original roller-pinned bearings, which presented significant

(a) (b) (c)

Figure 3.4 – Critical stages of the rehabilitation: (a) top deck removal; (b) strengthening of the top chords; (c) placing a steel module of the road deck.

signs of deterioration, were replaced by an elastomeric guided type device. Nonetheless, as shown in Figure 3.6, the cylindrical hinge that allows the longitudinal rotation of the bridge was kept (Appleton *et al.*, 2009).

Figure 3.5 – Bottom view of the Eiffel Bridge top deck, after the recent rehabilitation.

Figure 3.6 – View of a new support bearing.

3.3. Numerical analysis of the Eiffel Bridge

3.3.1. General remarks

The aim of this section is to present and discuss the most important and particular aspects of the Eiffel Bridge's structural behaviour regarding an easier understanding of the field results presented in the following sections. For that purpose, a finite-element model of the structure, representing the in-service performance, was developed. This model was used not only in this section but also to analyze and assess the field results presented in section 3.4.

The numerical model consists of three-dimensional beam-elements with six degrees of freedom at each end. The modelling of the structure was developed in accordance with the level of assessment under consideration. Therefore, the behaviour was assumed to be linear and elastic and it was considered continuity in the nodes (Sustainable Bridges, 2007). The structure geometry was defined in accordance with the data collected in the field, concerning not only the cross-section of the elements but also the coordinates of the nodes in the 3-D model (LisConcebe, 2007). Both the position and the connection between the elements were attended through the adequate offset of the barycenter of the cross-sections in relation to the reference axis and by appropriate constraints between the nodes. The Young's modulus of the wrought iron was assumed to be 180 GPa and that of steel, corresponding to the new elements, was 210 GPa. The coefficient of thermal expansion of the materials was assumed to be 11.7×10^{-6} per °C (LisConcebe, 2007). The pillars and the abutments, provided that their deformations are negligible, were not considered in the numerical model.

3.3.2. Flexural behaviour

The Eiffel Bridge comprises two decks: a road deck at the upper level and a railway deck, at the lower level. The upper deck is constituted by a set of precast steel modules that are simply supported over the nodes of the top chords. At the lower deck, the railway is supported over two parallel stringers sustained by floorbeams transferring the loads to the nodes of the bottom chords. Therefore, in both decks, the traffic loads are transferred to the nodes of the main girders.

Consider a point-load applied at mid-span of an intermediate span. According to the mechanism of load transfer, it must be divided in two point-loads per girder applied to the adjacent nodes. Figure 3.7 (a) depicts the deformed shape of the loaded span and the adjacent ones. The loaded span deflects downwards whereas the adjacent spans slightly deflect upwards. Furthermore, it may be observed that the deflection curve of the top chord in the loaded span is significantly different from the bottom one. Therefore, the overall deformed shape results from the combination of the global bending of the whole girder with the bending of each chord.

In general, a truss may be viewed as a beam where the web consists of a series of separate members instead of a continuous plate. Thus, the bottom and the top chords carry tension and compression, fulfilling the same function as the flanges of a beam, as shown in Figure 3.7 (b), wherein the axial force diagram of the bridge girder chords is depicted. In addition to this global behaviour, the bending of each chord, illustrated through the bending moment diagram depicted in Figure 3.7 (c), must be considered. Note that the magnitude of the bending moment is higher at the top chord, in which the load is directly transferred.

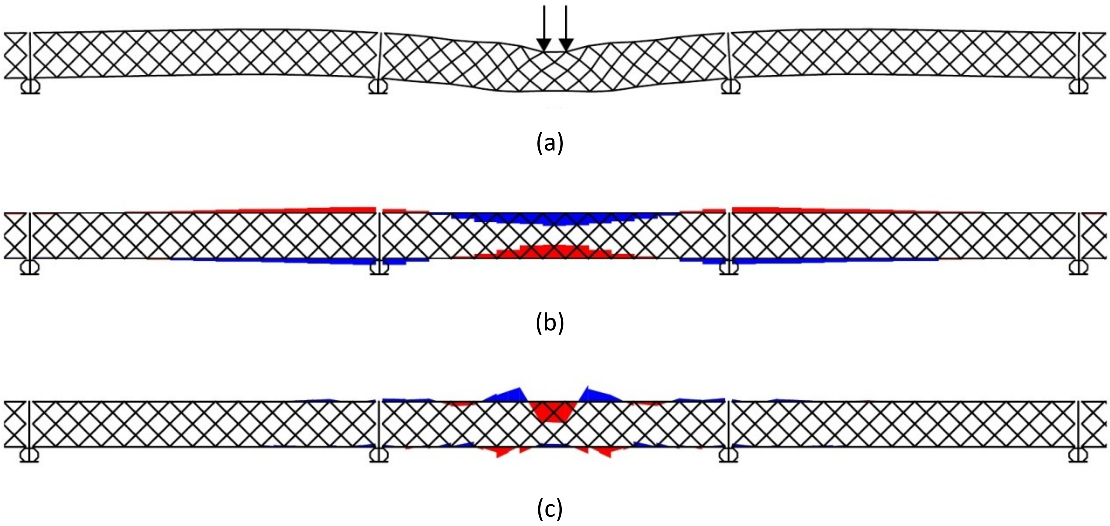
(a)

(b)

(c)

Figure 3.7 – Eiffel Bridge main girder subjected to two point-loads applied at mid-span of the top chord of an intermediate span: (a) deformed shape; (b) axial force diagram; (c) bending moment diagram.

3.3.3. The rotations of the joints

The observation of rotations in bridges is very useful as their measurement can reflect very adequately its global behaviour. As the measurement of rotations has many advantages in comparison with that of deflections, several methods to estimate the bridge deflection curves based on the observation of rotations have arisen (Burdet and Zanella, 2000; Hou *et al.*, 2005; Vurpillot *et al.*, 1998) .

Nevertheless, in this structure, the rotations do not reproduce the global behaviour of the structure. Using a traditional sensor to measure rotations, such as an inclinometer, the rotation to be measured concerns only to the rotation of the cross-section of the bar where the sensor is installed. However, the rotation of a cross-section of a given steel bar does not reflect the rotation of the entire cross-section of the girder. Therefore, the assumption of plane sections after deformation of the girder is not adequate. It is valid only for each bar individually. Consequently, the fundamentals about rotations and the derived methods referred above to estimate the bridge deflection are not applicable in this structure. Figure 3.8 depicts the deformed shape of the bridge subjected to a rotation introduced at an intermediate support. As shown, the girder does not deflect significantly. Most of the effect is produced near the node where the rotation is introduced. Thus, it is clearly shown that, in this structure, the rotations assume a local nature.

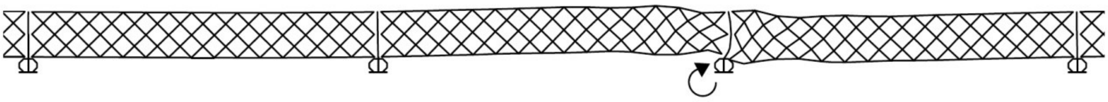

Figure 3.8 – Deformed shape of an Eiffel Bridge main girder subjected to a rotation introduced at an intermediate support.

3.3.4. The behaviour under temperature variation

Bridges expand and contract due to temperature change. This movement is accommodated by bearings and expansion joints or by deformation of the piers and abutments with integral construction. The joint displacements, $\varDelta$, may be computed by the equation:

$$\varDelta = \alpha \cdot L \cdot \varDelta T \tag{3.1}$$

where α is the coefficient of thermal expansion, L is the expansion length between the fixed support and the movable joint or bearing, and ΔT is the difference of temperature observed.

Taking the value of the coefficient of thermal expansion, 11.7 x 10^{-6} per °C, and the expansion length equal to half the total length of the bridge, 280.74 m, according to expression (3.1), the movement of the expansion joint is expected to be 3.28 mm per °C.

However, the external prestress leads to a significant decrease of the expectable movement. As the prestressing steel bars at the end span are anchored at a steel pillar placed outside the bridge (see Figure 3.3), when the temperature raises, due to the expansion of materials, the section over the first intermediate support, P1 (and P9), moves towards the steel pillar, leading to a significant loss of the prestressing forces at the end span, 1st span (and 10th span). Figure 3.9 (a) depicts the prestress loss at the end-span due to a uniform temperature rise. Nevertheless, as the steel bars are anchored to the main girder at the sections over the intermediate supports, the prestress loss at the other spans is negligible given that the expansion due to the temperature affects equally both "sub-structures". The unbalanced horizontal component in the prestressing bars over the first intermediate support, P1 (and P9), is transferred to the main chords of the girder, compressing the elements and, therefore, reducing the displacement at the expansion joints. As shown in Figure 3.9 (b), where the axial force at the chords of one of the main girders is depicted, all the intermediate spans are

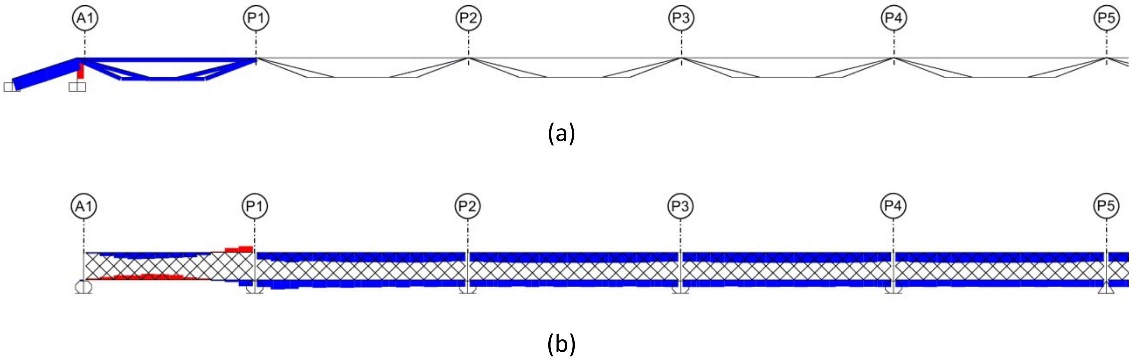

Figure 3.9 – Axial force diagrams for a uniform increase of temperature over the structure:
(a) in the prestressing bars; (b) in the main girder.

compressed and the end span presents a positive bending due to the decrease of the vertical forces resultant from the prestress loss.

Considering that the bridge may freely expand at the supports, the increase of 1 °C in every element in the numerical model leads to a displacement in the expansion joint of 2.73 mm, which is 17% lower than the displacement predicted with expression (3.1). However, in real conditions, the displacement at the supports may be partially restrained. As previously referred, the rehabilitation works comprised the replacement of the old steel rollers by an elastomeric guided type device. The elastomeric bearing pads serve to accommodate limited angular rotations around any axis whereas the horizontal movements occur in the plane of least resistance which is the bearing sliding surface faced with a polished stainless steel in contact with a PTFE sheet (FIP, 2007). Regardless the low frictional behaviour, the sliding bearing surface produces a frictional force that is applied to the superstructure, substructure, and the bearing itself (Taylor and Stanton, 2010). Therefore, when horizontal movements are induced in the structure, while these friction forces are not overcome the PTFE sheet does not slip. Consequently, the movement is accommodated by the distortion of the elastomer which leads to an horizontal force proportional to the shear stiffness of the elastomer, assumed to be 4.32 kN/mm (FIP, 2007). In this way, assuming that in every support the PTFE does not slip, the movement of the expansion joint predicted with the numerical model was 2.32 mm per °C.

Considering a value of 0.08 for the friction coefficient, in accordance with the values prescribed in the British Standard 5400 (BS - British Standards Institute, 1983), and 640 kN for the vertical force at the end support under the dead loads (A2P, 2007), the force required to slip the PTFE is 51.2 kN. Therefore, for temperature variations lower than 5 °C, as the displacement at the expansion joints is expected to be 11.6 mm and, consequently, the horizontal force at the end supports 50.1 kN, the PTFE does not slip. However, for higher temperature changes and thus, for higher displacements, as soon as the PTFE slips, the total movement is the combination of the distortion with the sliding. Therefore, it is expected that the bridge movements at the expansion joints may range from 2.32 mm per ºC – if the PTFE sheet does not slip – to 2.73 mm per ºC – if the bridge may freely expand at the supports.

3.4. Load test

3.4.1. General remarks

After the structural rehabilitation performed in 2007, a load test, involving the crossing of heavy road vehicles and a railway locomotive, was carried out. At the upper deck, two road vehicles, 30.2 ton of weight each, were used whereas at the bottom deck it was used a locomotive weighing 121 ton. The characteristics of the vehicles, namely the distances between the axles groups and the corresponding loads, are shown in Figure 3.10.

The load test was as much comprehensive as possible involving a large variety of load cases in order to assess the linearity and repeatability of the structural behaviour and to determine the most adverse effects. Thus, the load test comprised several load cases including a set of static positions of the vehicles at critical locations as well as a set of crossings along the structure with increasing speeds, using the vehicles individually and combining both the trucks and the locomotive.

The following sections contain a brief description of the measurement systems used and the most relevant results obtained, presented in detail in (Cavadas *et al.*, 2008). The results are then discussed with the support of the numerical model (Cavadas, 2008) and based on the numerical analysis of the Eiffel Bridge presented before.

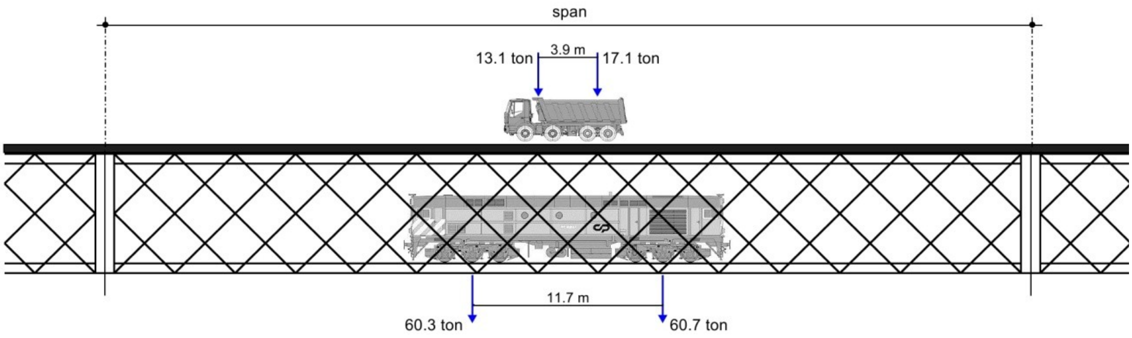

Figure 3.10 – Dimensions and load distribution of the vehicles used in the load test.

3.4.2. The measurement systems

The observation plan during the load test comprised the measurement of vertical displacements, rotations of the supports and strains at cross-sections of critical bars. A set of appropriate transducers and sensors and acquisition systems to register automatically all data was installed.

As the points wherein the deflections were required are over the river, using displacement gauges with reference to the ground was not possible. Therefore, the vertical displacements (VD) were measured using a specific electric levelling system developed at LABEST consisting in a hydraulic circuit through which vertical movements of the points under measurement are associated to the variation of liquid pressure (Figueiras *et al.*, 2005). A pressure sensor used to measure the change of liquid pressure is depicted in Figure 3.11 (a). This system enables a satisfactory precision (better than 0.5 mm) to measure the vertical displacements of the structure subjected to the loads under consideration. Figure 3.12 shows the cross-sections, in a total of 12, where the vertical displacements were measured (seven at the downstream girder (D) and five at the upstream girder (U) mid-spans).

The rotations (R) of the supports were obtained using electric inclinometers, as depicted in Figure 3.11 (b). These inclinometers are uniaxial sensors that measure the inclination in relation to the horizontal plane, ranging from -1° to 1°, with a precision better than 0.5° x 10^{-3}. Figure 3.12 shows the cross-sections, in a total of eight, where the rotations were measured (six at the downstream girder and two at the upstream girder sections over the supports).

The strains were obtained using fibre-optic sensors, namely surface bonded Fibre Bragg Gratings (FBG). These systems benefit from high sensitivity, small size, immunity to electromagnetic interference, high acquisition frequencies, and ability to support serial multiplexing schemes inherent to fibre-optic sensors (Measures, 2001; Udd, 1995). It was adopted a solution that integrates the fibre in a slight polyimide base, making a more robust


(a) (b) (c)

Figure 3.11 – Transducers and sensors used in the load test: (a) pressure sensor to measure the vertical displacements; (b) inclinometer; (c) FBG strain gauges.

sensor and simplifying the gluing procedure. Further information concerning the installation procedure, depicted in Figure 3.11 (c), can be found in (Rodrigues *et al.*, 2012). In order to thoroughly characterize the structural behaviour of the Eiffel Bridge, a total of 32 strain gauges were distributed over eight cross-sections of members located at the sixth span (6S). As shown in Figure 3.13 the observation program included the top (T) and bottom (B) chords (C), both at mid-span (M-S) and at the cross-sections near the support (P5), and two compression diagonals (D) near the support (P5). Additionally, a railway stringer, a railway bracing and a module of the road-deck were also observed.

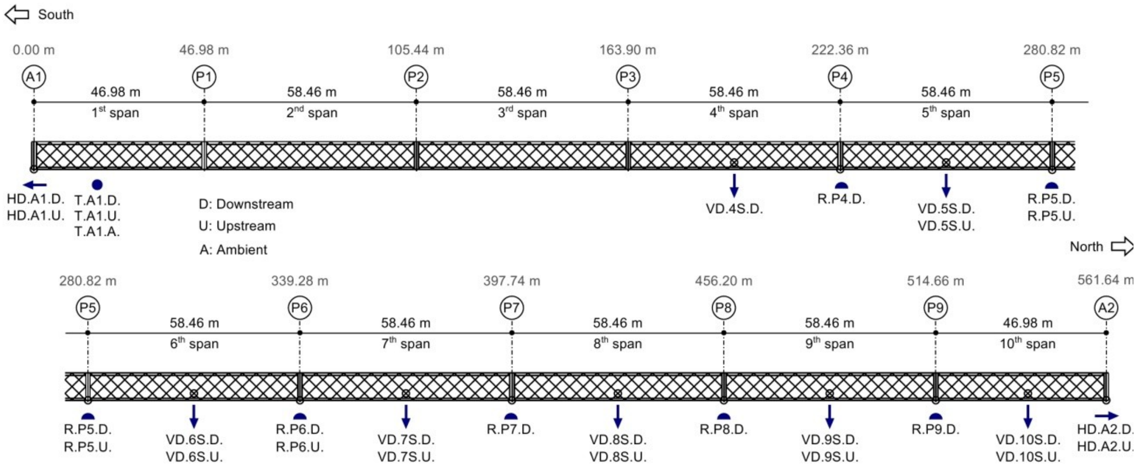

Figure 3.12 – Front view of the Eiffel Bridge, depicting the cross-sections where the vertical displacements (VD), the rotations (R), the horizontal displacements (HD) and the temperatures (T) were measured.

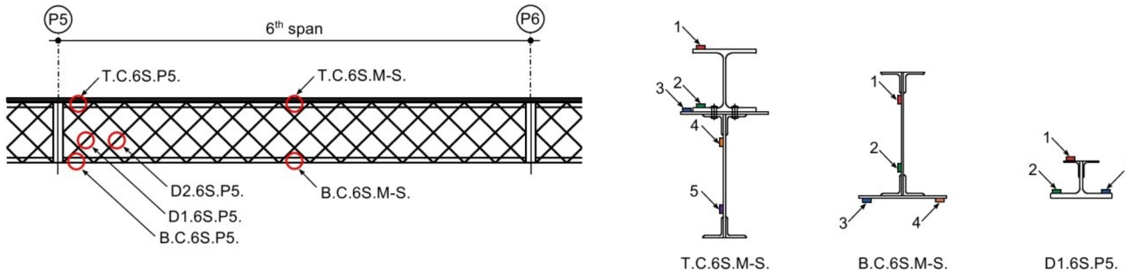

Figure 3.13 – Front view of the 6th span of the Eiffel Bridge depicting the location of the cross-sections where the strains were measured.

3.4.3. Results

3.4.3.1. Deflections

Figure 3.14 depicts the vertical displacements measured at spans 4, 6, 8 and 10, downstream, for a set of static positions in which the locomotive is placed at mid-span, from the 10th to the 4th spans. For the load cases in which the locomotive stands at the intermediate spans, the vertical displacement of the loaded and the adjacent spans is around, respectively, 11 mm, downwards, and 2 mm, upwards. When the locomotive stands at the end span, the vertical displacement is around 9 mm. It is also shown that when the bridge is unloaded its deflection returns to the initial position.

All the vertical displacements observed for a set of static positions when the loads are placed at the observed span, combining a pair of trucks and the locomotive, are summarized in Table 3.1. It includes the values measured during the load test (LT) and those obtained with the numerical model (Num). It is shown that both girders exhibit a similar behaviour in that the upstream (U) and downstream (D) vertical displacements are quite similar. Second, the vertical displacements observed under the locomotive are around twice those obtained under the pair of trucks, which is in accordance with the weight of the vehicles. Moreover, the vertical displacements under the locomotive and the road vehicles are very similar to the sum of those obtained under the loading of those vehicles separately. Finally, for each vehicle combination, there is a good agreement between the experimental and the numerical values.

Figure 3.15 depicts the comparison of the numerical with the recorded influence-line of the vertical displacement at the 6th span, upstream, for the slow crossing of the pair of trucks. The results show a good agreement between the field and the numerical influence-lines.

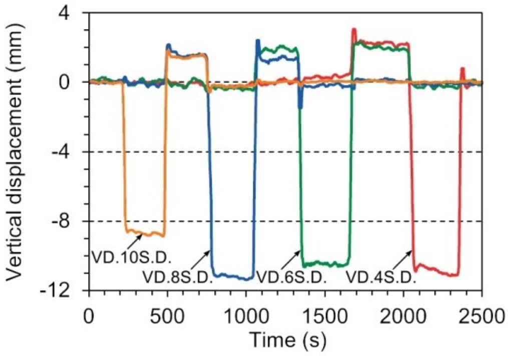

Figure 3.14 – Vertical displacements for a set of static positions in which the locomotive is placed at mid-span, from the 10th to the 4th spans.

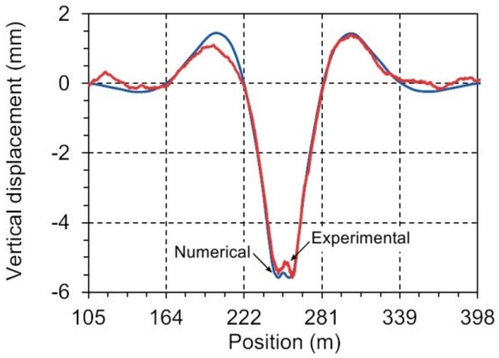

Figure 3.15 – Comparison of the numerical with the measured influence-line of the vertical displacements at the 6th span, for the slow crossing of a pair of trucks.

Table 3.1 – Comparison of the numerical with the measured vertical displacements (mm) for a set of static positions ranging from the 4th to the 10th spans when the vehicles are placed at mid-span.

	Sensor	VD.S4	VD.S5	VD.S6	VD.S7	VD.S8	VD.S9	VD.S10
	Loading	S4	S5	S6	S7	S8	S9	S10
Trucks	LT-D	5.5	5.0	5.5	5.5	5.5	5.5	4.5
	LT-U	-	5.0	5.5	6.0	-	6.0	4.5
	Num	5.5	5.5	5.5	5.5	5.5	5.3	4.1
Locomotive	LT-D	11.0	10.5	10.5	11.0	11.5	11.0	9.0
	LT-U	-	11.0	11.0	11.5	-	11.0	9.0
	Num	11.1	11.2	11.1	11.2	11.3	10.6	8.1
Trucks+Loc	LT-D	16.5	15.5	16.0	16.0	17.0	16.5	13.0
	LT-U	-	16.0	16.5	17.0	-	16.5	13.5
	Num	16.6	16.7	16.6	16.7	16.8	15.9	12.2

Moreover, the displacement observed for this load case, when the trucks are at mid-span, is very similar to that obtained for the static position of the same vehicles (see Table 3.1). An interesting detail of the behaviour is related to the fact that the maximum vertical displacement does not occur when the load is placed at mid-span. As the vertical displacement was measured at the intersection of two diagonals, near the bottom deck, for loads at the upper deck, the vertical displacement increases when the load is over the diagonals where the displacement transducer is installed and thus, it is lower when the load is exactly at mid-span.

3.4.3.2. Rotations

Figure 3.16 depicts the rotations measured at the supports over pillars P5, P7 and P9, downstream, for the same load cases shown in Figure 3.14 – a set of static positions in which the locomotive is placed at mid-span, from the 10th to the 4th spans. The observed rotations are around $15°\text{x}10^{-3}$. However, in comparison with the vertical displacements, the variability of the rotations measured along the bridge length is much higher. Nevertheless, as for the vertical displacements, when the bridge is unloaded, its rotation returns to the initial position.

As shown for displacements in Table 3.1, the rotations observed for a set of static positions when the loads are placed at the observed span, using a pair of trucks, the locomotive and using simultaneously the trucks and the locomotive, are summarized in Table 3.2. It includes the values measured during the load test and those obtained with the numerical model. As referred above, the variability of the rotations measured along the bridge is clear. In addition, for each vehicle combination, a not negligible difference between the measured rotations and those obtained with the numerical model may be observed. Even though, at the alignments where both upstream and downstream rotations were measured, the recorded values are quite similar. Moreover, the rotations observed under the locomotive are around twice those obtained under the pair of trucks, which is in accordance with the weight of the vehicles. Finally, the rotations under the locomotive and the road vehicles are very similar to the sum of those obtained under the loading of those vehicles separately.

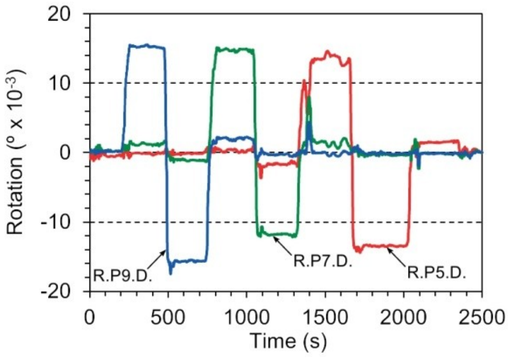

Figure 3.16 – Rotations for a set of static positions in which the locomotive is placed at mid-span, from the 10th to the 4th spans.

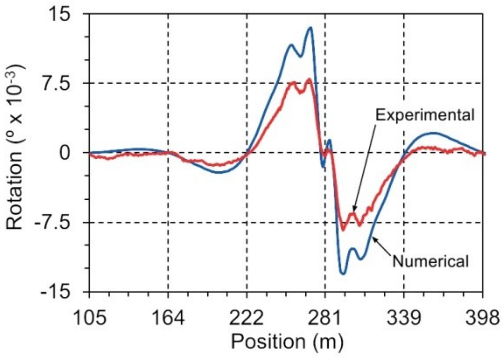

Figure 3.17 – Comparison of the numerical with the measured influence-line of the rotations at pillar P5, for the slow crossing of a pair of trucks.

Table 3.2 – Comparison of the numerical with the measured rotations (° x 10^{-3}) for a set of static positions ranging from the 4th to the 10th spans when the vehicles are placed at mid-span.

	Sensor	R.P4		R.P5		R.P6		R.P7		R.P8		R.P9	
	Loading	S4	S5	S5	S6	S6	S7	S7	S8	S8	S9	S9	S10
Trucks	LT-D	-6.5	6.5	-6.5	7.0	-5.5	5.5	-6.0	7.0	-8.0	7.0	-8.0	7.0
	LT-U	-	-	-6.5	6.0	-5.0	6.5	-	-	-	-	-	-
	Num	-11.7	11.5	-10.8	10.6	-11.7	11.4	-11.3	11.2	-11.6	11.1	-11.2	9.2
Locom	LT-D	-13.5	13.5	-13.5	13.5	-11.0	12.0	-12.0	14.5	-15.5	15.5	-15.5	15.5
	LT-U	-	-	-13.0	12.0	-11.0	12.5	-	-	-	-	-	-
	Num	-22.0	22.5	-21.0	21.0	-21.8	22.3	-21.4	21.5	-21.9	22.0	-21.0	19.0
Trucks + Locom	LT-D	-21.0	20.0	-21.0	20.0	-16.5	18.0	-18.5	22.0	-24.0	23.0	-24.0	22.5
	LT-U	-	-	-20.0	17.5	-16.5	19.5	-	-	-	-	-	-
	Num	-33.7	34.0	-31.8	31.6	-33.5	33.7	-32.7	32.7	-33.5	33.1	-32.2	28.2

Figure 3.17 depicts the comparison of the numerical with the recorded influence-line of the rotation at pillar P5, downstream, for the slow crossing of a pair of trucks. As observed before for the static positions of the locomotive, the rotation obtained with the numerical model is higher than that observed in the load test. This may be due to the type of modelling that was adopted. As the gusset plates of the nodes are not considered in the numerical model the nodes stiffness of the bridge is higher than that of the model. Notwithstanding, the form of the

influence-line measured in the bridge is very similar to that obtained with the numerical model. Moreover, the rotation observed for this load case, when the vehicles are at mid-span, is very similar to that obtained for the static position of the same vehicles (see Table 3.2). Although the rotations obtained in the numerical model do not match those obtained experimentally, the field and numerical vertical displacements agree quite well, as shown in section 3.4.3.1. Thus, the global structural response of this structure does not depend significantly on the rotations, which confirms the local nature of the rotations in this structure, as discussed in section 3.3.3.

3.4.3.3. Strains

Figure 3.18 depicts the strains observed at the cross-sections of both top and bottom chords, at mid-span, respectively, TC.6S.M-S and BC.6S.M-S (see Figure 3.13), for the slow crossing of a pair of trucks whereas the strains at the same cross-sections for the slow crossing of the locomotive are depicted in Figure 3.19. When the load is moving along the spans adjacent to the instrumented one, the deformation state of the chords cross-sections is very close to uniform. However, as soon as the vehicles reach the instrumented span, the deformation of each cross-section deviates significantly from the uniform state, indicating that each chord is bending. As discussed in section 3.3.2, the overall deformed shape of the Eiffel Bridge results from the combination of the global bending of the whole girder with the bending of each chord. When the vehicles are moving along the adjacent spans, the top and the bottom chords are, respectively, tensioned and compressed. Moreover, as the deformation state is close to uniform, the chords do not bend. However, when the vehicles move along the instrumented span, the chords bend. Thus, in addition to the compression and tension state at, respectively, the top and bottom chords, the bending of the chords must be taken into account.

In order to evaluate the magnitude of the bending moment at these cross-sections, the internal forces were estimated using a multiple linear regression model (Montgomery and Runger, 1999). Consider a generic cross-section whose area and moments of inertia about 3-3 and 2-2 axis are given, respectively by A, I_3 and I_2. According to the assumed sign convention, the stress, σ, at a point with coordinates x_2 and x_3, subjected to the axial force P and the bending moments about 3-3 axis and 2-2 axis, respectively, M_3 and M_2, is given by:

$$\sigma = \frac{P}{A} - \frac{M_3}{I_3} x_2 - \frac{M_2}{I_2} x_3 \qquad (3.2)$$

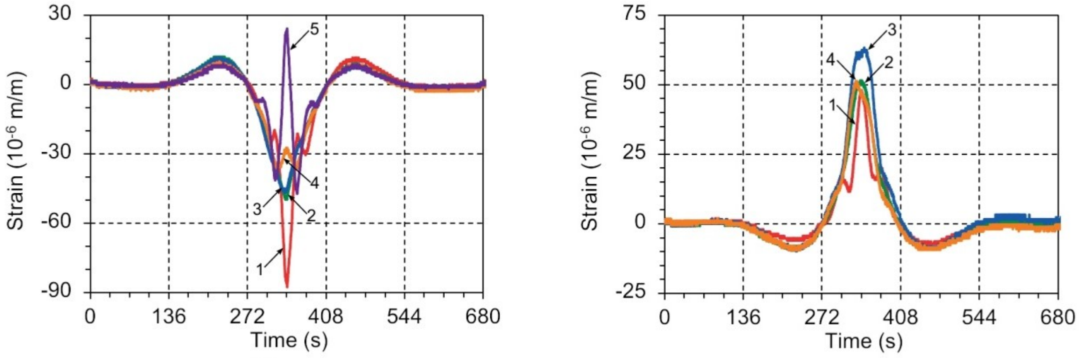

(a) (b)

Figure 3.18 – Strains measured at mid-span of the chords for the slow crossing of a pair of trucks: (a) top chord (T.C.6S.M-S); (b) bottom chord (B.C.6S.M-S).

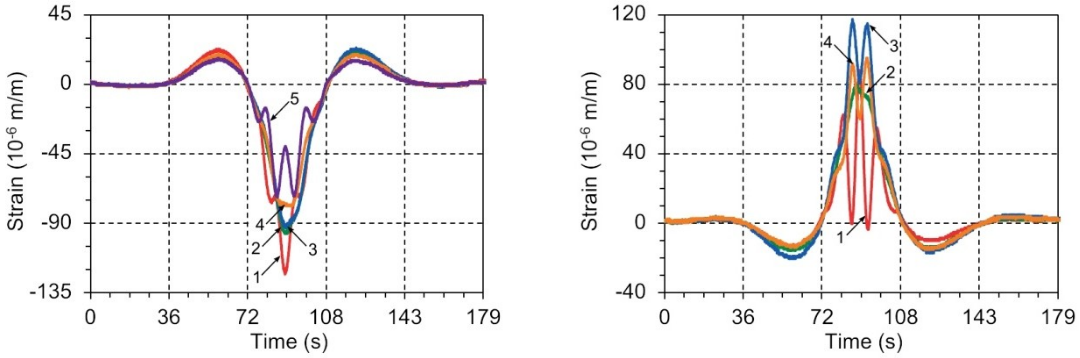

(a) (b)

Figure 3.19 – Strains measured at mid-span of the chords for the slow crossing of the locomotive: (a) top chord (T.C.6S.M-S); (b) bottom chord (B.C.6S.M-S).

Bearing in mind that within the linear elastic range the stress, σ, may be given by the product of the strain, ε, by the Young's modulus, E, equation (3.2) may be arranged and, thus, represent a multiple linear regression model with two regressor variables (Montgomery and Runger, 1999):

$$Y = \beta_0 + \beta_1 \cdot X_1 + \beta_2 \cdot X_2 \tag{3.3}$$

where the regression coefficients β_0, β_1 and β_2, to be estimated by the least squares method, are, respectively, the internal forces P, M_3 and M_2. The dependent variable, Y, is given by $E \cdot \varepsilon \cdot A$ and the independent variables X_1 and X_2 are given, respectively, by $-A \cdot \mathrm{x}_2/\mathrm{I}_3$ and $-A \cdot \mathrm{x}_3/\mathrm{I}_2$. In this way, using the strains recorded during the load test, the internal forces may be estimated for each time step.

Figure 3.20 and Figure 3.21 depict the comparison between the internal forces – the axial force and the bending moment about the highest moment of inertia axis – obtained with the numerical model and those estimated with equation (3.3) for the slow crossing of, respectively, a pair of trucks and the locomotive. In all cases, either for the vehicle type or the chord under consideration, the experimental internal forces reveal a good agreement with those obtained with the numerical model. Therefore, the bending behaviour discussed in section 3.3.2 is confirmed. Moreover, concerning specifically the top chord, it is shown that the strengthening is effective given that the compound section responds as a whole.

The effect of the chords bending is significantly higher when the load is transferred directly to the chord. Thus, the effect of bending is higher at the top and bottom chords for, respectively, the road and railway traffic. The bending on the other chord is due to the load transfer by the diagonals. Therefore, in spite of being present, it is not as significant as on the directly loaded chord. When the road vehicles are at mid-span the bending moment at the top chord (Figure 3.20 (a)) is significant. However, when the locomotive is placed at mid-span, due to the distance between the axles groups (see Figure 3.10), the bending moment observed at the bottom chord (Figure 3.21 (b)) is lower and, besides, is negative. The two peaks observed at

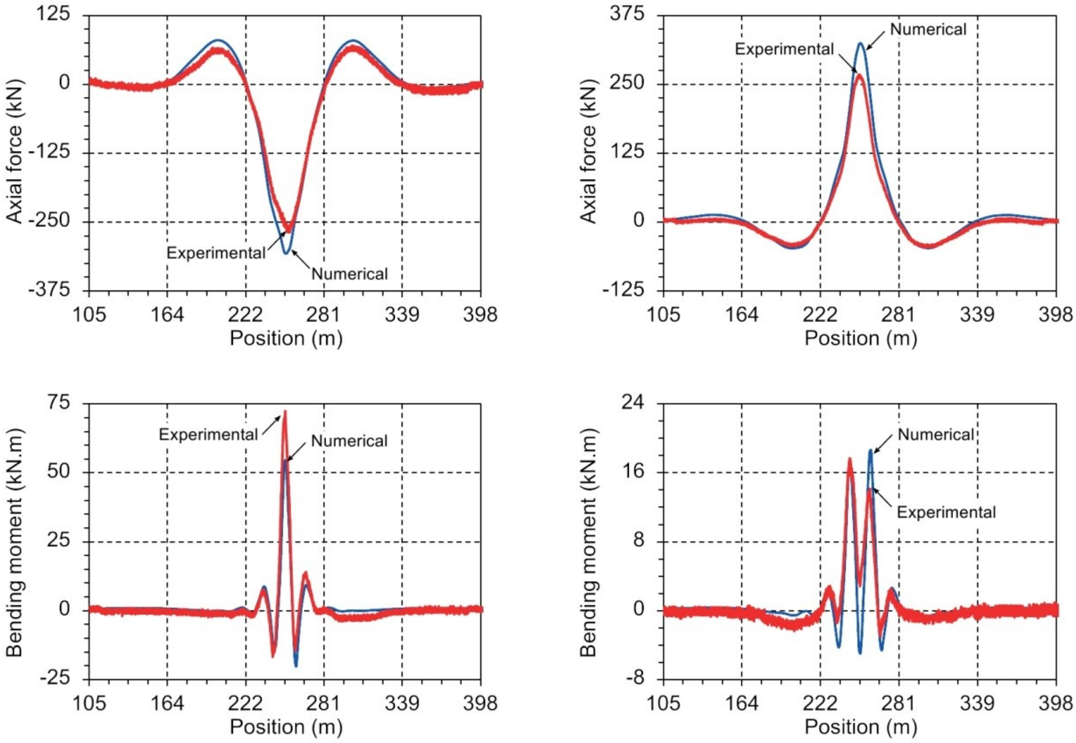

(a) (b)

Figure 3.20 – Comparison of the numerical with the estimated internal forces (axial force and bending moment) at mid-span of the chords for the slow crossing of a pair of trucks: (a) top chord (T.C.6S.M-S); (b) bottom chord (B.C.6S.M-S).

the bottom chord correspond to the successive passing of the two axles groups over the mid-span. For the slow crossing of the road vehicles, the maximum bending moment at the bottom chord (Figure 3.20 (b)) does not occur when the load is at mid-span. As previously referred, the bending on the opposite chord results from the load transfer through the diagonals. Thus, the maximum bending moment at the mid-span cross-section of the bottom chord occurs when the trucks pass over the diagonals that intersect the bottom chord near the mid-span, leading to two peaks. On the other hand, for the slow crossing of the locomotive, when the vehicle is at mid-span, due to the distance between the axles groups, the loads are placed in the region of the diagonals that intersect the top chord at mid-span. This leads to the peak present at mid-span in Figure 3.21 (a). The two remaining peaks correspond to the crossing of the first axles group over the diagonal on the left and the second axles group over the diagonal on the right.

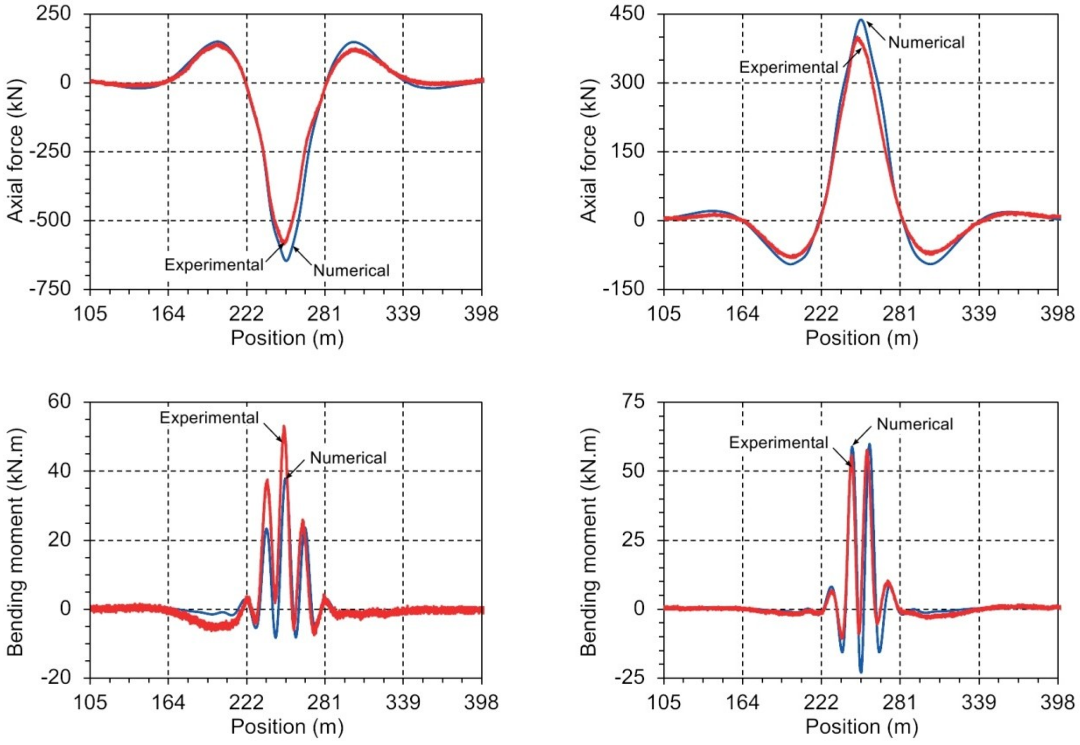

(a)

(b)

Figure 3.21 – Comparison of the numerical with the estimated internal forces (axial force and bending moment) at mid-span of the chords for the slow crossing of the locomotive: (a) top chord (T.C.6S.M-S); (b) bottom chord (B.C.6S.M-S).

3.5. Environmental test

3.5.1. General remarks

After completing the rehabilitation works, namely the replacement of the bearings' rollers, the bridge was instrumented with temperature sensors and displacement transducers to correlate the displacements at the expansion joints located at the two ends of the deck with the temperature. The objective was to assess the new bearings performance and to establish a reference for future evaluations.

Ni et al. (2007) proposed a procedure for the assessment of bridge expansion joints. Based on the measurement data of expansion joint displacement and bridge temperature, the normal correlation pattern between the effective temperature and thermal movement is established. This enables that in future evaluations alarms may be raised if the pattern deviates from this normal model. With the measurement data of displacement at expansion joints and effective temperature, a regression analysis can be carried out by assuming the following linear relationship:

$$\Delta = \beta_1 T + \beta_0 \tag{3.4}$$

where Δ is the displacement of an expansion joint and T is the effective temperature. The regression coefficients β_1 and β_0 can be obtained by the least-squares method. The rate of variation of displacement with the temperature is given by the coefficient β_1.

In this field test a total of three PT100 (platinum resistance thermometers) has been installed to measure: i) the temperature of the bottom chord of the downstream main girder (T.A1.D.); ii) the temperature of the bottom chord of the upstream main girder (T.A1.U.) and; iii) the ambient temperature (T.A1.A.). The horizontal displacements (HD) of the expansion joints were observed using a total of four LVDT (linear variable differential transformers) placed at the bottom chords of the main girders, upstream (U) and downstream (D), in both abutments, south (A1) and north (A2). The deployment of displacement transducers and temperature sensors is illustrated in Figure 3.12.

3.5.2. Results

Figure 3.22 presents the time histories of the temperatures and the average of the longitudinal displacements observed in the southern (HD.A1.) and northern (HD.A2.) expansion joints. The displacements are depicted in relation to the position of the expansion joints recorded at

7 a.m. in April, 16th. In general, both expansion joints exhibit a similar behaviour. Since the expansion length is equal for both expansion joints, as the temperature changes, the displacement varies in the same magnitude at both ends of the structure. The effect of the sun radiation on the structure is clear given that, on sunny days, during the day the temperature in the chords is higher than the air temperature. Besides, due to the bridge orientation (North-South), in the morning the temperature in the upstream chord is higher than that in the downstream chord whereas in the afternoon one can observe the opposite.

In order to determine the correlation between the temperature and the displacement the calculation of the effective temperature, which is an average of the temperature distributed along the cross-section, is required (Ni *et al.*, 2007). In this case it will be assumed that the effective temperature is the average of the temperatures of the chords.

Figure 3.23 (a) presents the correlation between the effective temperature and the displacement of the expansion joint at the downstream chord in the northern abutment (HD.A2.D) for the whole period of observation. The obtained correlation is significantly different from a linear relationship, contrarily to what would be expected. Due to the sun radiation, the effective temperature may not be representative of the temperature of the whole structure, leading to a weak relationship. Moreover, the plot shows several distinct "paths" for the relation between the temperature and the displacement. This may correspond to cooling or warming periods particularly when the effect of the sun radiation is more significant.

In order to overcome this problem, a much more comprehensive characterization of the temperatures along the structure would be required. However, this would significantly increase the cost of the monitoring system. Therefore, considering that the effect of the sun radiation is null and the rate of temperature variation reaches its minimum early in the

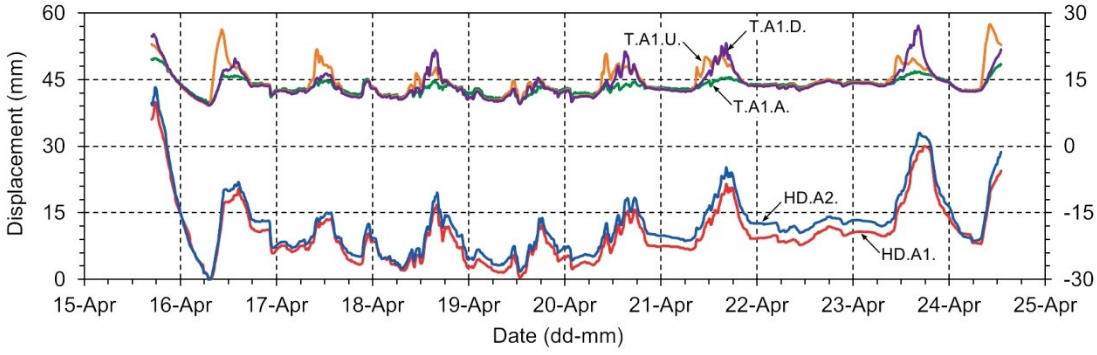

Figure 3.22 – Time-histories of the temperatures (T) and the horizontal displacements (HD) of the expansion joints.

morning, before the sunrise, computing the linear relationship using a single measurement taken every morning may lead to adequate results. Figure 3.23 (b) presents the correlation between the effective temperature and the displacement of the expansion joint also at the downstream chord in the northern abutment (HD.A2.D) using only the observations taken at 7 a.m. for the whole observation period. The plot clearly shows that the relationship is linear and thus may represent adequately the correlation between the displacements of the expansion joints and the effective temperature.

Table 3.3 summarizes the coefficients β_1 of the correlation between temperature and displacement, expressed by equation (3.4), for all the monitored movements, based on the observations taken at 7 a.m. during the whole observation period. Both at the northern and at the southern abutments the variation of displacement of the upstream chord is very similar to that of the downstream. However, despite the expansion length is equal for both expansion joints the variation rate at the northern abutment (A2) is 17% higher than that at the southern abutment (A1).

Although the time histories of the displacement presented in Figure 3.22 indicate a similar behavior of both expansion joints, a more detailed analysis shows some differences in the response to the temperature. Consider for example the measurements taken at 6 a.m. in three distinct days: i) 16th; ii) 22th and iii) 24th. In April 16th and 24th the displacements recorded in either expansions joint are very similar. However, in April 22th they are clearly different which means that the response of the structure under temperature variation is not linear. As discussed in section 3.3.4, as soon as the PTFE slips, the total movement is the combination of the distortion with the sliding, which may explain this non-linearity.

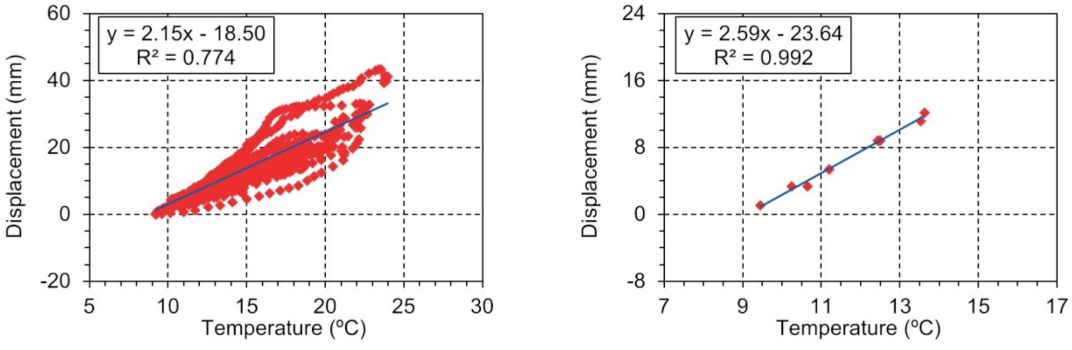

(a) (b)

Figure 3.23 – Correlation between the effective temperature and the horizontal displacements of the expansion joint at the downstream chord in the northern abutment (HD.A2.D) for: (a) the whole period of observation; (b) a set of observations taken at 7 a.m.

The actual response of the structure under temperature changes is hard to predict given that the friction coefficient depends on numerous factors such as sliding speed, contact pressure, air temperature and state of lubrication (Dolce *et al.*, 2005). The importance of this variability on the bridge response increases as the displacement depends on the behavior of several bearings along the expansion length. In addition, the shear stiffness of the elastomer to be used in the calculations, as the shear modulus is not easy to determine, may not be correctly estimated. Nevertheless, the values presented in Table 3.3 are not significantly different from those estimated in section 3.3.4.

Table 3.3 – Coefficient β_1 (mm/°C) of the correlation between the effective temperature and the joint displacement using the observations taken at 7 a.m.

Sensor	HD.A1.	HD.A2.
β_1 – D	2.18	2.59
β_1 – U	2.19	2.52
Average	2.185	2.555

3.6. Conclusions

This chapter presents the post-rehabilitation assessment of the Eiffel Bridge, a centenary double-deck bridge located in the North of Portugal. Recently, this bridge was submitted to rehabilitation works involving the replacement of the top deck, the strengthening of the top chords and the replacement of the support bearings. After the rehabilitation, a load test and an environmental test were carried out in order to: i) analyze the bridge behaviour and the live load distribution for the new structural conditions; ii) evaluate the effectiveness of the chords strengthening and; iii) establish the new baseline condition for future structural assessments. The analysis of the structural behavior and the interpretation of the field results were supported by an appropriate numerical model of the bridge. The main conclusions of this research are summarized below.

The deflection of the main girders chords results from the overlapping of both global and local behaviors. First, the truss may be viewed as a beam where the web consists of a series of separate members instead of a continuous plate. Thus, the bottom and the top chords carry tension and compression, fulfilling the same function as the flanges of a beam. In addition, the bending of each chord must be considered for the overall behaviour.

In this bridge, the rotations do not reproduce the global behaviour of the structure. The rotation of a cross-section of a given steel bar does not reflect the rotation of the entire cross-section of the girder. Therefore, the fundamentals about rotations in a beam and the derived methods to estimate the bridge deflection using rotations are not applicable to this structure.

The external prestressing system has a significant influence on the response of the structure to the temperature changes. As the prestressing bars are anchored outside the structure, the prestress losses lead to a significant decrease of the movements of the expansion joints. In addition, the movements may be partially restrained due to the friction forces at the bearings sliding surface.

Through the observation of strains during the load test, the effectiveness of the top chords strengthening was assessed. The internal forces estimated using a multiple linear regression model, based on the recorded strains, agree well with the internal forces obtained with the numerical model. Therefore, the response of the cross-section as a whole is confirmed.

The comprehensive field results comprising both a load test, where vertical displacements, rotations and strains were measured, and an environmental test carried out after the structural rehabilitation enabled the establishment of a reference state to perform, throughout its lifespan, the assessment of the structure's condition. Moreover, using an adequate numerical model of the bridge, the interpretation of the field results was more comprehensive and the structural behaviour was thoroughly characterized.

This research also provides valuable information regarding the installation of a permanent monitoring system for the surveillance of the bridge. Although the vertical displacements are one of the most significant quantities to be monitored, as they are difficult to directly measure, alternative parameters must be sought. In general, the rotations are an adequate alternative. However, in this bridge they may be useful only to monitor the performance of the support bearings hinge. The prestressing steel bars are paramount for the safety of the structure. Thus, monitoring the strains of the prestressing steel bars, particularly at the end spans where the prestress losses are significant, should be taken into account in a surveillance system. In addition, the strains of the chords, particularly at mid-span, as they give significant information about the load distribution, should be also considered. Finally, as an adequate performance of the bearings is crucial for the bridge safety and durability, the observation of the displacements of the expansion joints cannot be ignored.

Chapter 4

Analysis of the in-service behaviour of concrete bridges using a laboratorial model

4.1. Introduction

Structural health monitoring (SHM) of bridges and, in particular, the development of efficient and reliable damage detection methodologies have been given a huge attention over the last three decades, by both the scientific community and bridge owners (Chang *et al.*, 2003; Van der Auweraer and Peeters, 2003). Damage detection techniques may be categorized in dynamic, static and quasi-static approaches, depending on the used features and the nature of the collected measurements. In either approach, the comparison of the structure's response obtained in the monitoring stage with that of a baseline condition is needed for the successful detection of damage. In addition, it should be stressed that the damage detection process involves five increasing knowledge steps ranging between, in a first stage, signalizing the occurrence of damage and, in a last stage, assessing its effects on the safety and lifecycle of the bridge (Sohn *et al.*, 2004). Therefore, detailed assessment and characterization of the in-service behaviour of the structure is paramount for successfully completing the damage detection process.

Reinforced and prestressed concrete became very popular in the middle of the XX century and since then it has been regularly used in the construction of bridges (Menn, 1990). The possibility of avoiding permanently open cracks, leading to the improvement of both the durability and the overall stiffness of the structure, is one of the major advantages of prestressed structures (Collins and Mitchell, 1987). Therefore, one of these bridges' serviceability criteria imposes that the concrete surrounding prestressing tendons remains compressed under quasi-permanent combination of loads (decompression limit state) (CEN, 2004). However, during their lifecycle, bridges may be subjected to actions such as overloading (either in-service or during the construction), creep, shrinkage, temperature variations, etc., that may induce tensile stresses and cause cracking. Consequently, the in-service structural behaviour, even in compressed structures, can be different from that observed in uncracked structures. Therefore, as aforementioned, in order to successfully complete the damage detection process in concrete bridges it is crucial to thoroughly characterize and assess the structural response in a baseline condition, in which the structure may be already cracked.

With the aim of applying sound damage detection approaches based on the quasi-static component of moving-load responses (Cavadas *et al.*, 2013b) in concrete bridges, this chapter is devoted to the analysis of the in-service behaviour of these structures under moving-loads. The variation of the response due to a truck or carriage crossing a bridge, generally presented graphically in the form of influence-lines, provides significant information about its structural behaviour. Thus, these data may play an important role for characterizing the structural condition of a bridge (Hirachan and Chajes, 2005) as well as for early damage detection (Zaurin and Catbas, 2011). In this context, a reduced-scale laboratorial model of a reinforced and prestressed concrete frame, subjected to a moving-load, was chosen as the case study. Although the laboratorial structure is not a scaled-down model of a bridge, its response is representative of the behaviour of typical full-scale concrete frame bridges. In addition, this is a very versatile model that enables testing, under controlled conditions, the effects of different applied actions and boundaries, such as various moving-loads, different prestressing force scenarios, several support bearing situations, etc. Finally, it is important to mention that smeared cracking might be observed along the frame’s beam, which is typical in this type of concrete bridges.

The work described in this chapter includes an extensive set of experimental tests, which comprised the observation of the structural response due to a point-load crossing the structure, both forward and backwards, for different loads and under different prestressing force scenarios. In either case, it was observed that, even though the concrete beam remains entirely under compression during the point-load passage, the structural behaviour was not linear. Firstly, the response is not proportional to the load traversing the frame. Secondly, the response depends on the direction in which the moving-load crosses the structure. Neild *et al.* (2002) addresses the hysteretic response of cracked concrete structures under low magnitude cyclic loads. However, research addressing the nonlinear behaviour of concrete structures under moving-loads was not found in the literature, which was an additional motivation for the thorough assessment of the in-service response of the laboratorial model presented in this chapter. The analysis of the experimental results was supported by adequate numerical simulations, which included the nonlinear behaviour of cracked concrete beam-elements under low magnitude cyclic loads as well as the deformability of the support bearings. Both features were found to be determinant for the nonlinear response of the structure.

This chapter is divided in five sections, including this introduction and a final section where the main conclusions drawn are outlined. Section 4.2 presents a detailed description of the case study, comprising the structural characterization of the laboratorial model, and the description of the measurement and the loading systems used. In addition, illustrative results of the laboratorial-model nonlinear response are presented. The numerical modelling is addressed in the third section: firstly, with the aim of simulating the hysteretic response of cracked concrete structures, the local behaviour modelling is discussed, and its integration in the global model of the frame structure is described; then, the global finite-element model (FEM) developed to support the interpretation of the test results is presented; and finally, the additional iterative procedure needed for the implementation of the local hysteretic behaviour model in the global FEM is briefly described. Section 4.4 is devoted to the analysis of both the experimental and the numerical results: firstly, it is shown that both the nonlinear behaviour of cracked concrete beam-elements and the deformability of the support bearings determine the behaviour of the structure; secondly, a parametric analysis is carried out in order to assess the adequacy of the parameter values assumed in the numerical simulations; then, the consequences of varying the prestressing force are analysed; and finally, the influence of the moving-load magnitude is discussed.

4.2. Case study

4.2.1. General remarks

A reduced-scale laboratorial model of a reinforced and prestressed concrete frame (Figure 4.1), also used in previous research projects (Almeida, 2006; Félix, 2004), was chosen aiming at a very comprehensive research involving the experimental validation of damage detection techniques in different structural systems (Cavadas and Figueiras, 2014), within which the work presented in this chapter is included. It is a very compact and versatile experimental model that simulates a frame bridge typically used for overpasses and underpasses (Kylén, 2010). In addition, under moving-loads, the beam's response is similar to that of the central

Figure 4.1 – General view of the laboratorial model.

span of a 3-span continuous bridge, which is also a very usual structural system in bridges. Furthermore, by replacing one of the pinned bearings by a roller one, the behaviour of the frame's beam is the same as that of a simply supported beam. Therefore, in spite of not being a scaled-down model of a bridge, this is a very interesting laboratorial model as it enables, through simple modifications, studying several structural systems and simulating different applied actions under controlled conditions.

In addition, it should be stressed that smeared cracking can be observed along the frame's beam, as represented in Figure 4.2. In general, the cracks cross the entire cross-section. These cracks arose as a consequence of load histories (not known in detail) imposed during previous research projects (Almeida, 2006; Félix, 2004). The fact that the structure was heavily instrumented with sensors embedded in concrete and bonded to the reinforcing steel bars (Félix, 2004) affects the crack pattern, too. Still, with the aim of applying sound damage detection approaches based on the quasi-static component of moving-load responses (Cavadas *et al.*, 2013b) in concrete bridges, this structural condition is assumed as the baseline condition. In general, in new bridges, as long as the decompression limit state is observed, the structure is uncracked. However, during their lifecycle, due to overloading, either in-service or during the construction, creep, shrinkage, temperature variations, ageing, lack of maintenance, etc., some uncritical cracks may arise in the bridge. In these cases, the bridge owner may decide to monitor the structure in order to assess how those damages evolve. Hence, and in addition to the aforementioned features, it can be said that the behaviour observed in this structure is comparable to the structural response of full-scale bridges.

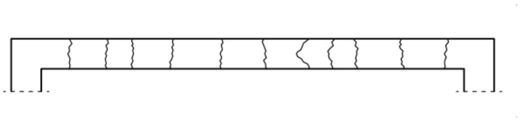

Figure 4.2 – Scheme of the crack pattern in the beam.

4.2.2. Structure geometry and materials

The laboratorial model is a single span reinforced and prestressed concrete frame, 150 cm high, 320 cm long, and 50 cm wide, as shown in the scheme depicted in Figure 4.3. The elements' thickness is 20 cm. The geometry of the frame's bases, 40 cm long and 20 cm thick, enables different positions for the supports. Within this work, two equal supports are placed in the alignment of the column axes. Each support, entirely made of steel, is composed by two plates and a pentagonal prism (see the detail in Figure 4.3). The top and the bottom plates are bolted to, respectively, the frame's basis and the floor slab. A thin layer of cement mortar ensures an adequate contact between the steel and the concrete surfaces. The upper vertex of the pentagonal prism fits the triangular shaped groove milled in the top plate, thereby preventing horizontal displacements and enabling longitudinal rotations.

Two seven-wire, straight, unbonded strands, having a cross-section area of 1.40 cm^2 each, were positioned at mid-depth of the beam cross-section. The ultimate wire strength is 1860 MPa, and thus the ultimate strength of each strand is about 260 kN. Two hydraulic jacks, one for each strand, were installed for tensioning and de-tensioning operations, which enables testing different prestressing force scenarios. The beam's ordinary reinforcement (characteristic yield stress of 500 MPa) consists of four 16 mm longitudinal bars (top and

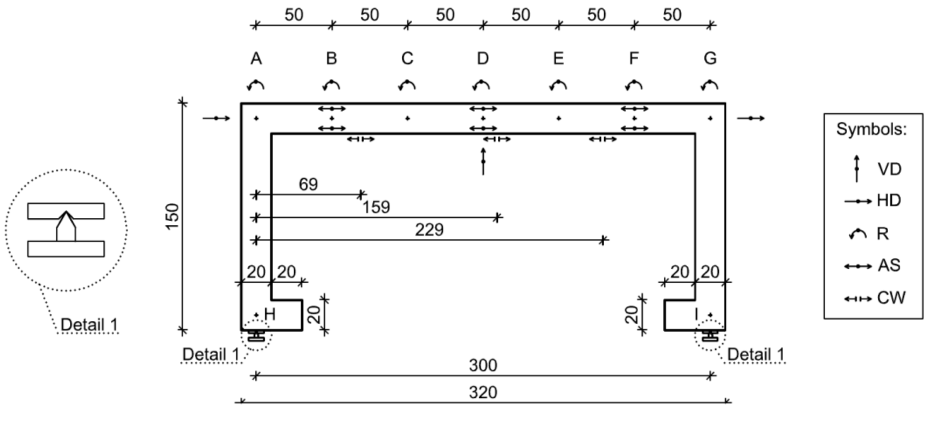

Figure 4.3 – Geometric characteristics of the laboratorial model and configuration of the measurement system.

bottom) with a concrete cover of 40 mm (with respect to the bar axis) and 6 mm stirrups spaced 15 cm apart. The concrete compressive strength and Young modulus were estimated at 37 MPa and 30 GPa respectively, based on the results of compression tests in 150 mm cube specimens, carried out 340 days after casting (Félix, 2004).

4.2.3. Measurement system

The assessment of the current performance of the structure and the early detection of anomalies in the structural response are among the objectives of installing a monitoring system in an existing or newly built bridge (Ko and Ni, 2005). In practical applications, the number of sensors that can be installed is limited which may introduce some uncertainty in the analysis of the results, namely as regards the detection of damage. It is, thus, essential that appropriate sensors are placed at locations such that the chances of detecting damage are maximized. Recently, several approaches have been developed to aid engineers in configuring measurement systems (Meo and Zumpano, 2005; Robert-Nicoud *et al.*, 2005b). However, due to the lack of a systematic approach for the configuration of measurement systems, engineers currently rely on their experience and judgement to decide upon the location and the type of sensors.

Within the scope of this work, the laboratorial model was heavily instrumented aiming at two main objectives. The first was to characterize and understand thoroughly the structural behaviour of cracked concrete bridges under moving-loads. The second, within the research involving the experimental validation of damage detection techniques (Cavadas and Figueiras, 2014), was to assess the most appropriate quantities, and corresponding locations, to be measured aiming at early detection of damage.

The monitoring system includes the measurement of the vertical displacement (VD) at mid-span, the horizontal displacements (HD) at the beam’s centroid in each end, the rotations (R) at seven equally spaced cross-sections, and the average strain (AS) at both the top and bottom of three cross-sections in order to obtain the corresponding curvatures (χ). Linear variable differential transformers (LVDT) were installed to measure both vertical and horizontal displacements. Rotations were measured by using electronic inclinometers. As the beam was cracked, average strains were determined by using displacement transducers with a base length of 300 mm. Crack-widths (CW) were measured at three cross-sections, with displacement transducers having a base length of 100 mm. In addition, to control the prestressing strands tensioning and de-tensioning as well as the variation of prestressing forces (PSF) under loading, two load cells, one for each strand, were installed. A scheme of the complete monitoring system may be found in Figure 4.3.

In general, in addition to the phenomenon under observation, the signals include random errors, which, regardless of their source, are typically described as noise. It is, thus, essential to remove as much of this noise as possible without, at the same time, unduly degrading the underlying information. Hence, a Savitzky-Golay filter (Savitzky and Golay, 1964), which is capable of smoothing data without distorting the intensity or the shape of the peak, may be applied. It consists in fitting successive sub-sets of adjacent data points with a low-degree polynomial by the method of linear least squares and then substituting back into the resulting equation the abscissa at the central point. The value obtained by this procedure is the best value at that point based on the least squares criterion, on the function which was chosen, and on the group of points examined.

As mentioned above, the focus of this work is the quasi-static component of the structural response as a moving-load crosses the structure. Furthermore, as in the tests carried out the crossing speed is appreciably low (see section 4.2.4), the dynamic component is inexistent. Still, with the objective of obtaining influence-lines as smoothed as possible without distorting the phenomena under observation, data were acquired at a rate higher than the one needed to adequately characterize the structural response. Hence, within this work, data was acquired at a rate of 50 samples per second, using a 16-bit analogue-to-digital converter (ADC). Then, a Savitzky-Golay filter using a third degree polynomial curve, with a moving window of 101 points of equal weight, was applied to smooth the acquired signals.

4.2.4. Loading system

As previously mentioned, this chapter focuses on the in-service behaviour of concrete bridges under moving-loads. For this purpose, a versatile loading system was developed, enabling the load to be mechanically moved along the beam, and also the total load to be easily modified. The loading system consists in a metallic structure comprising two hanging bases on which masses are laid down in order to change the total weight, as shown in Figure 4.1. This apparatus is supported on two steel wheels, transversely aligned, connected to an electrical motor, which drives the movement in both directions. The driving-motor is connected to an electrical frequency converter in order to ensure constant speed along the crossing. Hence, recording the crossing time at a set of positions allows estimating the position of the moving-load at each point-in-time, and thus, obtaining the experimental influence-lines. Furthermore,

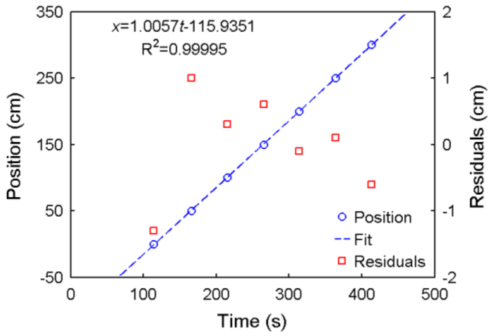

Figure 4.4 – Estimates of the load position over time, based on the records of the crossing time at a set of seven equally spaced (50 cm) pre-selected positions.

note that the position of the steel wheels leads to a point-load as regards the longitudinal direction, thereby facilitating the interpretation of the results.

In the tests carried out, in which the crossing speed was approximately 1 cm/s, the crossing time at a set of seven equally spaced (50 cm) pre-selected positions was recorded. Then, by fitting these data with a first-degree polynomial curve (assuming constant speed along the structure), the successive load positions over time were estimated. Figure 4.4, which depicts the application of the described procedure in a given crossing, shows its adequacy, as the absolute differences between the estimates and actual positions (denoted as residuals) are lower than 1 cm.

Finally, it should be mentioned that two auxiliary structures (3D steel truss towers) are placed next to both ends of the frame, as shown in Figure 4.1. Thus, in each crossing the moving-load departs and arrives outside the beam, ensuring that the structure is unloaded at both the beginning and the end of the crossing as well as allowing the load to move at constant speed while passing over the concrete structure.

4.2.5. Structural response

Within the scope of this work, an extensive set of experimental tests was carried out, which comprised the observation of the structural response due to a point-load crossing the structure, forward and backwards, for different loads and under different prestressing force scenarios. In either case, it was observed that, even when the concrete beam is entirely compressed (thus complying with the decompression limit state), the structural behaviour was not linear: the response is not proportional to the load magnitude and depends on the direction in which the moving-load crosses the structure.

To illustrate the nonlinear behaviour of the structure as regards the movement direction, representative transducer measurements were selected (Figure 4.5): the vertical displacement at mid-span, the horizontal displacement at the beam's centroid, the rotation at C and the curvature at B. These plots refer to a 10.2 kN point-load, moving forward (A-G) and backwards (G-A), when the prestressing force installed in the laboratorial model was about 230 kN (115 kN in each strand). The measurements are zeroed when the point-load crosses the first column axis (cross-sections A and G for forward and backward movements, respectively).

Except for rotations, the measurements taken both at the beginning and at the end of the crossing are approximately the same, irrespectively of the direction of movement. However, for intermediate positions, the response of the structure as the load moves forward may significantly differ from that as the load moves backwards. For example, the horizontal displacement at the beam's centroid (HD-G) when the load is at mid-span (position=150 cm) is approximately 0.08 and -0.04 mm as the load moves, respectively, forward and backwards. If the structural behaviour was linear and elastic, the response would be the same, irrespectively of the direction of movement. Furthermore, as the structure is symmetrical (except the cracks that are not symmetrical), the response would be null. Hence, the response of the laboratorial model seems to be determined by the nonlinear behaviour of the cracked beam.

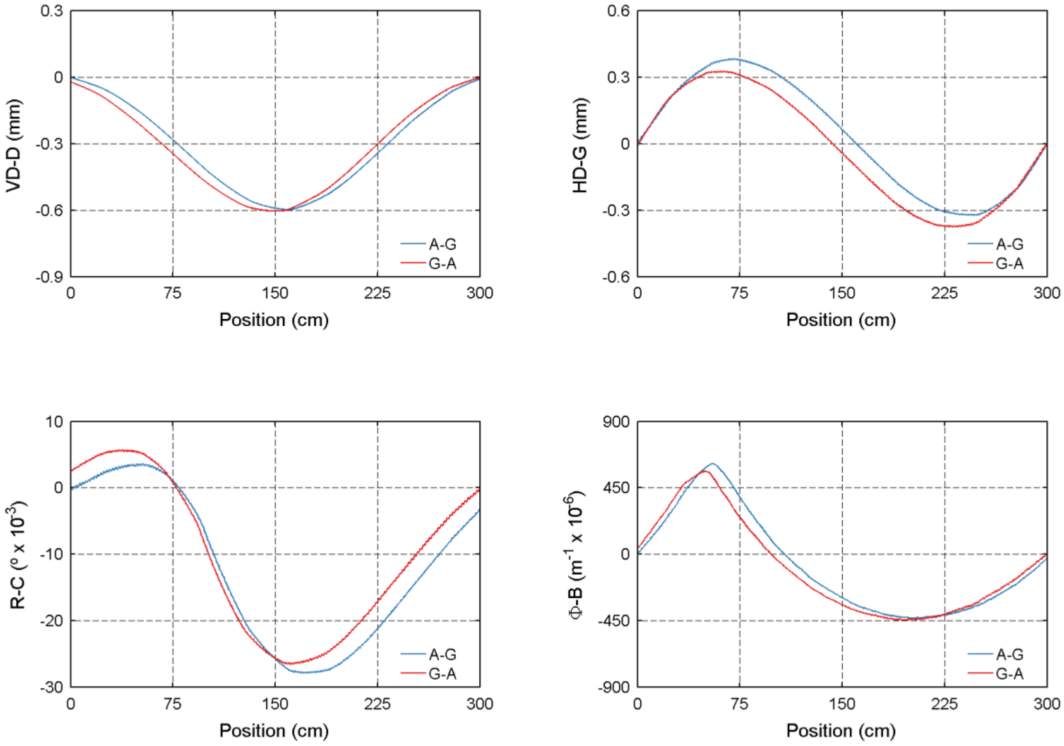

Figure 4.5 – Typical structural response of the laboratorial model.

As regards the rotations, in addition to the nonlinear behaviour discussed above, the response seems to be affected by the supports deformability. At the end of the crossings, negative (clockwise) and positive (counter-clockwise) residuals, as the load moves, respectively, forward and backwards, are observed.

Note that although the prestressing force installed in the laboratorial model is quite below the ultimate strength of the strands (about 44%), the decompression limit state is satisfied (i.e. the frame's beam remains compressed) under the effects of dead loads and a 10.2 kN moving point-load. Moreover, as these tests aimed at reproducing the in-service behaviour of concrete bridges under moving-loads, an additional criterion concerning the vertical deflection was attended. According to AASHTO LRFD (2010), the vertical deflection limit of bridges under vehicular loads is given by *span/800*. Thus, in this case, as the span length is 3 m, the vertical deflection must not exceed 3.75 mm, which is clearly higher than the deflection observed in the tests.

4.3. Numerical modelling

4.3.1. General remarks

In the previous section, the reinforced and prestressed concrete laboratorial model chosen as the case study for the research discussed in this chapter was presented. It was shown that the structural behaviour for a point-load moving across the beam was nonlinear. Therefore, the aim of this section is to develop a finite-element model (FEM), in which the main properties and features that govern the structural response must be included, with the goal of supporting the interpretation of the results obtained in the experimental tests. In addition, the numerical model, once validated, can be used to carry further analyses and supplement the information provided by the experimental tests as regards the in-service behaviour of concrete structures under moving-loads.

However, finding an adequate numerical model for a structure and the right explanations for its behaviour is often a challenge. Various hypotheses involving key parameters must be tested and validated (Robert-Nicoud *et al.*, 2005a; Strauss *et al.*, 2012). The analysis methods and software used, the combination between the accuracy of the results and the computational effort, and the objectives to be accomplished should be taken into account (Aktan *et al.*, 1998). It was shown before that the observed structural behaviour can only be numerically described if the analysis includes the nonlinear beam behaviour under cyclic loading and the supports deformability.

In this context, the behaviour of a cracked beam-element under low magnitude cyclic loads is firstly discussed, and a simplified model to describe the hysteresis loop is proposed. Thereafter, a 2D beam-element numerical model of the structure is implemented in the multi-purpose finite-element software package DIANA (TNO DIANA BV, 2011), in which a simplified model to describe the behaviour of cracked beam-elements as well as the supports deformability are included.

As a consequence of the adopted approach to implement, in DIANA, the hysteretic beam behaviour, in addition to the iterative calculations inherent to any nonlinear analysis, another iterative procedure was required, which is described at the end of this section.

4.3.2. Local behaviour modelling

When a moving-load crosses a structure, the latter undergoes a reloading/unloading cycle, with important variation of bending moments, M. If the loaded structure is cracked, it will exhibit a nonlinear response (Rotilio, 1998). In order to simulate, numerically, that response, it is important to explicitly take into account the following effects: the cyclic variation of bond stresses, τ, and corresponding slip values, s, at the interface between the longitudinal reinforcement and the surrounding concrete (Balázs, 1998); and the cyclic relationship between the crack opening, w, and the concrete stress, σ_c, normal to the crack (Hordijk, 1991). In this context, various numerical approaches have been proposed for cyclic analysis of a cracked member subjected to axial forces (Laurencet *et al.*, 1999; Sousa *et al.*, 2015; Zanuy *et al.*, 2010). All involve the discretization of a reinforced concrete member between two consecutive cracks (only half of this length is modelled owing to symmetry).

In the present work, the methodology proposed by Sousa *et al.* (2015)[1] was employed, for a simplified analysis of the monitored frame's beam, in the mid-span region, subjected to cyclic bending moments, in order to understand its response. For this purpose, the structure is simulated, in a simplified way, by considering that bending gives rise to axial forces in a top and a bottom chord, each of which being composed by the longitudinal steel reinforcement and the surrounding concrete (the chord depth is equal to 8 cm). The adopted material

---

[1] The fundamentals of the non-linear behaviour of cracked concrete exposed above were entirely due to the contribution of Prof. Carlos Sousa. Still, its inclusion in this thesis was crucial for the understanding of the whole text.

properties are shown in Figure 4.6. Note that a linear elastic behaviour was considered for concrete in compression owing to the low compression stress levels (the maximum compression stress was always lower than 5 MPa). After an initial deformation imposed to crack the structure, the prestress (N = -230 kN) and the self-weight (M = 1.1 kNm) effects are applied, followed by concrete creep and shrinkage deformations and moving-load effects (three reloading/unloading cycles with ΔM = 4.0 kNm). The distance between cracks was taken as 30 cm (compatible with the observed crack pattern). Figure 4.6 shows the obtained moment-relative rotation relationship, during the third reloading/unloading cycle. The third cycle was chosen noting that the response during the first constant-amplitude cycle (and, with less importance, also in the second one) is significantly different, because of the new trajectories tracked in the constitutive models. In Figure 4.6, one can observe that a significant hysteresis occurs, which is a consequence of the aforementioned constitutive behaviours (cyclic relationships τ-s and σ_c-w).

The employed numerical model (Sousa *et al.*, 2015) is thus a useful tool for explaining the observed hysteretic behaviour. However, the exact values of the parameters that define the τ-s and σ_c-w relationships are not known. Moreover, the previous history of loads applied to the rigid-frame is not known in detail. For those reasons, the cracked beam behaviour was implemented, in the FE analysis of the rigid frame, by means of a simplified moment-average curvature diagram comprising a reloading/unloading cycle. This diagram, composed by a set of moment-average curvature linear relationships, is characterized by parameters defining the secant stiffness and the hysteresis, which can be easily modified in a parametric analysis, in order to study the way how they affect the global frame response.

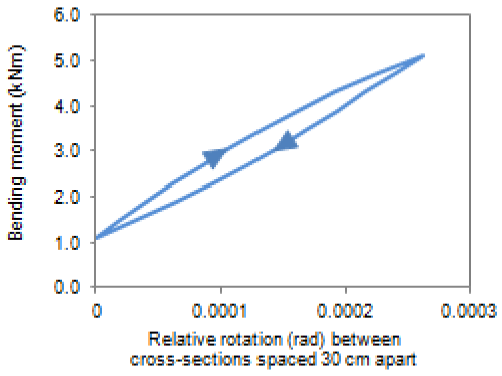

Concrete:
Compressive strength = 37 MPa
Young modulus = 30 GPa
Tensile strength = 2.9 MPa
Fracture energy = 0.075 kN/m
Shrinkage strain = 400 $\mu\varepsilon$
Creep coefficient = 2.5

Bond stress-slip relationship (monotonic envelope):
Farra (1995); poor bond conditions

Bond stress-slip relationship (unloading/reloading):
Sousa *et al.* (2015)
K_B = 400 MPa/mm
α_B = 0.25
β_B = 0.9

σ_c-w relationship:
Hordijk (1991)

Figure 4.6 – Adopted properties and typical behaviour of a cracked concrete beam-element under a low magnitude cyclic loading material.

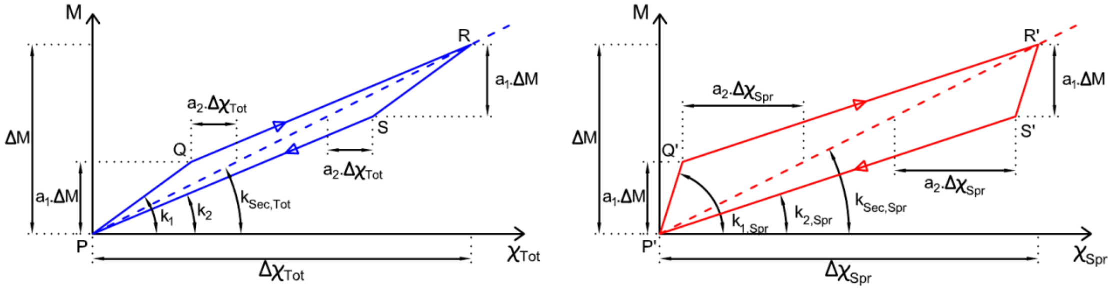

(a) (b)

Figure 4.7 – Scheme of the simplified multi-linear model used to reproduce the hysteresis loop: (a) total curvature; (b) curvature lumped in the spring.

Figure 4.7 (a) depicts the adopted diagram. The loading path is composed by two branches with stiffnesses K_1 and K_2. The same stiffnesses are found in the unloading path. This diagram is defined by the following parameters: the secant stiffness, $K_{Sec,Tot}$; the moment range, ΔM; the first hysteresis parameter, a_1, which establishes the moment range with stiffness K_1; the second hysteresis parameter, a_2, which establishes the fraction of the total curvature (denoted as $\Delta\chi$ and given by $\Delta\chi = \Delta M/ K_{Sec,Tot}$) that shifts points Q and S from the secant response.

With the objective of including this multi-linear model in 2D beam-element models for finite-element analysis of the in-service response of cracked concrete structures, nonlinear zero-length springs (Spr) connected in series with linear and elastic beam-elements (BE) are used. Therefore, the total deformation is given by the sum of deformation of both elements. The beam-element deformations are linear and elastic, with stiffness K_{BE}. If K_{BE} was equal to $K_{Sec,Tot}$, only the inelastic deformations of the assembly would be lumped into the spring (denoted as Spr), whose secant stiffness, $K_{Sec,Spr}$, would be infinite. In this case, undesirable negative stiffness branches would arise in the spring model (see Figure 4.8 (a)). It is thus necessary to reduce the secant stiffness of the spring. Bearing in mind that the stiffness values are related by equation (4.1), the reduction of the spring secant-stiffness, on one hand, must lead to positive stiffness in every branch of the spring model and, on the other hand, must be as small as possible so that most of the deformation of the assembly is given by the beam-element (see Figure 4.8 (b)).

$$\frac{1}{K_{Sec,Tot}} = \frac{1}{K_{BE}} + \frac{1}{K_{Sec,Spr}} \tag{4.1}$$

As mentioned before, the inelastic deformations of the assembly are lumped into the spring. Consequently, the multi-linear curve reproducing the hysteresis loop derived above must be

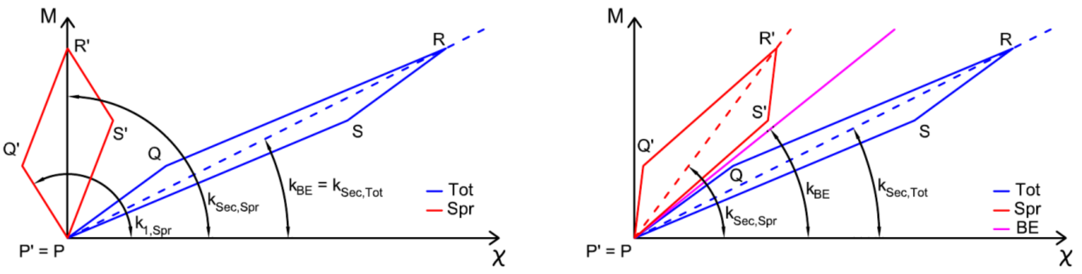

(a) (b)

Figure 4.8 – Scheme of simplified models for the assembly of a zero-length spring and a beam-element: (a) idealized; (b) adopted.

given by the spring, as depicted in Figure 4.7 (b). Given the secant-stiffness of the assembly, $K_{Sec,Tot}$, and once the stiffness of the beam-element, K_{BE}, is adequately chosen, as discussed above, the secant-stiffness of the spring, $K_{Sec,Spr}$, is obtained with equation (4.1). Thereafter, the multi-linear model of the spring can be derived as a function of the moment range, ΔM, and the hysteresis parameters a_1 and a_2. Hence, the stiffness of the first and second branches of the spring model are given, respectively, by equations (4.2) and (4.3).

$$K_{1,Spr} = \frac{\Delta M_{\mathrm{P'Q'}}}{\Delta \Phi_{P'Q'}} = \frac{a_1 \cdot \Delta M}{\dfrac{a_1 \cdot \Delta M}{K_{Sec,Spr}} - a_2 \cdot \dfrac{\Delta M}{K_{Sec,Tot}}} \tag{4.2}$$

$$K_{2,Spr} = \frac{\Delta M_{\mathrm{Q'R'}}}{\Delta \Phi_{Q'R'}} = \frac{\Delta M - a_1 \cdot \Delta M}{\dfrac{\Delta M}{K_{Sec,Spr}} - \dfrac{a_1 \cdot \Delta M}{K_{Sec,Spr}} + a_2 \cdot \dfrac{\Delta M}{K_{Sec,Tot}}} \tag{4.3}$$

In the multi-linear model presented above the cyclic loading ranges between zero and a positive moment. Either in this case or in a situation in which the moment ranges between zero and a negative value – scenarios in which the sign of the moment does not change in the cyclic loading –, the stiffness of the first and the second branches are, respectively, K_1 and K_2. Hence, in the former, the origin of the diagram, O', coincides with P', whereas in the latter, matches R'. However, when the moment ranges between negative and positive values – situations in which the sign of the moment changes in the cyclic loading – the hysteresis loop should be slightly different. Notwithstanding, for the sake of simplicity, a similar diagram was adopted. Therefore, depending on the "direction" in which the moment varies, two main scenarios arise, within each two situations are distinguished (see Figure 4.9). When the moment firstly varies towards positive values, the origin of the diagram is pulled along the bilinear curve P'Q'R'. If the portion of the moment range along which the stiffness is K_1 (given

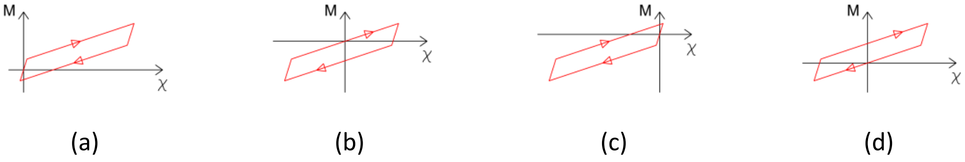

Figure 4.9 – Scheme of the multi-linear model for the rotation-spring used to reproduce the hysteresis loop, when the moment sign changes during cyclic loading: (a; b) when the moment firstly reaches the maximum positive value; (c; d) when the moment firstly reaches the "maximum" negative value.

by $a_1 \cdot \Delta M$) is greater than the highest negative value, the origin is shifted along P'Q' (Figure 4.9 (a)). Otherwise, the origin of the diagram is pulled along Q'R' (Figure 4.9 (b)). Conversely, when the moment firstly varies towards negative values, the origin of the diagram is pulled along the bilinear curve R'S'P'. If the portion of the moment range given by $a_1 \cdot \Delta M$ is greater than the highest positive value, the origin is shifted along R'S' (Figure 4.9 (c)). Otherwise, the origin of the diagram is pulled along S'P' (Figure 4.9 (d)). Note that when either the highest positive or negative values for, respectively, the first and the second scenarios addressed above, are lower than the portion of the moment range given by $a_1 \cdot \Delta M$, the stiffness of the first branch is K_1. On the contrary, when this portion is lower, the stiffness of the first branch is K_2. Still, it should be stressed that when the load reverses, the stiffness of the first branch is K_1 in either of the situations referred above.

4.3.3. Global behaviour modelling

The 2D FEM was implemented in the multi-purpose finite-element software package DIANA (TNO DIANA BV, 2011) and is constituted by beam-elements, with three degrees of freedom per node (two displacements and one rotation), springs to model the connection between contiguous beam-elements of the frame, and springs to simulate the supports stiffness also. The beam-elements axis is located along the geometrical centre of the beam and the columns, both with a rectangular cross-section, in accordance with the dimensions described in section 4.2.2. The beam-elements are based on the Timoshenko beam theory (shear deformation is taken into account).

As described in the previous section, with the objective of including the nonlinear behaviour of cracked concrete, zero-length springs are connected in series with the beam-elements of the frame. The beam-element deformations are linear and elastic and the inelastic deformations are given by the rotation-spring that connects contiguous beam-elements. The beam was discretized in 12 beam-elements of 25 cm in length (the nodes coinciding with measurement locations), which led to satisfactory results.

In the previous section, moment-curvature (M-χ) relationships for the beam-element and the rotation-spring were established with the goal of modelling the hysteresis loop of cracked concrete beam-elements. However, in DIANA, the rotation-spring's behaviour is defined through moment-relative rotation (M-$\Delta\theta$) relationships, denoted herein as rotational stiffnesses, K_R. The rotational stiffness of a beam-element with length L is given by:

$$K_R = \frac{EI}{L} \tag{4.4}$$

where E is the Young modulus and I is the moment of inertia of the cross-section. Hence, given the secant Young modulus of the assembly, $E_{Sec,Tot}$, and once the beam-element's Young modulus, E_{BE}, is adequately chosen, the corresponding rotational stiffnesses may be computed with equation (4.4), and then the rotation-spring secant-rotational-stiffness is given by equation (4.1).

In order to set the axial stiffness appropriately, a similar approach is required. Therefore, the beam-element is connected in series with a translation spring. As the variation of axial forces, when the moving-load crosses the structure was found minimal, a linear elastic axial behaviour is assumed. The axial stiffness, K_A, of a beam-element with length L is given by:

$$K_A = \frac{EA}{L} \tag{4.5}$$

where A is the cross-sectional area. Hence, given the secant Young modulus of the assembly, $E_{Sec,Tot}$, and once the beam-element's Young modulus, E_{BE}, is adequately chosen, the axial-spring secant-stiffness is given by equation (4.1).

In this context, two adjacent beam-elements are connected by both a rotation- and a translation-spring. In addition, compatibility of vertical displacements between pairs of nodes connected by springs was prescribed.

In DIANA, the rotation-spring's nonlinear behaviour can be specified by defining different spring stiffnesses for different relative rotation ranges. Moreover, multiple spring stiffness diagrams can be defined to model unloading-reloading cycles.

The columns were discretized in seven beam-elements of 20 cm in length, each. As these elements are not cracked, only beam-elements were used.

As regards the supports, experimental tests showed that their vertical deformability should be taken into account. This effect was assessed by measuring the rotation of a rigid aluminium bar (RAB) pinned to points H and I (positions shown in Figure 4.3) when a 10.2 kN point-load crosses the structure, moving forward (A-G) and backwards (G-A). Figure 4.10 depicts the measured rotations. The results are zeroed when the load passes cross-sections A and G (support alignments), as the load moves, respectively, forward and backwards (this being the approach also followed in section 4.2.5). Note that these plots include, in addition to the structural response observed as the load moves between the supports alignments (in which the position is equal, respectively, to 0 and 300 cm), the measurements recorded when the load is outside the structure (valuable information for the evaluation of the supports deformability). Focusing on the measurements collected when the load moves between the supports alignment, it is clear that the structure rotates clockwise and counter-clockwise as the load moves, respectively, forward and backwards. Moreover, by comparing these results with the maximum rotations depicted in Figure 4.5, it can be stated that the supports deformability should be taken into account in the interpretation of the experimental results.

In addition, in Figure 4.10, one can see that when the load is moving outside the structure, over the auxiliary steel truss towers (see Figure 4.1), the structure is unloaded, and thus, measurements remain constant. When the load “arrives” (“departs”) at the structure, due to the configuration of the rail over which the wheels of the moving-load system roll, the load is increasingly transferred to (from) the structure. Consequently, the support settles, and the rotation increases or decreases steeply as the load moves, respectively, forward or backwards.

Based on those results, the vertical stiffness of each support, K_V, can be estimated by equation (4.6), where P is the load value (10.2 kN), α is the difference between the rotations observed when the load is over the supports (approximately 0.002°, as shown in Figure 4.10), and L_S is

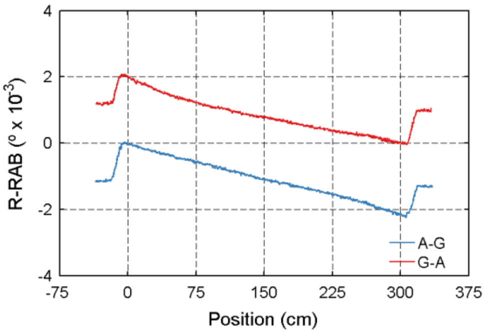

Figure 4.10 – Rotations measured during the experimental tests to assess the supports deformability.

the span length (3 m).

$$k_V = \frac{2 \cdot P}{\alpha \cdot L_S} \tag{4.6}$$

Expressing the parameter α in radians, the vertical stiffness of the supports is approximately 1.95×10^5 kN/m. This stiffness is simulated through a vertical translation-spring in each support. In addition, horizontal displacements are restrained whereas rotations are allowed.

In the analysis, the point-load passage was simulated with 301 load steps, in which a 10.2 kN point-load occupies successive positions spaced 1 cm apart. Dynamic effects are not considered for the reasons expressed above, in section 4.2.3.

4.3.4. Iterative procedure

In order to implement the hysteretic behaviour, a multi-linear model as described in section 4.3.2, with different diagrams for loading-unloading cycles, is defined for each rotation-spring, *i*. Given that the stiffness is prescribed as a function of the relative rotation, the transition-points' abscissa (points P', Q', R' and S' – see Figure 4.7.b and Figure 4.9) must be known beforehand. This implies that the minimum and maximum cyclic bending moments (respectively, M_{min} and M_{max}) are known before the constitutive model is defined for each rotation-spring. Therefore, an iterative analysis procedure was implemented. The moment ranges obtained in analysis *j* are used to define the constitutive models for each spring, *i*, in

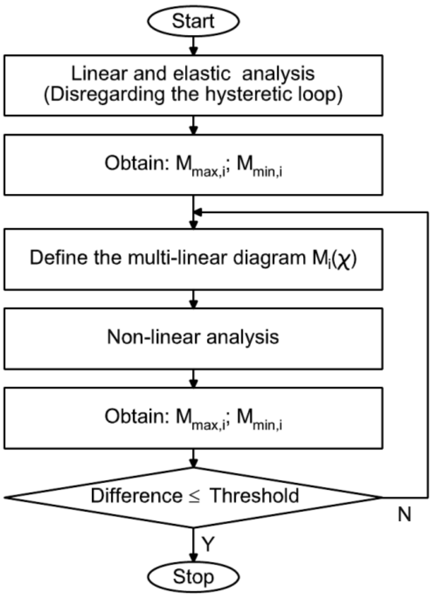

Figure 4.11 – Flowchart of the iterative procedure.

analysis *j*+1. The iterations stop when the difference between extreme bending moments in analyses *j* and *j*+1 is lower than a predefined threshold δ. This iterative procedure is summarized in the flowchart depicted in Figure 4.11. In the applications made in the present work, the final solution was always reached with less than seven iterations.

4.4. Analysis of the results

4.4.1. General remarks

As mentioned above, within the scope of this work, an extensive set of experimental tests was carried out, comprising the observation of the structural response due to a point-load crossing the structure, both forward and backwards, for different loads and under different prestressing force scenarios. Even though the concrete beam remains under compression during the point-load passage (with compression stresses lower than 5 MPa), it was observed that the structural behaviour was not linear. Both the nonlinear behaviour of cracked concrete under cyclic loading and the supports deformability were pointed as the main causes for the measured structural response due to moving-loads.

In this context, with the goal of supporting the interpretation of the experimental test results, namely as regards the differences observed in the response as the load moves forward and backwards, FEM analyses were carried out. Hence, the main purpose of this section is to evaluate the hypotheses raised above and to assess the adequacy of the numerical model described in the previous section. In addition, the effect of varying the prestressing force on the structural response, namely in terms of the nonlinear structural behaviour as regards the movement direction, is also assessed. Finally, based on the results of a set of tests in which the only varying parameter is the point-load magnitude, the proportionality of the response in relation to the load level crossing the structure is evaluated.

4.4.2. Comparison between numerical and experimental results

In section 4.2.5, the measurements of a set of representative quantities were selected to illustrate the nonlinear behaviour of the structure as regards the movement direction. Those results concern experimental tests with a 10.2 kN point-load and a prestressing force of 230 kN. With the goal of assessing the hypotheses raised above (nonlinear behaviour of the cracked concrete beam-elements under cyclic loading and the supports deformability), this section presents the results of three FEM analyses, identified in Table 4.1. The first one

Table 4.1 – Specificities of FEM analyses 1 to 3.

	Hysteretic beam behaviour	Deformable supports
FEM1	Yes	No
FEM2	No	Yes
FEM3	Yes	Yes

(FEM1), includes only the nonlinear behaviour of cracked concrete whereas the second (FEM2), includes only the supports deformability. Finally, the third one (FEM3) includes both effects.

The Young modulus of the columns, as they are uncracked, was taken as 30 GPa, in accordance with the results of compression tests (see section 4.2.2). On the contrary, a lower stiffness was expectable for the beam, as it was cracked along its entire length. Preliminary linear elastic analyses (disregarding the hysteresis loop) revealed that a reasonable match with the maximum measured values could be obtained if the beam's Young modulus, E_{sec}, was taken as 9 GPa, this being the value adopted to define the secant stiffness of the beam.

In the analyses including the hysteretic behaviour (FEM1 and FEM3), bearing in mind the constraints discussed in section 4.3.2, the beam-element's Young modulus was taken as 12 GPa. Plausible values were adopted for the hysteresis parameters a_1 and a_2 which define the hysteresis loop: $a_1 = 25\%$ and $a_2 = 4.175\%$. The adequacy of these values is discussed below, with the support of a parametric analysis with that purpose.

In the analyses wherein the supports deformability is taken into account (FEM2 and FEM3), the stiffness of the translation-spring is equal to 1.95×10^5 kN/m, the value determined in section 4.3.3.

The estimates obtained with these three FEM as well as the experimental results are compared in Figure 4.12. As aforementioned, these plots refer to a 10.2 kN point-load, moving forward (A-G) and backwards (G-A), and express the variation of the selected quantities in relation to the measurements taken when the load passes the cross-sections A and G (support alignments), as the load moves, respectively, forward and backwards.

The estimates obtained with FEM1, in which only the nonlinear behaviour of cracked concrete is taken into account, show, in general, a reasonable agreement with the experimental results. In this model, the nonlinear behaviour of the structure as regards the direction in which the load crosses the structure is clearly reproduced. However, in the calculated rotations, the "residuals" observed at the end of the crossings are not replicated.

Conversely, in FEM2, in which only the deformability of the supports is taken into account, these "residuals" are clearly reached. However, as this model is linear and elastic, the nonlinear behaviour of the structure as regards the direction of movement is not reproduced. As a consequence of the supports deformability, a "rigid body" rotation takes place, and the influence-lines of the rotations are "rotated" leading, thus, to the aforementioned "residuals" at the end of the crossing. Furthermore, as the reference value selected to plot the results depends on the movement direction, the influence-lines for forward movement is shifted in relation to those obtained when the load moves backwards. It should be stressed, however, that the influence-lines for vertical displacement at mid-span and for curvatures, obtained in either direction, are completely overlapped. In the former case, as the support stiffnesses are assumed to be equal, the additional displacement due to the "rigid body" rotation is the same regardless the movement direction. In the latter, as the vertical reactions do not depend on the vertical stiffness of the supports, the internal forces, and consequently the curvatures, are also the same regardless the movement direction.

By combining both the effects (FEM3), in general, in all quantities observed, a good agreement between the numerical estimates and the experimental results is found. Hence, it is clearly shown that the nonlinear response of the structure as regards the direction of movement observed in the tests is caused by both the nonlinear behaviour of the cracked concrete beam-elements under cyclic loading, and the supports deformability.

As regards the nonlinear hysteretic behaviour of cracked concrete under low amplitude cyclic loading modelled in the previous analyses, with the objective of assessing the adequacy of the adopted values for the hysteresis parameters a_1 and a_2, a parametric study was carried out. As referred in section 4.3.2, the previous loading history of the structure under analysis as well as parameters required to define the constitutive model are not known in detail. Hence, the typical hysteresis loop was simplified as a multi-linear diagram defined by two hysteresis parameters a_1 and a_2, whose values must be properly chosen in order to reproduce the energy dissipated in the hysteresis loop and, thus, the global behaviour of the structure.

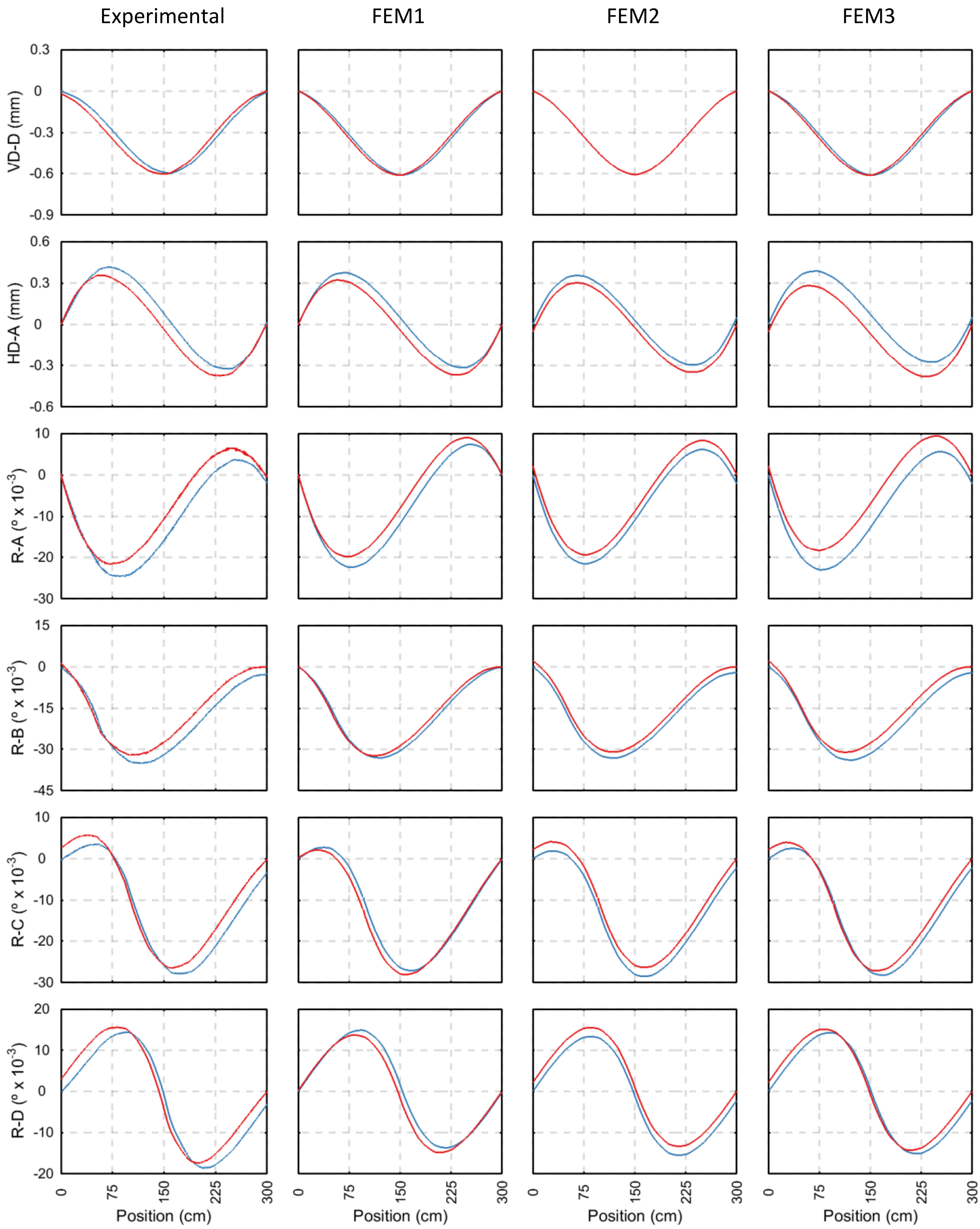

Figure 4.12 (i) – Comparison of experimental results with estimates provided by three FEM combining the nonlinear behaviour of cracked concrete and the supports deformability (A-G, blue line, and G-A, red line).

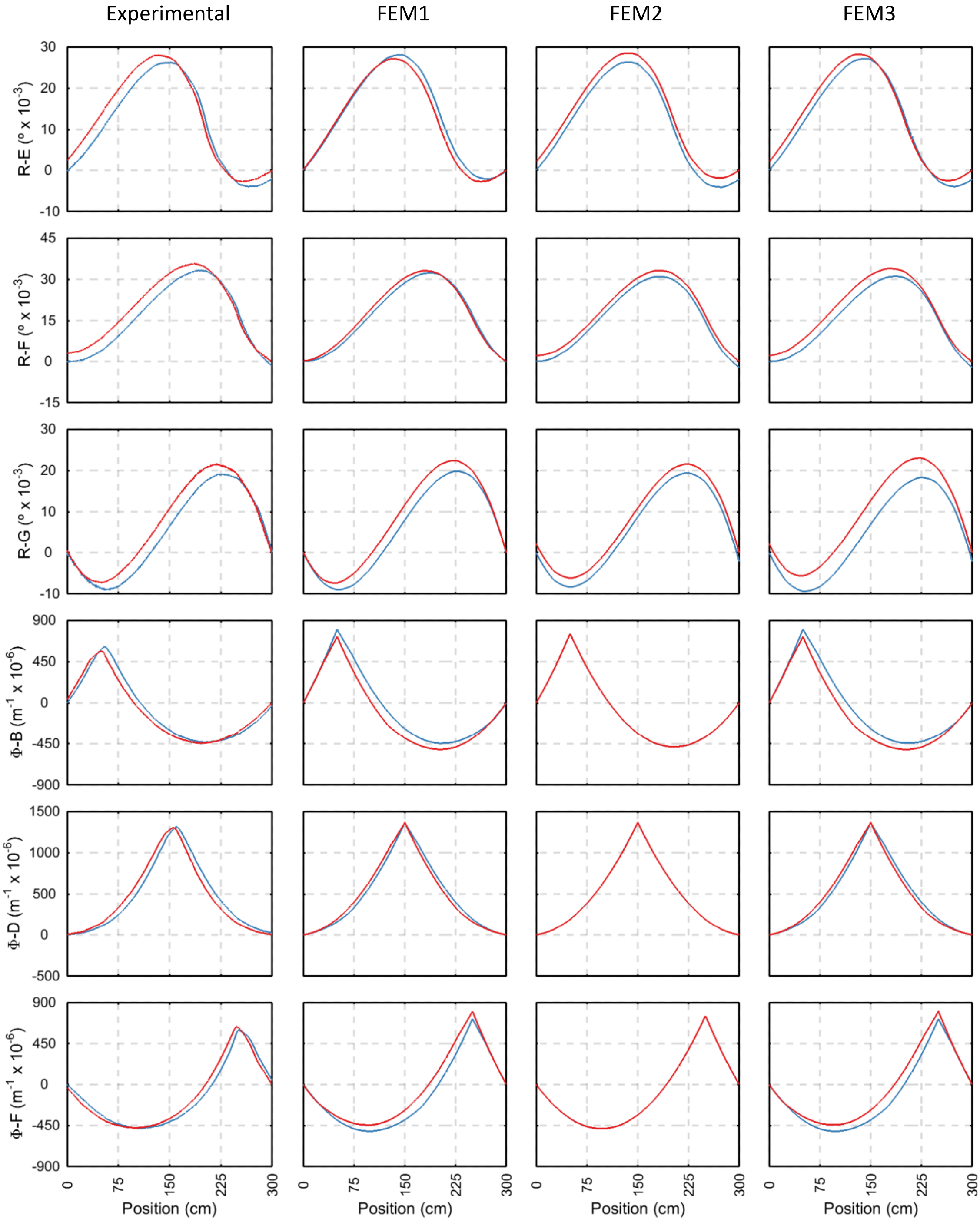

Figure 4.12 (ii) – Comparison of experimental results with estimates provided by three FEM combining the nonlinear behaviour of cracked concrete and the supports deformability (A-G, blue line, and G-A, red line).

Figure 4.13 (a) depicts the hysteresis loop, denoted as H2, as modelled in the previous analyses (FEM1 and FEM3) in which the hysteresis parameters were assumed to be $a_1 = 25\%$ and $a_2 = 4.175\%$. Two additional multi-linear diagrams are depicted, in which the dissipated energy of the hysteresis loop is halved (H1) and doubled (H3). The values of the hysteresis parameters for each scenario are summarized in Table 4.2. For the sake of clarity, the multi-linear diagrams of the rotation-spring in which the nonlinear behaviour of the assembly is lumped, (as described in section 4.3.2) are also depicted (see Figure 4.13 (b)).

The estimates provided by FEM analyses with different hysteresis scenarios, as well as the experimental results, are compared in Figure 4.14. In these analyses, the effect of the supports deformability is also included. Consequently, FEM3 coincides with H2.

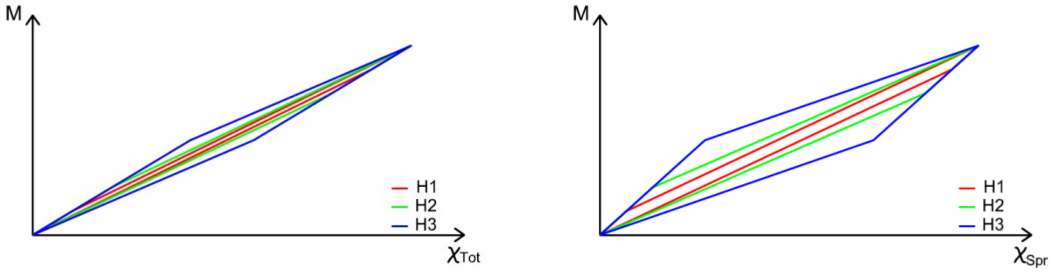

(a) (b)

Figure 4.13 – Moment-curvature relationships assuming different hysteresis parameters a_1 and a_2: (a) assembly; (b) rotation-spring.

Table 4.2 – Hysteresis parameters.

	a_1	a_2
H1	12.5%	2.088%
H2 ≡ FEM3	25.0%	4.175%
H3	50.0%	8.350%

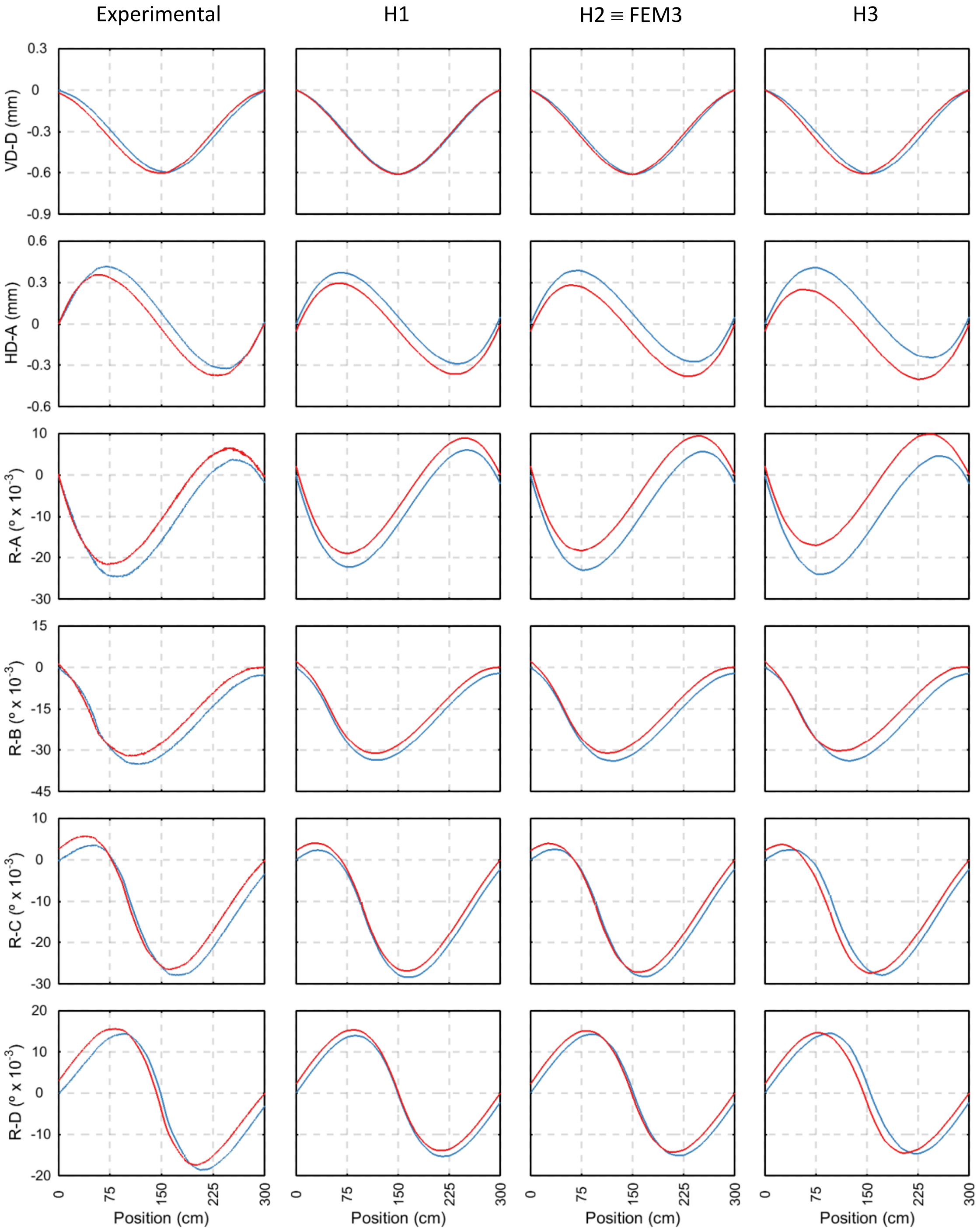

Figure 4.14 (i) – Comparison of experimental results and estimates provided by three FEM assuming different hysteresis parameters (A-G, blue line, and G-A, red line).

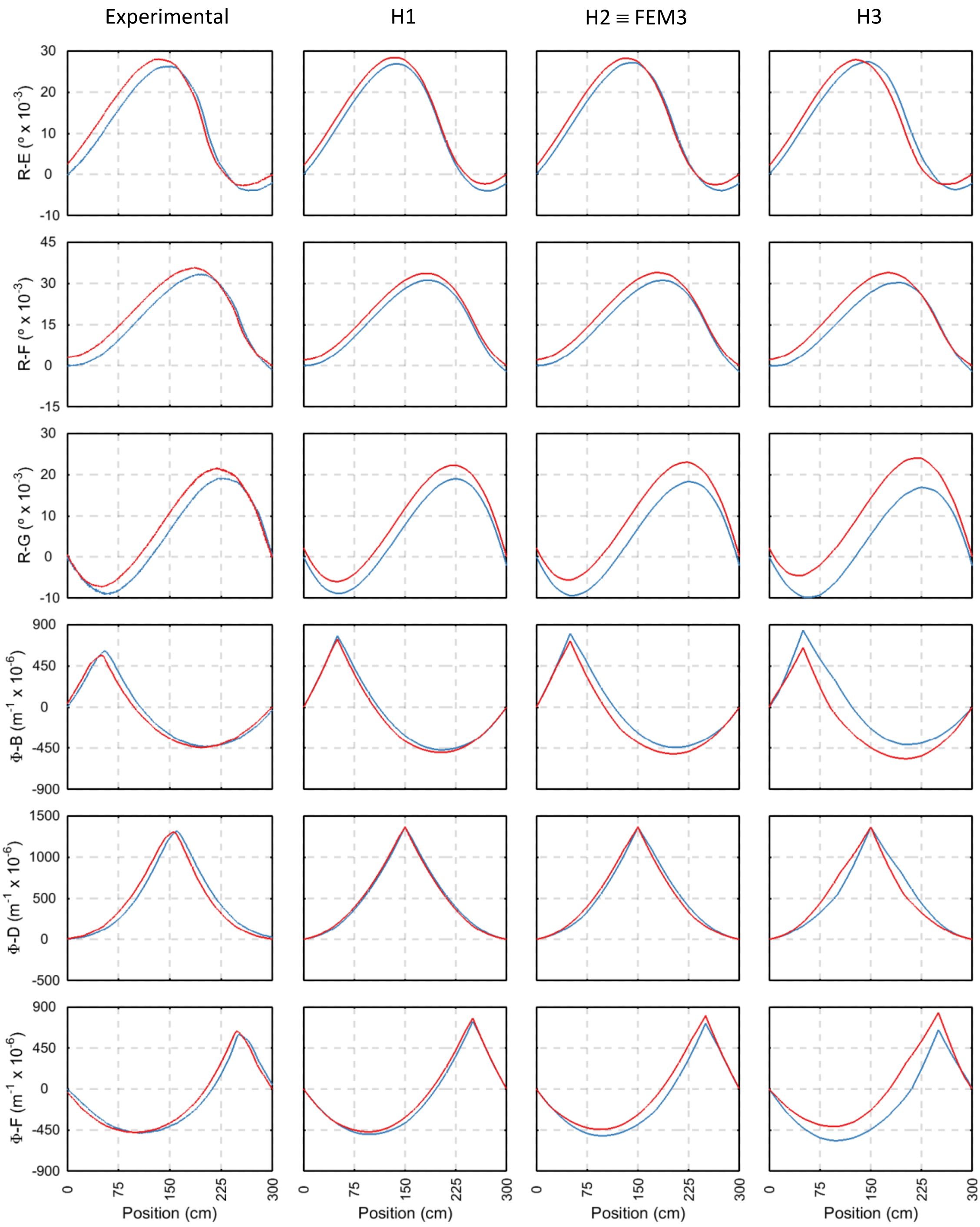

Figure 4.14 (ii) – Comparison of experimental results and estimates provided by three FEM assuming different hysteresis parameters (A-G, blue line, and G-A, red line).

By comparing the experimental results with the numerical estimates provided by H3, one can see that the dissipated energy in this scenario is excessive. Conversely, focusing on the estimates for vertical displacement and mid-span curvature (VD-D and ϕ-D), the energy of the hysteresis loop assumed in model H1 seems to be insufficient. Thus, even though the estimates provided by model H2 (≡ FEM3) are not exactly equal to the measured values for all the observed parameters, the results indicate that this is a plausible model for the hysteretic behaviour of the cracked beam.

4.4.3. Evaluation of the effect of varying the prestressing force

In the tests whose results were presented in section 4.2.5, the prestressing force installed in the laboratorial model was 230 kN (115 kN in each strand). Although this prestressing force is quite below the ultimate strength of the strands (approximately 44%), the decompression limit state under both the dead-load and a 10.2 kN point-load is comfortably ensured. Still, the structural response is highly determined by the nonlinear behaviour of cracked concrete under cyclic loading, as shown in the section above. With the goal of assessing the effect of varying the prestressing force on the structural response, the prestressing force was increased to 330 kN (165 kN in each strand, approximately 64% of the ultimate strength). Figure 4.15

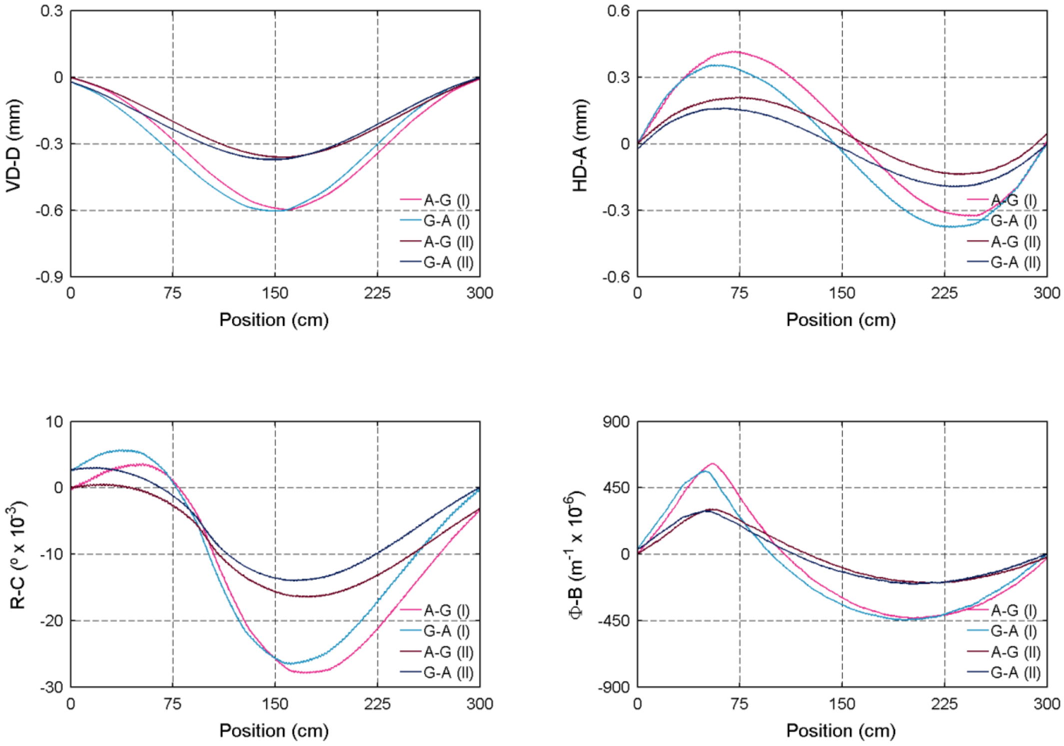

Figure 4.15 – Structural response of the laboratorial model under two different prestressing force scenarios.

depicts the structural response of the laboratorial model under a 10.2 kN point-load, moving forward (A-G) and backwards (G-A), for the two different prestressing force levels mentioned above, denoted respectively as I and II.

Although the decompression limit state is comfortably ensured in both cases, and thus every cross-section is compressed when the load crosses the structure, the structural deformation decreases when the prestressing force is increased. It may be concluded that the beam stiffness increases for higher compression stress levels. Besides that, the nonlinear behaviour observed under the lowest prestressing force level (I) is also observed under the highest one (II), although it is less pronounced. In addition, it should be mentioned that, as the “residuals” observed in the rotations at the end of the crossings are exactly the same in both prestressing force scenarios, these results emphasize that the supports deformability must be taken into account in the interpretation of the structure’s behaviour.

The results depicted in Figure 4.15 clearly show the stiffness increase as the presstress force increases. However, no indication is given regarding the proportionality of the influence-lines obtained in both cases. Hence, Figure 4.16 depicts the results obtained in both scenarios as the load moves forward (A-G) normalized by the highest absolute value: the measurements concerning scenario II are multiplied by a scale factor λ given by the ratio $\delta_{max,I}/\delta_{max,II}$, where

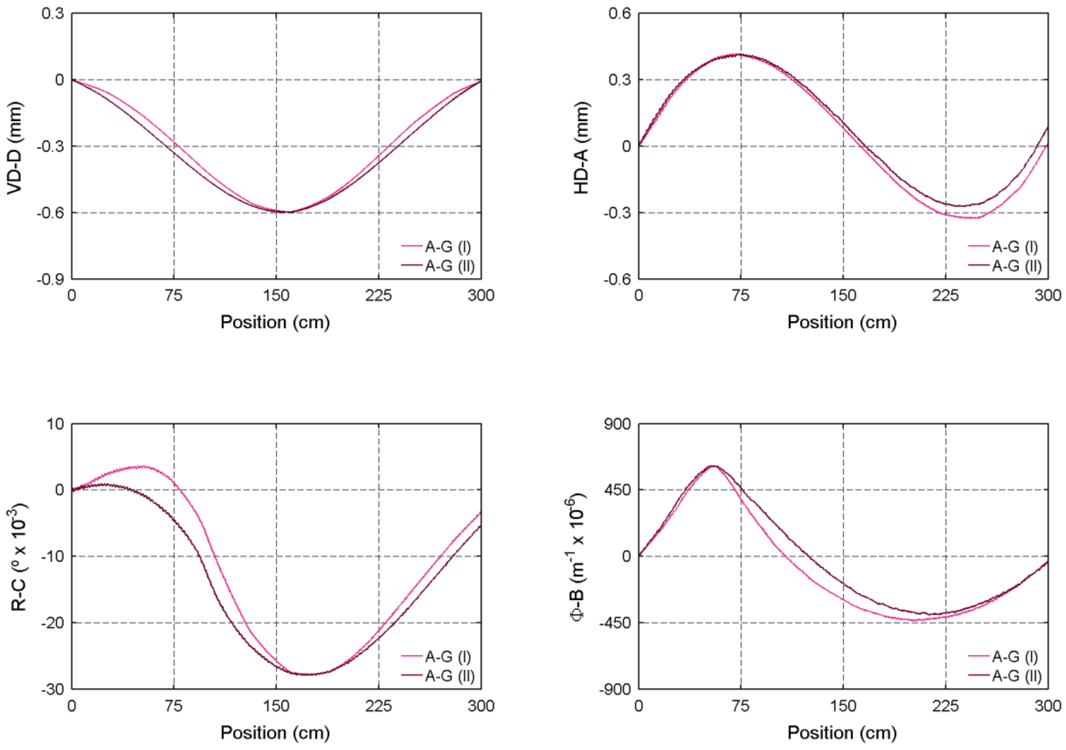

Figure 4.16 – Structural response of the laboratorial model, normalized by the maximum measurement, under two different prestressing force scenarios.

$\delta_{max,I}$ and $\delta_{max,II}$ are the maximum measurements recorded, respectively, in scenarios I and II. It is shown that the influence-lines obtained in the second scenario are not proportional to those obtained in the first one. As discussed above, the stiffness of the beam increases as the prestressing force increases. Therefore, the ratio between the beam and columns stiffnesses is changed. Consequently, as the structure is statically indeterminate, the distribution of the internal forces varies and, thus, the influence-lines' shape is different.

4.4.4. Analysis of the structural response under different load levels

With the purpose of assessing the proportionality of the response in relation to the magnitude of the moving point-load, a set of tests under different loads were carried out in similar conditions (namely under the same prestressing force). Figure 4.17 shows the tests results for nine load levels ranging between 8.8 kN and 14.6 kN, when the load moves forward (A-G). The prestressing force was 330 kN (165 kN in each strand). It should be stressed that even for the highest load level (14.6 kN) the decompression limit state is comfortably ensured. The results show that, on one hand, the structural response varies in accordance with the load level, and, on the other hand, the shape of the influence-lines looks similar for every case. Thus, despite the nonlinear behaviour discussed in the sections above, for a given prestressing force scenario, the structural response obtained when the load moves in a given direction appears to be proportional to the load level.

In order to assess the proportionality of the response in relation to the load level, Figure 4.18 depicts the results shown in Figure 4.17 normalized by the load level. The measurements for a given passage are multiplied by a scale factor λ_L given by the ratio P_{max}/P_i where P_{max} is the maximum load level ($P_{max} = 14.6$ kN) and P_i is the load in the passage under consideration. Although the resulting curves are very similar, slight differences may be noticed, namely as regards the maximum values. As the load level decreases, the scaled maximum values also decrease, although very marginally. Therefore, one may say that as the load level decreases the global stiffness of the structure increases. This conclusion is in accordance with the conclusion drawn in the previous section: as the prestressing force decreases, the global stiffness also decreases. Herein, as the load level increases, the compression state in the tensile chord decreases and, thus, the stiffness also decreases. Consequently, the structural response is not proportional to the load level.

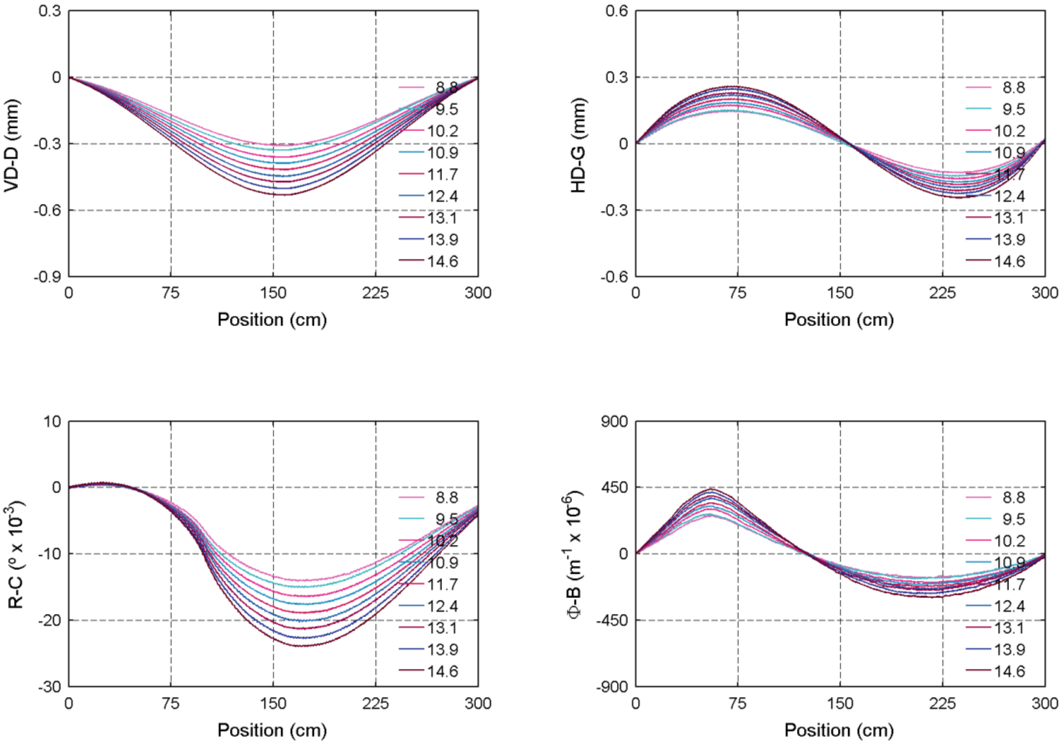

Figure 4.17 – Comparison of the structural response obtained for different load levels.

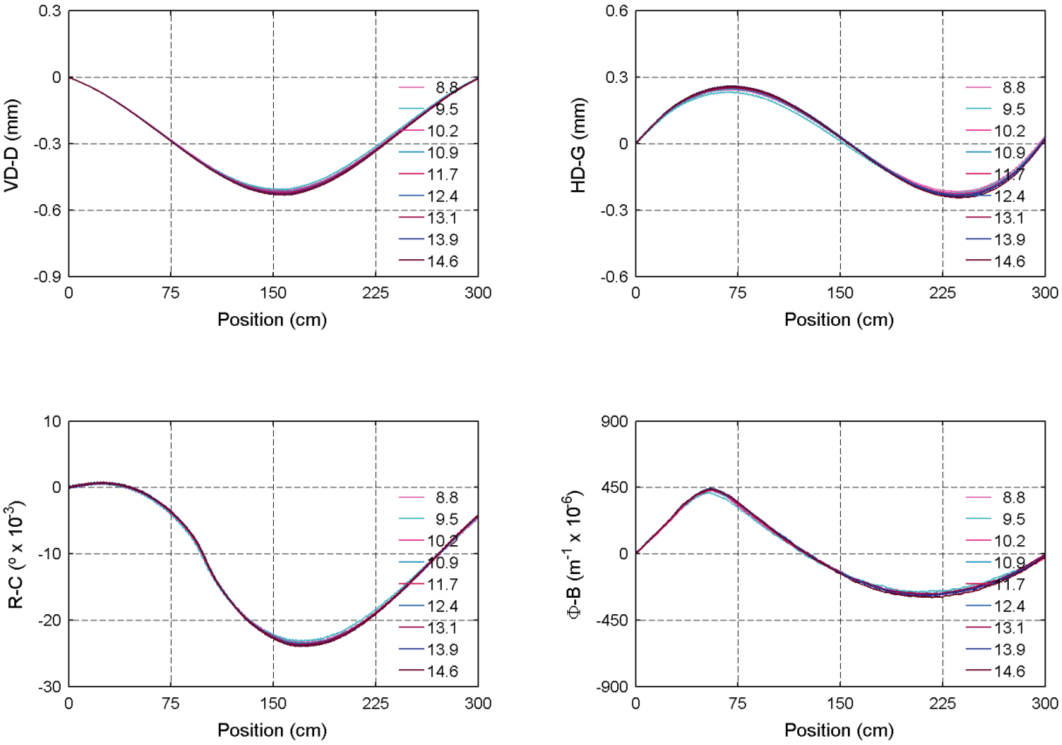

Figure 4.18 – Comparison of the structural response, normalized by the load level, obtained for different load levels.

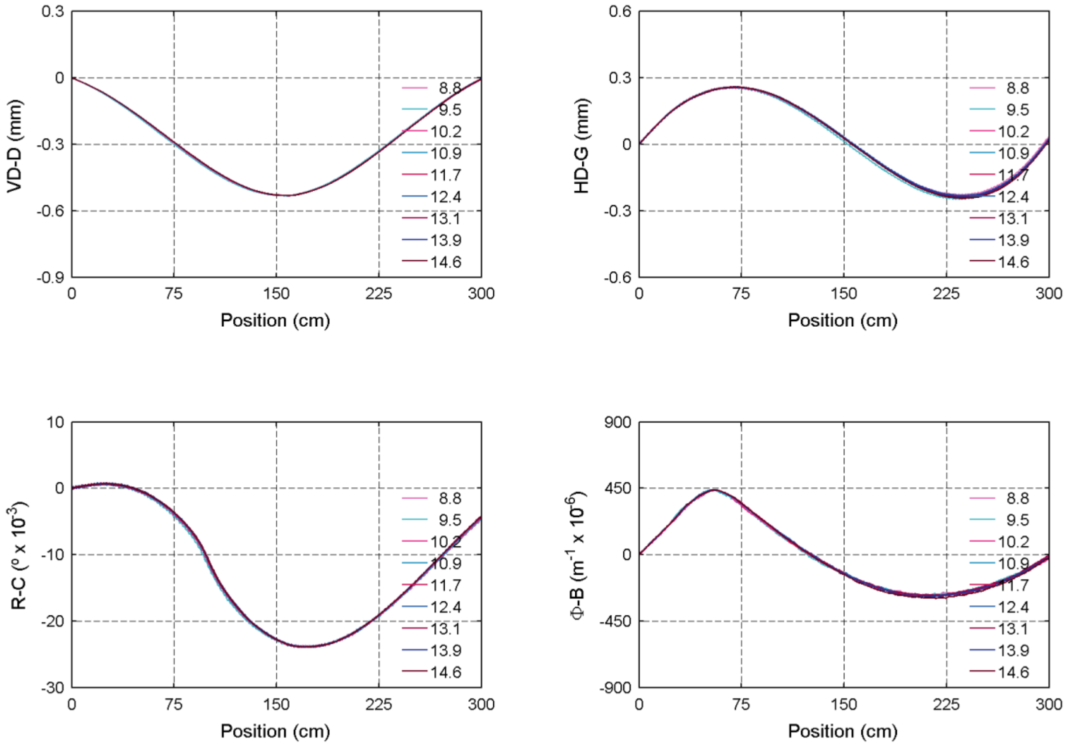

Figure 4.19 – Comparison of the structural response, normalized by the maximum measurement, obtained for different load levels.

However, when the results are normalized by the maximum response value, the various curves are overlapped, as shown in Figure 4.19. In these plots, the measurements for a given passage are multiplied by a scale factor λ_M given by the ratio $\delta_{max,Pmax}/\delta_{max,Pi}$ where $\delta_{max,Pmax}$ is the maximum measurement observed under the maximum load employed in the tests, and $\delta_{max,Pi}$ is the maximum measurement observed in the passage under consideration. As the scaled curves are equal, the shape of the influence-lines is the same for every load level. Hence, although the response is not linear with respect to the load level (see Figure 4.18), it is proportional to a fictitious load given by an adequate scaling of the actual load.

4.5. Conclusions

A deep understanding of the in-service behaviour of structures is paramount for successfully completing the damage process. In this context, this chapter discusses the in-service behaviour of reinforced and prestressed concrete bridges under moving-loads. A reduced-scale laboratorial model of a reinforced and prestressed concrete frame, subjected to a moving-load, was chosen as the case study. The experimental results showed that, although the concrete beam remains entirely under compression during a point-load passage, the structural behaviour was not linear. The analysis of the experimental results, supported by adequate numerical simulations, enabled to draw the conclusions addressed below.

Accurate measurements could be obtained for the structural response (displacements, rotations, average deformations and crack widths) of a bridge model crossed by a moving-load, by using a versatile loading system (enabling the load to be mechanically moved along the structure, and the total load to be easily modified) and by applying a Savitzky-Golay filter to smooth the measured data without distorting the intensity or the shape of the peak.

The laboratorial work provided useful information about the structural response due to a point-load crossing the structure, both forward and backwards, for different loads and under different prestressing force scenarios. The beam under analysis exhibits small-width cracks. However, all the cross-sections remain entirely under compression during the point-load passages, as a consequence of the applied prestressing forces. This is typical in real prestressed bridge decks, where decompression is prevented for normal traffic loading. In the tests, it was observed that, even though the cracks are closed (i.e. compressed) and the compression stress level is reduced, the structural behaviour was not linear. Firstly, the experimental influence-line depends on the direction in which the moving-load crosses the structure. Secondly, the response is not proportional to the magnitude of the moving-load. Thirdly, the response to a constant point-load crossing the structure depends on the applied prestressing force.

The dependency on the movement direction was justified and explained with the aid of finite-element analyses. It was demonstrated that, on one hand, that behaviour is due to the nonlinear behaviour of cracked concrete. On the other hand, the supports deformability also contributes to the dependency of the experimental influence-lines with respect to the movement direction. It was demonstrated that both effects exist in the structure under analysis.

It was shown that the frame’s beam exhibits a hysteretic behaviour during the reloading-unloading cycle that occurs when the point-load crosses the structure. That hysteresis can be observed in the moment-average curvature relationship. It was analysed with a numerical model which explicitly includes the cyclic constitutive behaviour at the interface between the longitudinal reinforcement and the surrounding concrete (bond effects) and the cyclic relationship between the crack opening and the concrete stress normal to the crack. It could be concluded that these effects justify the hysteretic behaviour of the beam when it is subjected to cyclic bending moments.

It was shown that, if the moving-load magnitude is changed while the prestressing force is kept constant, the structural response is not directly proportional to the load level. Still, the influence-lines for the different load magnitudes get coincident if they are normalized with respect to the maximum recorded value for the response parameter under analysis.

Finally, it was shown that the beams' bending deformations significantly decrease when the prestressing force is increased. Moreover, it was shown that the experimental influence-lines for different prestress values are not proportional. That lack of proportionality is justified by the structure hyperstaticity.

The previously exposed conclusions are relevant in the context of structural assessment of bridges based on the analysis of experimental influence-lines. The issues pointed out in this chapter regarding the nonlinear behaviour of bridges are, in general, neglected, either in laboratorial or field results. However, with the objective of applying sound damage detection techniques, aiming at a timely preventive maintenance and conservation of bridges, a detailed assessment providing an accurate characterization of the in-service behaviour of the structure is paramount.

Chapter 5

Damage identification based on moving-loads responses using numerically-simulated data

5.1. Introduction

Complex infrastructure systems ensure economic prosperity and quality of life. Therefore, maintaining civil infrastructure so that it is safe and reliable for daily use is important to all countries. However, existing infrastructure has suffered from decades of neglect and overuse, leading to accelerated deterioration of bridges, buildings, municipal and transportation systems, and resulting in a situation that has been described as "A global infrastructure crisis" (Bisby, 2004). Due to the age of existing bridges, increasing loads and changing requirements for use, maintenance and strengthening of bridges is becoming more and more important (Davis *et al.*, 2013; Kaschner *et al.*, 1999; Lounis, 2007). Often, the high costs of building new bridges are economically justifiable only through promise of longer service lives together with smaller maintenance costs compared with structures that are being replaced. Therefore, corrective maintenance of old structures is increasingly becoming a cost efficient alternative to the building of new structures (Sedlaccek *et al.*, 2007).

Structural health monitoring (SHM) is a term that describes the use of a range of measurement systems on structures, including data interpretation. The aim of these systems is to assist and inform owners of continued “fitness for purpose” of structures under gradual or sudden changes to their state and to learn about loading and response mechanisms (Brownjohn, 2007). SHM has potential to identify structural damage before it becomes critical, and thus represents a promising strategy in the ongoing challenge to achieve sustainable infrastructure (Farrar and Worden, 2007).

Today, many bridges are monitored using sophisticated measurement systems employing hundreds of sensors. These systems generate large amounts of data and it is often difficult to detect early damage (Zhang and Zhou, 2007). There is thus a need for data interpretation techniques that provide reliable information to assist engineers in structural management. The choice and implementation of algorithms to process the data and carry out the identification is arguably the most crucial ingredient of a SHM system. Before choosing the data-interpretation algorithm, it is necessary to choose between two complementary approaches to the challenge: model-based (*inverse strategy*) or data-driven (*pattern recognition*) (Worden and Dulieu-Barton, 2004). Model-based methods require the development of detailed numerical models of the structure. Measurements are compared with those predicted by the model with the aim of discovering anomalies in the behaviour of the structure. However, for civil infrastructure, creating such models is often difficult and expensive and this approach may not be successful in identifying the right anomaly. Data-driven methods consist of looking for changes in a "signature" of the structure that is related to its structural response under excitation. Anomalous behaviour is detected without information of physical processes requiring only initial conditions (no-anomalies) for training. Thus, these methods are generally faster than model-based methods as they do not require the evaluation of computation-intensive numerical models. Strengths and weaknesses of both classes have been summarized in (ASCE, 2011).

Since data-driven methods involve only tracking changes in signals, they are appropriate for analysing measurements during continuous monitoring of the performance of structures. Moyo and Brownjohn (2002) applied the wavelet analysis and Omenzetter and Brownjohn (2006) used auto-regressive integrated moving average (ARIMA) models to identify events and changes in the structural state in a bridge. Lanata and Del Grosso (2006) applied the proper orthogonal decomposition (POD) to identify in time and locate in space the initiation of damage. Posenato *et al.* (2010) presented two statistical methods: moving principal component analysis (MPCA) and robust regression analysis (RRA) for damage detection during continuous static monitoring of civil structures. Through a comparative study with other statistical analyses, they observed superior performance of these methods for damage detection.

Some methods have used the regular traffic responses to detect damage. Cardini and DeWolf (2009) presented an approach based on determining the live load distribution factors for the girders, peak strains and the neutral axis locations from the strain data collected from normal truck traffic (Chakraborty and DeWolf, 2006) to provide a continuous picture of the structural integrity of multi-girder steel bridges. Zaurin and Catbas (2011) proposed a method in which video images and sensor data are correlated and used to create a series of unit influence-lines (UIL) that are used as input features to detect and localize damage in the structure.

When periodic static loading tests are available, damage may be detected by comparing either the deflection curves or the influence-lines of displacements and rotations before and after damage. Choi *et al.* (2004) derived and proposed an *elastic damage load theorem* (EDLT) and demonstrated that the variations of the displacement reach the maximum at the damaged location independent of the location. Stohr *et al.* (2006) showed that the differences between the influence-lines of inclination measured under original and under modified structural conditions indicate clearly the existence and locations of stiffness changes. However, the application of these methods involves periodic static-load tests under controlled conditions, requiring the interruption of regular traffic. Furthermore, they imply knowing precise load levels used in the tests. Thus, in order to detect damage using influence-line data, development of other strategies is necessary.

This work presents an approach to perform damage detection based on moving-load data of regular traffic. The exact load level that is crossing the structure does not need to be known. The approach consists of applying two data-driven methods – MPCA and RRA – that have already been shown to be successful in continuous monitoring, to another type of data, influence-line information. It is worth noting that only the quasi-static component of the response is taken into consideration in the study. The objective is to detect and to localize the damage. Section 5.2 presents the framework and the approach adopted in order to use these two methods on influence-line data. In the third section the use of each method for SHM is briefly described. Finally, using numerically-simulated data, section 5.4 presents the results obtained with each method.

5.2. Methodology

5.2.1. General remarks

This section describes how influence-line data may be used for damage detection. The shape and magnitude of the influence-line of a bridge load effect is representative of its static behaviour. However, the regular traffic response may contain a dynamic component. Dynamic components are particularly present in light-weight steel pedestrian bridges. In the case of a concrete medium-span bridge with smooth wear surface and joints, the dynamic component caused by a moving vehicle on the bridge response is generally negligible (González and OBrien, 2008). However, in some situations the dynamic component in the signal cannot be neglected. Therefore, the removal of the dynamic component of the signal prior to the application of this methodology is required. Paultre *et al.* (1995) proposed the application of a digital low-pass filter to the measured time-series whereas González and OBrien (2008) employed wavelet analysis to extract the total static component from the measured bridge response. Thus, considering these filtering techniques to remove the dynamic component of the signal, the present methodology takes into consideration the quasi-static response of the structure only. The damage detection procedure proposed herein is illustrated by using a simple frame. The need for employing advanced methodologies to process the influence-line data obtained under different load levels is first demonstrated. Then, the approach proposed for using moving-load measurements for model-free interpretation is presented.

5.2.2. Description of the frame

The structure adopted to illustrate the employment of data-driven methods applied to moving-load responses for damage detection was a simple frame, 150 cm high and 320 cm long, as shown in Figure 5.1. The elements are 50 cm wide and 20 cm thick. The geometry of the frame’s bases, 40 cm long and 20 cm thick, allow different positions for the supports. In normal operating conditions the supports are centred in the middle of the columns cross-section. The left support is a roller bearing, allowing horizontal displacements and rotations over the longitudinal direction. The right support is a pinned bearing, restraining the horizontal displacement but allowing the rotation over the longitudinal direction. Therefore, considering vertical loads only and ensuring this bearings configuration, the response of this frame is the same as that of a simply supported beam.

This structure was chosen because of planned future research involving the experimental validation of the methodology. Through simple modifications, the study of several structural systems is possible. The structural response of the frame for the support conditions described above is equivalent to that of a simply supported beam. However, by replacing the roller bearing by a pinned one, this structure becomes a concrete rigid-frame that resembles a bridge which is typically used for either overpasses or underpasses. In addition, under these support conditions, the beam’s response is similar to that of the central span in a 3-span continuous beam. Finally, considering once again the support conditions and loading illustrated in Figure 5.1, it may be viewed as a model of a beam where the distance of the support bearings to the longitudinal axis of the beam is amplified. This facilitates studies of bearing stiffness properties for investigations of the effects of bearing malfunction. Therefore, in the context of future research into the validation of this methodology in the laboratory as well as other studies, this very compact and versatile model enables testing of a wide variety of scenarios.

The response is assumed to be linear and elastic, where the Young's modulus has been assumed to be 15 GPa. This relatively low value was obtained through experimental testing. Using the numerical model, the structural response is estimated for a set of successive positions along the beam, which, for practical applications, is numerically equivalent to monitoring the structure while a point-load moves across the frame at a slow speed. The results are presented graphically in the form of influence-lines that represent the variation of response at a given point due to a load traversing the structure. As depicted in Figure 5.1, the response of the structure is characterized through two displacements – the vertical deflection at mid-span (VDM) and the horizontal displacement at the roller support (HDR) – and two rotations – the rotation over the left support bearing (RLB) and the rotation over the right support bearing (RRB).

In order to make the study more realistic, noise was added to the simulated data. Sensor noise was assumed to have a uniform probability density function. The range, assumed to be ±0.01 mm for displacements and $\pm 1° \times 10^{-3}$ for rotations, is based on observations made during preliminary laboratory testing that was aimed at quantifying the precision of the sensors as well as ambient electrical noise.

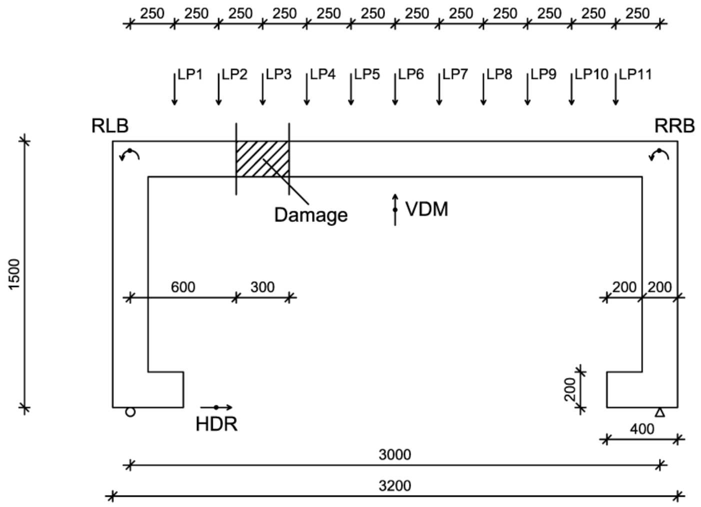

Figure 5.1 – Frame model.

5.2.3. The problem of detecting damage under different load levels

Consider a damage scenario corresponding to a local crack in a pre-stressed and reinforced concrete element. For the sake of simplicity it will be represented as a 20% stiffness reduction in a 30 cm length beam-element, as depicted in Figure 5.1. This damage scenario leads to an increase of 2% in the vertical deflection at mid-span under a point-load placed at mid-span. For example, under a service load of 8.75 kN, the vertical deflection varies from 1.00 mm to 1.02 mm before and after damage, respectively.

Comparing the responses, under a given load value, before and after the stiffness reduction, both the occurrence and the location of the damage can be detected. As shown in the plots of

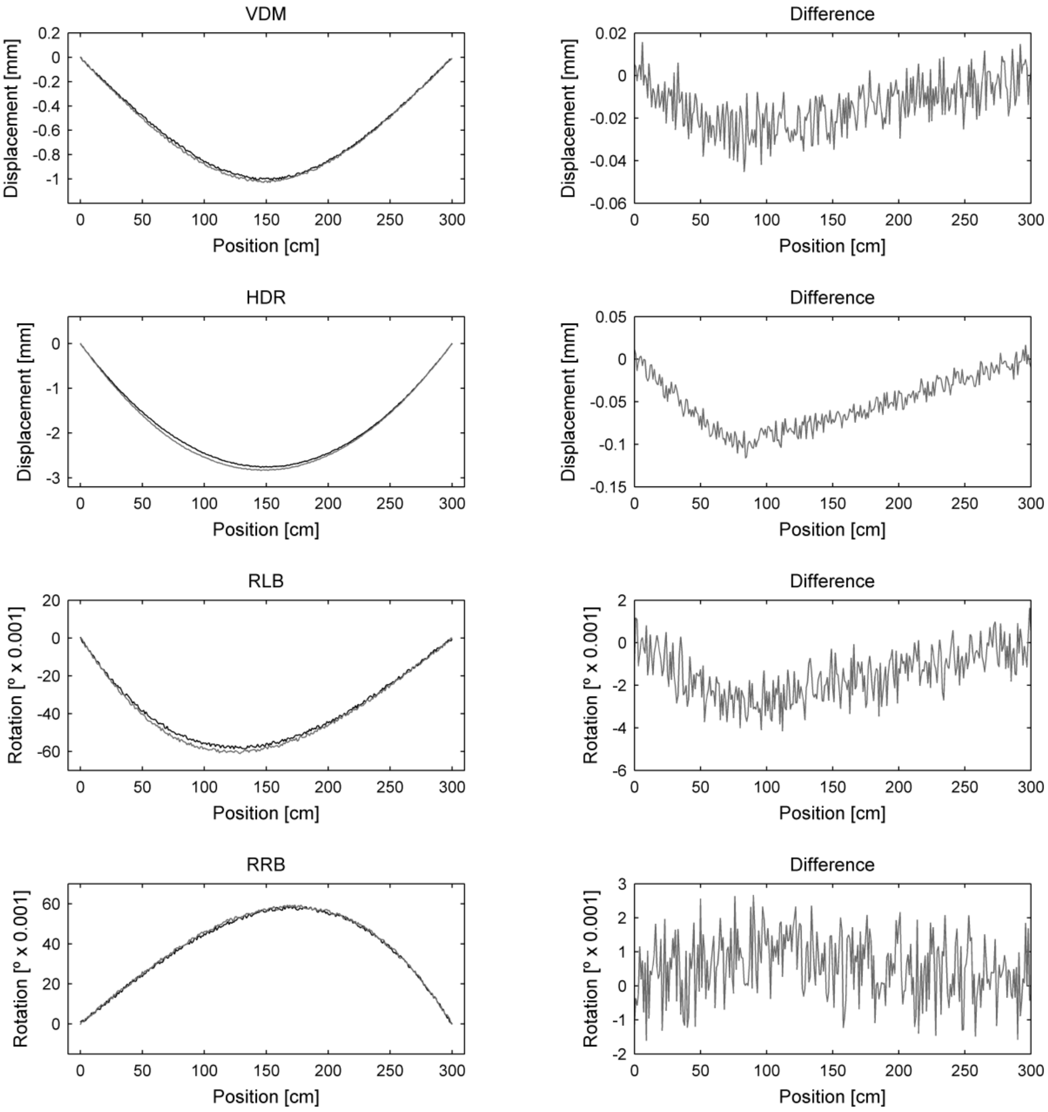

Figure 5.2 – Comparison of the influence-lines in the baseline condition (black) and in the damaged condition (gray), left, and the corresponding differences between the responses, right.

Figure 5.2 (left), since the influence-lines obtained before (black) and after (gray) damage are slightly different, comparing them can be a means of detecting changes in the structural condition. However, the location of the damage remains unknown. Nevertheless, as shown in (Choi *et al.*, 2004) and (Stohr *et al.*, 2006), computing the differences between the influence-lines, allows the determination of the damage location, which corresponds to the position of the highest difference. As depicted in the plots of Figure 5.2 (right), the position of the largest differences corresponds to the region of the stiffness reduction. However, if the load crossing the structure is not exactly the same before and after the occurrence of damage, no significant difference may be noticed and, thus, the occurrence of damage may not be detected.

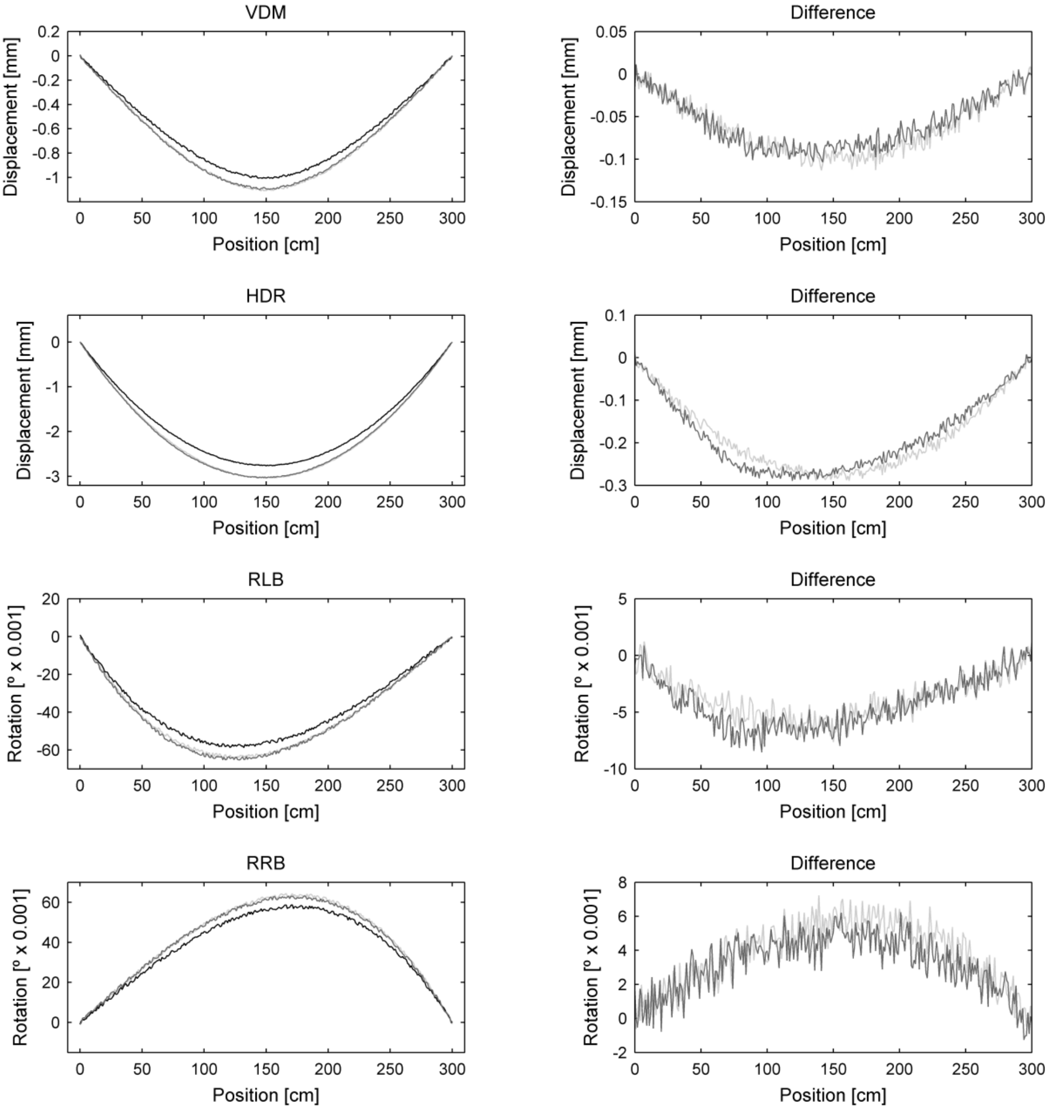

Figure 5.3 – Comparison of the influence-lines in the: i) baseline condition, under the reference moving-load – ML (black); ii) baseline condition, under 1.10xML (light gray); iii) damaged condition, under 1.07xML (gray), left, and the differences between the responses ii-i (light gray) and iii-i (gray), right.

Consider, for example, that the uncertainty in quantifying the load is ±10%. Figure 5.3 presents the responses of the structure: i) under the reference moving-load (ML), before damage (black); ii) under 1.10xML, before damage (light gray); and iii) under 1.07xML, after damage (gray). The difference between the influence-lines for a load 10% higher than the reference load before damage and for a load 7% higher than the reference load after damage is negligible (Figure 5.3, left). Furthermore, the differences between these influence-lines and those obtained under the reference load before damage are very similar (Figure 5.3, right). Therefore, when the load cannot be quantified accurately, and thus, is uncertain, the occurrence of damage may not be detected. Therefore, in order to detect the occurrence of damage using influence-line data, the application of another strategy is necessary.

5.2.4. Model-free interpretation of moving-load measurements

The approach proposed in this chapter regarding the application of data-driven methods to detect damage involves building time-series using moving-load data. Consider a period in which n_c crossings of vehicles were recorded and, in each passage, the response at n_p equally spaced points was recorded. Two types of time-series – type i and type ii – can be built.

A time-series type ii involves the whole influence-line. Whenever a load crosses the structure its response is collected and recorded in a time-series that includes the previous crossings, leading to a time-series containing n_m measurements, in which $n_m = n_c \times n_P$. The i^{th} measurement in the time-series corresponds to the value recorded at the q^{th} position on the structure during the k^{th} passage, as expressed in equation (5.1):

$$i = (k-1) \cdot n_p + q \tag{5.1}$$

Figure 5.4 presents a time-series containing 29 influence-lines ($n_c = 29$) of the vertical displacement at mid-span (VDM), under a load uncertainty of ±10%, ranging from 0.90 to 1.10 times a service load of 8.75 kN, according to a uniform probability density function. Each influence-line involves 301 measurements ($n_p = 301$), leading to a total of 8729 observations.

A time-series type i involves the response at a given load position (LP) for the successive crossings. Therefore, each time-series contains n_c measurements. Based on the response recorded by each sensor one can build as many time-series as the number of load positions considered for the data acquisition. In Figure 5.5 the time-series of the vertical displacement at mid-span (VDM) when the load was also at mid-span, load position 6 (see Figure 5.1), is presented. Note that this time-series is based on the same data presented in Figure 5.4.

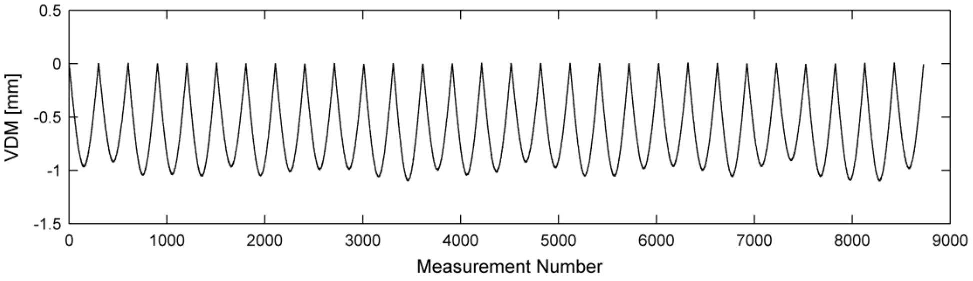

Figure 5.4 – Time-series type ii, of the vertical displacement at mid-span (VDM)

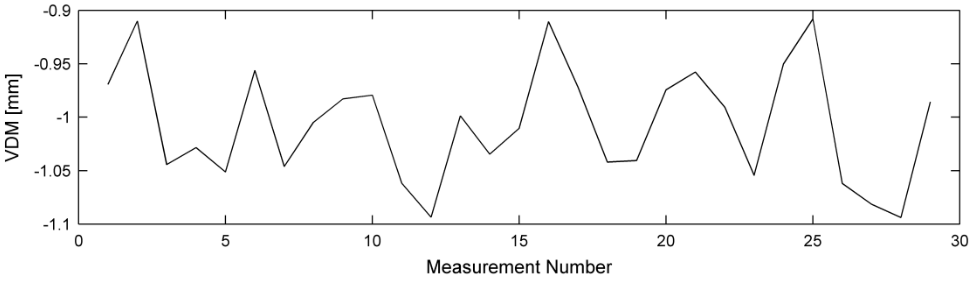

Figure 5.5 – Time-series type i, of the vertical displacement at mid-span (VDM) when the load is at mid-span, LP6.

Using these two types of time-series, the damage detection procedure will be carried out using two data-driven methods: moving principal component analysis (MPCA) and robust regression analysis (RRA).

5.3. Data interpretation methods

5.3.1. Moving principal component analysis

The purpose of the principal component analysis (PCA) is to identify dependencies behind a multivariate stochastic observation in order to obtain a compact description. Consider a dataset, $X\epsilon\ \mathfrak{R}^{n\times p}$, as expressed in equation (5.2), consisting of n observations on p variables. The rows are p-dimensional vectors representing the measurements of the variables at a given instant, whereas the columns are n-dimensional vectors corresponding to the time-history of each variable.

$$X = \begin{bmatrix} X_{1,1} & X_{1,2} & \cdots & X_{1,\mathrm{p}} \\ X_{2,1} & X_{1,2} & \cdots & X_{2,\mathrm{p}} \\ \cdots & \cdots & \cdots & \cdots \\ X_{\mathrm{n},1} & X_{\mathrm{n},2} & \cdots & X_{\mathrm{n},\mathrm{p}} \end{bmatrix} \tag{5.2}$$

The goal of PCA is to reduce the dimensionality of the data matrix by finding r new variables, where r is less than p. Termed principal components, these r new variables together account for as much of the variance in the original p variables as possible while remaining mutually uncorrelated and orthogonal. Each principal component is a linear combination of the original variables, and so it is often possible to ascribe meaning to what the components represent. The first component corresponds to the direction in which the projected observations have the largest variance. The second component is then orthogonal to the first and again maximizes the variance of the data points projected on it. Continuing in this manner, it is possible to compute all the principal components (Hubert *et al.*, 2005). Equation (5.3) expresses the matrix of the observations, $[X]$, as a linear combination of a set of p orthogonal vectors, $[U_j]$.

$$[X] = \sum_{j=1}^{p} [Z_j][U_j]^T \tag{5.3}$$

$[Z_j]$ is a vector containing the component scores corresponding to the j^{th} variable and $[U_j]$ is the j^{th} orthogonal vector. The component scores correspond to the coordinates of the original data in the new coordinate system defined by the orthogonal vectors, which are the eigenvectors computed from the covariance matrix $S \epsilon \Re^{p \times p}$ of the dataset. As the first eigenvalues represent the most important terms, it is possible to choose only the first r eigenvectors so that the final dataset can be rewritten without significant loss of information, as expressed in equation (5.4):

$$[X] \cong \sum_{j=1}^{r} [Z_j][U_j]^T \tag{5.4}$$

In the structural health monitoring field, PCA may be used for three primary purposes (Figueiredo *et al.*, 2009): (i) evaluation of patterns in the data; (ii) data cleansing; and (iii) data compression.

In the context of this work, it is used to enhance the discrimination between features of undamaged and damaged structures. The analysis of the behaviour in time of eigenvalues and eigenfunctions of the covariance matrix of the dataset gives a good indication of the damage initiation and can provide information about the severity of the damage (Lanata and Del Grosso, 2006). However, as the observation period increases, and therefore, the number of measurements becomes high, the time to detect the structural change also increases. When damage occurs, the influence of measurements in the undamaged state is much higher than that of the new measurements, leading to an increase in the time required for the eigenvector values to change enough in order to indicate damage.

To overcome this shortcoming, Posenato *et al.* (2008) proposed moving principal component analysis (MPCA) that computes the principal components inside a moving window of constant size, containing n_w measurements $(n_w < n)$. For the k^{th} observation, the matrix X of the measurements becomes the following:

$$X(k) = \begin{bmatrix} X_{k-n_w+1,1} & X_{k-n_w+1,2} & \cdots & X_{k-n_w+1,p} \\ X_{k-n_w+2,1} & X_{k-n_w+2,2} & \cdots & X_{k-n_w+2,p} \\ \cdots & \cdots & \cdots & \cdots \\ X_{k,1} & X_{k,2} & \cdots & X_{k,p} \end{bmatrix} \tag{5.5}$$

Then, the monitoring is carried out by observing the evolution of the principal components – the eigenvectors that are related to the first few eigenvalues. Damage is identified when there is a change in the values of the principal components. Considering that each $\left[Z_j\right]$ describes a major trend of the original data and that each component $U_{i,j}$ of the vector $\left[U_j\right]$ describes the influence of $\left[Z_j\right]$ for the i^{th} sensor, MPCA can be applied for anomaly detection in the continuous static monitoring of civil structures. If the group of series considered in the analysis are correlated and if the structure has not been damaged then the main eigenvalues and the corresponding eigenvectors remain stable with time. When something occurs in the structure, the signals of some sensors may vary with respect to others. As a consequence, eigenvector components $U_{i,j}$ of the sensors closest to the zone involved by the new situation should highlight the variation. This feature enables not only the damage identification but also the damage localization (Lanata and Del Grosso, 2006; Posenato *et al.*, 2008).

Application of MPCA for damage detection using continuous monitoring data involves two phases: training and monitoring. In the training phase, the structure is assumed to behave in an undamaged condition. The aim of this initialization period is to estimate the variability of the time-series and to define the thresholds for detecting anomalous behaviour in the monitoring phase. To do this, each eigenvector U_j at every time step during the reference period is stored and values, in each coordinate, $U_{i,j}$, for mean, $\mu_{i,j}$, and standard deviation, $\sigma_{i,j}$, are determined in order to define the corresponding thresholds. In the monitoring phase, the window continues moving along time-series to compute new eigenvalues and eigenvectors at each time step. If there is no anomaly, the eigenvectors remain within these thresholds. When damage occurs, the components of the covariance matrix change and as a consequence, so do values of eigenvalues and eigenvectors. If the value of the c^{th} coordinate of the eigenvector U_j ($U_{c,j}$) exceeds the threshold bounds, an anomaly is flagged by sensor c at time k (Laory *et al.*, 2011).

A key issue of MPCA is the dimension of the window, n_w. The value n_w should be sufficiently large so that it is not influenced by measurement noise and small enough to allow fast anomaly detection. Additionally, if the time-series has periodic variability, the window size should be a multiple of the period, so that mean values are stationary and eigenvalues of the covariance matrix do not have periodic behaviour (Posenato, 2009).

Comparing MPCA with PCA, the use of a moving window rather than all measurements has three main advantages. First, the calculation of process parameters is faster. Second, detection of anomalous behaviour is more timely because the old measurements do not bias the results. Finally, once new behaviour is identified, the definition of a new training phase corresponding to the new state of the structure allows detection of further anomalies (Posenato *et al.*, 2008).

5.3.2. Robust regression analysis

Many problems in engineering and science involve exploring the relationships between two or more variables. Regression analysis is a statistical technique that is very useful for this type of problems (Montgomery and Runger, 1999). It is normally used to detect anomalous behaviour in two ways. One method consists in evaluating how the distance between the points and the regression line change with time. The other consists of observing the evolution of the coefficients of the regression. Anomalies are identified whenever a significant variation is observed (Posenato, 2009).

The algorithm involves the calculation of a robust regression line between two sensors for the reference period which is used to discover anomalies in the trends of the measurements. The linear relation between two variables, X and Y, can be written as:

$$\hat{y} = \beta_0 + \beta_1 \cdot x \tag{5.6}$$

Where $\hat{y}$ represents the value of y calculated according to the linear relation and β_0 and β_1 are the coefficients of the robust regression line estimated from measurements in the training phase. The method used to compute the coefficients in equation (5.6) consists in assigning a weight to each data point. Weighting is done automatically and iteratively using a process called *iteratively reweighted least squares*. In the first iteration, each point is assigned equal weight and model coefficients are estimated using ordinary least squares. At subsequent iterations, weights are recomputed so that points farther from model predictions in the previous iteration are given lower weight. Model coefficients are then recomputed using weighted least squares. The process continues until the values of the coefficient estimates converge within a specified tolerance (MatLab, 2012). An advantage of robust regression in comparison with traditional regression is its insensitivity to outliers.

In this work damage detection is based on the first approach presented above, which involves the calculation of $\hat{y}_i$ at every instant of observation and the corresponding differences $e_i = y_i - \hat{y}_i$. As in the MPCA, application of RRA for anomaly detection during continuous monitoring includes two phases: training and monitoring. In the training phase the structure is assumed to behave normally (no damage). During the reference period, the mean, μ_j, and the standard deviation, σ_j, of the differences e_i are determined in order to define the corresponding thresholds. In the monitoring phase, at each time step k, if the differences e_i in N_{out} measurements within a window ranging from time step $k - N_{test}$ to k, in which $N_{out} \leq N_{test}$, are out of the threshold bounds, the anomaly is detected by the variable pairs X and Y.

In addition to the advantage of being insensitive to outliers and missing data, RRA is capable of adapting to the new state of a structure for identifying further anomalies by redefining a new training phase after an anomaly is identified.

5.4. Application to numerically-simulated data

5.4.1. Simulated data

The proposed approach will be tested on data obtained through using the numerical model presented in section 5.2.2. A load variability of ±10% around a service load of 8.75 kN and uniformly distributed noise in the measurements as also described in section 5.2.2 will be assumed. Consider a period of observation in which the response of 1500 crossings of the structure was collected. The first 1000 crossings are the baseline condition (undamaged) and the latest 500 are the damaged condition. As described above, the damage scenario under consideration consists of a 20% reduction in the stiffness of a 30 cm long beam-element (see Figure 5.1).

According to the two types of time-series that can be built using the moving-load data presented above, the following two types of analysis are performed:

a) 4 time histories of type ii (4 transducers employed);

b) 44 time histories of type i (11 load positions, as depicted in Figure 5.1, times 4 transducers).

Figure 5.6 and Figure 5.7 present respectively, a time-series of type ii and type i, for the rotation over the left support (RLB). The former involves the whole influence-line whereas the latter is for load position 3, which is the damage location (see Figure 5.1). Figure 5.6 (b) and Figure 5.7 (b) are magnifications of parts of Figure 5.6 (a) and Figure 5.7 (a), respectively, considering 23 crossings before and after the occurrence of damage. No significant differences in the signals, indicating the occurrence of damage, can be observed. Although in Figure 5.7 there is a slight difference between the response before and after damage, a small increase in the load variability would hide this difference and, thus, the occurrence of damage might not be detected. Therefore, the application of more sophisticated data-processing is necessary.

In this section, using these two types of time-series, two data-driven methods – moving principal component analysis (MPCA) and robust regression analysis (RRA) – will be applied to detect both the occurrence and the location of damage. The capability of each method, as well as the time to detection will be evaluated. Throughout this chapter the time to detection, also referred to as *delay*, corresponds to the number of crossings observed between the occurrence and the detection of the damage.

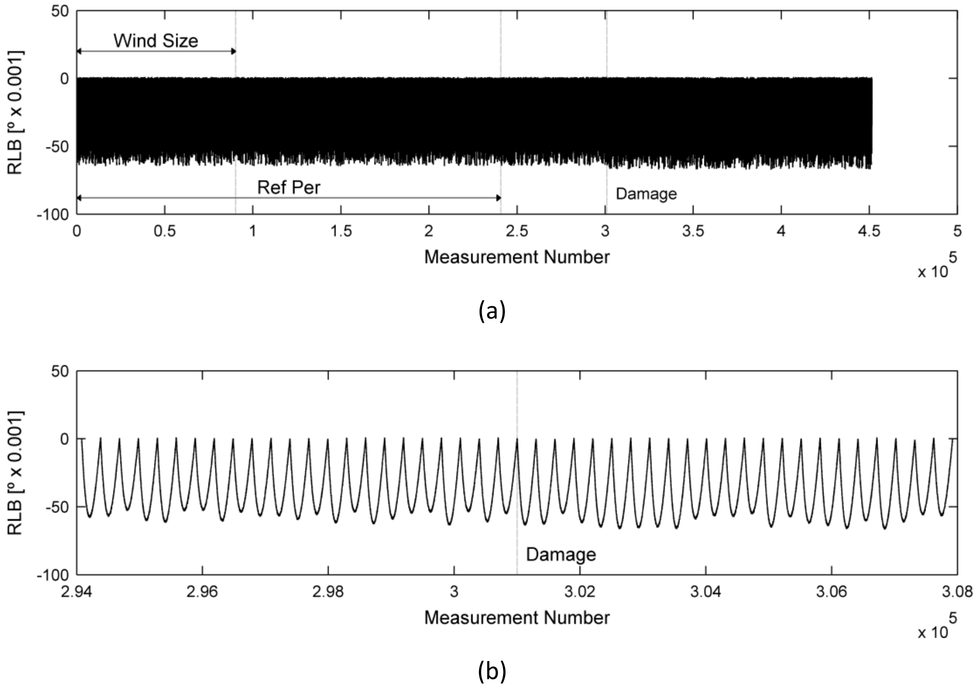

(a)

(b)

Figure 5.6 – Time-series type ii, of the rotation over the left support (RLB): (a) whole period; and (b) expansion of part of the whole period.

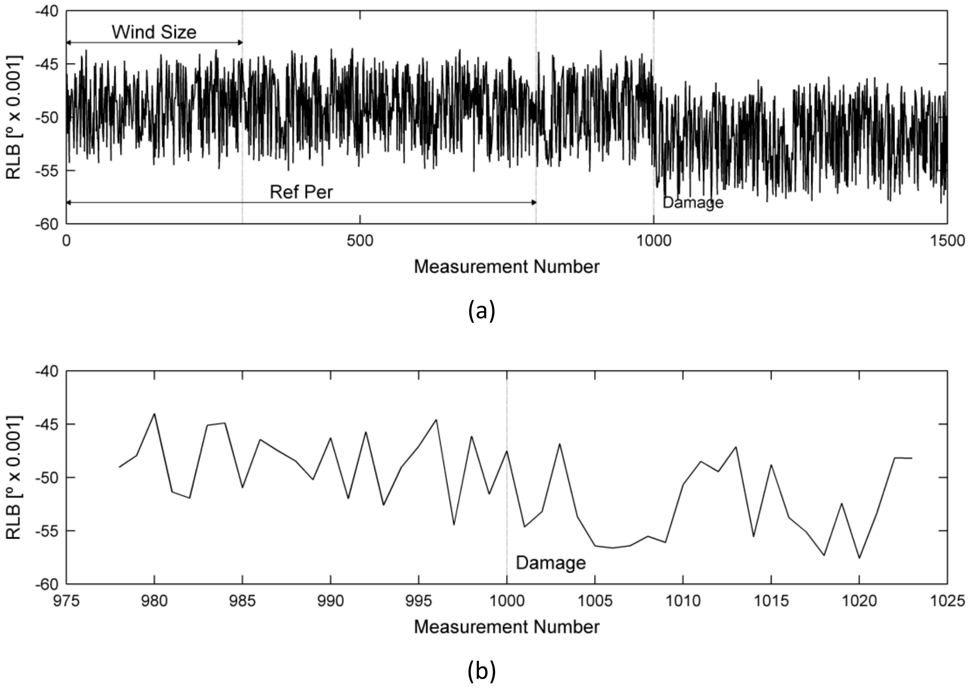

Figure 5.7 – Time-series type i, of the rotation over the left support (RLB): (a) whole period; and (b) expansion of part of the whole period.

5.4.2. Moving principal component analysis

MPCA was applied to both datasets – type I and type II. To compare the performance of the method the parameters such as reference period, window size and thresholds, were assumed to have the same values for both types of analysis.

As mentioned above, application of MPCA to structural health monitoring involves an initial phase where the structure is assumed to behave normally and this is called the training phase. The aim of this reference period is to estimate the variability of the time-series and to define thresholds for detecting anomalous behaviour. In this study, the training phase comprised 800 crossings, in which both the mean, μ, and the standard deviation, σ, were computed in order to define thresholds for damage detection.

During the monitoring phase, as soon as n_{cp} consecutive points exceed the threshold a structural change is flagged. The requirement of n_{cp} consecutive points exceeding the thresholds in order to flag a structural change increases the reliability of the methodology by preventing false positive indications of damage. In this work, the thresholds were assumed to be $\mu \pm 9\sigma$ and $n_{cp} = 10$. These unusually high levels are necessary to avoid false-positives arising from the response of a beam subjected to moving-loads. The window size, n_w, was defined by taking into account the features of the time-series.

The time-series type ii presents periodic variability (Figure 5.6), corresponding to the number of positions observed in each crossing ($n_p = 301$). Therefore, the window size should be a multiple of n_p. In addition, the time-series type i does not present periodic variability (Figure 5.7) given that each time-series contains the response at a given position for the successive crossings. Therefore, the variability is due to both the measurement noise and the variability in the load. Thus, a window comprising 300 crossings, leading to $n_w = 300$ and $n_w = 300 \times 301$ for, respectively, time-series type i and type ii. This size enables that calculations are not significantly influenced by measurement noise in time-series type i. The window size (Wind Size) and the reference period (Ref Per) are marked both in Figure 5.6 and Figure 5.7.

The application of MPCA requires computing the principal components (PC) inside a moving window of constant size along the time-series. In practice, computing PCs of a dataset X_0 entails (Shlens, 2009):

i. subtracting off the mean of each measurement type, as expressed in equation (5.7) – denoted as normalization a – where $X_{0,i}$ represents the time-series of the variable i (which may be the time-history of a given sensor in the dataset of type ii or the time-history of a given sensor for a given load position in the dataset of type i) and μ_i is the corresponding mean;

$$X_i = X_{0,i} - \mu_i \tag{5.7}$$

ii. computing the eigenvectors of the covariance matrix S of the dataset.

As previously described, when something occurs on or in the structure, measurement data from some sensors may vary with respect to data from other sensors. As a consequence, the main eigenvalues change and the eigenvector components $U_{i,j}$ of the sensors closest to the zone involved by the new situation should highlight a variation. If the value of the c^{th} coordinate of the eigenvector U_j ($U_{c,j}$) exceeds the threshold bounds, an anomaly is flagged by sensor c at time k and, thus, it is expected that damage is located close to sensor c. The figures presented below illustrate the results of the MPCA. They show the evolution of the coordinate of the first principal component (eigenvector) that first exceeds the thresholds, i.e., the coordinate that first flags the damage. As the sensors closest to the damage should highlight the variation, it is expected that the sensor related to this coordinate may be near the damage. In particular, for time-series type i, as each time-series is related to a load position, it may be seen as a time-series of a sensor. Therefore, it is expected that damage may be localized by the time-series related to LP3, placed over the damage, or LP2 or LP4, close to the damage.

Figure 5.8 presents the time-series of the coordinate related with RLB of the first principal component given by MPCA using the time-series of type ii. Figure 5.9 presents the time-history of the coordinate related with HDR and load position 3 of the first principal component using the time-series of type i. As can be seen in the figures, the data-processing using MPCA allows the early detection of changes in the structural response and the location of damage. Using the time-series type ii, the damage was detected 15 crossings after the occurrence of the damage (Figure 5.8). Using the time-series type i, the first coordinate of the first principal component exceeding the thresholds (Figure 5.9) corresponds to load position 3, which matches the location of the stiffness reduction (see Figure 5.1). In this case, the delay was 27 crossings.

However, as it will be shown, after performing several analysis adopting different random sequences, in terms of load variability and noise in the measurements, it was observed that the damage location is seldom correctly identified.

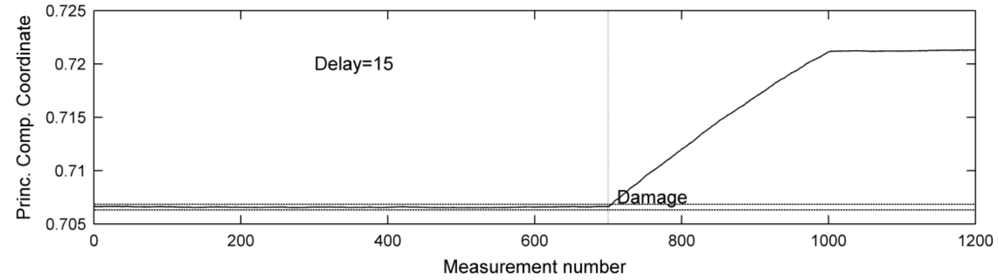

Figure 5.8 – Time history of the coordinate corresponding to the RLB of the first principal component applying MPCA on time-series type ii using normalization a.

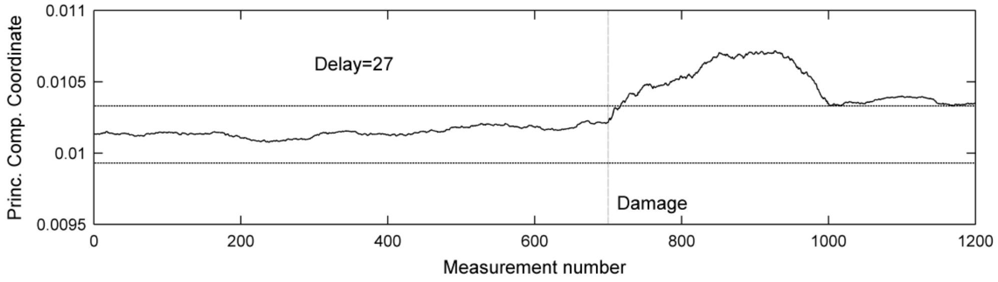

Figure 5.9 – Time history of the coordinate corresponding to the HDR for load position 3 of the first principal component applying MPCA on time-series type i using normalization a.

Consider an additional step prior to the calculation of the eigenvectors. After subtracting the mean of each measurement type, the data is divided by the standard deviation of each variable, σ_i, as expressed in equation (5.8). This procedure will be denoted as normalization b.

$$X_i = \frac{X_{0,i} - \mu_i}{\sigma_i} \tag{5.8}$$

The results presented in Figure 5.10 and Figure 5.11 refer to the MPCA using pre-processed data through the normalization b. Figure 5.10 presents the time-history of the coordinate corresponding to RRB of the first principal component using the time-series type ii. The time-history of the coordinate corresponding to RLB at load position 3 of the first principal component using the time-series type i is depicted in Figure 5.11. As in the normalization a procedure, the results adopting the normalization b procedure show that the occurrence and the location of the damage may be detected. Again, the coordinate of the principal component that first exceeds the threshold corresponds to the load position 3. The delay using time-series of type ii and i was, respectively, 79 and 32 crossings.

As previously noted, damage is detected when a coordinate value of a principal component exceeds the threshold bounds. Afterwards, as soon as the moving window contains data of the damaged condition only, a new state of the structure is defined. In Figure 5.8 and Figure 5.10, as after damage the value of the coordinate stabilizes in a different value than that before damage, the modification into a new state is clear. In Figure 5.9, in spite of being very close, the new state is different from the old one. However, in Figure 5.11 the two states are similar. This is due to the type of data and normalization used. As the data is divided by the standard deviation, the normalized data of the new state happens to be similar to that of the old state. The same does not happen in Figure 5.10 because it includes all the influence-lines and as their shape change due to damage, the new state is different from the old one, even after normalization b.

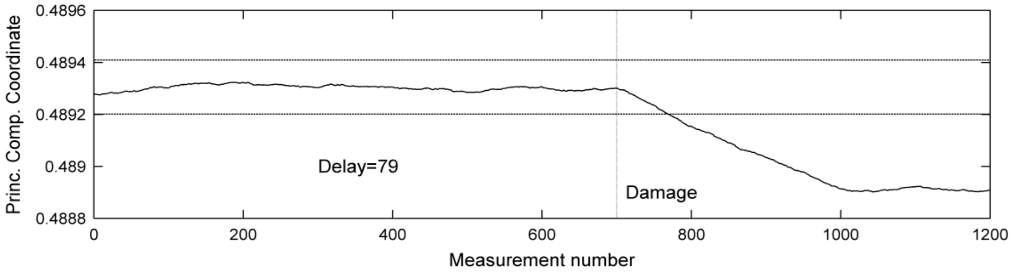

Figure 5.10 – Time-history of the coordinate corresponding to the RRB of the first principal component applying MPCA on time-series type ii using normalization b.

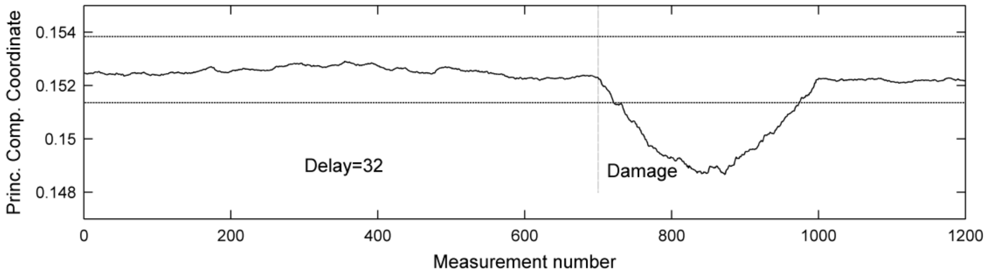

Figure 5.11 – Time history of the coordinate corresponding to the RLB for load position 3 of the first principal component applying MPCA on time-series type i using normalization b .

Comparing Figure 5.8 with Figure 5.10, it is observed that the time to detect the damage occurrence is much more pronounced in the latter than in the former. Furthermore, in Figure 5.8 the variation in the coordinate is much clearer. Therefore, the normalization a is more suitable than normalization b to detect the occurrence of damage using time-series type ii. Comparing Figure 5.9 with Figure 5.11 one observes the opposite. Although in this case the time to detect the occurrence of damage using the normalization a is smaller, as it will be shown, the normalization b leads to lower time to detection and to more reliable results regarding the localization of damage.

In order to validate the conclusions drawn above, 100 analyses adopting different random sequences, in terms of load variability and noise in the measurements, were performed. The study involved the two types of datasets – type ii and i – and the two normalization procedures – a and b. The results are summarized in Table 5.1 to Table 5.3.

Using time-series type ii, there is no false-positive indication of damage in either normalization procedures. This means that the occurrence of damage is correctly identified in every case. Table 5.1 presents the comparison in terms of time to detection, given by MPCA applied to the time-series type ii, between both normalization procedures. It is observed that the normalization procedure a provides the best results regarding the time to detection of damage. The time to detection using the normalization a is significantly smaller than that using normalization b.

The comparison in terms of damage location, given by MPCA applied to the time-series type i, between both normalization procedures is shown in Table 5.2. The false-positive indication of damage is similar in each normalization procedure – 2% and 3% in normalization procedures a and b, respectively. However, concerning the identification of the damage location, the results obtained using the normalization procedure b are significantly better. The damage location is correctly identified – LP3 – in more than 70% of the cases. Furthermore, considering that the identification of contiguous load positions (LP2 and LP4) is also acceptable regarding the location of damage (see Figure 5.1), only in 15% of the cases the damage location is not correctly identified. On the other hand, using the normalization procedure a the location of damage is incorrectly identified in almost 40% of the cases.

Table 5.3 presents the comparison in terms of time to detection, given by MPCA applied to the time-series type i, between both normalization procedures. The data presented in the table includes the true-positive damage detection cases associated with load positions 2, 3 and 4 only. The time to detection using the normalization procedure b is smaller. Therefore, the normalization procedure b applied before the MPCA on the dataset of type i provides the most reliable results in terms of damage location and lower times to detection.

Table 5.1 – Number of crossings required for damage identification using time-series type ii.

Normalization	a	b
Minimum	13	25
Maximum	28	157
Mean	18.4	58.6
Standard deviation	3.2	23.9

Table 5.2 – Damage location (load position that signalizes the occurrence of damage) using time-series type i.

Normalization	a	b
False-positives	2	3
Load position 3	31	72
Load positions 2 and 4	31	13
Other load positions	36	12

Table 5.3 – Number of crossings required for damage identification using time-series type i.

Normalization	a	b
Minimum	13	16
Maximum	92	63
Mean	41.2	31.3
Standard deviation	16.9	9.5

5.4.3. Robust regression analysis

The procedure adopted to detect damage using RRA involves determining whether there are points lying far from the regression line estimated during a reference period. This requires calculation of $\hat{y}$ and the differences $e_i = y_i - \hat{y}_i$, denoted as residuals, during the training and monitoring phases. As in the MPCA, the training phase involved 800 crossings, in which the mean, μ_i, and the standard deviation, σ_i, were computed in order to define thresholds for damage detection. During the monitoring phase, as soon as at least 9 points (N_{out}) out of 10 consecutive points (N_{test}) exceeded the threshold, assumed to be $\mu \pm 3\sigma$, a structural change is flagged. The procedure of flagging damage only when at least N_{out} points, out of N_{test} consecutive points, exceed the threshold bounds improves the reliability of the method, preventing false-positive indications.

In statistics the correlation coefficient is a measure of the correlation (linear dependence) between two variables X and Y. It is widely used as a measure of the strength of linear dependence between two variables. Consider a dataset of type ii containing one crossing only, with noise in the measurements as described in section 5.2.2. Table 5.4 presents the correlation coefficients for the influence-lines of the four sensors.

Although values for the correlation coefficients for all sensor pairs are relatively high (higher than 0.8), the relation between the sensors response is not linear. Figure 5.12 presents the relation between the vertical displacement at mid-span (VDM) and the horizontal displacement at the roller support (HDR) during one crossing. Figure 5.12 (a) presents both the relation between the measurements and the corresponding regression line whereas Figure 5.12 (b) presents the residuals between the measurements and the predictions computed with

Table 5.4 – Correlation coefficients between the sensors (taking into account one crossing).

	VDM	HDR	RLB	RRB
VDM	1	0.997	0.953	-0.954
HDR	0.997	1	0.956	-0.957
RLB	0.953	0.956	1	-0.832
RRB	-0.954	-0.957	-0.832	1

the regression line. Although the correlation coefficient is very close to 1 ($\rho = 0{,}997$), it is clear that the relationship between responses VDM and HDR is not linear, see Figure 5.12 (b).

Figure 5.13 presents the relationship between the vertical displacement at mid-span (VDM) and the rotation over the left support bearing (RLB) during one crossing. Figure 5.13 (a) presents both the relationship between the measurements and the corresponding regression line whereas Figure 5.13 (b) presents the residuals between the measurements and the predictions computed with the regression line. In both figures it is clear that the relationship between these responses (VDM and RLB) is not linear. Therefore it may not be appropriate to apply the RRA using time-series type ii.

Consider a dataset of time-series type i, 100 crossings, in the baseline condition, with load variability of ±10% around a service load of 8.75 kN and noise in the measurements as described in section 5.2.2. Figure 5.14 presents the relationship between the vertical displacement at mid-span (VDM) and the horizontal displacement at the roller support (HDR) when the load is, in both cases, at mid-span, LP6 (see Figure 5.1). Figure 5.14 (a) presents both

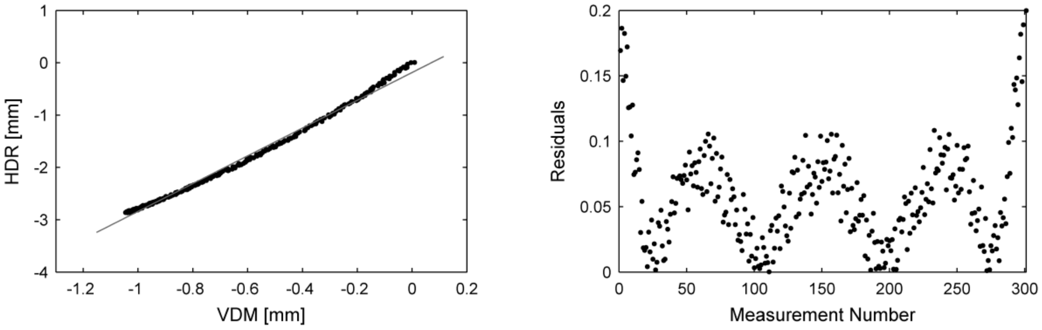

(a) (b)

Figure 5.12 – Relationship between VDM and the HDR: (a) measurement values; (b) residuals from the robust regression.

the relationship between the measurements and the regression line whereas Figure 5.14 (b) presents the residuals of taking the difference between measurements and the predictions computed with the regression line. The relationship between these responses is linear.

Therefore the RRA will be applied using only the time-series type i. The results of the RRA applied on the dataset of type i, containing 44 time histories, as described in section 5.3.1, are presented below.

Figure 5.15 presents the residuals of measurements and predictions computed with the regression line using RRA obtained with the time-series corresponding to the HDR response for load position 2 and the VDM for load position 5 – one of the pairs that present the smallest time to detection. The damage is detected nine crossings after its occurrence. The plot shows a clear change in the structural condition.

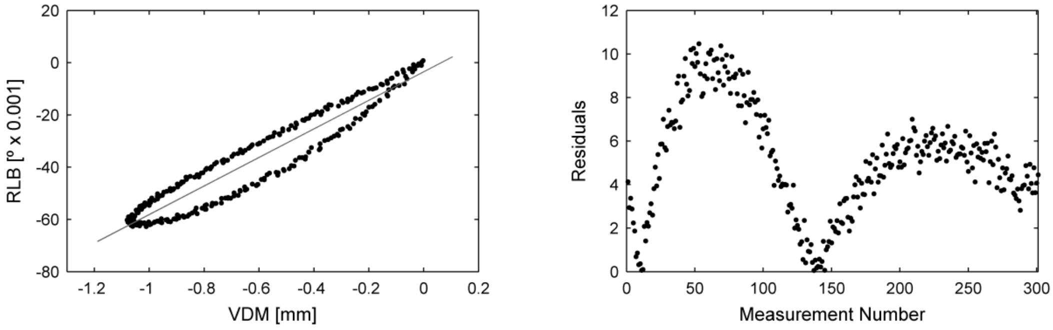

(a) (b)

Figure 5.13 – Relationship between VDM and the RLB: (a) measurement values; (b) residuals from the robust regression.

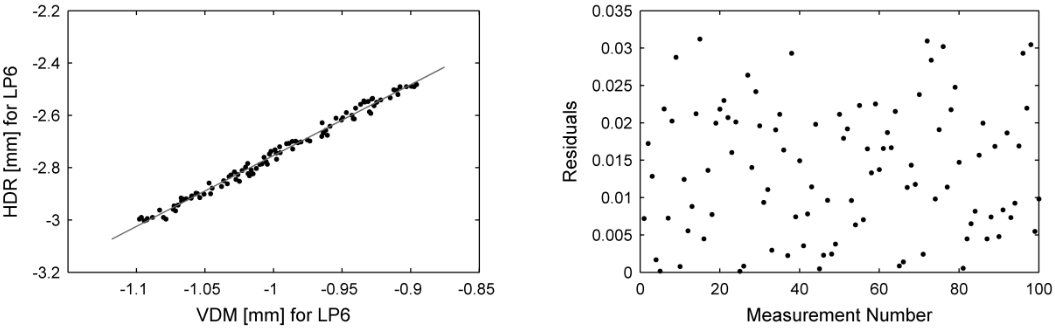

(a) (b)

Figure 5.14 – Relationship between the VDM and HDR when the load is at mid-span, LP6: (a) measurement values; (b) residuals from the robust regression.

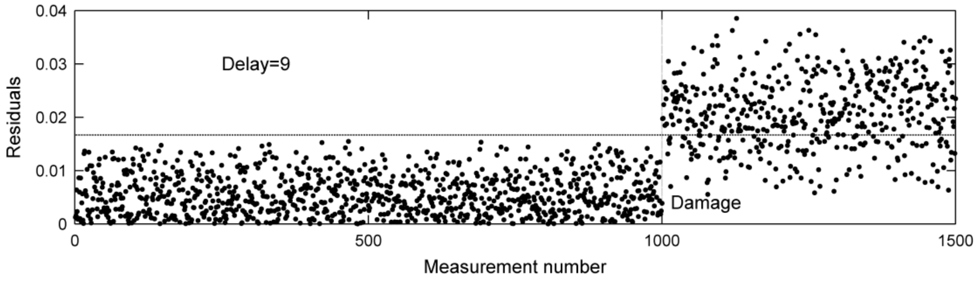

Figure 5.15 – Time history of the residuals of measurements and predictions computed with the regression line using RRA obtained with the time-series type II corresponding to the HDR response for load position 2 and the VDM for load position 5

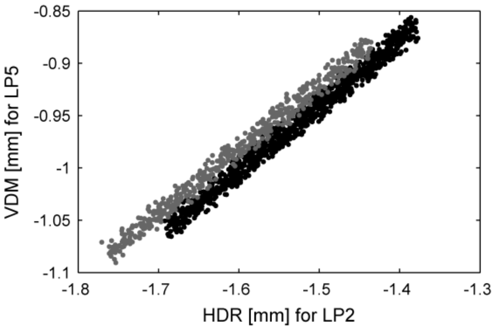

Figure 5.16 – Relationship between the time-series type II of the HDR for load position 2 and the VDM for load position 5 before (black) and after (gray) damage.

Figure 5.16 presents the relationship between the responses recorded by the HDR for load position 2 and the VDM for load position 5 before (black) and after (gray) damage. The effect of the occurrence of damage is clearly flagged by the shift of the relationship between the responses before and after damage.

In order to validate the applicability of the RRA as a reliable damage detection procedure, using time-series type i, 100 analysis adopting different random sequences, both in terms of load variability and noise in the measurements, were performed. In every case, the occurrence of damage was correctly identified. Moreover, the time to detection in every situation was nine crossings.

5.5. Conclusions

This chapter discusses the application of data-driven methods on moving-load data in order to detect the occurrence as well as the location of damage. The present methodology takes into account the quasi-static structural response only and thus, the dynamic component is not included. Using a damage scenario of a local crack in a reinforced concrete element, simulated as a stiffness reduction in a beam-element, time-series of moving-load data are useful inputs for behaviour-model-free (non-physics-based) methods. Two types of time-series were addressed. The first, denoted as type i, regards the response observed when the load is at a given position. The second, denoted as type ii, includes the whole influence-line. Based on the results described in this chapter, the conclusions drawn are presented in the following paragraphs.

Data-processing using MPCA allows the early detection of changes in the structural response and the location of damage. Two types of normalization of the data prior to the calculation of the principal components were tested. Normalization a consists of subtracting the mean prior to the calculation of the covariance matrix. In normalization b, the data is also divided by the standard deviation. The results showed that: i) using time-series type ii and normalization a, MPCA allows the earliest detection of damage; ii) using the time-series type i and normalization b locates damage the best.

Applying RRA on time-series type ii was not appropriate because the response relationships are not linear. Using time-series type i, the occurrence of damage was detected. However, the method does not provide information related to damage location.

In general, the time to detection using RRA is smaller than MPCA. Therefore, the combination of both methods provides the most complete information on structural condition.

Chapter 6

Damage identification in a laboratorial model based on experimental moving-loads responses

6.1. Introduction

The surveillance of bridges and viaducts is an issue that has been given a huge attention during the last decades (Farhey, 2005; Housner *et al.*, 1997), within which special emphasis has been devoted to the installation of modern structural health monitoring (SHM) systems and to the development of damage detection procedures. The SHM systems include a set of sensors used to obtain structural response data that must be stored, processed and analysed in order to inform owners about the condition of structures, thereby supporting surveillance, maintenance and other management tasks (Wong, 2007). However, although many bridges are today endowed with modern measurement systems providing huge amounts of data (Sousa *et al.*, 2011), the detection of damage and anomalies in the structures is still a challenge (Zhang and Zhou, 2007). In this context, particular attention must be paid to the development of techniques for processing and analysing data in order to obtain from the SHM systems useful and reliable information concerning the condition of the structure (Catbas *et al.*, 2008; Worden *et al.*, 2009).

This chapter focuses, therefore, on the early detection of damage in reinforced and prestressed concrete bridges. Among the problems that may arise in this type of structures, the prestress losses are one of the most critical. The possibility of avoiding permanent cracks, leading to the improvement of both the durability and the overall stiffness of the structure, is one of the major advantages of prestressed structures (Collins and Mitchell, 1987). In fact, a significant prestress loss may lead to severe problems in the serviceability and safety of the structure (Bažant *et al.*, 2012; Lan *et al.*, 2012). Furthermore, malfunctions of support bearings, although not an exclusive issue for concrete bridges, may cause major problems for these structures (Liu *et al.*, 2009). As a result of both the development of corrosion between their components and the accumulation of detritus, the movements that the support bearings are designed for are, often, partially restrained, and, in the most severe situations, completely prevented (Ryan *et al.*, 2006). In these cases, stresses not predicted during the design stage may arise and lead to severe damages in the superstructure and in the substructure, which can grow progressively worse if ignored, and ultimately result in the bridge failure (NYSDOT, 2005; Splitstone *et al.*, 2010). In this context, this chapter addresses these two types of damage: prestress losses and malfunctions of support bearings.

The variation of the response due to a truck or carriage traversing a bridge, graphically presented in the form of influence-lines, provides significant information as regards its structural behaviour (Ghali *et al.*, 2009). Thus, these data may play a key role for characterizing the structural condition of a bridge (Hirachan and Chajes, 2005) as well as for early damage detection. Choi *et al.* (2004) and Štimac Grandić *et al.* (2011) had shown that both the occurrence and the location of damage may be identified by comparing influence-lines. However, this approach implies the comparison of influence-lines obtained under the same load. This requires the execution of periodic load tests under controlled conditions, which is, in general, very difficult to accomplish. Therefore, a more sophisticated data-processing procedure is needed in order to identify damage on bridges based on moving-loads responses.

The approach for damage detection presented herein is based on moving-loads responses, which do not require, however, to be originated by equal loads in terms of magnitude. This approach is based on in-service traffic responses and involves, firstly, building time-series of influence-lines data, and, secondly, the analysis of the measurements using an adequate data-processing algorithm. As demonstrated in chapter 5, using numerically-simulated data, this approach has shown to be successful for damage detection. However, the effectiveness of the method remains to be evaluated with the use of real data. Therefore, this work concerns to the application of this approach for early damage detection using experimental moving-loads responses collected in laboratorial tests.

Aiming at the application of the aforementioned approach on full-scale bridges using in-service moving-loads responses, the laboratorial tests were designed in order to meet the following aspects. Firstly, a reduced-scale laboratorial model of a reinforced and prestressed concrete frame, resembling a prestressed concrete bridge, was chosen as case study. Secondly, two typical damage scenarios of concrete bridges, such as prestress losses and restraints for the longitudinal rotation of support bearings, were simulated through suitable modifications in the structure. Finally, a moving-load system specially developed for these experiments enabled to easily obtain influence-lines under different load levels, thus replicating in-service traffic loads of bridges.

This chapter is divided in five sections, including this introduction and a final section in which the main conclusions drawn are presented. The second section is devoted to the presentation of the case study. This includes a brief description of the laboratorial model, the measurement system installed and the analysis of the structural behaviour under normal operating conditions, as well as those regarding the damage scenarios addressed herein. In the third section, the approach for damage detection is presented together with the data-processing algorithms applied: robust regression analysis (RRA); moving principal component analysis (MPCA); and influence-line assurance criterion (ILAC). The fourth section is devoted to the analysis of the results of the methodology applied in either damage scenario. Firstly, the procedure to obtain time-series of experimental laboratorial data is described. In addition, taking advantage of the comprehensive monitoring system installed in the laboratorial model, the performance of different measurement systems, combining different number and distinct types of sensors, is assessed. Both the advantages and the shortcomings of each data-processing algorithm are discussed, namely as regards the ability and time required for damage detection, and the suitability of different monitoring systems analysed.

6.2. Case study

6.2.1. General remarks

This chapter aims at the application of damage identification methodologies in reinforced and prestressed concrete bridges based on experimental moving-loads responses. A reduced-scale laboratorial model of a reinforced and prestressed concrete rigid-frame subjected to a moving point-load was chosen as case study. This structure was selected aiming at a broad research programme with the objective of assessing and validating, in different structural systems, damage identification techniques in bridges using experimental data. This is a very compact and versatile laboratorial model that resembles a rigid-frame bridge commonly used for overpasses and underpasses. However, when a pinned bearing is replaced by a roller one, the behaviour of the frame’s beam is the same as that of a simply supported beam. In addition, this laboratorial model was designed aiming at the implementation of structural changes with the goal of simulating, under controlled conditions, typical issues observed in reinforced and prestressed concrete bridges, such as different prestressing force scenarios and several support bearing conditions. Furthermore, the system used for replicating moving-loads on bridges enables the movement in both directions and a swift change of the load magnitude.

In general, a damage detection approach involves the comparison of a set of selected structural parameters obtained in two stages: the reference and the monitoring periods. Therefore, prior to the application of any damage detection procedure, the structural condition in the reference period must be thoroughly characterized, which was done as carefully discussed in chapter 4. In the baseline scenario (BS) the prestressing force installed in the laboratorial model was about 330 kN (165 kN in each prestressing strand, which is about 64% of the ultimate strength), and both supports were under normal operating conditions, i.e., preventing longitudinal displacements and enabling longitudinal rotations. In these conditions, although the decompression limit state is satisfied, it was shown that the structure exhibits nonlinear behaviour, as a result of smeared cracking that might be observed along the frame's beam. Although this structural state may be considered as damage, in the context of this work, with the aim of assessing and validating damage detection techniques for concrete bridges, it is assumed as the reference condition. On such a basis, two damage scenarios were simulated. The first, denoted as damage scenario 1 (DS1), regards a prestress loss, and the second, designated as damage scenario 2 (DS2), concerns to a restraint for the longitudinal rotation of a support bearing.

In either structural condition, a very comprehensive campaign of laboratorial tests was carried out. The tests included several crossings under different load levels in both directions. However, as shown in chapter 4, the structural response heavily depends on the direction in which the load crosses the structure. Therefore, a successful application of a damage detection strategy requires the analysis of data for crossings in the same direction. Consequently, hereafter, only the results collected in one selected direction were considered.

This section gives a detailed description of the laboratorial model, including the characterization of the structure's geometry and materials, and the overview of the measurement system installed. In addition, with the objective of assisting the interpretation of the results obtained with the approach for early damage detection proposed herein, this section presents and describes the main changes on the structural response observed after the deployment of the damage scenarios.

6.2.2. Description of the laboratorial model

The laboratorial model, depicted in Figure 6.1, is a single span reinforced and prestressed concrete frame, 150 cm high, 320 cm long and 50 cm wide (see Figure 6.2). The elements' thickness is 20 cm. The geometry of the frame's bases, 40 cm long and 20 cm thick, enables different positions for the support bearings. In the baseline condition two equal supports, carefully designed to prevent horizontal displacements and to allow longitudinal rotations (see detail depicted in Figure 6.2), are placed in the alignment of the column axes.

Two seven-wire strands, straight and unbounded, with a cross-sectional area of 1.40 cm^2 each, were placed at mid-depth of the beam's cross-section. The ultimate strength of the wires is 1860 MPa (leading to an ultimate strength of about 260 kN for each strand) and the modulus of elasticity is 195 GPa. Two manually-operated hydraulic jacks, one for each strand, were installed in order to perform both prestressing tensioning and de-tensioning operations, thereby enabling different prestressing force scenarios. The beam's ordinary reinforcement, with a characteristic yield stress of 500 MPa, consists of four 16 mm longitudinal bars, both at the top and the bottom, and 6 mm stirrups spaced 15 cm apart. Compression tests in 150 mm cube specimens, carried out 340 days after the cast (Félix, 2004), led to estimates for the concrete modulus of elasticity and the compressive strength of, respectively, 30 GPa and 37 MPa. However, due to the cracking along its length, the beam exhibits a lower stiffness. The analysis of the experimental results have shown that the assumption of a value of 9 GPa for the beam's modulus of elasticity would lead to a reasonable match between measured values and numerical estimates (see chapter 4).

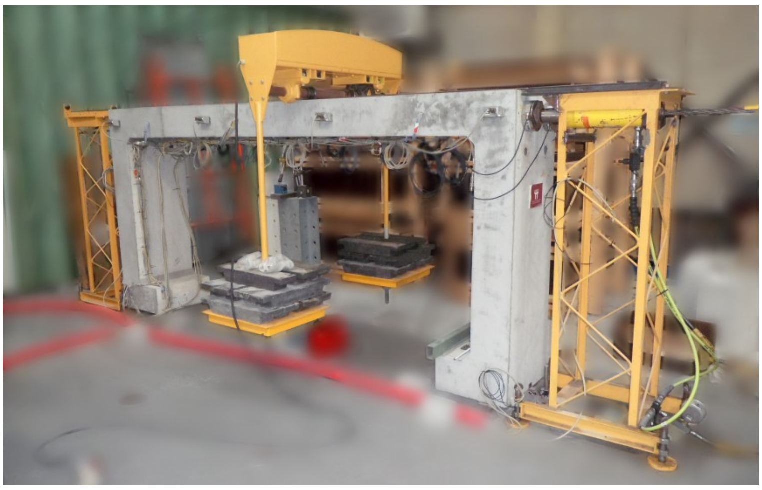

Figure 6.1 – General view of the laboratorial model.

The damage detection techniques presented in this work are based on the structural response under moving-loads. Thus, a versatile system, in which the load is mechanically moved along the beam, and the total load is easily changed, was developed. The loading system consists in a metallic structure, supported over two steel wheels (transversely aligned leading to a point-load as regards the longitudinal direction) connected to an electrical motor, which is responsible for the movement in both directions. This metallic structure is equipped with two hanging bases on which masses are laid down in order to change the total weight, as shown in Figure 6.1. The electrical motor was connected to an electrical frequency converter in order to ensure constant speed along the crossing. Then, by recording the crossing time at a set of pre-determined locations, the estimation of the moving-load position at each recording time instant is made possible and thus, obtaining experimental influence-lines. In this respect, two auxiliary structures (3D steel truss towers) are placed next to both ends of the frame, as depicted in Figure 6.1. Therefore, in each crossing, the moving-load departs and arrives outside the beam, ensuring, on one hand, the structure is unloaded at both the beginning and the end of the crossing, and, on the other, the load moves at constant speed while passing over the concrete frame.

The measurement system included the collection of: (i) the vertical displacement (VD) at mid-span, using linear variable differential transformers (LVDTs); (ii) the horizontal displacements (HD) at the beam's centroid in each end, also with LVDTs; (iii) the rotations (R) at seven equally spaced cross-sections, by using electronic inclinometers; (iv) the average strain (AS) at both the top (T) and bottom (B) of three cross-sections, using 300 mm long displacement transducers; (v) the crack-width (CW) at three cross-sections, with 100 mm long displacement transducers; and (vi) the prestressing force (PSF) in each strand, using load cells. A scheme of the complete monitoring system is depicted in Figure 6.2. It is noteworthy to mention that, although the laboratorial model used within this research was heavily instrumented, in full-scale applications, the number of sensors that can be installed is limited. In addition, although several approaches have been developed to aid engineers in configuring measurement systems, there is still a long way ahead (Castro-Triguero *et al.*, 2013; Kripakaran and Smith, 2009). Therefore, this comprehensive measurement system aimed two main objectives. The first was to thoroughly characterize the structural behaviour both at the baseline and at the damaged conditions. The second, within the objective of developing sound and reliable damage detection techniques, was to assess the most appropriate structural quantities to be measured in order to attain an early detection of damage.

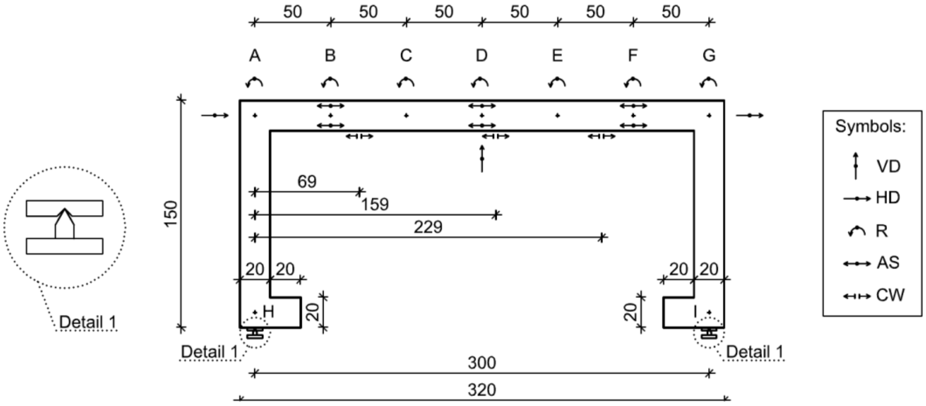

Figure 6.2 – Geometric characteristics of the laboratorial model and configuration of the measurement system.

This work focuses on the quasi-static component of the structural response as a moving-load traverses the structure. As in the tests carried out the crossing speed is appreciably low, the dynamic component is inexistent. However, the measurements are polluted with noise. Therefore, firstly, data was acquired at a rate of 50 samples per second (which is significantly higher than the acquisition frequency needed to adequate characterize the structural response), using a 16-bit analog-to-digital converter (ADC). Then, a Savitzky-Golay filter (Savitzky and Golay, 1964) using a third degree polynomial curve, with a moving window of 101 points of equal weight, was applied to smooth the acquired signals.

6.2.3. Damage scenarios

6.2.3.1. Prestress loss

By taking advantage of the tensioning system of the prestressing strands installed in the laboratorial model, which enables changing the prestressing forces easily, a 15% prestress loss was simulated. Therefore, the prestressing force was changed from about 330 kN (165 kN in each prestressing strand, which is about 64% of the ultimate strength), in the baseline scenario (BS), into 280 kN (140 kN in each prestressing strand, which is about 54% of the ultimate strength), in the damaged scenario 1 (DS1).

Figure 6.3 depicts the influence-lines for a set of selected quantities obtained under a 11.65 kN point-load moving forward (in the A-G direction), both in the baseline (BS) and in the damaged (DS1) scenarios. As a result of this structural change, every structural quantity experiences a significant increase in the measurements. However, the increase is not equal for every cross-section. For instance, the vertical displacement at mid-span (VD-D) increases about 35% whereas the crack-width opening at the cross-section near the mid-span (CW-D) almost triples the values observed in the baseline condition. Although the prestressing force in both scenarios is quite below the ultimate strength of the strands, the decompression limit state, under both the dead load and a 11.65 kN point-load, is comfortably satisfied. However, when the prestressing force is higher, the structural deformation is lower. Therefore, as shown in chapter 4, as the compression state decreases, the "global stiffness" of the beam also decreases.

Furthermore, it is noteworthy to mention that this structural modification leads to changes in the shape of the influence-lines. As the structure is statically indeterminate, the change on the beam's stiffness leads to a modification on the ratio between this one and the stiffness of the columns. Consequently, the distribution of the internal forces varies and, thus, the shape of the influence-lines is different. Even though, the changes observed among the measured quantities differ. Figure 6.4 depicts the results shown in Figure 6.3 normalized by the highest absolute value: the measurements concerning the baseline scenario (BS) are multiplied by a scale factor λ given by the ratio $\delta_{max,DS1}/\delta_{max,BS}$, where $\delta_{max,DS1}$ and $\delta_{max,BS}$ are, respectively, the maximum measurements recorded in the damaged and the baseline scenarios. Although the changes in the shape of the influence-lines for the crack-width at the cross-section near the mid-span (CW-D) and for the rotations at the ends of the beam (R-A and R-G) are clear, the differences observed at the remaining quantities are almost negligible. Note that for the vertical displacement at mid-span (VD-D), the scaled influence-line in the baseline condition almost overlaps that obtained in the damaged condition. Therefore, taking into account that for a given structural condition the response is proportional, within certain limits, to the load level, the increase observed in the vertical displacements, as a result of the prestress loss, may be incorrectly ascribed to a higher load level. Nevertheless, it is noteworthy to mention that a higher prestress loss would lead to changes in the shape of the influence-line (see chapter 4).

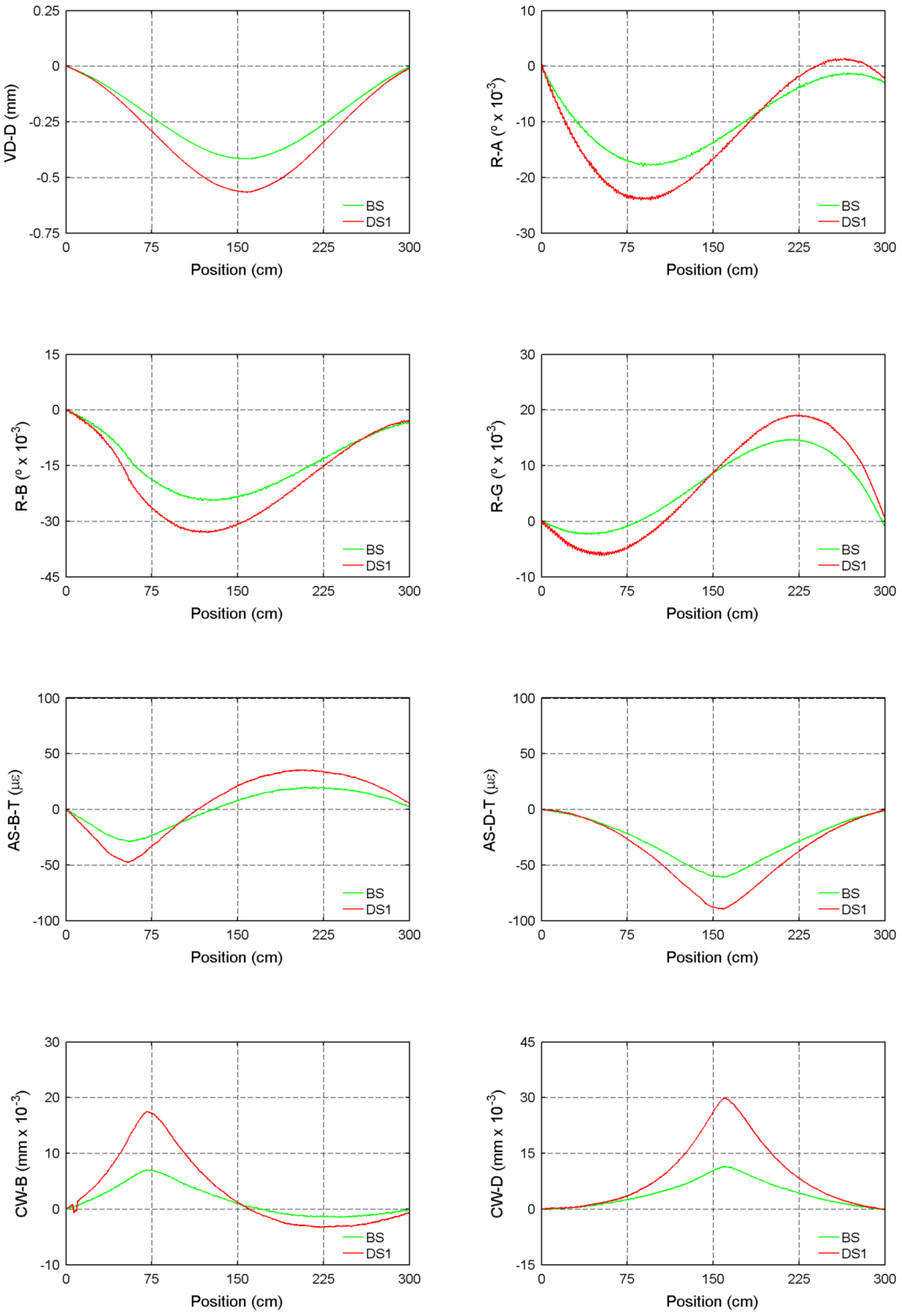

Figure 6.3 – Comparison of the structural response under a 11.65 kN point-load, crossing the structure in the A-G direction, in the baseline condition (BS) and after a 15% prestress loss (DS1).

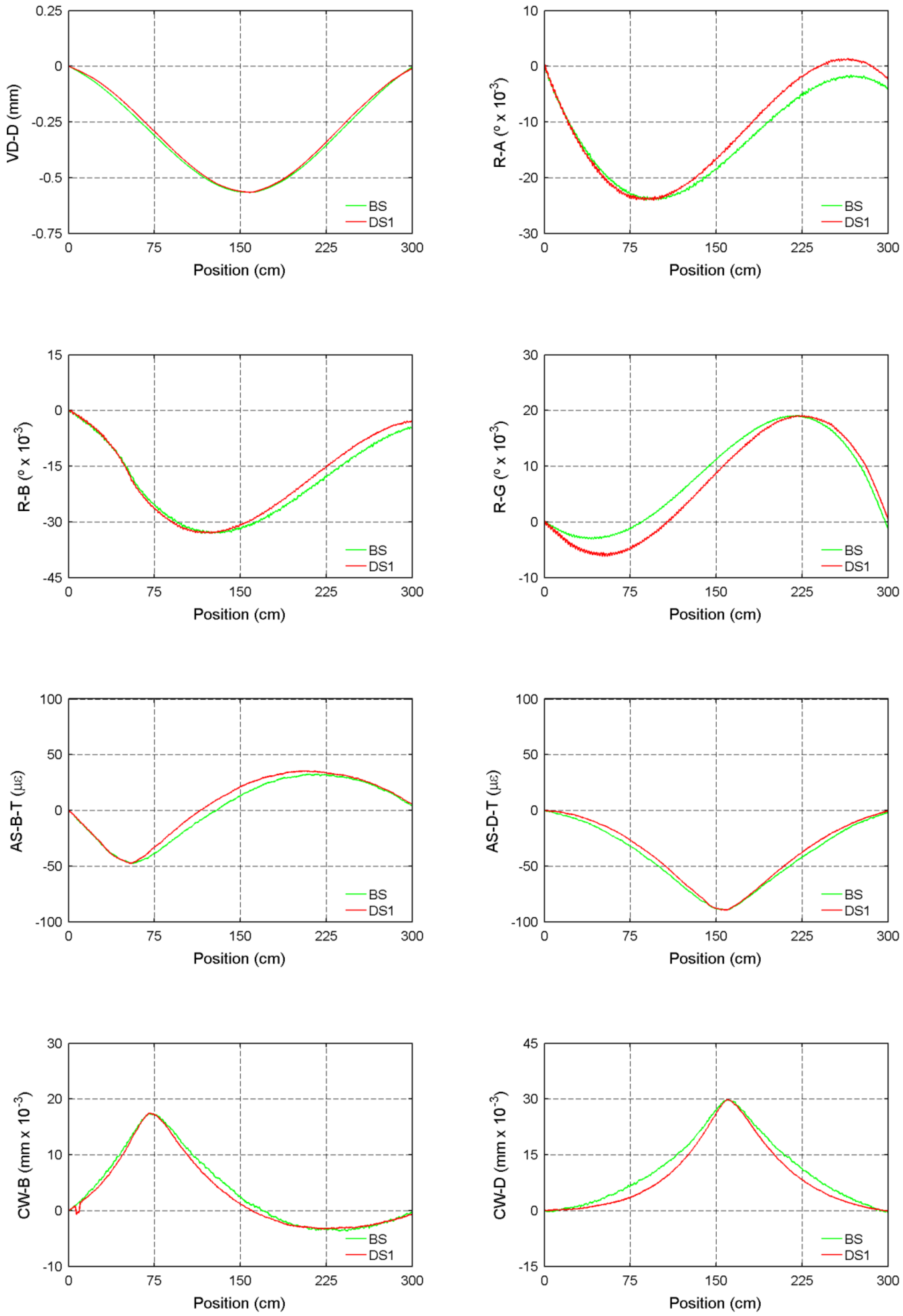

Figure 6.4 – Comparison of the structural response under a 11.65 kN point-load, crossing the structure in the A-G direction, in the baseline condition (BS) and after a 15% prestress loss (DS1), normalized by the highest absolute value.

6.2.3.2. Restraint for the longitudinal rotation of a support bearing

With the objective of simulating a partial restraint for the longitudinal rotation of a support bearing in the laboratorial model, an auxiliary system, as depicted in Figure 6.5, was deployed under the alignment G. This system is composed by a set of two steel bars fastened to the floor, on one end, and fixed to a steel profile attached to the frame's base, on the other. Consider the scheme shown in Figure 6.5 (c) representing the relation between the rotational and the axial stiffnesses of the auxiliary system. The axial stiffness, k_{L}, of the set composed by two 12 mm of diameter steel bars and the steel profile was estimated in approximately 100 000 kN/m, and the distance, d, between the rotation axis and the auxiliary system was 0.28 m. Thus, according to expression (6.1), the rotational stiffness, k_{R}, was estimated in approximately 7840 kN.m.

$$k_{\mathrm{R}} = k_{\mathrm{L}} \cdot d^2 \tag{6.1}$$

(a) (b) (c)

Figure 6.5 – Auxiliary system to simulate a partial restraint for the longitudinal rotation of the support bearing: (a) side view; (b) front view; and (c) working scheme.

It is noteworthy to mention that, contrary to the simulation carried out in this laboratorial test, the restraints for the movements of the support bearings, either the displacements or the rotations, due to malfunctions are, in general, not linear. Even though, this approach constitutes a good approximation to real situations and enables, under controlled conditions, to assess the effects of the support bearings malfunctions on the structural response under moving-loads.

Figure 6.6 depicts the influence-lines for a set of selected quantities obtained under a 11.65 kN point-load moving forward (in the A-G direction), both in the baseline (BS) and in the damaged (DS2) scenarios. The changes produced by the restraint for the longitudinal rotation of the support bearing simulated herein are, in general, not significant. The influence-lines obtained in both scenarios for the vertical displacement at mid-span (VD-D) are clearly identical. As

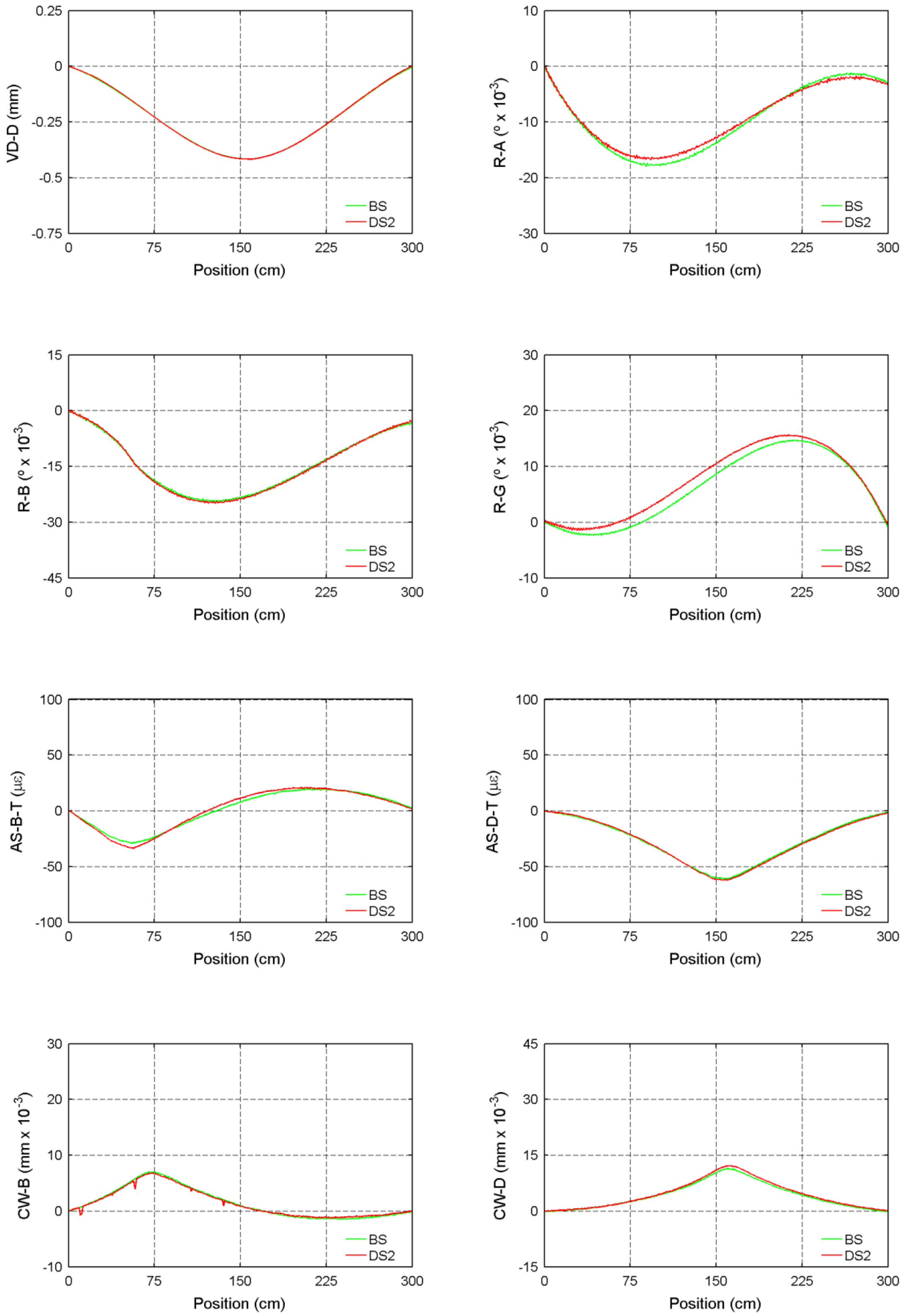

Figure 6.6 – Comparison of the structural response under a 11.65 kN point-load, crossing the structure in the A-G direction, in the baseline condition (BS) and under a partial restraint for the longitudinal rotation of the support bearing in the alignment G (DS2).

regards the average strains (AS) and the crack-widths (CW), minor changes may be observed, namely in the highest absolute values. However, the rotations at the ends of the beam (R-A and R-G) experience clear changes both in the shape of the influence-line and in the highest absolute value.

It should be noted that in a rigid-frame whose behaviour is linear and elastic, a restraint for the longitudinal rotation would lead to a decrease of the highest absolute values of the rotations at the ends of the beam. However, although the highest absolute value of the rotation at the alignment A decreases, that of the rotation at the alignment G increases. It is noteworthy to mention that, as thoroughly discussed in chapter 4, the beam is cracked and, thus, the structure exhibits nonlinear behaviour. Furthermore, in addition to the elastic restraint for the longitudinal rotation deployed in the support bearing, a “permanent” deformed shape of the structure, induced between the baseline condition and this damage scenario, should be taken into account. As a moving-load traverses the beam, the structure bends and, thus, the supports rotate. Therefore, with the objective of ensuring the effectiveness of the elastic restraint for the longitudinal rotation during the entire crossing, prior to the experimental tests, the steel bars integrated in the auxiliary system were pre-tensioned, which led to the aforementioned “permanent” deformed shape. In this context, this condition together with the nonlinear behaviour of the structure may explain the changes observed in the rotation at the alignment G. Still, with the goal of confirming these hypotheses, further investigation, through adequate nonlinear analysis of the structure, should be carried out (not included herein in that this analysis surpasses the aim of this work).

6.3. Data-driven approach for early damage detection

6.3.1. General remarks

The comparison of influence-lines obtained under the same load level, before and after damage, allows the identification of the occurrence of the structural change, as shown above and as demonstrated by Choi *et al.* (2004) and Štimac Grandić *et al.* (2011). Although the differences observed in some quantities may be negligible (such as the vertical deflection at mid-span (VD-D) under a partial restraint of the support bearing rotation, depicted in Figure 6.6), the changes in other quantities may be significant (such as the crack-width at mid-span (CW-D) under a 15% prestress loss, depicted in Figure 6.4). However, if the structural responses derive from different load levels the damage identification through a straightforward comparison may be compromised, as shown in chapter 5. Therefore, with the goal of performing damage identification in bridges using moving-loads data, more sophisticated data-processing techniques are required.

In this context, the approach for damage identification based on moving-loads data proposed in this work, involves building time-series of influence-lines, in accordance with the approach presented in chapter 5. Consider a monitoring period during which the structural response of n_c crossings is collected. In the context of this work, two types of time-series were addressed. The first, denoted as i, regards the highest absolute values collected by each of the n_S sensors included in the monitoring system during each crossing. Therefore, the database includes n_S time-series with n_c measurements each. The second type, designated as ii, includes the whole influence-line. Therefore, if for each crossing the structural response is obtained for n_p positions, the database includes n_S time-series with n_m $(n_c \times n_P)$ measurements each.

In this chapter, three data-processing algorithms carefully selected to be applied on each type of time-series mentioned above were evaluated with the objective of detecting changes in the structural behaviour due to either prestress losses or restraints for the longitudinal rotation of a support bearing. Robust regression analysis (RRA) and influence-line assurance criterion (ILAC) were used to process data concerning time-series of, respectively, type i and type ii. Moving principal component analysis (MPCA) was used to process time-series of both types. A brief description of each data-processing algorithm is given below.

6.3.2. Data-processing algorithms

6.3.2.1. Robust regression analysis

Regression analysis is a statistical technique that is very useful for many problems in engineering and science, which involves exploring the relationships between two or more variables. Consider a set of n data points concerning two variables X and Y: (x_1, y_1), (x_2, y_2), ..., (x_n, y_n). If there is a strong indication that the points lay scattered randomly around a straight line, it is reasonable to assume that the variable Y is related to X by a linear relationship. Therefore, the fitted or estimated regression line is given by:

$$\hat{y} = \beta_0 + \beta_1 \cdot x \tag{6.2}$$

where β_0 and β_1, respectively, the intercept and the slope of the line, are the regression coefficients of the simple linear regression model. Note that each observation i, (x_i, y_i), satisfies the following relationship:

$$y_i = \beta_0 + \beta_1 \cdot x_i + e_i \tag{6.3}$$

where e_i, given by $e_i = y_i - \hat{y}_i$ and denoted as the residual, describes the error in the fit of the model to the i^{th} observation (Montgomery and Runger, 2003).

The regression coefficients are estimated using a process denoted as *iteratively reweighted least squares*, which is based on the least squares method. This iterative and automatic process involves assigning a weight to each data point. In the first iteration, each point is assigned equal weight and regression coefficients are, thus, estimated using ordinary least squares method. At subsequent iterations, weights are computed so that points farther from model predictions in the previous iteration are given a lower weight. Regression coefficients are then recomputed using weighted least squares. The process continues until the values of the coefficients estimates converge within a specified tolerance (Huber, 1981). Traditional regression analysis using the least squares method produces very good results when all of its assumptions are valid (Montgomery and Runger, 2003). However, when some of these assumptions are invalid, least squares method can perform poorly. Therefore, robust regression analysis (RRA) arises as an alternative to traditional regression, working with less restrictive assumptions and providing much better regression coefficients estimates on the presence of outliers in the data (Huber, 1981).

In the field of damage identification, linear regression analysis may be used to identify changes in the structural behaviour in two ways. The first approach consists in observing the evolution of its coefficients (Yao and Pakzad, 2014) and the second is based on monitoring the variation of the residuals (Posenato *et al.*, 2008) in time. In both cases anomalies are identified when a significant variation is observed. In this work, the identification of damage occurrence is based on the latter method.

6.3.2.2. Moving principal component analysis

The principal component analysis (PCA) is used to reduce the dimensionality of a dataset consisting of a large number of interdependent variables to a much smaller number of uncorrelated variables while retaining as much as possible of the variation present in the original dataset (Jolliffe, 2002). Consider a matrix $X \in \Re^{n \times p}$, denoted as features matrix, containing n observations for p features written as a linear combination of a set of orthogonal vectors $U_j = (U_{1,j},\ U_{2,j}, \dots, U_{p,j})$ as follows:

$$[X] = [Z][U]^T \tag{6.4}$$

where $Z \in \Re^{n \times p}$ is the scores matrix and $U \in \Re^{p \times p}$ is the loadings matrix. The scores correspond to the coordinates of the original data in the new coordinate system defined by the orthogonal vectors U_j.

In the PCA this new set of uncorrelated variables, the principal components (PCs), are ordered so that the first principal component corresponds to the direction in which the observations exhibit the largest variance. The subsequent components are orthogonal to the previous ones and maximize the variance of the data points projected on it (Hubert *et al.*, 2005; Jolliffe, 2002). In the classical approach, the principal components correspond to the eigenvectors computed from the covariance matrix $S \in \Re^{p \times p}$ of the dataset $X \in \Re^{n \times p}$. The k^{th} principal component is the eigenvector U_k corresponding to the k^{th} largest eigenvalue (Jolliffe, 2002). In order to PCA work properly, the mean of all observations included in each feature of the dataset must be subtracted before the calculation of the covariance matrix S.

As mentioned above, the first few principal components retain most of the variation present in all of the original variables. Therefore, for a p-dimensional dataset, it is possible to choose only the first r principal components and obtain the original data without significant loss of information. Thus, a good approximation of the features matrix $X \in \Re^{n \times p}$ can be obtained as follows:

$$[X] = [\bar{Z}][\bar{U}]^T \tag{6.5}$$

where $\bar{Z} \in \Re^{n \times r}$ and $\bar{U} \in \Re^{p \times r}$ are, respectively, the r-dimensional matrices of the scores and the loadings.

In the context of structural health monitoring, PCA has been widely used with three major objectives (Figueiredo *et al.*, 2009): (i) evaluation of patterns in the data; (ii) data cleansing; and (iii) data compression.

With the goal of early damage detection Lanata and Del Grosso (2006) have shown that the analysis of the evolution of the eigenvalues and the eigenvectors of the covariance matrix of the dataset gives a good indication of changes on the structural response. However, as a result of a higher influence of old measurements (in the undamaged state) than that of the new measurements (in the damaged state), a significant delay between the occurrence of damage and its identification was noticed. Therefore, Posenato *et al.* (2008) proposed an extension of the PCA, the moving principal component analysis (MPCA) with the goal of overcoming this drawback. The approach consists in the calculation of the principal components of the data comprised in a window of constant size moving along the entire dataset. Therefore, the influence of old measurements is reduced. As in the original approach, a change in the values of the principal components coordinates suggests the occurrence of damage. For a group of correlated sensors, if the structural conditions do not change, the main eigenvalues and the corresponding eigenvectors, remain stable with time. However, if a change occurs, the measurements collected by some sensors may vary with respect to others, thus leading to changes in the eigenvalues and eigenvectors.

6.3.2.3. Influence-line assurance criterion

The influence-line assurance criterion (ILAC), based on the modal assurance criterion (MAC) usually applied to match mode shapes (Allemang, 2003), is a statistical indicator that yields the degree of consistency between influence-lines. This parameter, proposed herein for early damage detection based on moving-loads data, may be defined as:

$$ILAC(r_A, q_B) = \frac{\left|\{\Upsilon_{r,A}\}^T\{\Upsilon_{q,B}\}\right|^2}{\left(\{\Upsilon_{r,A}\}^T\{\Upsilon_{r,A}\}\right)\left(\{\Upsilon_{q,B}\}^T\{\Upsilon_{q,B}\}\right)} \tag{6.6}$$

where $ILAC(r_A, q_B)$ is the ILAC between the r^{th} influence-line of a dataset A, $\Upsilon_{r,A}$, and the q^{th} influence-line of a dataset B, $\Upsilon_{q,B}$.

If datasets A and B are obtained in different time-instants, the diagonal terms of the ILAC matrix may provide a good indication of the occurrence of damage in the structure. If the influence-lines under consideration are identical, i.e, exhibit a consistent relationship, the ILAC value should approach the unity. A greater deviation from unity indicates that the influence-lines are not identical, which suggests changes in the structural response, and thus, the occurrence of damage.

Still, with the objective of using moving-loads data for early damage detection, an additional parameter, the AutoILAC, which is based on the AutoMAC presented by (Pastor *et al.*, 2012), is proposed herein. The AutoILAC quantitatively compares all the possible combinations of influence-lines pairs for only one set of influence-lines. Therefore, instead of finding the influence-lines included in a given dataset that exactly match, the objective lies on the surveillance of the evolution of the AutoILAC values along a monitoring period. Therefore, if the structural conditions do not change, the AutoILAC values remain stable with time. Deviations of these values suggest changes in the structural response, and thus the occurrence of damage.

6.4. Application and discussion

6.4.1. General remarks

The approach proposed herein for damage detection based on moving-loads responses has shown an appropriate performance using numerically-simulated data (see chapter 5). The objective of this chapter is to validate its performance using experimental data. For that purpose, a very comprehensive campaign of tests was carried out on the reinforced and prestressed concrete laboratorial model described above. As explained earlier, this approach involves building time-series of influence-lines, which must comprise two stages: a reference and a monitoring period. Therefore, the structural response under a moving point-load was collected for both the baseline condition and each of the damaged scenarios addressed herein. Moreover, this work aims to provide reliable information regarding the applicability of this approach in full-scale bridges using in-service traffic data. Therefore, the laboratorial tests included a set of crossings under a point-load for different load levels, thereby replicating in-service traffic data. This section describes in detail the tests carried out as well as the procedure to obtain the corresponding time-series.

Taking advantage of the comprehensive measurement system installed in the laboratorial model, the assessment of the most appropriate quantities to be measured in order to attain early damage detection was an additional objective of this work. In this context, five different measurement systems (MS), as summarized in Table 6.1, were regarded. The first, denoted as MS-a, consists in a mixed system comprising the vertical displacement at mid-span (VD-D), the rotations at the ends of the beam (R-A and R-G) and the average strains (AS), both at the top and bottom of the three instrumented cross-sections. However, vertical displacements are difficult to measure (Chung *et al.*, 2008; Hou *et al.*, 2005). Therefore, the second measurement system (MS-b) evaluated is similar to the former, except, however, for the vertical displacement at mid-span which is not considered. The last three measurement systems include only quantities of a single type. The third one, designated as MS-c, comprises four rotations (R): two at the ends and two at the thirds of the beam’s length. The fourth (MS-d),

Table 6.1 – Monitoring systems under consideration.

	VD D	R A	R C	R E	R G	AS B-T	AS B-T	AS B-T	AS B-T	AS B-T	AS B-T	CW B	CW D	CW F
MS-a	x	x			x	x	x	x	x	x	x			
MS-b		x			x	x	x	x	x	x	x			
MS-c		x	x	x	x									
MS-d						x	x	x	x	x	x			
MS-e												x	x	x

includes all the instrumented average strains. The fifth, denoted as MS-e, comprises the crack-widths at the three observed cross-sections.

In this context, this section presents and discusses in detail the results of the application of the data-processing algorithms described above, within the approach proposed herein for early damage detection based on moving-loads, using experimental datasets regarding the measurement systems addressed above.

6.4.2. Time-series of experimental laboratorial data

The time-series of experimental data built within this work comprise two distinct stages. The first stage concerns to the baseline condition whereas the second stage concerns to one of the damaged conditions simulated above. Moreover, as this work aims to provide reliable information regarding the applicability of this approach in full-scale bridges using in-service traffic data, the laboratorial tests included a set of crossings under a point-load for different load levels. Therefore, for each structural condition (including the baseline (BS) and both the damaged scenarios (DS1 and DS2)), a set of four passages in each direction under different load levels ranging between 8.8 kN and 14.6 kN were carried out. As an example, Figure 6.7 shows the influence-lines for the rotation on the alignment G (R-G) for a crossing under each load level in the baseline condition. The corresponding experimental results for each of the damage scenarios simulated within this work are depicted in Figure 6.8. As regards the influence-lines obtained under the same load level, a careful analysis of the results have shown that, disregarding small differences inherent to experimental tests, for a given

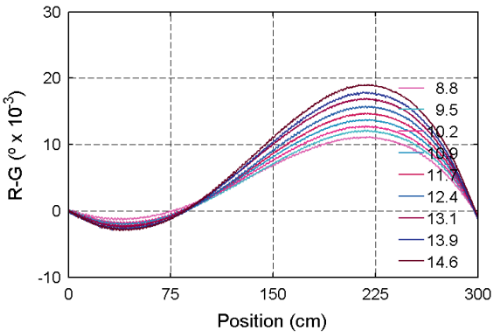

Figure 6.7 – Influence-lines for the rotation on the alignment G (R-G) for a crossing, in direction A-G, under each load level in the baseline condition.

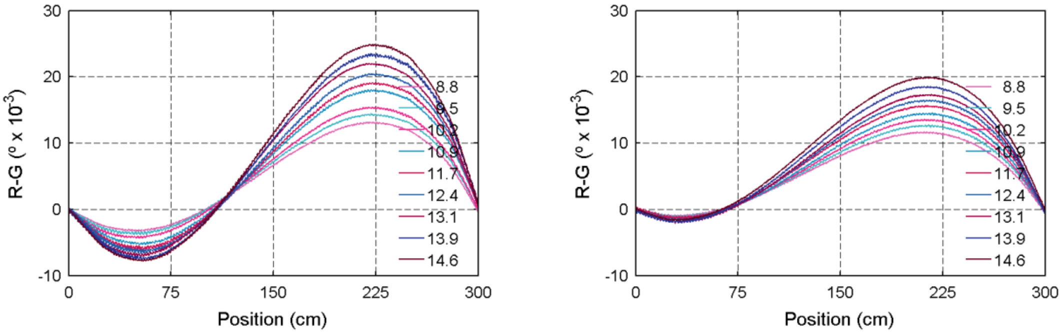

(a) (b)

Figure 6.8 – Influence-lines for the rotation on the alignment G (R-G) for a crossing, in direction A-G, under each load level, for: (a) a prestress loss (DS1); and (b) a restraint for the longitudinal rotation of a support bearing (DS2).

structural condition the curves are very similar. In addition, it is noteworthy to mention that although the response is not linear in terms of the load level, it appears to be proportional to a fictitious load given by an adequate scaling of the actual load (see chapter 4).

Despite these experimental tests aimed to simulate, in some way, the results of in-service traffic for a full-scale bridge, two major differences may be pointed out. On one hand, the load variability regards only nine different load levels. On the other, the number of influence-lines collected is low ($9 \cdot 4 = 36$ influence-lines for each structural condition). However, in the context of laboratorial tests, increasing both the variability, as regards the load level, and the number of crossings collected would be very time-consuming, and, ultimately, could be unfeasible. Still, in order to “artificially” generate longer time-series, this limited number of passages (36 for each structural condition) was carefully combined as follows. Firstly, a randomly simulated data series was produced in order to replicate the variability of the load level. For the sake of simplicity, a Gaussian distribution with mean, μ, equal to 11.7 kN and standard deviation, σ, equal to 1.17 kN (10% of the mean value) was assumed. It is noteworthy to mention that for this distribution about 99.7% of the values lie within the range [8.19; 15.21] (given by $\mu \pm 3 \cdot \sigma$), which comprises the range of the experimental load levels. Secondly, the correspondence between each randomly simulated load level and the closest experimental load value was established. Finally, one out of the four crossings carried out for the load level selected in the previous step was chosen on the assumption of same likelihood for each.

In this work, the time-series include 1500 crossings. The first 1000 correspond to the baseline scenario (BS), in which the structure was assumed to behave normally. The last 500 correspond to each of the damage scenarios described above (DS1 or DS2). Therefore, as the number of crossings obtained experimentally is lower than that assumed in the time-series, a given crossing may be included several times along the time-series. Besides, as the time-series include only the nine load levels tested experimentally, the load variability is not continuous. Even though, based on the proportionality observed in the structural responses, these “artificially” generated time-series constitute a good approximation to more realistic time-series in which the load levels distribution is continuous.

Consider, for instance, the rotation on the alignment G (R-G). Time-series of type i, i.e., including only the highest absolute values of each influence-line, for either the prestress loss or the restraint for the rotation of the longitudinal bearing are depicted in Figure 6.9. The transition from the baseline condition into the damaged condition is marked through a magenta dotted line. In accordance with the results depicted in Figure 6.7 and Figure 6.8, even under a significant load variability, a structural change may be clearly identified by simply observing the time-series regarding the prestress loss. Conversely, as the changes produced on

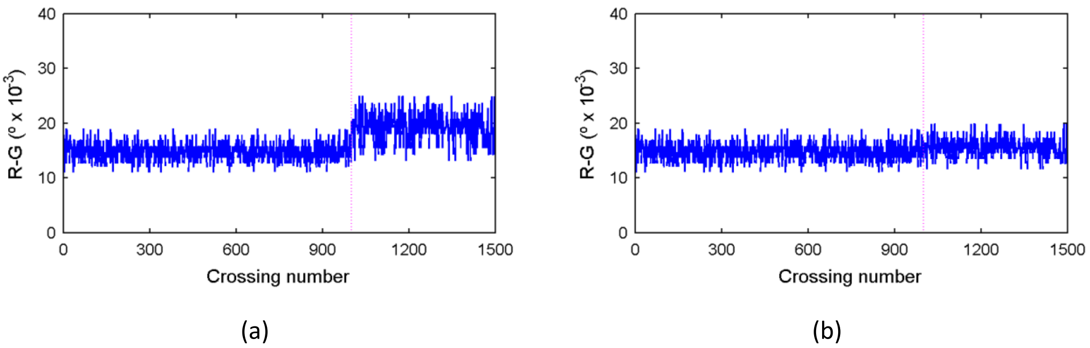

(a)

(b)

Figure 6.9 – Time-series of type i (including only the highest absolute values of each influence-line) of the rotation on the alignment G (R-G) for: (a) a prestress loss (DS1); and (b) a restraint for the longitudinal rotation of a support bearing (DS2).

the highest absolute values of the rotation in the alignment G by the restraint for the longitudinal rotation of the support bearing are negligible, this structural change may not be detected in the time-series.

6.4.3. Results

The approach for damage detection based on time-series of moving-loads data proposed herein requires an initial stage – the training period – in which the structure is assumed to behave normally. The purpose of this initial period is to estimate the variability of the control parameters selected in the data-processing algorithm under analysis, and to establish the thresholds for damage identification in the monitoring phase. As referred above, the control parameters for each data-processing algorithm are as follows: the residuals for robust regression analysis (RRA), computed on the basis of the regression model established in the reference period; the coordinates of the first principal component for moving principal component analysis (MPCA); and the measure of consistency for the influence-line assurance criterion (ILAC).

Within this work, the training period comprises 800 crossings. The thresholds for flagging damage were based on the average, μ, and on the standard deviation, σ, of the control values obtained in the training period. The thresholds for normal operation were given as $\mu \pm k \cdot \sigma$, in which k is a parameter that determines the amplitude of the interval. This parameter is carefully chosen in order to, on one hand, enable a swift damage identification and, on the other, prevent false-positive indication of damage. Therefore, in this work this parameter was set equal to 4. In addition, with the objective of increasing the reliability of this approach by avoiding false-positive indication of damage, changes in the structural response are signalized only when 10 consecutive control values exceed the thresholds. The application of MPCA requires the definition of an additional parameter: the size of the moving-window, which was assumed equal to 300 crossings.

As aforementioned, RRA and ILAC were used to process data concerning time-series of, respectively, type i (including only the highest absolute value of each influence-line) and type ii (including the measurements of the whole influence-line). MPCA was used to process time-series of both types. The results of the application of these data-processing algorithms to the time-series regarding either the prestress loss (DS1) or the restraint for the longitudinal rotation of a support bearing (DS2) are summarized in Table 6.2. When damage is correctly identified, the time for damage detection in terms of the number of crossings required to

Table 6.2 – Results of the application of the data-processing algorithms, in terms of the number of crossings required to identify the occurrence of damage, for time-series regarding both damage scenarios 1 and 2 (respectively, DS1 and DS2). ND and FP regards cases in which the damage was not detected and there was a false-positive indication of damage, respectively.

	RRA (i)		MPCA (i)		MPCA (ii)		ILAC (ii)	
	DS1	DS2	DS1	DS2	DS1	DS2	DS1	DS2
MS-a	10	10	FP	FP	11	11	11	11
MS-b	10	10	FP	FP	FP	FP	11	11
MS-c	10	10	11	41	16	12	11	11
MS-d	10	10	11	42	12	11	11	17
MS-e	26	18	11	25	11	15	11	ND

identify the occurrence of damage, is indicated. No detection and false-positive indication of damaged are identified, respectively, as ND and FP.

As shown in the table above, RRA flags the occurrence of damage for both changes in the structural condition simulated herein, using either monitoring system under analysis. Figure 6.10 depicts the residuals resulting from the application of RRA between the measurements collected by R-A and R-E (sensors included in the monitoring systems MS-a to MS-c), for both damage scenarios. For the first damage scenario (DS1), the changes in the magnitude of the highest absolute values of the rotations are significant, thus leading to a significant increase in the residuals computed in relation to the regression model established in the training period (see Figure 6.10 (a)). As regards the second damage scenario (DS2), although the changes in

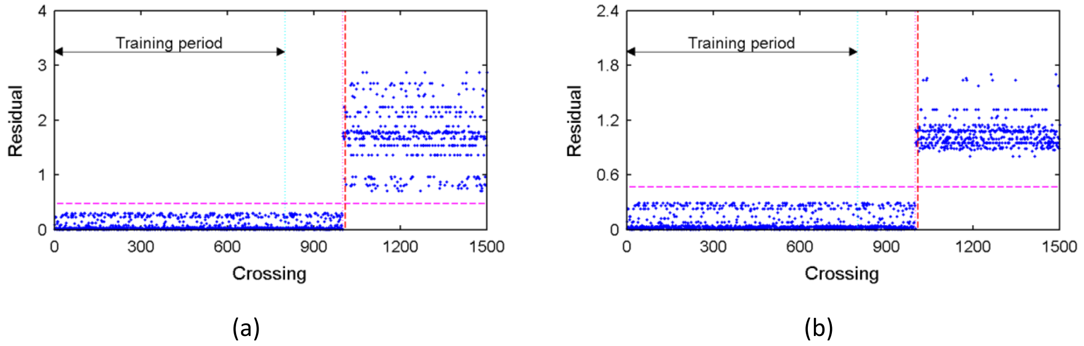

(a) (b)

Figure 6.10 – Residuals resulting from the application of RRA (i) between the measurements collected by R-A and R-E for the damage scenarios: (a) DS1; and (b) DS2.

the structural response are less pronounced, the application of the RRA enables to enhance this structural modification (see Figure 6.10 (b)).

It is noteworthy to mention that, even for the cases in which the modifications in the highest absolute values are very slight, this data-processing algorithm enables to detect the structural changes. Consider, for instance, the results of the crack-widths (included in the monitoring system MS-e), for the restraint of the support bearing longitudinal rotation. As shown in Figure 6.6, this structural change induces very slight changes both in the highest absolute values and in the shape of the influence-line. Nevertheless, a slight decrease and a small increase are noticeable in the measurements of respectively, CW-B and CW-D. Figure 6.11 (a) depicts a scatter plot of the measurements collected by both sensors. Blue and red points regard, respectively, the baseline and the damaged conditions. Note that although the modifications in the measurements collected by each sensor are very slight, the scatter plot comparing both sensors enhances the structural change. Consequently, the residuals computed in relation to the regression model estimated for the training period register a significant increase, as shown in Figure 6.11 (b). Even though, the time for detection is slightly higher than that obtained with the remaining monitoring systems.

As regards the application of MPCA on time-series of type i (including only the highest absolute value of each influence-line), the results of the monitoring systems MS-a and MS-b show a false-positive indication of damage for both anomalous scenarios simulated in this work. Figure 6.12 shows the coordinate of the first principal component related with R-A for the application of MPCA on the time-series regarding the damage scenario DS1, for both MS-a and MS-b. It is clear that although the control values exceed the thresholds at a time-instant in which the structural condition is equal to that of the training period, thus resulting in a false-positive indication, when damage occurs the variations are clearly higher. Therefore, a slight

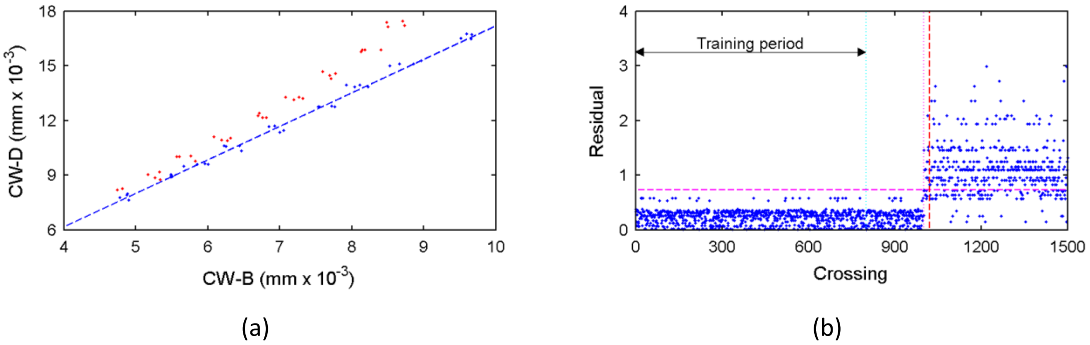

Figure 6.11 – Results from the application of RRA (i) between the measurements collected by CW-B and CW-D for the damage scenario DS2: (a) scatter plot, in which the blue and the red points regard, respectively, the baseline and the damaged conditions; and (b) residuals.

increase in the threshold bounds would prevent the false-positive indication of damage without compromising the promptness of damage identification.

Note that even in the cases in which the changes in the highest absolute values are slight, similarly to the situation discussed above for RRA (i), this data-processing algorithm enables also to detect the structural changes. See Figure 6.13 in which the evolution of a selected coordinate of the first principal component regarding either the application on MS-d (comprising only average-strains measurements) and MS-e (including only crack-widths opening) is depicted. However, the changes in the coordinates of the first principal component are less pronounced. Consequently, the number of crossings required for detection is higher.

The application of MPCA to time-series of type ii enables to detect both damage scenarios, using either monitoring system under analysis. Even though, the results of this data-processing algorithm using the monitoring system MS-b show a false-positive indication of damage in both scenarios. Figure 6.14 shows the time-history of the coordinate of the principal component for the application of MPCA for damage scenario DS1 using either MS-a or MS-b.

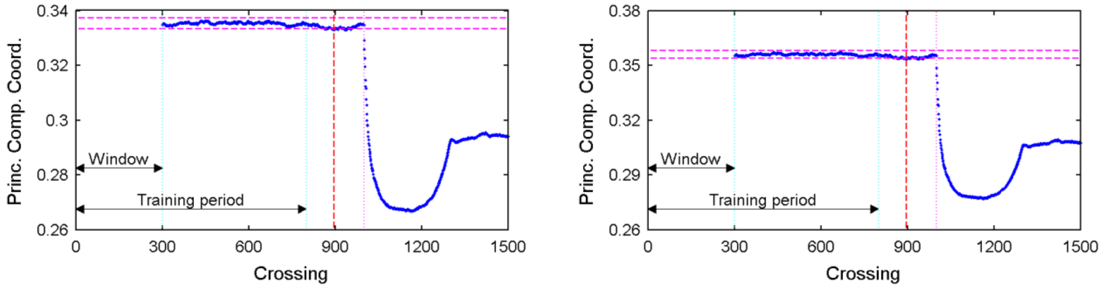

(a) (b)

Figure 6.12 – Coordinate of the first principal component related with R-A for the application of MPCA (i) on the time-series regarding the damage scenario DS1, for the monitoring system: (a) MS-a; and (b) MS-b.

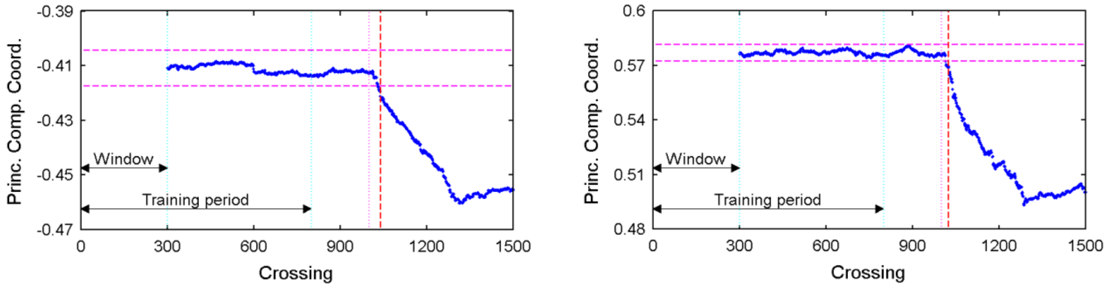

(a) (b)

Figure 6.13 – Coordinate of the first principal component, for the application of MPCA (i), related with: (a) AS-D-B, included in MS-d; and (b) CW-B, included in MS-e; for damage scenario DS2.

Note that in both cases a significant change in the control values is observed when damage occurs. However, for the monitoring system MS-b (see Figure 6.14 (b)) the control values exceed the thresholds before the change on the structural condition takes place, thus resulting in a false-positive indication of damage. Still, a slight increase in the threshold bounds would prevent the false-positive indication of damage without compromising the swiftness of damage identification.

In the cases in which the changes produced in the influence-lines by the structural changes are very slight, this data-processing algorithm is also capable of detecting the damage occurrence. Consider for instance the cases of the monitoring systems comprising either the average strains (MS-d) or the crack-widths opening (MS-e). As shown in Figure 6.15, the changes in the coordinates of the first principal component when the structural condition is modified are clear for both cases.

As regards the application of ILAC on time-series of type ii (including the measurements of the

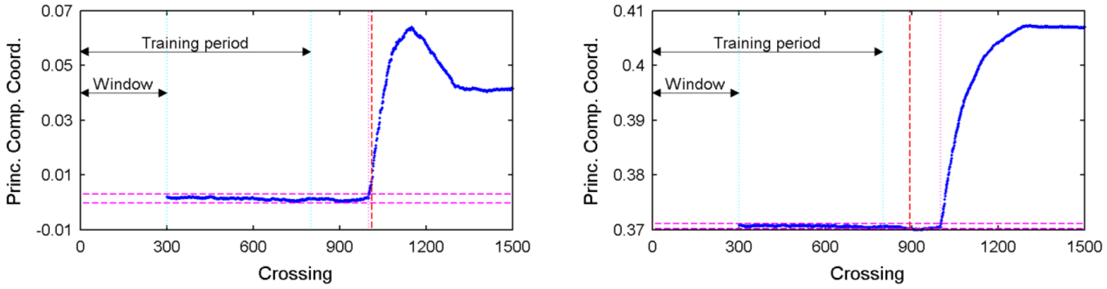

(a) (b)

Figure 6.14 – Coordinate of the first principal component, for the application of MPCA (ii), related with: (a) VD-D, included in MS-a; and (b) R-A, included in MS-b; for damage scenario DS1.

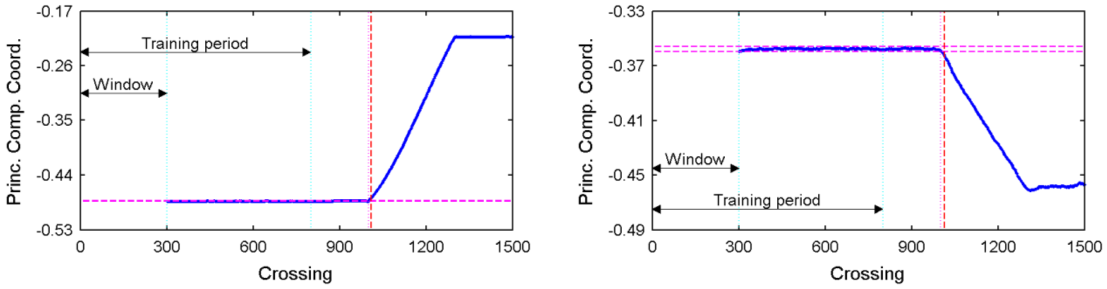

(a) (b)

Figure 6.15 – Coordinate of the first principal component, for the application of MPCA (ii), related with: (a) AS-F-T, included in MS-d; and (b) CW-B, included in MS-e; for damage scenario DS2.

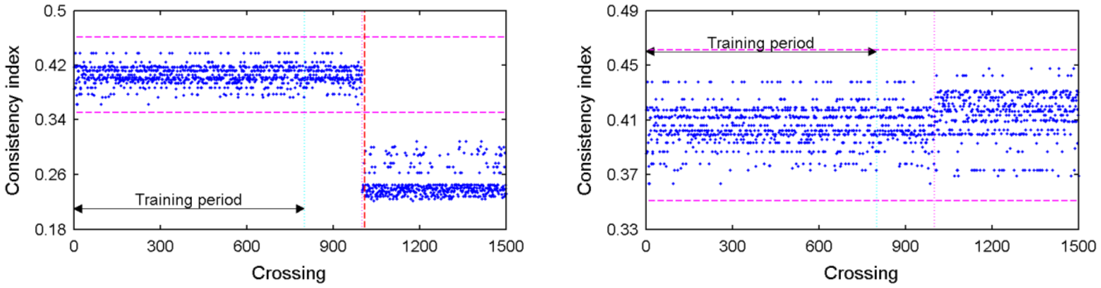

(a)

(b)

Figure 6.16 – Measures of consistency resulting from the application of ILAC (ii) between the measurements collected by CW-D and CW-F for the damage scenarios: (a) DS1; and (b) DS2.

whole influence-line), the results show that, in general, damage may be promptly detected. Figure 6.16 (a) depicts the evolution of the measures of consistency resulting from the application of ILAC between the measurements collected by CW-D and CW-F for the prestress loss (DS1). The changes are clear and, thus, damage is swiftly detected. However, as regards the restraint for the longitudinal rotation of a support bearing (DS2), given that the changes produced in the shape of the influence-lines are not significant, the changes in the measures of consistency are also slight (see Figure 6.16 (b)). Therefore, the structural change is not flagged.

6.5. Conclusions

This chapter addresses the application of an alternative approach for early damage detection using experimental influence-lines data provided by loads of different magnitude. This methodology involves, firstly, building time-series of moving-loads responses, and, secondly, data-processing using adequate algorithms. This methodology has shown to be successful for early damage detection when applied to numerically-simulated data. Therefore, the aim of this chapter was to assess its performance when applied to experimental responses.

A reduced-scale reinforced and prestressed concrete laboratorial model was chosen as case study. Moreover, aiming at the later application of this approach in full-scale bridges, the tests were designed with the purpose of replicating as close as possible two typical damage scenarios: a prestress loss (DS1) and a partial restraint for the longitudinal rotation of a support bearing (DS2). In addition, time-series based on experimental data concerning both damage scenarios were built following an especially devoted approach. Two types of time-series were addressed. The first, denoted as type i, regards the highest absolute values collected for each crossing. The second, denoted as type ii, includes the whole influence-line.

Then, these data were analysed by three selected algorithms for early damage detection. Robust regression analysis (RRA) and influence-line assurance criterion (ILAC) were used to process data concerning time-series of, respectively, type i and type ii. Moving principal component analysis (MPCA) was applied to process time-series of both types. In addition, taking advantage of the comprehensive monitoring system installed in the laboratorial model, the performance of different measurement systems, regarding the most appropriate quantities to be observed, as well as the number and type of sensors to be adopted, was also assessed.

The results show that, in general, either algorithm provides satisfactory results, irrespectively the monitoring system considered or the damage scenario under analysis. However, for the damage scenario 2, ILAC is not able to detect damage when the monitoring system under analysis comprises only crack-widths data. In addition, MPCA, using either time-series of type i or type $ii,$ gives a false-positive indication of damage when mixed measurement systems were considered. Still, a deeper insight into the results enabled to observe that if the threshold bounds are slightly increased this false-positive indication of damage is prevented without jeopardizing the ability of promptly detecting damage.

Finally, it is worth mentioning that the damages applied to the structure caused very different impact in the measured quantities, not producing significant effects in some of them. Therefore, an appropriate development of the monitoring system, regarding the number and type of sensors to be installed and cross-sections to be instrumented, is paramount to obtain reliable field data for successfully detecting the occurrence of damage, regardless of the adopted technique.

Chapter 7

Characterization of the railway traffic of a centenary steel bridge – The Luiz I Bridge

7.1. Introduction

In the last decades road freight transport has grown significantly, which, together with the strong competition between transport modes and companies, led to an increase in the number of fully loaded trucks and of their gross weight (WAVE, 2001a). However, trucks exceeding the legal weight limits pose to road transport operations serious problems such as: (i) increase of the risk of traffic accidents; (ii) occurrence of severe impacts on the safety and durability of the infrastructures, namely on pavements and bridges; and (iii) increase of an unfair competition between transport modes and companies (Jacob and Feypell de La Beaumelle, 2010). Therefore, it is critical to ensure truck compliance to weight regulations. In this context, it is essential for road authorities to have at their disposal up to date and on-line measurements of axles and vehicles weights. These data can be further used to improve knowledge of traffic for economic surveys, statistics and management, and to support both the design and maintenance of the infrastructures (WAVE, 2001a).

In this context, weigh-in-motion (WIM) systems, that allow to estimate vehicles parameters such as gross weight, speed, number of axles, axle loads, the distance between axles, etc., without affecting the traffic flow, have been developed in the last decades. WIM systems were introduced in the United States in the mid 1950’s and since then many developments and progresses have taken place (Jacob and Feypell de La Beaumelle, 2010; Jacob and Loo, 2008; Jacob and O'Brien, 2005). Although WIM systems have been developed for road traffic (Quilligan, 2003), the separation between the railway infrastructures administrators and train operators has led to the need of monitoring and controlling the train loads and, subsequently, to the deployment of these systems in the railway infrastructure (Liljencrantz, 2007). There are primarily two categories of WIM systems (MAINLINE, 2013; Quilligan, 2003): pavement- or track- and bridge-based. The former systems consist of sensors embedded in or bonded to the pavement, perpendicular to the traffic direction, in the case of road infrastructures, and installed on the track in the case of railway lines. The latter use an instrumented bridge as a large scale calibrated to weigh axles and vehicles.

Bridge weigh-in-motion (B-WIM) systems were introduced in the USA in the late 1970's by Moses (1979). The proposed system combined traffic sensors and strain gauges on highway bridge girders to obtain axle and gross weights. The method has been extended much further and today, due to safety, durability and congestion implications of having sensors on the road surface, the focus is on Nothing-On-Road (NOR) systems (O'Brien *et al.*, 2008). Despite the differences between B-WIM on railways and on roads (Karoumi *et al.*, 2007), these systems have several advantages in comparison with traditional WIM (Karoumi *et al.*, 2007; WAVE, 2001b). However, the method has not been widely adopted for the weighing of road vehicles and is much less used in the railway infrastructure.

Liljencrantz *et al.* (2007) implemented a B-WIM system in a short span concrete integral bridge, carrying two ballasted railway tracks. The system comprised four strain transducers embedded in concrete and enabled to determine the axle distances, static axle loads, speed and acceleration of the train, and the direction and the track on which the train was crossing. This work was extended and Liljencrantz and Karoumi (2009) report the application of the methodology in an eleven span prestressed concrete structure carrying two unballasted tracks and in a simply supported composite bridge carrying one ballasted track, using a minimum of four strain transducers installed to measure the transverse effect of passing trains. Pimentel *et al.* (2008) presented a system using only three fibre Bragg grating (FBG) sensors to determine the speed and weigh distribution of trains in a short span railway bridge. In this application, the deformation measurements of the rail were used instead of those of the bridge for the identification of the geometry and speed of the train. The axle loads were estimated by using a third measurement of deformation in one of the bridge's beam. Recently, González Silva and Karoumi (2015) presented a B-WIM system comprising only two strain gauges, implemented in a bridge consisting of a continuous steel grillage with six spans. The bridge has two tracks with wooden sleepers resting directly on the stringer beams. As both sensors were installed in a stringer, the system only enables to characterize the traffic on one track.

This chapter presents a B-WIM system implemented in a centenary steel truss bridge, the Luiz I Bridge located in Porto, carrying two unballasted tracks integrated in the metro rail network. The system comprises only two fibre-optic strain gauges installed at the mid cross-section of two crossbeams. Hence, it enables the characterization of the traffic, irrespectively of the track on which the vehicles are crossing.

This work has been motivated by an increasing interest from the infrastructure administrator in taking the maximum advantage of the comprehensive monitoring system installed in the bridge, within the rehabilitation and strengthening works carried out to allow the integration of its upper deck in the Porto metro light rail network (Costa and Figueiras, 2012). This system was initially implemented with two primary objectives. The first was to appraise the strengthening solutions performance by comparing the results of two load tests carried out before and after the rehabilitation works. The second was to monitor the bridge's structural health by identifying changes in the measured deformations of key elements due to unexpected loading events or caused by the surrounding environment, namely temperature variations. In this work, the traffic characterization emerges as a third application of this monitoring system. Furthermore, the record of the structure response combined with the knowledge of the corresponding inducing loads is of great interest in monitoring the structural condition, not only on issues related to fatigue (Treacy and Brühwiler, 2011) but also for damage detection purposes (Cantero *et al.*, 2015). In this context, in addition to the characterization of the traffic, this B-WIM system will be also used to obtain influence-line data of the in-service vehicles crossings, for later application of damage detection methodologies based on moving-load responses (Cavadas *et al.*, 2013b).

This chapter is divided in six sections, including this introduction and a final section in which the main conclusions drawn from this work are summarized. In the second section, the Luiz I Bridge is described and in the third section the main aspects regarding the structural response under metro traffic are discussed. The fourth section is devoted to the description of the procedure for identifying vehicles crossing the bridge and for determining the direction and the travelling speed. This section includes, in addition, the description of the approach for obtaining influence-lines data. Finally, the procedure for estimating the vehicles loads is presented in the fifth section.

7.2. The Luiz I Bridge

7.2.1. General remarks

Luiz I Bridge spans the Douro River, connecting the cities of Porto and Vila Nova de Gaia, in the north of Portugal (Figure 7.1). This Porto’s iconic double-deck bridge was designed by the Belgian Engineer Théophile Seyrig, a former partner of Gustave Eiffel, and constructed by the *Société Anonyme de Constructions et des Ateliers de Willebroeck*. Inaugurated in 1886, it was at that time the longest steel arch in the world (Figueiras *et al.*, 2005).

The bridge is constituted by a metallic double hinged arch, supporting simultaneously two decks at different levels over the river crossing (Figure 7.2). The arch has a parabolic geometry, both in the vertical and plan views, with a span length of 172 m and a height of 45.1 m. Its apparent vertical thickness is variable, ranging from 16.7 m at the supports to 7.1 m at the crown. The lower deck, 8 m wide and 174.3 m long, is supported at the abutments and suspended from the arch by four ties 36 m apart. The upper deck, 10 m wide and 391.25 m long, is supported by the arch crown, seven piers, either made of masonry or steel, and the abutments. Both decks have at the abutments bearing devices that enable longitudinal displacements. The connections between the upper deck and the piers located over the river banks are accomplished by similar supports whereas the piers supported by the arch are rigidly connected at both ends. Besides the pedestrian traffic, the lower deck carries a roadway and the upper deck holds, at the present time, a double tram-train railway line. The upstream track is devoted to the vehicles that cross the bridge in the south-north direction (denoted in this work as direction 1) whereas the downstream track is devoted to the north-south direction (denoted herein as direction 2). In addition, on the upper deck, the circulation of emergency road vehicles is allowed.

Figure 7.1 – General view of the Luiz I Bridge (South (Gaia) on the left and North (Porto) on the right).

Despite some operations of rehabilitation and maintenance or minor changes carried out to accommodate the passage of new types of vehicles, the structure has been in continuous operation since its construction. However, in 2005 a major strengthening and rehabilitation process took place on this bridge aiming at the integration of its upper deck in the infrastructure of the Porto metro light rail network. During this process, a very comprehensive fibre Bragg grating (FBG) based monitoring system was implemented with two main purposes (Costa and Figueiras, 2012). The first was to appraise the strengthening solutions performance by comparing the results of two load tests carried out before and after the rehabilitation works. The second was to monitor the bridge's structural health by identifying changes in the measured deformations of key elements due to unexpected loading events or caused by changes in the surrounding environment, namely temperature variations.

In this work, the implementation of a B-WIM system to characterize the metro traffic on the upper deck emerges as a third application of this monitoring system. In addition, this B-WIM system will be also used to obtain influence-line data of the in-service vehicles crossings for later application of damage detection methodologies based on moving-loads responses (Cavadas *et al.*, 2013b). By default, within the continuous monitoring of the structural health of the bridge, the acquisition program collects the sensors signals at intervals of five minutes. These data are suitable for the characterization of the bridge response induced by ambient actions, namely temperature, and allows capturing significant behaviour variations in time caused by degradation or gradual damage. In the context of this study, a specific area of the upper deck was selected, which holds sensors distributed among four optical branches, and whose signals were recorded with a frequency of 50 Hz. These data have allowed to properly characterize the traffic in terms of type of metro composition crossing the bridge, the track and the direction in which the vehicles travel, the speed and the vehicles loads, as well as it has enabled the collection of influence-lines for later application of damage detection methods.

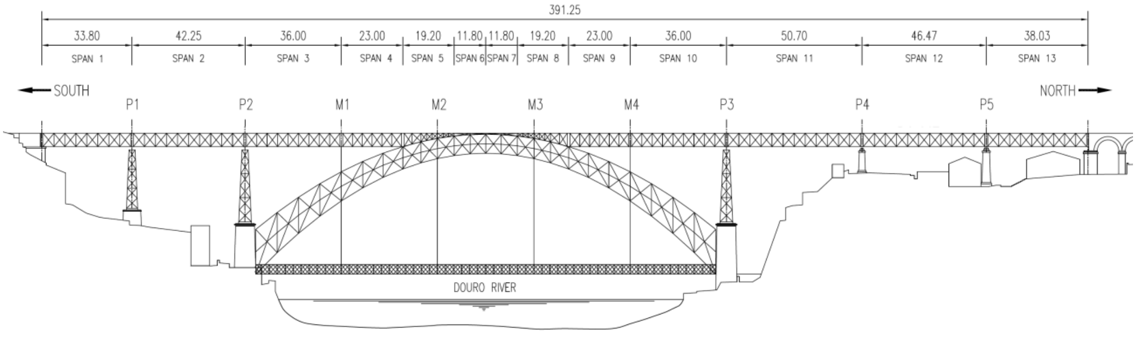

Figure 7.2 – Scheme of the side view of the Luiz I Bridge.

7.2.2. Structural characterization of the upper deck

The upper deck, 391.25 m long and 10 m wide, comprises two continuous truss girders, 4.65 m apart, supported by the arch crown, seven piers and the abutments, materializing a total of 13 spans (Figure 7.2). These truss girders are laterally braced by diagonal and transverse beams at the chords' levels, in the verticals alignment. In general, the girders are 5 m high. However, in the area where the upper deck and the arch merge, these girders have variable height. At the two central spans, the truss girders are replaced by I-profiles.

The floor system combines two load transfer systems. The first one consists of a set of secondary stringers and transverse beams carrying a steel cladding plate to which the pedestrian and emergency road vehicles loads are applied. The second one is formed by the rails and the wooden sleepers (see Figure 7.3.a), and receives the loads of the metro vehicles. Both systems are supported on a main grid of stringers and crossbeams (see Figure 7.3.b), which are transversely extended by means of cantilevers in order to comprise the 1.75 m wide lateral sidewalks. The crossbeams deliver the loads to the girders' top chords at the nodes in each vertical alignment. In this way, the upper deck loads are not directly applied to the girders' chords, thereby preventing that adverse additional local forces to the original steel may arise.

(a) (b)

Figure 7.3 – General view of the upper deck of the Luiz I Bridge: (a) top view; and (b) bottom view.

7.2.3. Monitoring system

The monitoring system installed on the bridge during the rehabilitation works consists in a fibre-optic network comprising 15 optical channels containing multiple FBG sensors connected in series. It enables the measurement of: (i) strains in selected truss elements of the bridge structure; (ii) horizontal displacements of the bridge upper deck; and (iii) temperature of the ambient air and experienced by the steel. The strains were measured in 59 cross-sections of selected truss elements, through a pair of strain sensors installed in each, distributed as follows: 30 in the upper deck, 14 in the arch, 9 in suspension ties and 6 in piers. Eight fibre-optic-based displacement transducers were installed to measure the relative horizontal movements between the bridge upper deck and both the abutments (three in each end of the deck, of which two at the bottom chords level and one close to the floor system) and the pier P5 (two at the bottom chords level). The temperature sensors were distributed as follows: six in the arch chords (four at the crown and two at the south support) and four in the upper deck bottom chords, at the first spans over the river banks (Costa and Figueiras, 2012).

As referred above, this monitoring system has been used for long-term continuous observation of the bridge behaviour due to changes in the surrounding environment, namely temperature variations, as well as shifts induced by slow deterioration phenomena. For this purpose, the sensors signals have been acquired every five minutes, which constitutes a low reading frequency for fully capturing the structural response under the metro vehicles crossing. Therefore, in the context of the work presented herein, two spans of the upper deck instrumented with sensors allocated to four channels were selected, for which the data acquisition rate was set at 50 Hz. This upgraded setting has allowed a complete characterization of the traffic in terms of speed, travelling direction and bogies' loads, as well as the collection of influence-lines, without jeopardizing the primary objective of the monitoring system.

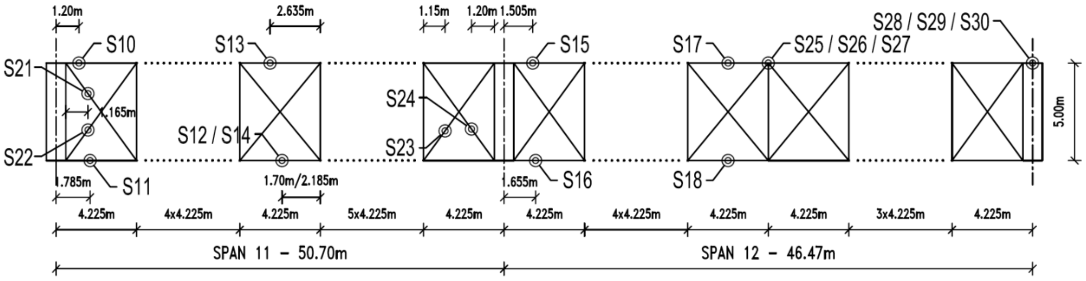

Figure 7.4 – Scheme of the side view of the upper deck depicting the location of the instrumented cross-sections.

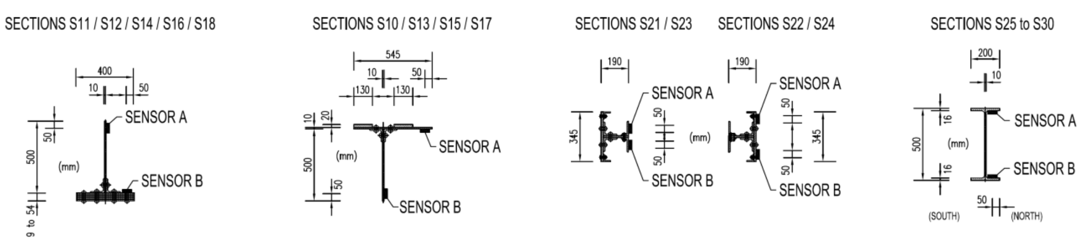

Figure 7.5 – Scheme of the instrumented cross-sections.

The selected region comprises 19 instrumented cross-sections distributed as follows: (i) five at the bottom chords; (ii) four at the top chords; (iii) four in diagonals; and (iv) six in crossbeams. Except for the cross-section denoted as S12, located at mid-span of the upstream bottom chord at the 11th span, both the bottom and top chords, as well as the diagonals, were instrumented in the downstream girder. Two crossbeams were instrumented at the mid cross-section (S26 and S29) and at cross-sections near the downstream (S25 and S28) and upstream (S27 and S30) girders. Figure 7.4 depicts the location of the instrumented cross-sections in the upper deck spans under study and Figure 7.5 presents the corresponding layout of the applied strain sensors.

7.2.4. Loading system

The upper deck of the Luiz I Bridge holds the Yellow double railway Line (D) integrated in the Porto Metro Network, in which the travelling vehicles are *Eurotram* trains produced by *Bombardier Transportation*, with a capacity for 80-seated places and capable of reaching 80 km/h. One or two coupled vehicles may constitute the metro compositions. However, this work has targeted only one-vehicle compositions. The dimensions of the vehicle as well as the loads corresponding to its tare weight are depicted in Figure 7.6.

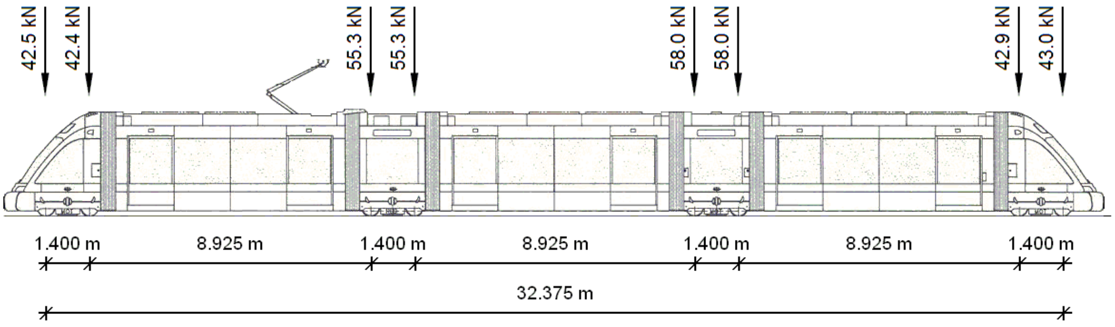

Figure 7.6 – Scheme of a metro vehicle.

7.3. Analysis of the structural response under metro traffic

7.3.1. General remarks

The instrumented spans of the upper deck selected with the objective of characterizing the metro traffic and collecting influence-lines for later application of damage detection methodologies, include a set of cross-sections instrumented in different truss elements and in distinct positions along the spans (see section 7.2.3). Consequently, significant differences in the structural response under the metro traffic, both in terms of magnitude and shape, are expected over the instrumented cross-sections. Hence, with the goal of selecting the most adequate truss elements and cross-sections to accomplish the objectives referred above, the analysis of the structural behaviour is essential. In this context, the structural response under the metro crossing is simulated with an adequate finite-element (FE) model of the bridge (Costa, 2012), and compared with the measurements. The main objectives are: (i) evaluating the contribution of each internal force (axial force and bending moments) in the overall deformations measured by the sensors; and (ii) assessing the effects of the successive passage of the vehicle axles over the instrumented truss elements.

7.3.2. Brief description of the numerical model

The FE model of the bridge used herein to simulate the structural response induced by the metro crossing was developed with the objective of appraising the performance of the strengthening solutions adopted in the bridge rehabilitation (Costa, 2012). It consists in a complete 3D FE linear and elastic model (see Figure 7.7) that simulates the bridge condition after the rehabilitation and strengthening works. The model was created on the basis of two-node frame elements, which have three translational degrees of freedom (DOFs) and three rotational DOFs at each node. Consequently, in correspondence with the DOFs, these elements account for one axial force, two shear forces, one torsion moment and two bending moments. The deformation holds contributions from the shear forces. In addition, four-node shell

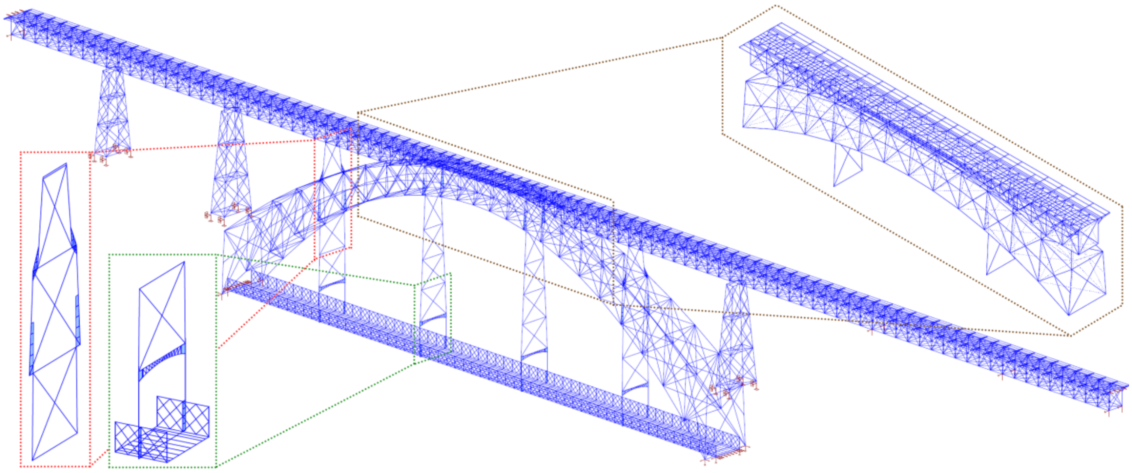

Figure 7.7 – General view of the FE model (Costa, 2012).

elements have been adopted in order to simulate the slab and plate actions of thin 2D structural elements. Further details concerning the numerical modelling can be found in (Costa, 2012)[2].

7.3.3. Results

With the objective of assessing the structural behaviour of the bridge under the metro traffic this section presents the comparison between the measurements and the numerical estimates. As referred above, the instrumented cross-sections are mainly located in the downstream truss girder. Therefore, the comparison presented herein regards a crossing of a 1-vehicle composition, with no passengers, traversing the bridge in the direction 2 (north-south), in which the vehicle travels in the downstream track. The results are presented graphically and show the variation of strain as the metro traverses the bridge. The abscissas correspond to the position of the vehicle centre.

Figure 7.8 depicts the field results and the corresponding numerical estimates of the strains collected at the chords cross-sections instrumented both at mid-span and near the supports. As carefully detailed in (Costa, 2012), it is clearly perceptible that these cross-sections deformations hold two main components. The first is caused by the axial force acting in the truss element as a result of the upper deck bending, which can be seen as the global response of this structural component. The bending moment acting in the upper deck is carried by a couple of longitudinal forces, one at the top chords and the other at the bottom chords. Therefore, the axial stiffness of the chords determines the bending stiffness of the upper deck. The second component is caused by the chords bending, which can be regarded as the local response of these elements. Consequently, the strain state induced by the first component is attenuated on one side of the cross-section and magnified on the other. The strain gradients registered in the cross-sections may be more or less significant, depending on the magnitude of the bending moment experienced by the chords.

As the metro traverses the 12th span, the cross-section located at mid-span of the bottom chord (S18), is subjected to tensile stresses due to the upper deck bending. In addition, due to the chord's bending, the tensile deformation of the flange (sensor B) is increased and that of the web (sensor A) is decreased (see Figure 7.8.b). On the contrary, the cross-section located at mid-span of the top chord (S17) is under compressive stresses. As regards the local

---

[2] The finite element model as well as the numerical simulations was entirely developed by Dr. Bruno Costa. Still, its inclusion in this thesis was crucial for the understanding of the whole text.

response, although the axles effects cannot be separated, the results exhibit a set of local maxima/minima, which correspond to the passage of the bogies over the instrumented truss element (see Figure 7.8.a). In addition, it is noteworthy that as the bogies reach the instrumented element the bending of the chord leads to such a decrease of the compressive deformation in the web so that tensile strains are induced. The behaviour exhibited at the cross-sections instrumented near the supports (see Figure 7.8.c and d) is similar to that observed at the mid-span cross-sections. Both the upper deck and the chords bending are clearly perceptible in the response. In addition, the successive passage of the bogies over the instrumented cross-sections, although more pronounced at the top chord cross-sections, may be detected. However, it should be referred that as the vehicle traverses the adjacent spans of the support near which the elements are instrumented, due to the deck bending, the top and bottom chords are, respectively, under tensile and compressive strains.

In general, the numerical estimates show a good agreement with the field results. Even though, the correlation between the field data and the numerical estimates is significantly better for the sensors installed in the flanges than those in the webs. As the distance from the centre of gravity of the cross-section to the sensor located in the web is higher than that to the sensor installed in the flange, slight differences in the estimates of the bending moment may lead to higher deviations in the strain estimates in the former than in the latter. Still, both the global and the local behaviour of the upper deck chords is satisfactorily reproduced by the FE model.

The field results and the corresponding numerical estimates of the strains collected at the instrumented cross-sections of two diagonals are depicted in Figure 7.9. Bearing in mind their position in the span, the strain pattern observed in both is quite similar. First, under the passage of a 1-vehicle composition the cross-section is in a compressive state. Second, the results show small strain gradients, although that observed at cross-section S22 is clearly higher than that at S24. Third, the measurements exhibit a set of local minima, which correspond to the passage of each bogie over the instrumented truss element. This is clearly shown in the figure inasmuch the vehicle positions are in correspondence with each local minimum. Note that, as detailed in section 7.2.2, the railway loads are carried to the girders by the crossbeams at the intersection nodes of the top chord, the verticals and the diagonals. Consequently, the aforementioned local minima occurs when the bogies pass over these intersection nodes (located 4.225 m apart the supports alignment, as marked by circles in Figure 7.9). Finally it should be stressed that a good agreement between the field results and the numerical estimates was found, although the former are slightly higher than the latter.

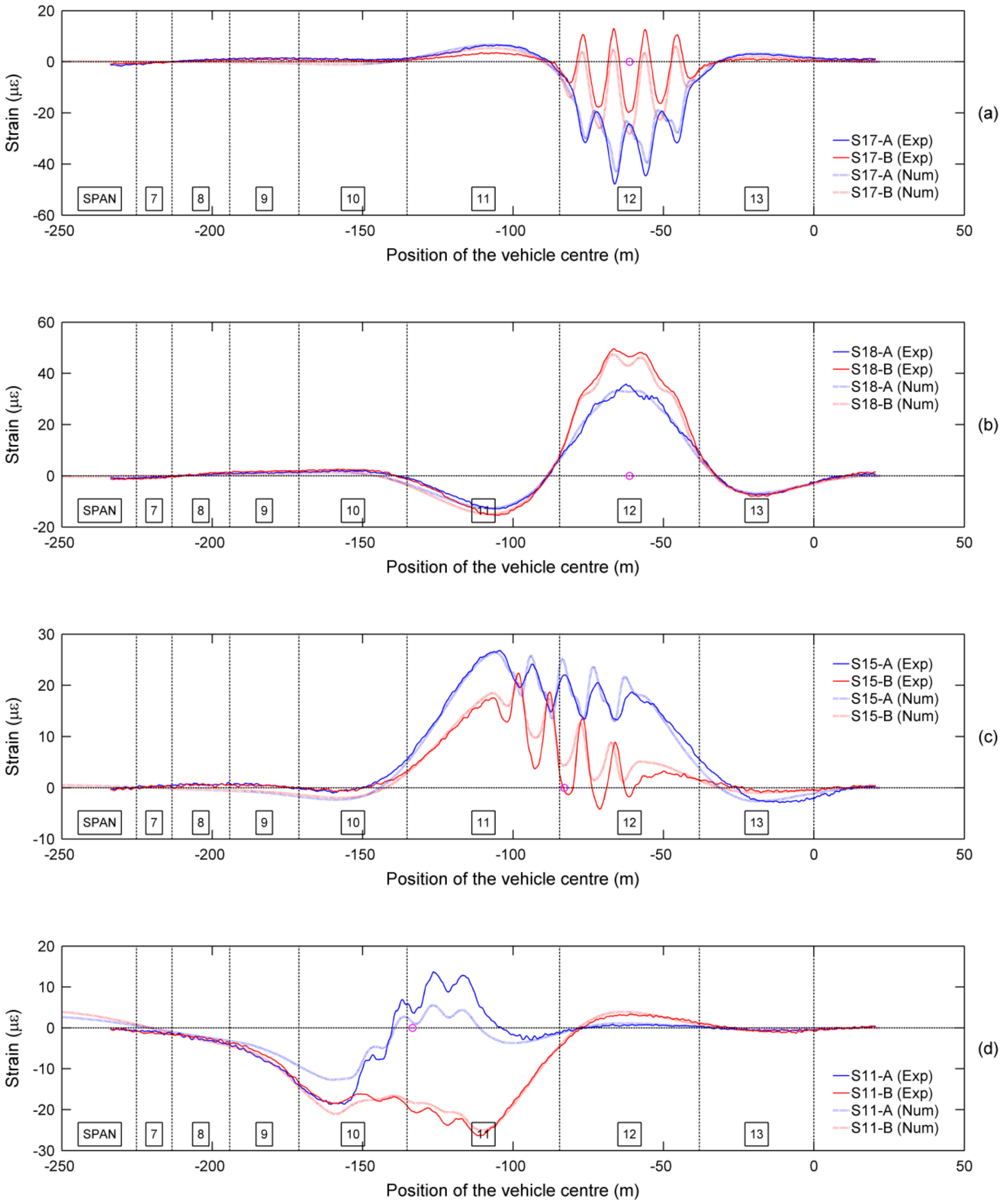

Figure 7.8 – Comparison between the measurements and the FE model estimates of the strains at the chords cross-sections, induced by a 1-vehicle composition crossing the bridge in the direction 2: (a) top chord at mid-span – S17; (b) bottom chord at mid-span – S18; (c) top chord near the support – S15; and (d) bottom chord near the support – S11.

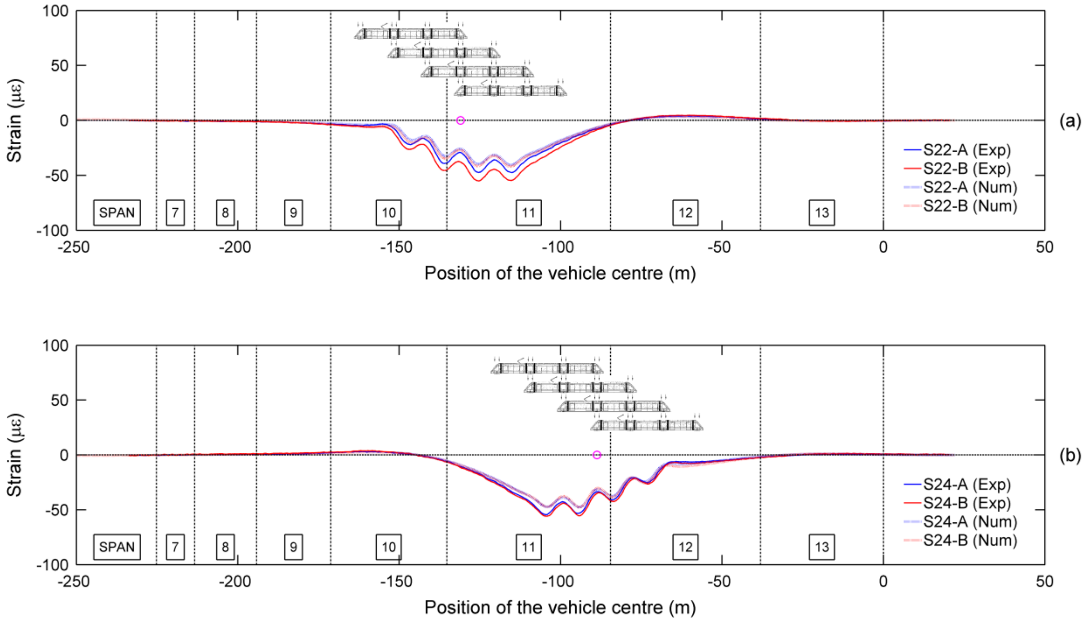

Figure 7.9 – Comparison between the measurements and the FE model estimates of the strains at the diagonals cross-sections, induced by a 1-vehicle composition crossing the bridge in the direction 2: (a) S22; and (b) S24.

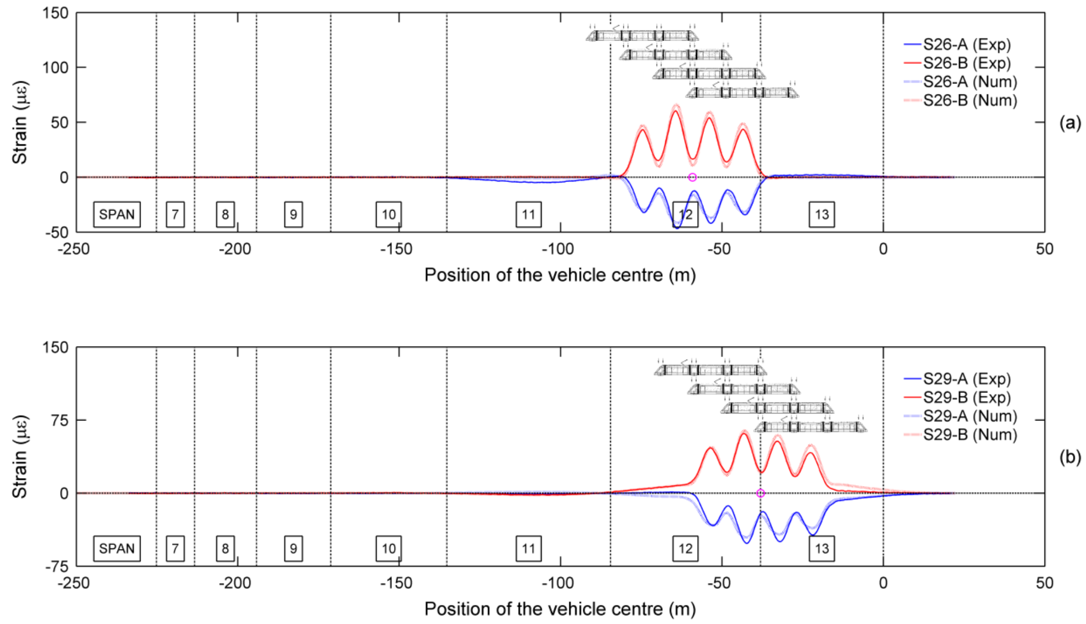

Figure 7.10 – Comparison between the measurements and the FE model estimates of the strains at the crossbeams cross-sections, induced by a 1-vehicle composition crossing the bridge in the direction 2: (a) mid cross-section of the crossbeam at mid-span – S26; and (b) mid cross-section of the crossbeam over the support – S29.

Figure 7.10 depicts the field results and the corresponding numerical estimates of the strains collected at the crossbeams cross-sections. These deformations hold two main components. The first is caused by the fact that the axes of the crossbeams are displaced from the horizontal alignment defined by the girders upper nodes. The transverse rotation of these nodes leads to the development of axial forces in those members. The second component is caused by the crossbeams bending. Still, the major contribution to the overall deformation of these cross-sections lies on the second component. The results exhibit a set of local maxima/minima, which correspond to the passage of each bogie over the instrumented cross-section. As depicted in Figure 7.9, the vehicle positions in correspondence with each local maximum/minimum are also shown herein. Again, a good agreement between the field results and the numerical estimates was found. Therefore, it is shown that the FE model satisfactorily reproduces the behaviour of the bridge, and, thus, it is reliable to support the structural analysis.

7.4. Crossing direction and travelling speed estimates

7.4.1. General remarks

In general, B-WIM systems are used to estimate vehicle parameters such as speed, number of axles, the distance between axles, axle loads, etc. In this case study, as for most bridges (Liljencrantz *et al.*, 2007), although the effects of each bogie in the structural response in a set of instrumented cross-sections can be recognized, the effects of the individual axles of a given bogie cannot, however, be separated. As aforementioned, the measurements in the cross-sections at mid-span of the top chords and of the diagonals exhibit a set of local maxima/minima, which correspond to the passage of each bogie over the instrumented truss element, when the vehicle moves in the track in the same alignment of the girder under analysis. However, the results obtained for crossings in the track in the opposite alignment show that the effects of each bogie cannot be separated. As regards the mid cross-sections of the crossbeams, as for the cross-sections referred above, the measurements exhibit a set of local maxima/minima, which correspond to the passage of each bogie over the instrumented element. In addition, the general pattern of the results obtained for crossings in both tracks is similar, as shown in Figure 7.11. Hence, these cross-sections, located in two crossbeams 21 m apart, are suitable for the characterization of the metro traffic in both tracks. Moreover, as the data regarding the vehicles parameters that may be extracted with the measurements of both sensors installed in the same cross-section is similar, the results of a single sensor of each

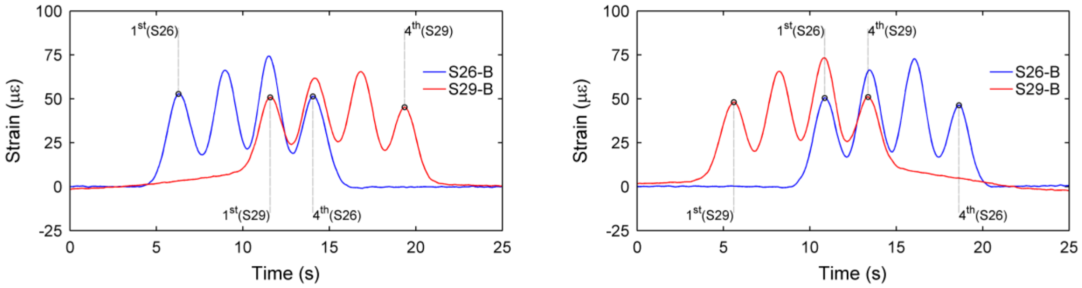

(a)

(b)

Figure 7.11 – Strain measurements taken with the sensors installed in the bottom flange of the mid cross-sections of the crossbeams, induced by a 1-vehicle composition crossing the bridge in: (a) direction 1; and (b) direction 2.

cross-section are enough to obtain all the information needed to characterize the metro traffic in the upper deck of the Luiz I bridge. Hence, the sensors installed in the bottom flange (S26-B and S29-B) were selected.

In general, within the characterization of the traffic, the vehicles geometry, namely the number and the distances between axles, are not known, either in road or railway bridges. In this case study, as aforementioned, the metro traffic in the upper deck of the Luiz I Bridge includes only 1- or 2-vehicles compositions. Figure 7.11 depicts the structural response under a 1-vehicle composition, in which the effects of each bogie can be recognized, leading to four local maxima. The results for crossings of 2-vehicles compositions showed that the effects of the end and first bogies of, respectively, the first and the second vehicles cannot be separated. Therefore, the measurements exhibit seven local maxima. In this context, the identification of the number of local maxima in the results enables to determine the number of vehicles included in a composition, and, thus, the geometry is immediately known.

This section aims at describing the procedure adopted in order to characterize the metro traffic in the upper deck of the Luiz I Bridge, namely: (i) the detection of vehicles traversing the bridge; (ii) the identification of their travelling direction; and (iii) the estimate of the corresponding speed. In addition, with the objective of later application of damage detection methods, the process of obtaining influence-line data is described. As aforementioned, this work focuses on 1-vehicle compositions. However, the procedure described herein can be easily adapted for targeting the characterization of 2-vehicles compositions.

7.4.2. Data acquisition and smoothing

The first step of any procedure whose objective is to estimate vehicle parameters based on the structural response of a bridge is to acquire data at a sufficiently high rate that enables adequately characterizing the structural response. However, in this work, the inherent data-processing was not carried out in real-time. Consequently, without jeopardizing its objective, the acquisition rate should be as low as possible in order to prevent the storage of huge amounts of data. The results of preliminary tests showed that the metro compositions cross the bridge at a speed lower than 10 m/s, and the dynamic component of the structural response is negligible. Hence, an acquisition rate of 50 samples per second (which leads to at least five samples per meter in terms of the vehicle influence-line) was found appropriate.

Nevertheless, in addition to the phenomenon under observation, the fibre-optic based signals include errors (Kong *et al.*, 2012), which, regardless of their source, are typically described as noise. In order to remove this noise as much as possible without, at the same time, unduly degrading the underlying information, a Savitzky-Golay filter (Savitzky and Golay, 1964), using a fourth degree polynomial curve, with a moving window of 45 points of equal weight, was applied to smooth the acquired signals. Moreover, the data smoothing is essential for the vehicle detection in that it lays on the identification of local maxima in the time-series.

7.4.3. Vehicle detection

A FBG is a type of distributed Bragg reflector inscribed in a short segment of the optical fibre that reflects particular wavelengths of light and transmits all others (Moyo *et al.*, 2005). The grating central wavelength, λ_B, in the reflected spectrum shifts by $\Delta\lambda_B$ in response to strain, $\Delta\varepsilon$, or temperature, ΔT, variations through the following equation (Othonos, 1997):

$$\frac{\Delta\lambda_B}{\lambda_B} = P_\varepsilon \cdot \Delta\varepsilon + [P_\varepsilon \cdot (\alpha_M - \alpha_F) + (\alpha_F + \zeta)] \cdot \Delta T \tag{7.1}$$

where P_ε is the gain factor for strain and ζ is the thermo-optic coefficient, whereas α_M and α_F stand as the coefficients of thermal expansion of the host structural material and of the fibre itself, respectively. Consequently, in addition to the strains induced by the metro crossings, the measurements also include the temperature variations as well as the strains due to the temperature changes along the period of observation. Figure 7.12 depicts the measurements taken with sensor S26-B along a day of observation, in the period in which the metro is in service (from 6 a.m. to 1 a.m.). During the day, the wavelength shift related to temperature variations (general trend) is clearly higher than that related to the metro crossings (several

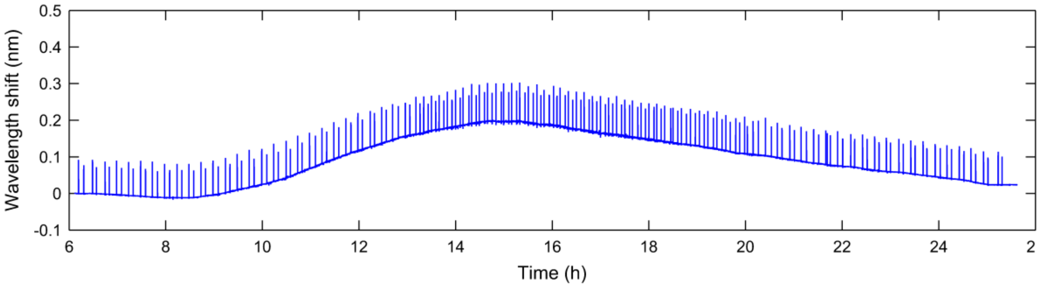

Figure 7.12 – Measurements taken with sensor S26-B, during a day of observation.

peaks). Consequently, in order to identify the passage of vehicles, the effects due to temperature variations must be removed. In general, this is done by subtracting the best fit of a low order polynomial curve. Then a max-to-min difference over a short period of time is used to identify the sections of the signal that correspond to passing vehicles (González Silva and Karoumi, 2015).

An alternative procedure that consists in finding measurements above a given threshold in relation to the general trend, in a window that moves along the data, is adopted herein. The window size was chosen bearing in mind two primary conditions. First, it should be as large as needed in order to ensure that the major effects of a passing composition shall be comprised in a window. Second, it should be as small as possible so that, unless for the case in which two vehicles travelling in opposite directions cross each other near the cross-section under analysis, the window encompasses the strains induced by only one composition.

When a vehicle traverses the structure the sensors signal deviates from the trend associated to temperature variation, and, thus, it may be detected by finding measurements above a given threshold. If the window size is sufficiently small, the signal change due to temperature variations is approximately null and, therefore, the trend is approximately constant. Since the effect of the passing vehicle is observed in less than a half-window, the median value reflects the general trend of the data. Conversely, the average value may only reflect the trend value if the number of measurements in which the effect of the vehicle is observed is quite lower than the remaining measurements. Consequently, by expressing the trend through the median value one obtains smaller window sizes, and, thus, the probability of the effects of two vehicles crossing the bridge in opposite directions be comprised in the same window is decreased. As explained above, the trend estimate based on the median value requires that the window size must be at least twice the period in which a vehicle strains the cross-section under analysis.

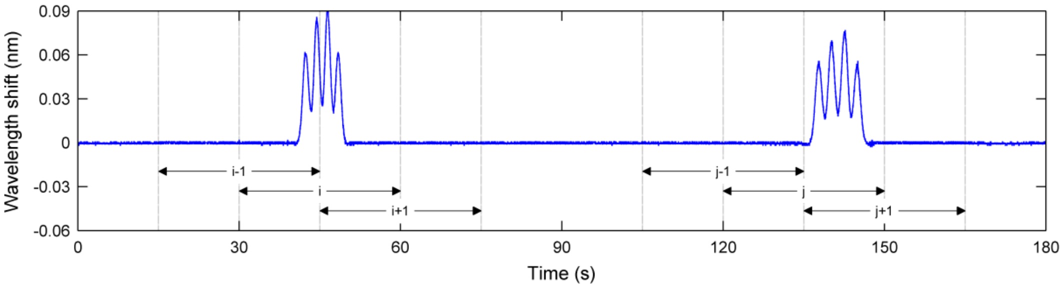

Figure 7.13 – Measurements taken with sensor S26-B for a 3-minutes period of observation during which two 1-vehicle compositions crossed the bridge.

Figure 7.13 depicts the measurements taken with sensor S26-B, for a period of three minutes, in which two 1-vehicle compositions may be detected. The size of the moving window was assumed as 30 seconds. As the window size is such that the effect of the vehicle is observed in less than half-window, the step was assumed to be half-size of the moving window. Hence, the whole effect of every passing vehicles in the cross-section under observation is comprised in at least one window. On one hand, if the effect of the vehicle is centred in a given window i, neither the preceding, i-1, nor the following, i+1, windows comprise the whole effect of the vehicle. On the other, for a given window j, if the whole effect of the vehicle is comprised in the second half-window, the same vehicle is detected in the following window, j+1. In this case, the vehicle detection in window j+1 is disregarded.

As aforementioned, the procedure adopted herein consists in finding measurements above a given threshold in relation to the general trend. Figure 7.14 depicts the measurements taken with sensor S26-B for a 40-seconds period, comprising the window i marked in Figure 7.13. In addition to the raw data, the smoothed data obtained as described in section 7.4.2 are also depicted. The median value of the measurements comprised in the window and the threshold, 0.010 nm above the median, were computed and marked in the figure (see magenta dotted and red dashed lines, respectively). Within the window under analysis a set of measurements are above the threshold which suggests the passage of a vehicle. Still, a further step is required. As discussed above, the response of 1-vehicle and 2-vehicles compositions, which constitutes the metro traffic on the upper deck of the Luiz I Bridge, includes, respectively, four and seven local maxima. Therefore, the vehicle detection requires the identification of an accordant number of peaks in the measurements above the threshold. In this context, the previous step of smoothing data is important both to eliminate undesirable noise in the data and to facilitate the search of local maxima in the experimental data. It is noteworthy that this procedure for vehicle detection enables to determine the type of the passing composition with

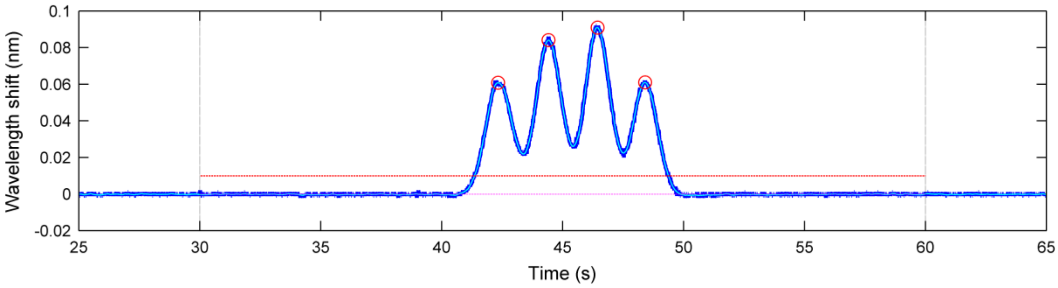

Figure 7.14 – Measurements taken with sensor S26-B during a 40-seconds period in which a 1-vehicle composition is detected.

no further steps. Hence, the measurements comprised in the window depicted in Figure 7.14 results from a 1-vehicle composition traversing the bridge, in that four local maxima are identified (red circles). Finally, once a vehicle is detected the set of time-points in correspondence to the local maxima, which are in accordance with the passage of each bogie over the instrumented cross-section, is recorded in a matrix, denoted as $M_{S26\text{-}B}$, for later use.

7.4.4. Crossing direction

In the previous step, the procedure to identify passing vehicles on the bridge based on the measurements taken with sensor S26-B was described. As aforementioned, for each passing vehicle a set of time-points corresponding to the passage of each bogie over the instrumented cross-section is recorded in the matrix $M_{S26\text{-}B}$. However, in order to determine both the crossing direction and the speed, equivalent data for another cross-section is required. Hence, the procedure described for detecting vehicles based on the measurements taken with sensor S26-B was also carried out with data acquired by sensor S29-B. Therefore, an additional group of time-points sets is obtained: $M_{S29\text{-}B}$. It is noteworthy that both groups of time-points sets are obtained independently. Moreover, two vehicles traversing the bridge in opposite directions may be identified in a given cross-section and may not be detected in the other, namely if they pass over the latter approximately at the same time. Consequently, prior to any further step, the time-points sets stored in each group ($M_{26\text{-}B}$ and $M_{29\text{-}B}$) must be matched, i.e., to a given set in the former group must be associated a set stored in the latter originated by the same vehicle.

As the distance between the instrumented crossbeams (about 21 m) is lower than the length of the shortest composition (about 30 m for a 1-vehicle composition), within a range of positions the vehicle strains both truss elements simultaneously (see Figure 7.11). Hence, the first and the last time-points recorded in each group may be related in order to match the time-points sets. Evidently, when the vehicle travels in direction 1 (from south to north), each bogie reaches the cross-section S26 before S29. Moreover, as a result of the relation between the vehicle's length and the distance between the instrumented cross-sections, the first bogie reaches S29 before the last one reaches S26. Conversely, for direction 2 (in which the vehicles cross the bridge from north to south), each bogie reaches S29 before S26. Furthermore, the first bogie reaches S26 before the last one reaches S29. In this context, irrespectively of the crossing direction, two conditions may be imposed in order to match the time-points sets identified in the strain time-series of each cross-section and recorded in the corresponding group $M_{26\text{-}B}$ and $M_{29\text{-}B}$ (see Figure 7.11): (i) the time-instant corresponding to the first local maximum in S26 must be lower than the last one in S29; and (ii) the time-instant corresponding to the first local maximum in S29 must be lower than the last one in S26.

Once the time-points sets related to vehicles crossings identified with each sensor are matched, the identification of the crossing direction is straightforward. If the vehicle first reaches cross-section S26, the vehicle moves in direction 1, otherwise, it travels in direction 2.

7.4.5. Travelling speed

In general, the time-points corresponding to the passage of the bogies over each cross-section under analysis as obtained above are used to estimate both the speed and the axles distances. Taking into account the time a bogie takes to travel from one cross-section to the other, one estimate of the speed is obtained for each bogie. Thereafter, using the estimates of the speed and the time that two consecutive bogies take to pass over the instrumented cross-section, the axles distances are determined (González Silva and Karoumi, 2015). However, in this case study, the geometry of the vehicle was determined within the vehicle detection (see section 7.4.3). Therefore, this knowledge may lead to more accurate travelling speed estimates.

The analysis of the results showed that successive local maxima observed in the measurements collected with the sensors under analysis (S26-B and S29-B) correspond to the successive passage of each bogie over the instrumented truss element (see section 7.3.3). Hence, a well-known position of the vehicle, in a total of eight (four for each cross-section) for 1-vehicle compositions, may be assigned to each time-point corresponding to the local maxima, as depicted in Figure 7.10. Building on this knowledge, the position of the vehicle over time may be estimated by adjusting a polynomial curve to the data, in which the x-data are the time-points referred above and the y-data are the successive positions of the vehicle. Therefore, by using the appropriate derivative functions both the speed and the acceleration may be obtained. In this work, two different situations were assumed. In the first, the vehicle

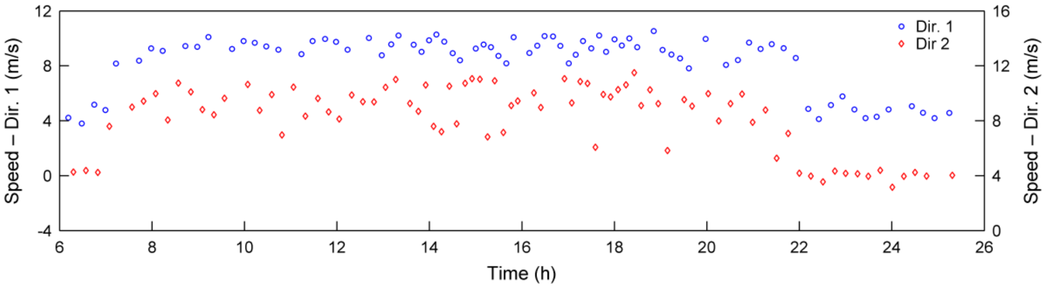

Figure 7.15 – Speed estimates during a day of observation.

speed was assumed constant and, thus, a first-degree polynomial curve was used. In the second, the vehicle speed was assumed variable with constant acceleration and, thus, a second-degree polynomial curve was adopted.

The estimates of the vehicles speed based on a first-degree polynomial curve obtained during a day of observation are shown in Figure 7.15. The speed estimates in direction 1 and 2 can be read, respectively, in the left and in the right axes, thereby facilitating the analysis of the results. In general, the vehicles cross the bridge at about 10 m/s in both directions. However, for security reasons, in the night, the vehicles speed does not exceed, in general, 4 m/s.

7.4.6. Vehicle influence-line

An additional goal of implementing this B-WIM system in the upper deck of the Luiz I Bridge is to obtain influence-line data of the in-service vehicles crossings, for later application of damage detection methodologies based on moving-loads responses. An unit influence-line (UIL), also denoted simply as influence-line, shows the value of a quantity (such as bending moment, shear force, normal force, displacement, etc.) at any given cross-section due to the application of a unit load at any point on the structure (Ghali *et al.*, 2009). When a vehicle traverses a structure, its response may be obtained in order to generate the respective vehicle influence-line (VIL). Thereafter, by knowing the weight and location of each axle, it is possible to extract the UIL of the structure (O'Brien *et al.*, 2006).

In the previous section, with the objective of estimating both the speed and the acceleration of the passing metro compositions on the upper deck of the Luiz I Bridge, the position of the vehicle over time was estimated. Therefore, the VIL can be generated by assigning the response measured at a given time-instant to the respective position of the vehicle. Figure 7.16 depicts the influence-line of both sensors S13-A and S17-A (installed in the mid-span cross-sections of the top chords at, respectively, the 11th and the 12th spans) obtained for a set of five 1-vehicle compositions crossings, in which a second-degree polynomial curve was used to estimate the vehicle positions. It should be underlined that the loads of the vehicles under observation are not the same. Consequently, the magnitude of the measurements varies. Still, as discussed in section 7.3.3, the local minima observed in the response of each passing vehicle correspond to the passage of the successive bogies over the cross-section. The vertical cyan dotted lines depicted in the figure correspond to the positions of the vehicle centre in which each bogie is over the instrumented cross-section.

For every passing-vehicle under observation, the position of the local minima of the measurements collected with sensor S17-A (12th span), shows a good agreement with that of the vertical lines. However, the abscissas of the local minima of the measurements collected with sensor S13-A (11th span) are clearly dissimilar from those of the vertical lines. In particular, the farther the vehicle is from the cross-sections whose data was used to estimate the vehicle position (S26 and S29), the larger is the discrepancy. Therefore, it may be concluded that the polynomial fit based on the time-points identified in the measurements of the sensors S26-B and S29-B poorly estimates the vehicle position in the regions beyond the segment comprised between the instrumented crossbeams.

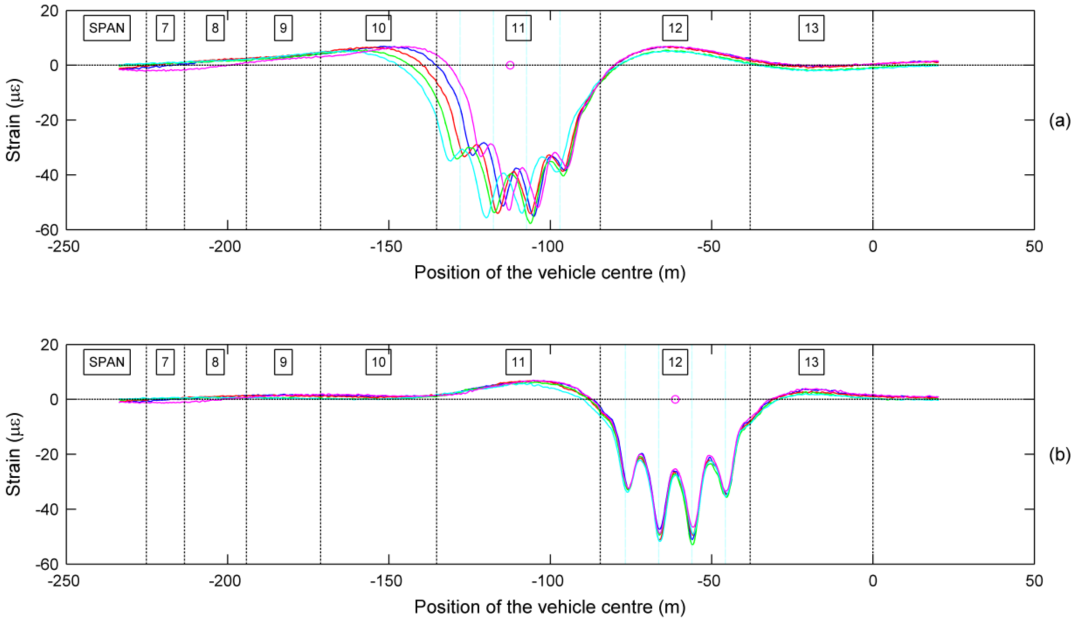

Figure 7.16 – Vehicle influence-lines of the strain measurements taken with sensors: (a) S13-A; and (b) S17-A. The estimates of the vehicle position are based on a second-degree polynomial curve and on the time-points identified in the strain measurements of the crossbeams cross-sections (S26 and S29).

As most of the sensors selected to obtain influence-line data are located in the 11th span, a more accurate estimate of the vehicle position along this span must be sought. According to the response results of the set of cross-sections under observation, estimates based on the strain measurements of the diagonals cross-sections may lead to satisfactory results, as these are instrumented at the ends of this span. In addition, the analysis of the measurements of the sensors installed in cross-sections S22 and S24 showed that the effects of each bogie may be clearly recognized in the response pattern (see Figure 7.9). Hence, as for the crossbeams cross-sections, a well-known position of the vehicle, in a total of eight (four for each cross-section) for 1-vehicle compositions, may be assigned to each time-point corresponding to the local minima identified in the response of both sensors S22-B and S24-B. An additional relationship between time and vehicle position may be thus obtained by adjusting a polynomial curve to these data. Figure 7.17 depicts second-degree polynomial curves estimated with the time-points identified both in the cross-sections of the crossbeams (S26 and S29), denoted as fit i, and of the diagonals (S22 and S24), denoted as fit ii, for a vehicle crossing. For the sake of clarity of the figure, the x-data are the vehicle positions and the y-data are the time-points. The figure shows that the estimates of the vehicle position over time based on fit i are different from those obtained with fit ii. Consequently, the vehicle position assigned to a given time-instant using both fits i and ii is different, and, thus, the VILs obtained are dissimilar. As referred above, the farther the vehicle is from the cross-sections whose data was used to estimate its position, the larger is the discrepancy.

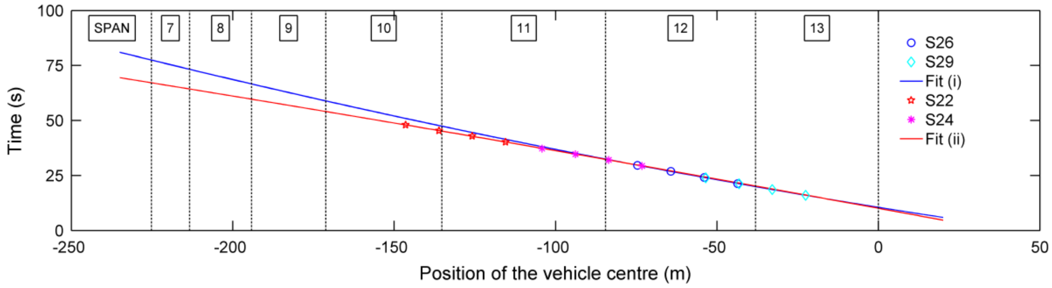

Figure 7.17 – Comparison of the estimates of the vehicle position based on a second-degree polynomial curve and on the time-points identified in the strain measurements of the cross-sections of the (i) crossbeams (S26 and S29) and of the (ii) diagonals (S22 and S24).

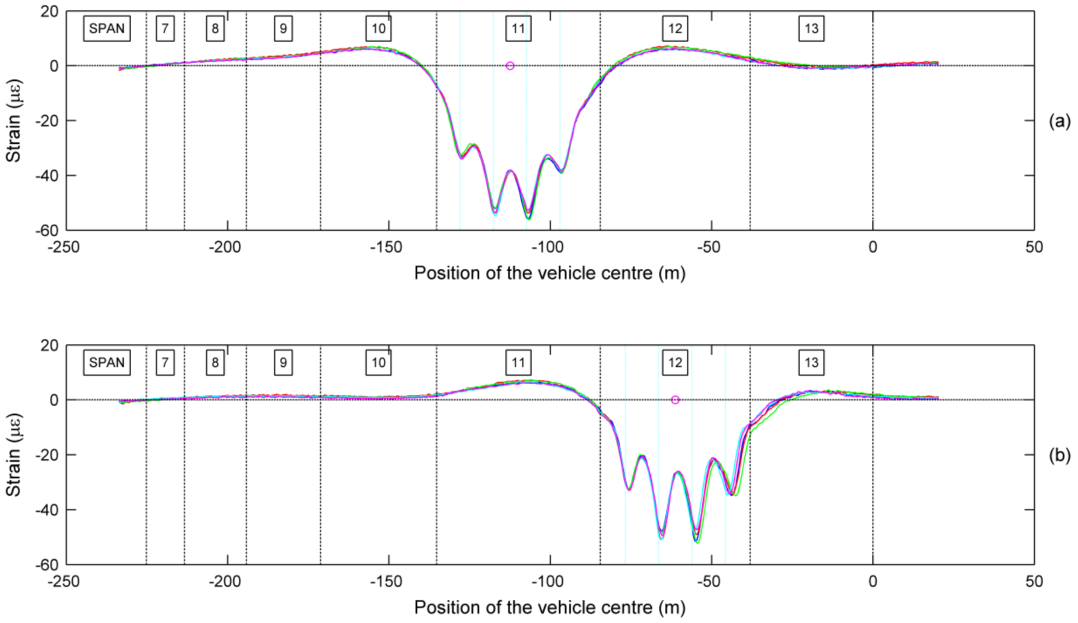

Figure 7.18 – Vehicle influence-lines of the strain measurements taken with sensors: (a) S13-A; and (b) S17-A. The estimates of the vehicle position are based on a second-degree polynomial curve and on the time-points identified in the strain measurements of the diagonals cross-sections (S22 and S24).

Figure 7.18 depicts the influence-line of both sensors S13-A and S17-A (installed in the mid-span cross-sections of the top chords at, respectively, the 11th and the 12th spans) obtained for the same set of five 1-vehicle compositions crossings depicted in Figure 7.16. In this case, a second-degree polynomial curve estimated with the time-points identified in the strain data of the diagonals cross-sections (S22 and S24) was used to obtain the vehicles positions. On the contrary of the VILs depicted in Figure 7.16, herein, the position of the local minima of the measurements collected with sensor S13-A (11th span) shows a good agreement with that of the vertical lines. As regards the abscissas of the local minima of the strain measurements collected with sensor S17-A (12th span), although the positions are not clearly dissimilar, slight changes may be noticed. Hence, according to the positions of the instrumented cross-sections along the spans, strain VILs of the crossbeams cross-sections as well as of cross-sections S17 and S18 should be estimated by using fit i. Strain VILs for the remaining cross-sections should be obtained with fit ii.

7.5. Vehicle load estimates

7.5.1. General remarks

The procedure adopted in the B-WIM system implemented in the upper deck of the Luiz I Bridge for identifying the type of composition, the crossing direction and the vehicles speed, was presented above. Thus, this section is devoted to the approach for estimating the vehicles loads, and, therefore, completing the estimation of the main parameters required in any B-WIM system.

As with the other parameters, the estimates of the vehicles loads are based on the strain measurements of the sensors installed in the bottom fibre of the mid cross-sections of the crossbeams (sensors S26-B and S29-B). The general pattern of the response of these sensors obtained for crossings in both tracks is similar, as shown in section 7.4.1, leading to equal ability for estimating the vehicles loads, irrespectively of the track in which the composition traverses the bridge. In addition, the results exhibit a set of local maxima, which correspond to the passage of each bogie over the instrumented truss element (see section 7.3.3). However, as referred above, the effects of the individual axles of a given bogie cannot be separated. Consequently, the approach proposed herein only enables the identification of the bogies loads.

7.5.2. Description of the approach

In a structure whose behaviour is linear and elastic, the response may be obtained by the superimposition of the effects of each load computed separately. Thus, the response of a vehicle with several axles may be given by the sum of the contribution of each axle. Taking advantage of the unit influence-line (UIL) concept, the contribution of a given axle is obtained by multiplying the axle load by the ordinate value of the UIL at the axle position. However, as aforementioned, the effects of individual axles of a bogie cannot be separated. Still, on one hand, the axles distances of every bogie are equal (1.40 m), and on the other, according to the information given by the operating company, the axles loads of a bogie are approximately equal, irrespectively of the vehicle occupation. Hence, instead of using the individual axles loads and the UIL, the structural response of a vehicle may be obtained by multiplying the bogie load by the ordinate value of an idealized bogie influence-line (BIL). The BIL shows the variation of the quantity under analysis as two 0.5 kN point-loads, 1.40 m apart, move along the structure.

Within the procedure for the detection of vehicles traversing the bridge, the type of composition (including 1- or 2-vehicles) is identified, and, consequently, its geometry is immediately determined (see section 7.4.3). As aforementioned, this work focuses on 1-vehicle compositions. Hence, the geometry of every vehicle under analysis is the same. Furthermore, the bogies centres are equally spaced by a distance d = 10.325 m (see Figure 7.6). Therefore, as the vehicle moves forward d, the abscissas of bogies B_1, B_2 and B_3, in the former position, and those of bogies B_2, B_3 and B_4, in the latter, are, respectively, the same. Consider the vehicle position that leads to the first local maximum of the response of one of the cross-sections under analysis (S26 and S29). As shown in Figure 7.10 (see section 7.3.3), the centre of the first bogie, denoted as B_1, is over the instrumented crossbeam, located at abscissa x_i. The other bogies, B_2, B_3 and B_4, are, respectively, at abscissas x_{i-1}, x_{i-2} and x_{i-3}, whose distance between each other is d. When the vehicle moves forward d, the second bogie, B_2, is over the instrumented truss element, which leads to the second local maximum of the response. At this vehicle position, bogies B_2 and B_3, are, respectively, at abscissas x_{i-1} and x_{i-2} whereas bogie B_1 is at abscissa x_{i+1}. Following the same pattern for the vehicle positions in which bogies B_3 and B_4 are located at the instrumented truss element (at abscissa x_i), the local maximum strains, denoted, respectively, as $\varepsilon_{1,i}$, $\varepsilon_{2,i}$, $\varepsilon_{3,i}$ and $\varepsilon_{4,i}$ are given, in the matrix form, as follows:

$$\begin{bmatrix} \varepsilon_{1,i} \\ \varepsilon_{2,i} \\ \varepsilon_{3,i} \\ \varepsilon_{4,i} \end{bmatrix} = \begin{bmatrix} y_i & y_{i-1} & y_{i-2} & y_{i-3} \\ y_{i+1} & y_i & y_{i-1} & y_{i-2} \\ y_{i+2} & y_{i+1} & y_i & y_{i-1} \\ y_{i+3} & y_{i+2} & y_{i+1} & y_i \end{bmatrix} \begin{bmatrix} P_1 \\ P_2 \\ P_3 \\ P_4 \end{bmatrix} \tag{7.2}$$

where P_1, P_2, P_3 and P_4 are the bogies loads and y_{i-3} to y_{i+3} are the ordinate values of the BIL at, respectively, x_{i-3} to x_{i+3}. Hence, the bogies loads, $[P]$, may be estimated based on the local maxima strains $[\varepsilon_i]$ recorded when a 1-vehicle composition traverses the bridge.

However, the ordinate values of the BIL, y_{i-3} to y_{i+3}, must be obtained previously. As referred above, the BIL shows the variation of a quantity at any given cross-section as two 0.5 kN point-loads, 1.40 m apart, move along the structure. Thus, it may be obtained by using the UIL of the quantity under analysis. The UIL can be, in turn, generated numerically (e.g., using the finite element method) either by calculating the quantity of interest as a unit load moves on the structure or by making use of the Muller-Breslau's principle (Ghali *et al.*, 2009). However, bridge performance determined on the basis of field measurements has typically been found to be better than that predicted based on analytical models (Hirachan and Chajes, 2005). In this context, consider the equations expressed above re-written as follows:

$$\begin{bmatrix} \varepsilon_{1,\mathrm{i}} \\ \varepsilon_{2,\mathrm{i}} \\ \varepsilon_{3,\mathrm{i}} \\ \varepsilon_{4,\mathrm{i}} \end{bmatrix} = \begin{bmatrix} P_4 & P_3 & P_2 & P_1 & 0 & 0 & 0 \\ 0 & P_4 & P_3 & P_2 & P_1 & 0 & 0 \\ 0 & 0 & P_4 & P_3 & P_2 & P_1 & 0 \\ 0 & 0 & 0 & P_4 & P_3 & P_2 & P_1 \end{bmatrix} \begin{bmatrix} y_{\mathrm{i}-3} \\ y_{\mathrm{i}-2} \\ y_{\mathrm{i}-1} \\ y_{\mathrm{i}} \\ y_{\mathrm{i}+1} \\ y_{\mathrm{i}+2} \\ y_{\mathrm{i}+3} \end{bmatrix} \qquad (7.3)$$

In a controlled "calibration" test under a vehicle of known loads, by substituting the parameters $\varepsilon_{j,i}$ and P_k, in the expression written above, for, respectively, the values of the recorded strains and the bogies loads, one obtains a problem of four equations and seven unknowns (y_{i-3} to y_{i+3}). Consequently, an additional test, in which the vehicle loads must be distinctly distributed over the bogies, is required in order to obtain at least as many equations as unknowns. Still, with the goal of estimating ordinate values as accurate as possible, further tests should be performed in order to obtain a higher number of equations. The required ordinate values of the BIL are then estimated by solving a minimization problem based on the minimum least squares method.

7.5.3. Results

The "calibration" tests carried out with the objective of obtaining the ordinate values, y_{i-3} to y_{i+3}, included only crossings of out-of-service vehicles. Thus, the vehicle loads were those described in section 7.2.4. Still, as the *Eurotram* trains move "forward" and "backwards", and the tare weight is asymmetrically distributed over the bogies, two distinct situations of load distribution are experienced. Consequently, eight equations (four for each load case) with seven unknowns may be established, and, thus, the BIL ordinate values may be obtained. However, numerical simulations carried out have shown that when the number of equations is not significantly higher than the number of unknowns, small differences either in the strain measurements or in the load distribution over the bogies may lead to important variations in the estimates of the BIL ordinate values.

Consider the measurements taken with sensors S26-B and S29-B during a 1-vehicle composition crossing on the upper deck of the bridge, shown in Figure 7.19. The abscissas of the vehicle centre corresponding to positions in which each bogie is over the instrumented cross-section, denoted as $X_{1,i}$ to $X_{4,i}$, are marked with cyan dotted lines. As discussed above, these positions are in correspondence with those of the local maxima of the strain measurements. In addition, the abscissas of the vehicle centre corresponding to positions in which the first and the fourth bogies are d=10.325 meters apart the instrumented element, denoted, respectively, as $X_{0,i}$ and $X_{5,i}$, are also marked (red dotted lines). As shown, in the former position ($X_{0,i}$), the first bogie is located at the same abscissa of the second one when the vehicle centre is at $X_{1,i}$ (in which the first bogie is over the instrumented element). Hence, when the vehicle centre is at $X_{0,i}$, bogies B_1, B_2 and B_3 are, respectively, at abscissas x_{i-1}, x_{i-2} and x_{i-3}, whereas bogie B_4 is at abscissa x_{i-4}, and the response is given by the superimposition of the contributions of each bogie by multiplying the bogie load by the corresponding BIL ordinate value: y_{i-4} toy_{i-1}. Similarly, in the latter position ($X_{5,i}$), the fourth bogie is located at the same abscissa of the third one when the vehicle centre is at $X_{4,i}$ (in which the fourth bogie is over the instrumented element). Hence, when the vehicle centre is at $X_{5,i}$, bogies B_2, B_3 and B_4 are, respectively, at abscissas x_{i+3}, x_{i+2} and x_{i+1}, whereas bogie B_1 is at abscissa x_{i+4}, and the response is given by the superimposition of the contributions of each bogie by multiplying the bogie load by the corresponding BIL ordinate value: y_{i+1} to y_{i+4}.

As regards sensor S26-B, the strain measurements recorded for both vehicle positions $X_{0,i}$ and $X_{5,i}$ are negligible. Furthermore, when the vehicle is at farther positions the effects on the instrumented element are also insignificant. Therefore, one may conclude that the BIL ordinate values y_{i-j} and y_{i+j}, for $j = 1, 2, \ldots$ are negligible and only the ordinate value at the abscissa of the instrumented element – y_i – is non-negligible. Still, the BIL ordinate values at

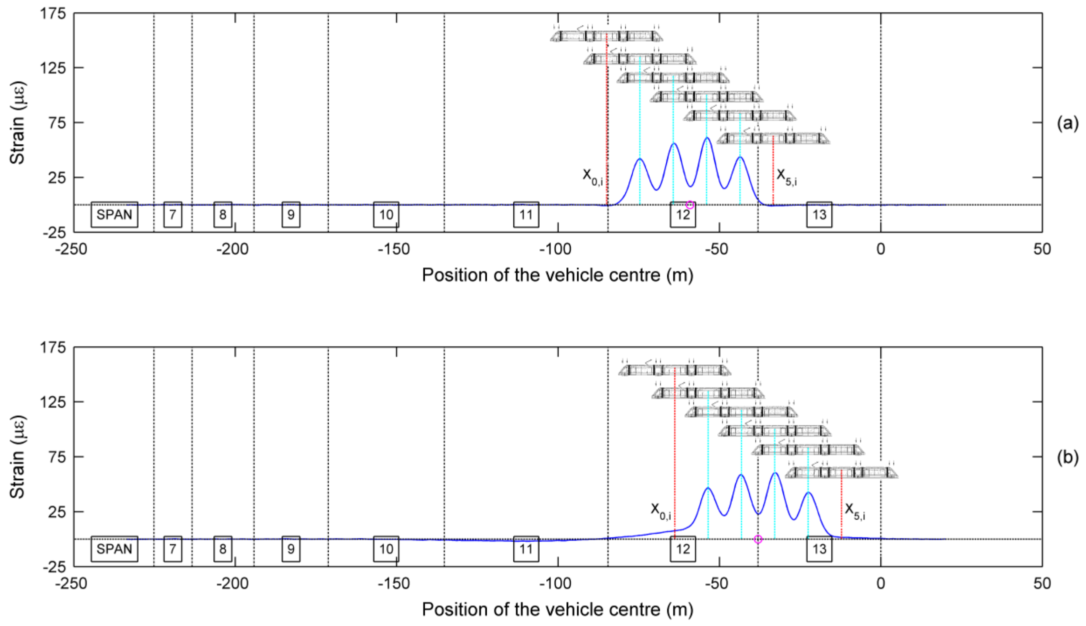

Figure 7.19 – Strain measurements taken with the sensors installed in the bottom flange of the mid cross-section of the crossbeams, induced by a 1-vehicle composition crossing the bridge: (a) S26-B; and (b) S29-B.

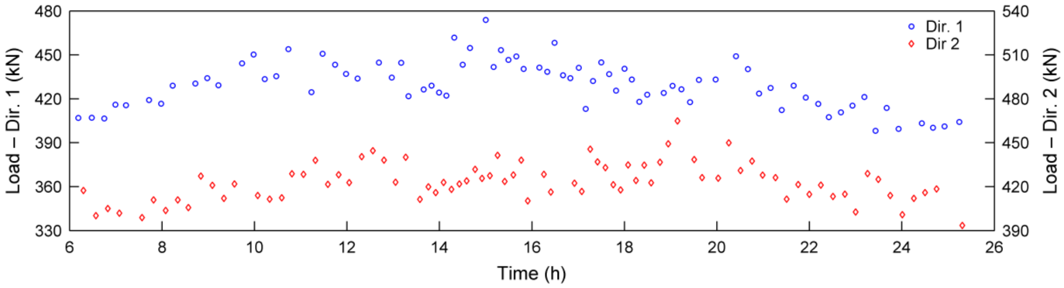

Figure 7.20 – Load estimates during a day of observation.

adjacent positions – y_{i-1} and y_{i+1} – were also assumed non-negligible. Consequently, by substituting, in equation (7.3), the BIL ordinate values y_{i-3}, y_{i-2}yi-2, y_{i+2} and y_{i+3} by zero and the parameters $\varepsilon_{j,i}$ and P_k by, respectively, the values of the recorded strains and the bogies loads, one obtains eight equations (four for each load case) with three unknowns. The BIL ordinate values were then obtained by solving a minimization problem based on the minimum least squares method. The results showed, as expected, that the BIL ordinate values at adjacent positions – y_{i-1} and y_{i+1}– are negligible.

As regards sensor S29-B, although the strain measurements when the vehicle is at $X_{5,i}$ are negligible, when the vehicle is at $X_{0,i}$, the response is significant. Consequently, the BIL ordinate values y_{i-3} to y_{i-1}, may not be assumed null. As a result, the number of unknowns is increased which may lead to inappropriate estimates of the BIL ordinate values. Therefore, as aforementioned, it is recommended to perform additional "calibration" tests in which the vehicle load must be distinctly distributed over the bogies.

As the number of tests carried out was limited, the BIL ordinate values for sensor S29-B were not estimated. However, the tests have enabled to obtain suitable BIL ordinate values for sensor S26-B which, by using equation (7.2), allows to estimate the vehicle loads. Figure 7.20 depicts the estimates of the total loads of the vehicles that crossed the bridge upper deck during a Sunday in both directions. The loads estimates in direction 1 and 2 can be read, respectively, in the left and in the right axes, thereby facilitating the analysis of the results. The total load of the metro compositions ranges between about 390 kN (corresponding to the vehicles tare weight) and 480 kN along the day, in both directions. Still, under exceptional load conditions, the total load of a metro vehicle can reach 650 kN.

7.6. Conclusions

This chapter has presented a bridge weigh-in-motion (B-WIM) system installed in a centenary double-deck steel truss bridge. The purpose was the characterization of the traffic, namely in terms of speed and vehicles loads, of the upper deck, which holds a double tram-train railway line. An additional objective of this work was to obtain vehicle influence-line data for latter application of damage detection methodologies based on moving-load responses.

This B-WIM system comprises only two fibre-optic strain gauges, applied in two crossbeams. These sensors are part of a very comprehensive system previously installed in the bridge to monitor the structural health by measuring the deformations of key elements due to changes in the surrounding environment. Without jeopardizing the primary objective of the existing monitoring system, an upgraded setting applied to a key instrumented region of the upper deck has allowed to collect the fundamental strain data at a rate that enables to adequately characterize the structural response under metro traffic. As the dynamic component of the structural response under in-service metro traffic is negligible, the traffic characterization proposed in this work is based on the quasi-static component only.

Taking into account that the structural response is due to several simultaneous actions and factors, a procedure for the adequate separation of the effects associated to the crossing of the metro vehicles has been presented. The process of detecting their passage and crossing directions was also described, as well as the technique adopted for computing their travelling speed, an utmost aspect to obtain accurate vehicles influence-lines by shifting the data domain from time to space. Finally, the general approach to estimate the bogies' loads was detailed, which is based on the principle of the superimposition of the effects assuming linear and elastic structural behaviour.

Although the sensors chosen for the B-WIM system were not primarily installed with this objective, the results have shown a good quality in terms of speed and load estimates, irrespectively of the track in which the vehicle crosses the bridge. It should be stressed, however, that the quality of the results depends on the accuracy of the measurements. In this case study, the application of a FBG based monitoring system enabled to obtain suitable measurements and, consequently, a satisfactory traffic characterization has been achieved.

This work focused on 1-vehicle compositions, being already planned the extension of the traffic characterization to 2-vehicles compositions, ultimately aiming at the assessment of the number of passengers using the metro line. In railway bridges devoted to train traffic, the compositions formation as well as the vehicles geometry present a higher variability than that of the metro-compositions under analysis in this chapter. Nevertheless, the number of different vehicles that travel in a given railway line is limited. Therefore. a database including the characteristics of every vehicle that might cross the bridge may be previously created for a later use aiming at the identification of the vehicles. In this context, the general procedures proposed herein to characterize the traffic in a tram-train railway line may be adopted in train railway bridges.

Chapter 8

Physics-based and data-driven damage identification in a centenary steel bridge – The Luiz I Bridge

8.1. Introduction

Bridges are susceptible to structural damage due to many factors, such as, ageing, operating loads, fatigue, corrosion and unforeseen defects (Rucker *et al.*, 2006; Ryan *et al.*, 2006). Undetected damage can lead to the failure of the structure, which may be very costly in both economic and human lives terms (Chavel and Yadlosky, 2011; Zhu *et al.*, 2010). Therefore, ensuring the integrity and safety of structures is of paramount importance. In this context, over the last decades, structural health monitoring of bridges, and in particular the development of reliable and efficient damage detection techniques, has been attracting a huge attention from both the infrastructure owners and the scientific community (Aktan *et al.*, 2002; Doebling *et al.*, 1996; Dong *et al.*, 2010).

Most of the existing damage detection approaches are based on either dynamic (Abdel Wahab and De Roeck, 1999; Huth *et al.*, 2005) or static (Laory *et al.*, 2013; Rucka and Wilde, 2006) features obtained in a continuous basis. Notwithstanding, in the last years, methodologies based on the quasi-static responses originated by moving-loads on bridges, although less common, have also arisen (Cantero and González, 2014; Orcesi and Frangopol, 2010). This chapter presents an alternative approach for damage detection in full-scale bridges based on the vehicle influence-lines of in-service traffic. The proposed methodology involves, in a first stage, building time-series of moving-loads responses and, in a second stage, processing data using an adequate algorithm to detect changes in the structural behaviour. The work presented in this chapter follows previous studies in which the applicability of this approach using either numerically-simulated (Cavadas *et al.*, 2013b) or reduced-scale laboratorial-model experimental (Cavadas and Figueiras, 2014) data has been shown to be successful.

In this work, with the purpose of demonstrating the feasibility of successfully extending this approach to full-scale bridges, the Luiz I Bridge was selected as a case study. This Porto's centenary steel arch double-deck bridge was recently subjected to major rehabilitation and strengthening works in order to allow the integration of its upper deck in the Porto metro light rail network. In this context, a very comprehensive monitoring system was implemented in the bridge, which has been used to continuously monitor its structural response under environmental actions, namely the temperature variation (Costa and Figueiras, 2012). For the work presented herein, a set of sensors were selected to monitor the railway traffic of the upper deck. The responses of in-service metro compositions, in the form of vehicle influence-lines, were collected in a continuous basis using an appropriate B-WIM system developed to characterize the metro traffic (see chapter 7). These data were then used to build time-series of the structural response under in-service metro traffic. Thereafter, either moving principal component analysis (MPCA) or influence-line assurance criterion (ILAC) were used for processing data with the purpose of detecting changes in the structural response, and, thus, identify the occurrence of damage.

Support bearings, structural devices positioned between the bridge superstructure and the substructure, are critical components in the operating conditions of a bridge (Fasheyi, 2012). Bearings have two main functions (Feng and Chen, 2000): (i) to transmit loads from the superstructure to the substructure; and (ii) to accommodate relative movements between the superstructure and the substructure. Movements include translations (caused by creep, shrinkage and temperature variations) and rotations (due to traffic loading and uneven settlement of the foundation). However, malfunctioning bearings may prevent these movements, leading to stresses and moments both in the superstructure and in the substructure, that can grow progressively worse if ignored, and ultimately may result in the bridge failure (Balassone, 2010).

The upper deck of the Luiz I Bridge is equipped with segmental rocker nest bearings, which consist of a group of segmental rockers (Ryan *et al.*, 2006), allowing both longitudinal-translations and -rotations. When clean, rocker nests work well. However, this assembly offers many places for dirt and moisture, which leads to wear and corrosion of the rollers, and, consequently, to bearing malfunctions. Field results regarding the structural response under in-service metro traffic obtained in periodic tests within the surveillance program of the bridge structural integrity have shown restraints for the longitudinal displacements of the support bearings (Cavadas *et al.*, 2013a). It is noteworthy to mention that the support bearings of the upper deck of the Luiz I Bridge, as a result of the anti-symmetric deformation of the arch under vehicle loads (Costa, 2012), must accommodate longitudinal translations also under traffic loading. In this context, with the aim of assessing the applicability of the aforementioned damage detection approach based on moving-loads data, this work focuses on bearings malfunctions.

In order to supplement the field results, a suitable finite element model of the bridge was used to simulate the in-service condition of the bridge both in normal and under damaged operating conditions. First, the field results collected in the periodic tests, in which restraints for the longitudinal displacements were identified, were carefully analysed through adequate numerical simulations. Secondly, the finite element model was used to obtain numerically-simulated data regarding normal and damaged operating conditions, with the objective of building time-series of vehicle influence-lines for latter application of data-processing algorithms for damage detection.

In the context of the numerical simulation of data, it must be borne in mind that, in operating conditions, even with no modification on the structural conditions, the vehicle influence-lines regarding different crossings may vary as a result of: (i) the variability of the vehicles loads; (ii) uncertainty about the vehicle position; and (iii) noise in the measurements. Therefore, with the aim of reproducing the experimental conditions, a procedure to take into account these factors that lead to the variability of the field results was carried out in the development of the numerically-simulated time-series.

This chapter is divided in seven sections, including this introduction and a final section in which the main conclusions drawn from this work are summarized. The second section is devoted to the description of the Luiz I Bridge and the monitoring system installed in the structure. In the third section the main aspects regarding the modifications on the structural response under metro traffic as a result of damage-induced changes, namely bearings malfunctions, are discussed. The fourth section is devoted to the presentation of the approach for early damage detection proposed herein, including a brief description of the algorithms used for data-processing: MPCA and ILAC. The fifth section is devoted to the assessment of the performance of these methodologies using numerically-simulated data. A detailed description of the procedure to take into account the variability of the field results in the development of the numerically-simulated time-series is also given in this section. The results of the application of these methodologies to field data collected during a 3-months monitoring period of the Luiz I Bridge are presented in the sixth section.

8.2. The Luiz I Bridge

8.2.1. Brief description of the bridge

Luiz I Bridge spans the Douro River, connecting the cities of Porto and Vila Nova de Gaia, in the north of Portugal (Figure 8.1). This Porto's iconic double-deck bridge, designed by the Belgian Engineer Théophile Seyrig, was inaugurated in 1886, and it was at that time the longest steel arch in the world (Figueiras *et al.*, 2005).

The bridge is constituted by a metallic double hinged arch, with a span length of 172 m and a height of 45.1 m, supporting simultaneously two decks at different levels over the river crossing (Figure 8.2). The lower deck, 8 m wide and 174.3 m long, carries a roadway, and is supported at the abutments and suspended from the arch by four ties 36 m apart. The upper deck, 10 m wide and 391.25 m long, holds a double tram-train railway line, and is supported by the arch crown, seven piers, either made of masonry or steel, and the abutments. Both decks have at the abutments bearing devices that enable both longitudinal-translations and -rotations. The connections between the upper deck and the piers located over the river banks are accomplished by similar supports whereas the piers supported by the arch are rigidly connected at both ends.

The upper deck, which is the focus of this work, comprises two continuous truss girders, 4.65 m apart, supported by the arch crown, seven piers and the abutments, materializing a total of 13 spans (Figure 8.2). These truss girders are laterally braced by diagonal and transverse beams at the chords' levels, in the verticals alignment. The floor system combines two parallel load transfer systems. The first one consists of a set of secondary stringers and transverse beams carrying a steel cladding plate to which the pedestrian and emergency road vehicles loads are applied. The second one is formed by the rails and the wooden sleepers and receives the loads of the metro vehicles.

Figure 8.1 – General view of the Luiz I Bridge (North (Porto) on the left and South (Gaia) on the right).

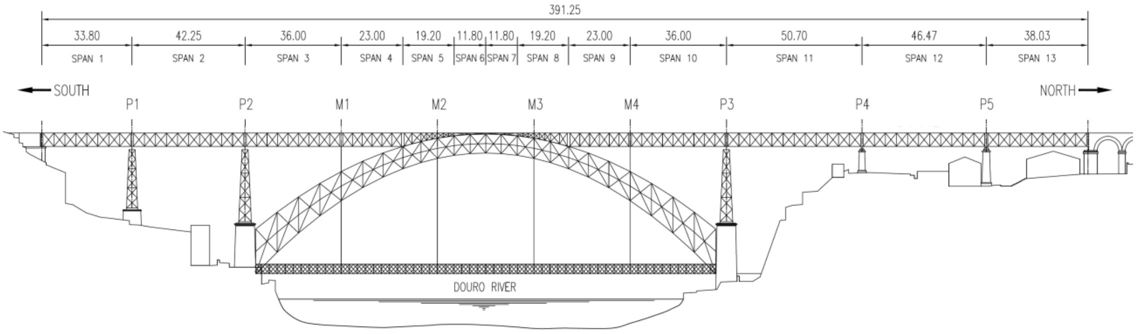

Figure 8.2 – Scheme of the side view of the Luiz I Bridge.

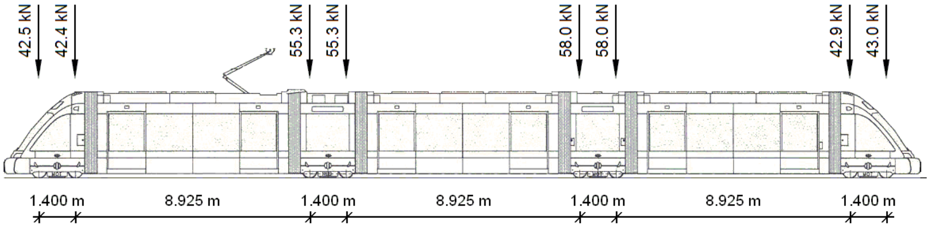

Figure 8.3 – Scheme of a metro vehicle.

Integrated in the Porto Metro Network, the upper deck of the Luiz I Bridge holds the Yellow double railway Line (D), in which the travelling vehicles are *Eurotram* trains produced by *Bombardier Transportation*, with a capacity for 80-seated places and capable of reaching 80 km/h. The vehicles cross the bridge in the upstream track in the South-North direction, denoted herein as direction 1, whereas North-South crossings, denoted as direction 2, take place in the downstream track. One or two coupled vehicles may constitute the metro compositions. However, this work has targeted only 1-vehicle compositions. The dimensions of the vehicle as well as the axles loads corresponding to its tare weight are depicted in Figure 8.3.

8.2.2. Monitoring system

In 2005 a major strengthening and rehabilitation process was carried out on this bridge aiming at the integration of its upper deck in the infrastructure of the Porto metro light rail network. During this process, a very comprehensive fibre Bragg grating (FBG) based monitoring system was implemented with the purpose of, first, appraising the performance of the strengthening solutions, and, second, monitoring the bridge's structural health by measuring the deformations of key elements due to the traffic loading and to changes in the surrounding environment, namely temperature variations. The monitoring system installed on the bridge consists in a fibre-optic network comprising 15 optical channels containing multiple FBG sensors connected in series. It enables the measurement of: (i) strains in 59 cross-sections of selected truss elements, through a pair of strain sensors installed in each; (ii) relative horizontal displacements of the bridge upper deck, by using eight fibre-optic-based displacement transducers; and (iii) temperature of the ambient air and experienced by the steel, through 10 temperature sensors (Costa and Figueiras, 2012).

Recently, with the objective of taking the maximum advantage of the measurement system installed in the bridge, two additional applications have emerged. First, a B-WIM system to characterize the metro traffic on the upper deck was implemented (see chapter 7). Second, a structural health monitoring approach using in-service vehicle influence-line data of metro vehicles as described in this work was deployed. By default, within the continuous monitoring of the structural health of the bridge, the acquisition program collects the sensors signals at intervals of five minutes. In the context of the additional applications mentioned above, a specific area of the upper deck was selected, which holds sensors distributed among four optical channels, and whose signals were recorded with a frequency of 50 Hz. These data has allowed to properly characterize the traffic in terms of type of metro composition, the track and the direction in which the vehicles travel, speed and vehicles loads, as well as the collection of vehicle influence-lines for later application of damage detection techniques, without jeopardizing the primary objective of the monitoring system.

The monitoring system selected within the context of this work comprises eight cross-sections instrumented both in the 11th and in the 12th spans of the downstream girder, distributed at the lower (S11, S14 and S16) and the upper (S10, S13 and S15) chords, and the compression diagonals (S22 and S24). Figure 8.4 depicts the location of the instrumented cross-sections and Figure 8.5 presents the corresponding layout of the applied strain sensors. Although the cross-sections installed in the legs of pillar P3 (S56 and S57) and at mid-span of the 12th span (S17 and S18) are not comprised in the selected monitoring system, their results have been assessed in the analysis of the structural behaviour under restraints for the longitudinal displacements of the support bearings.

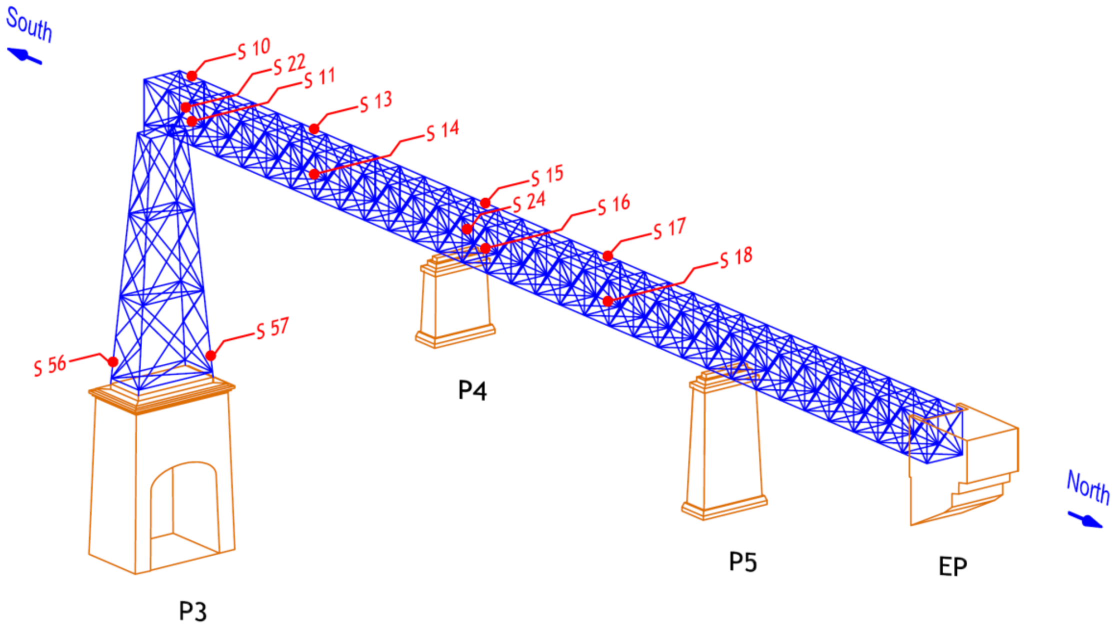

Figure 8.4 – 3D scheme of the bridge depicting the location of the instrumented cross-sections.

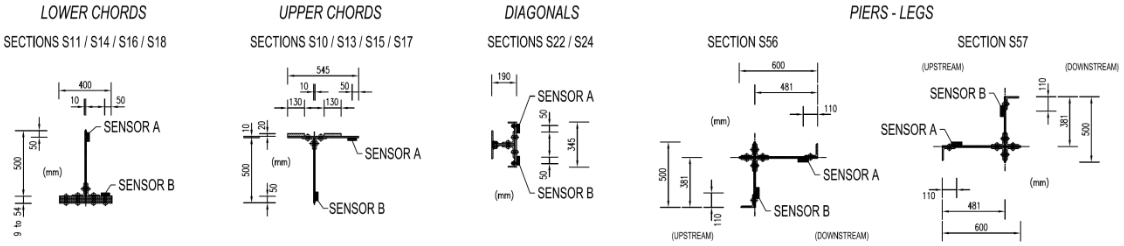

Figure 8.5 – Scheme of the instrumented cross-sections.

8.3. Analysis of damage-induced changes in the structural response

8.3.1. General remarks

This section is devoted to the analysis of the effects of support bearings malfunctions on the structural response of the Luiz I Bridge. As mentioned above, the support bearings of the upper deck allow rotations as well as displacements in the longitudinal direction. This work addresses two damage scenarios related with constraints for the longitudinal displacements of

(a) (b)

Figure 8.6 – General view of the support bearings installed on the upper deck of the Luiz I Bridge: (a) pillar P3; and (b) pillar P4.

the support bearings installed over: (i) pillar P3 (denoted herein as DS1); and (ii) pillar P4 (denoted herein as DS2).

Although the support bearings installed both on pillars P3 and P4 are similar, the effects of constraints for the longitudinal displacement on the structural behaviour, namely on the response of the instrumented cross-sections, are significantly different. On one hand, the former pillar, made of steel and with a meaningful height, is less rigid than the latter, made of masonry and considerably smaller (see Figure 8.2). On the other hand, the relative position of the instrumented cross-sections between the arch crown – the rigidity centre of the upper deck for longitudinal displacements (Costa, 2012) – and each pillar is different. As regards pillar P3, all the cross-sections included in the monitoring system are located away the region comprised between the arch and the pillar, whereas as regards pillar P4, part of the measurement system is located within the area delimited by the arch crown and the pillar (see Figure 8.4).

Within this chapter, the effects that the constraints for the longitudinal displacements produce on the structural behaviour of the bridge under the passage of the metro are assessed through both field results and adequate numerical simulations. In relation with the constraints for the longitudinal displacements of the support bearings installed on pillar P3, the results of a periodic campaign carried out with the objective of monitoring the in-service behaviour of the bridge under the metro traffic had shown an abnormal response (Cavadas *et al.*, 2013a). The strains of the cross-sections instrumented on the pillar legs (see Figure 8.4) pointed out the occurrence of bending on the pillar caused by horizontal forces at its top related to constraints for the horizontal movements of the support bearings during the passage of the metro. Adequate finite element analysis, in which the horizontal movements of the supports were restrained, enabled to attest this hypothesis inasmuch as the numerical estimates were similar to the field results. As regards the effects on the structural behaviour of a constraint for the longitudinal displacements of the support bearings installed on pillar P4, only numerical simulations were carried out.

The numerical model of the bridge used herein to simulate the structural response under the metro crossing consists in a complete 3D finite element linear and elastic model created on the basis of two-node frame elements, which have three translational degrees of freedom (DOFs) and three rotational DOFs at each node. Further details concerning the numerical modelling can be found in (Costa, 2012)[3].

8.3.2. Restriction of the horizontal movement over the pillar P3

Figure 8.7 depicts the numerical estimates of strains on the cross-sections instrumented on the legs of pillar P3 for the crossing of a 1-vehicle composition in direction 2, under idealized operating conditions of the support bearings, i.e., on the assumption that both the rotation and the displacement in the longitudinal direction are totally allowed. Under these conditions, denoted herein as baseline scenario (BS), only vertical loads are transferred to the pillar. As the vehicle moves over spans adjacent to pillar P3 (spans 10 and 11), the pillar is compressed whereas when the vehicle moves farther, due to the deck bending, the vertical load on the pillar decreases leading to tensile strains on the legs. The differences between the strain estimates at cross-sections S56 and S57, located, respectively, at upstream and downstream legs (see Figure 8.4), are explained by the eccentricity of the load at the deck's cross-section: vehicle crossings in direction 2 correspond to passages on the downstream track of the upper deck.

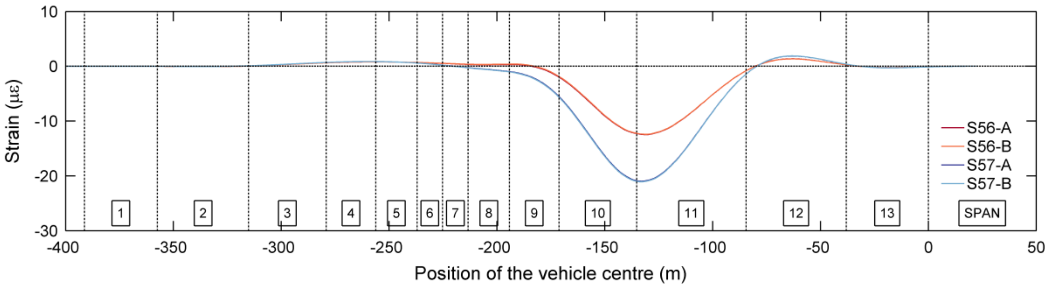

Figure 8.7 – Numerical estimates of the cross-sections strains generated in the legs of pillar P3 for the crossing of a 1-vehicle composition in direction 2, under idealized operating conditions of the support bearings.

---

[3] The finite element model as well as the numerical simulations was entirely developed by Dr. Bruno Costa. Still, its inclusion in this thesis was crucial for the understanding of the whole text.

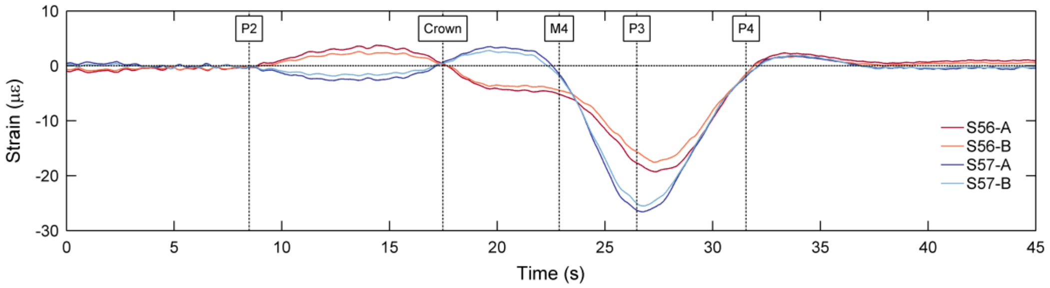

Figure 8.8 – Field results of the strains at the cross-sections instrumented in the legs of pillar P3 collected during the crossing of a 1-vehicle composition in direction 2.

Figure 8.8 depicts the field results of the strains at the cross-sections instrumented in the legs of pillar P3 collected during the crossing of a 1-vehicle composition in direction 2. These measurements, obtained in periodic tests within the surveillance program of the bridge structural integrity, where collected under in-service metro traffic (Cavadas *et al.*, 2013a). The B-WIM system installed to obtain vehicle influence-lines of the structural response under in-service metro traffic (see chapter 7) was not installed when these results were obtained. Consequently, the axles loads of the vehicle are not known. Still, the strains of other sensors recorded together with those of the legs of the pillars enabled to match a set of time instants with remarkable positions of the vehicle along the crossing, as marked in the figure.

The comparison of Figure 8.7 with Figure 8.8 shows that, disregarding the strains magnitudes, the shape of the field results is different from that of the numerical estimates obtained under idealized operating conditions of the support bearings, namely when the vehicle is moving between pillars P2 and P3. First, when the vehicle traverses spans 3 to 6, comprised between pillar P2 and the arch crown, the numerical estimates indicate slight tensile strains on both legs. However, although the field results also show that cross-section S56 registers tensile strains, the magnitude is clearly higher. In addition, cross-section S57 is under compressive strains. Second, when the vehicle crosses spans 7 to 9, comprised between the arch crown and M4, the numerical estimates for cross-section S56 are approximately null whereas cross-section S57 records slight compressive strains. As regards the field results, the measurements show tensile stresses for S57 and compressive stresses for S56. Finally, when the vehicle crosses span 10, comprised between M4 and P3, the trends of both the numerical estimates and the field results are similar. Still, the variation rate of the compressive strains of the numerical estimates for cross-sections S56 and S57 appears to be, respectively, higher and lower than that of the field results.

Regarding these results, it is noteworthy to mention that, as a result of an anti-symmetric loading on the arch, its deformation impels a horizontal translation of the upper deck as if it was a rigid body (Costa, 2012). As shown in Figure 8.9, when 1-vehicle composition is located on spans 3 to 6, comprised between pillar P2 and the arch crown, the arch deformation impels a horizontal translation of the upper deck to the right (in the South-North direction). Therefore, in the case of the horizontal displacement at the supports over pillar P3 is restrained, a force in the same direction applied at its top arises, which bends the pillar. The resulting bending moment gives rise to a pair of tensile and compressive forces on, respectively, the left (on the South side) and right (on the North side) legs. This pattern matches the field results observed when the vehicle traverses spans 3 to 6, in which S56 and S57 are, respectively, under tensile and compressive stresses.

On the other hand, when the vehicle traverses spans 7 to 10, comprised between the arch crown and pillar P3, the arch deformation impels a horizontal translation of the upper deck to the left (in the North-South direction), which leads to a force in the same direction at the top of the pillar. The resulting bending moment gives rise to compressive and tensile forces on, respectively, the left (on the South side) and right (on the North side) legs. As the vehicle crosses spans 7 to 9, comprised between the arch crown and the suspension tie M4, the field results agree with this behaviour: S56 and S57, register, respectively, compressive and tensile strains. When the vehicle reaches span 10, comprised between M4 and pillar P3, the vehicle loads are increasingly transferred to pillar P3 and, therefore, both legs experience compressive strains. Still, as a result of the previously installed state of strain due to the bending moment on the pillar, the variation rate of the compressive strains of the field results for cross-sections S56 and S57 appears to be, respectively, lower and higher than that of the numerical estimates.

Therefore, the field results on the cross-sections instrumented in the legs of pillar P3 collected

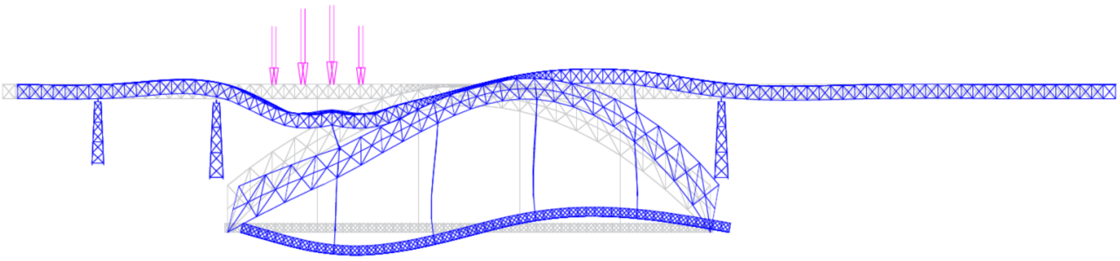

Figure 8.9 – Deformed mesh of the structure when 1-vehicle composition is located on spans 3 to 6, comprised between pillar P2 and the arch crown, under idealized operating conditions of the support bearings.

during the crossing of a 1-vehicle composition in-service clearly show a constraint for the longitudinal displacement at the support bearings over pillar P3.

The constraints for the longitudinal displacement due to malfunctions on the support bearings exhibit, in general, nonlinear behaviour. However, with the aim of replicating the field results with the numerical model, for the sake of simplicity, the constraint for the longitudinal displacement was simulated by introducing horizontal springs connecting the lower chords of the upper deck and the top of pillar P3, one at each support position. Among several scenarios analysed, it was concluded that the numerical estimates obtained on the assumption of a stiffness of 3500 kN/m in each spring (depicted in Figure 8.10) show a good agreement with the field results (see Figure 8.8).

Figure 8.11 depicts the numerical estimates of the horizontal reactions (HR) at the supports over pillar P3, both at upstream (U) and downstream (D), for the crossing of a 1-vehicle composition in direction 2, under an elastic restraint of 3500 kN/m. In the figure, positive values correspond to forces applied at the lower chords of the upper deck, over pillar P3, from South to North (from the left to the right). These results are in accordance with the horizontal movement of the upper deck, as a result of the anti-symmetric loading on the arch. When the vehicle traverses spans 3 to 6, the upper deck displaces to the right and, thus, horizontal reactions arise to the left (negative values). Conversely, when the vehicle crosses spans 7 to 10, the upper deck moves to the left and, therefore, horizontal reactions arise to the right (positive values). In addition, according to the action-reaction law, the forces applied on the pillar, at its top, are symmetric to the reactions at the supports. Those forces lead to bending moments on the pillar, which give rise to pairs of tensile and compressive forces on the legs. This explains the differences observed in the numerical estimates of the strains of cross-sections S56 and S57 between the damage scenario 1 (DS1) – under an elastic restraint of 3500 kN/m in each support bearing over pillar P3, depicted in Figure 8.10 – and the baseline

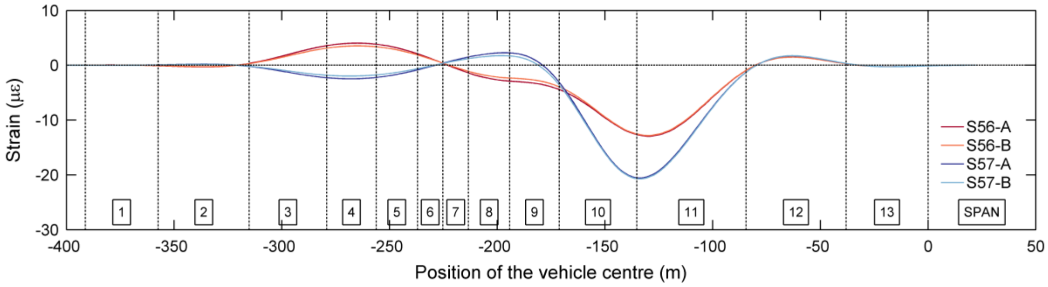

Figure 8.10 – Numerical estimates of the strains generated in the cross-sections instrumented in the legs of pillar P3 for the crossing of a 1-vehicle composition in direction 2, under an elastic restraint of 3500 kN/m in each support bearing over pillar P3.

scenario (BS) – under idealized operating conditions, depicted in Figure 8.7.

It is noteworthy to mention that the horizontal reaction force at the supports arising from the restraint simulated herein is below 3 kN. As the vertical reaction for dead loads at each support is about 600 kN, it may be concluded that a small constraint for the horizontal movements of the support bearings (below 0.5% of the vertical load) leads to noticeable changes of the strains measured in the legs of the pillar, during the crossing of metro vehicles. However, as regards the remaining cross-sections included in the monitoring system as described in section 8.2.2, this structural change does not produce significant modifications on the estimated strains, as shown in Figure 8.12.

As aforementioned, as regards the severity of the constraint for the horizontal displacement at the support bearings over pillar P3, several scenarios were analysed, ranging between no constraint and total restraint. Still, even in the later case, similarly to the situation whose results are depicted in Figure 8.12 (regarding an elastic restraint of 3500 kN/m in each support bearing), this structural change does not produce significant modifications on the measured strains. Therefore, the cross-sections selected to monitor the structural health of the bridge based on moving-loads using the strains collected during crossings of in-service metro vehicles are not appropriate to detect constraints for the horizontal displacements of the support bearings over pillar P3. On the contrary, the cross-sections instrumented on the legs of pillar P3 are particularly suitable for that purpose in that, as shown above, small magnitude constraints at the top of the pillar produce significant modifications on the measured strains, acting, therefore, as a scale.

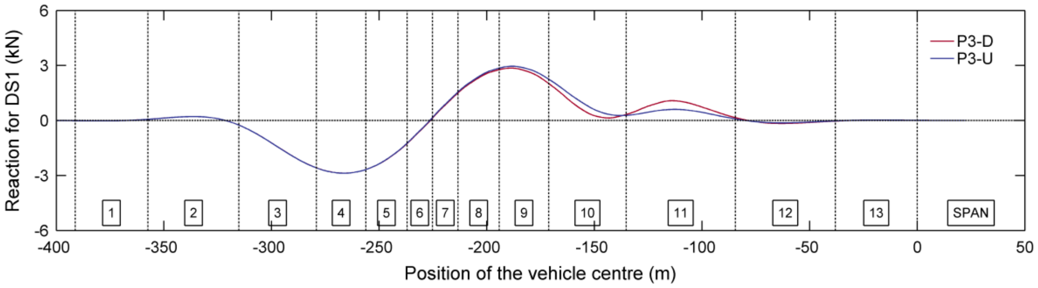

Figure 8.11 – Numerical estimates of the horizontal reactions at the supports over pillar P3 for the crossing of a 1-vehicle composition in direction 2, under an elastic restraint of 3500 kN/m in each support bearing over pillar P3.

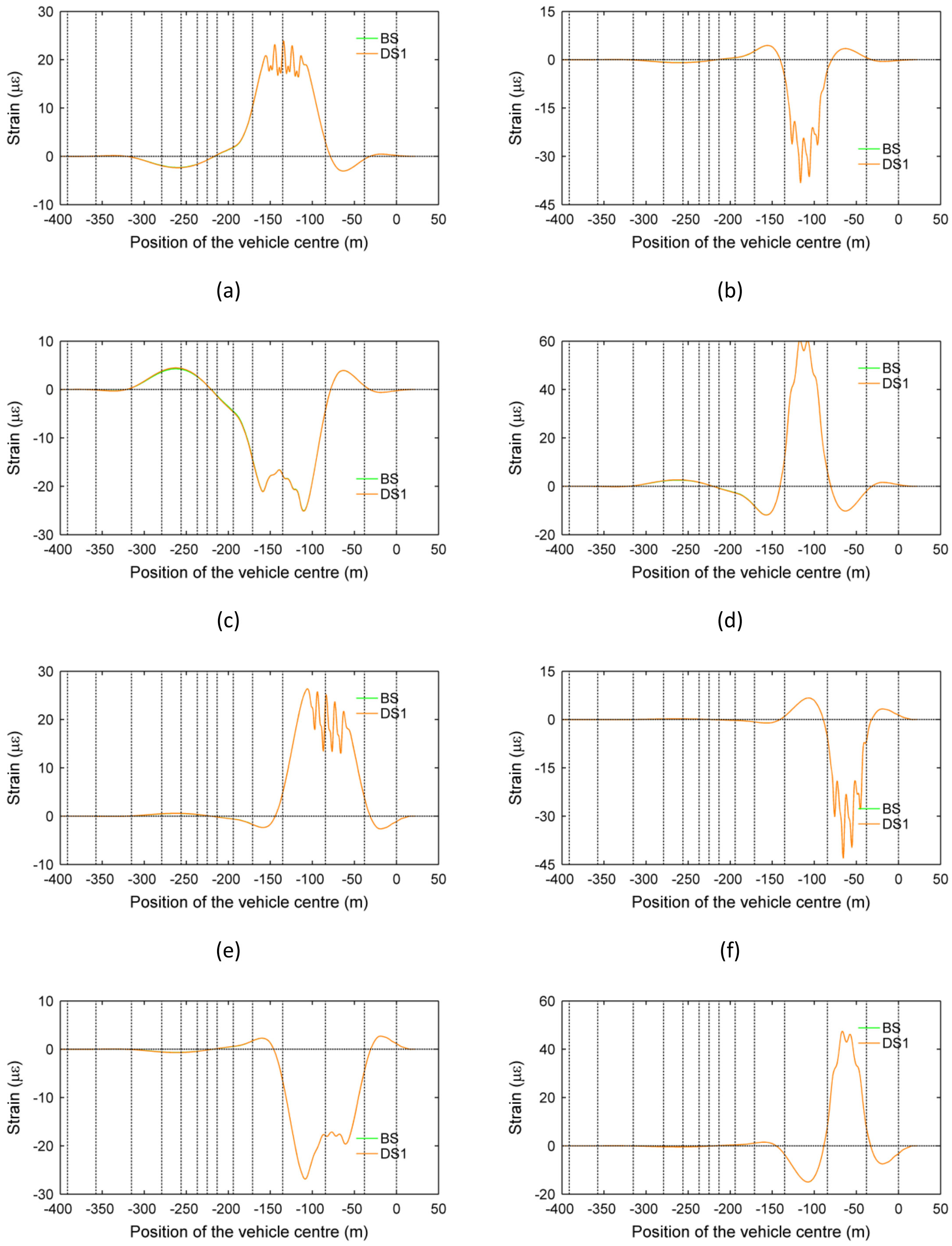

(a) (b)

(c) (d)

(e) (f)

(g) (h)

Figure 8.12 – Comparison of the numerical estimates of the flanges strains of the instrumented cross-sections, for the crossing of a 1-vehicle composition in direction 2, under the following scenarios: BS1 (under idealized operating conditions of the support bearings); and DS1 (under an elastic restraint of 3500 kN/m in each support bearing installed over pillar P3). The selected cross-sections are: (a) S10; (b) S13; (c) S11; (d) S14; (e) S15; (f) S17; (g) S16; and (h) S18.

It should be noted that, even in the case of total restraint for the longitudinal movement of the support bearings over pillar P3, due to its flexibility (as a result of being meaningfully high and materialized by a steel truss structure), the displacement of the upper deck is only partially constrained. The results of adequate numerical simulations have shown that the pillar stiffness for horizontal movements at its top is around 8900 kN/m (leading to 4450 kN/m at each support). Consequently, in either scenario analysed, the elastic constraint for the longitudinal displacement of the upper deck does not exceed 4450 kN/m at each support bearing.

As referred above, with the objective of obtaining numerical estimates similar to the field results, the elastic restraint in each support bearing was set at 3500 kN/m. Consequently, the elastic restraint for the longitudinal displacement of the upper deck in each support bearing over pillar P3 is about 1960 kN/m – resulting rigidity of two springs of stiffness 3500 kN/m (representing the elastic restraint at the support bearings) and 4450 kN/m (simulating the pillar rigidity for horizontal movements at its top) attached in series. Thus, the constraint for the horizontal displacement of the upper deck in this scenario is only a little smaller than half of that of the case in which the horizontal displacement of the support bearings is totally restrained, whose stiffness is provided only by the pillar.

8.3.3. Restriction of the horizontal movement over the pillar P4

In the section above, it was shown that an elastic restraint for the longitudinal displacement of the upper deck over pillar P3 does not produce significant modifications in the measured strains on the cross-sections included in the monitoring system selected in the context of this work. It is noteworthy that, keeping the longitudinal displacements totally allowed in the remaining support bearings, either over the pillars or on the abutments, the horizontal forces arising at the top of pillar P3, as a result of the referred constraint, are balanced by the arch, at its crown. As shown in Figure 8.4, all the instrumented cross-sections are placed away the region of the bridge comprised between pillar P3 and the arch crown. Conversely, a significant number of cross-sections are located within the area delimited by pillar P4 and the arch crown. Therefore, with the objective of assessing the effects regarding the position of the instrumented cross-sections in relation to the region comprised between the arch crown and the alignment in which the longitudinal displacements are constrained, an elastic restraint of 1960 kN/m was simulated in each support bearing over pillar P4. As this pillar is both considerably small and made of masonry, the horizontal displacement at its top was considered negligible. Therefore, the restraint for the longitudinal displacement of the upper deck is straightforwardly given by the elastic restraint prescribed at the support bearings.

As shown in Figure 8.13, an elastic restraint of 1960 kN/m in each support bearing over pillar P4, denoted herein as damage scenario 2.i (DS2.i), does not produce significant modifications on the measured strains. As regards the horizontal reactions at the supports, both at upstream (U) and downstream (D), the extreme values do not exceed 3 kN (see Figure 8.14). These results are very similar to those obtained in damage scenario 1 (DS1), in which an elastic restraint of 3500 kN/m in each support bearing over pillar P3 was simulated. On one hand, although the restraint for the horizontal movements of the support bearings is different (3500 kN/m in DS1 and 1960 kN/m in DS2.i), the restraint for the longitudinal displacement of the upper deck is similar (1960 kN/m in both damage scenarios). On the other hand, the displacements that lead to the horizontal reactions at the supports that drive the structural response arise from the anti-symmetric loading on the arch, which is similar in both situations. Even though, as the vehicle approximates the pillars under analysis, the bending of the upper deck impels horizontal displacements at the lower chord that explain the slight differences observed when the vehicle approximates the supports.

As mentioned above, the ratio between the horizontal reaction force at the supports arising from this restraint (below 3 kN) and the vertical reaction for dead loads at each support (about 600 kN) is very small (below 0.5%). Therefore, an additional scenario, denoted herein as damage scenario 2.ii (DS2.ii), in which the restraint for the longitudinal displacement of the support bearings over pillar P4 was taken as 19600 kN/m (10 times the stiffness of the scenario discussed above), was simulated. Note that even under these conditions the ratio between the horizontal reaction force (below 25 kN, as shown in Figure 8.14) and the vertical reaction for dead loads is still very low (below 4.2%).

As depicted in Figure 8.13, except for the cross-sections located at mid-span of the 12th span (S17 and S18), the restraint for the horizontal displacement of the support bearings installed over pillar P4 simulated for DS2.ii produces significant changes in the strains measured in the cross-sections included in the monitoring system. The most significant modifications take place when the vehicle moves along the spans directly supported by the arch.

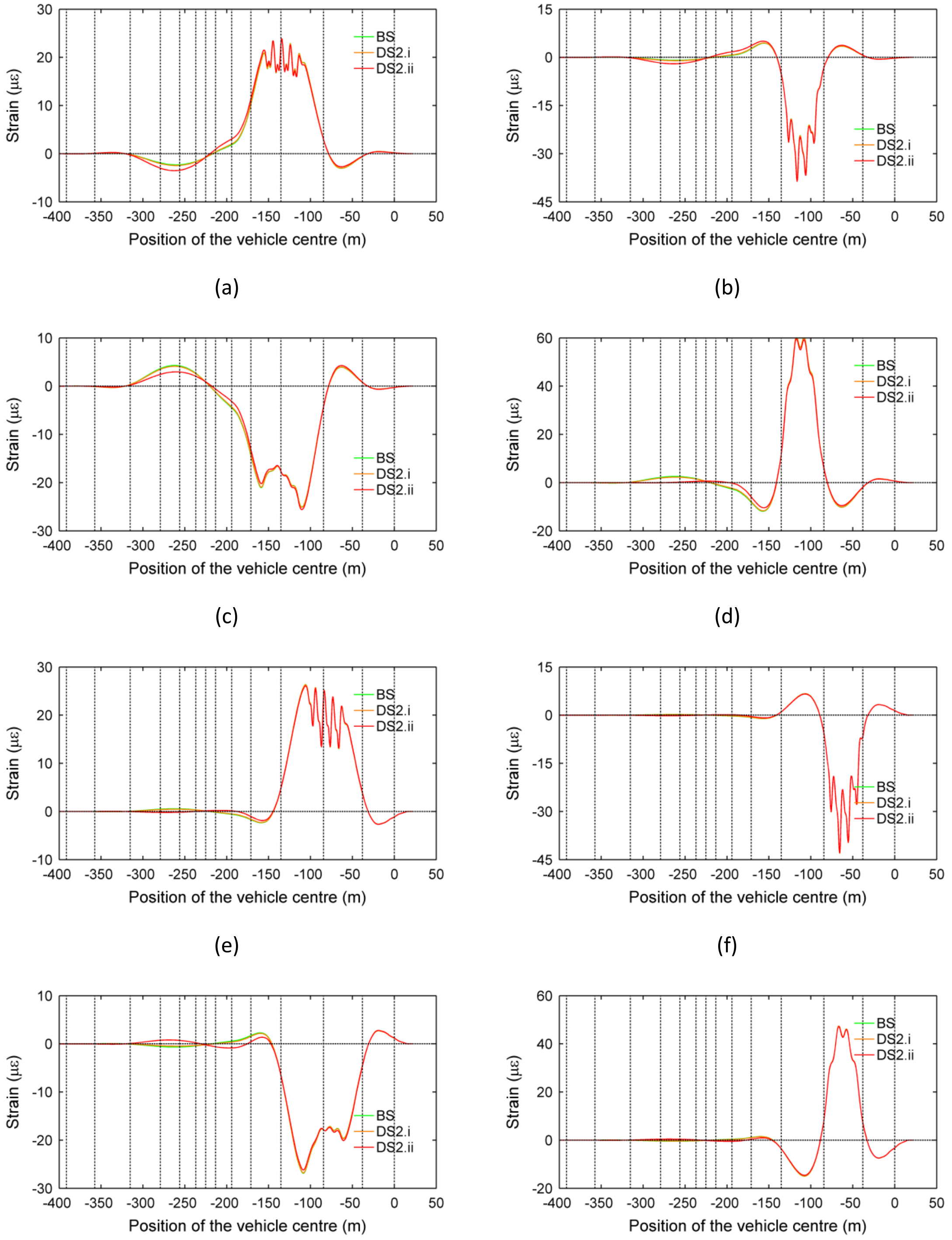

(a) (b) (c) (d) (e) (f) (g) (h)

Figure 8.13 – Comparison of the numerical estimates of the flanges strains of the instrumented cross-sections, for the crossing of a 1-vehicle composition in direction 2, under the following scenarios: BS1 (under idealized operating conditions of the support bearings); DS2.i (under an elastic restraint of 1960 kN/m in each support bearing installed over pillar P4); and DS2.ii (under an elastic restraint of 19600 kN/m in each support bearing installed over pillar P4). The selected cross-sections are: (a) S10; (b) S13; (c) S11; (d) S14; (e) S15; (f) S17; (g) S16; and (h) S18.

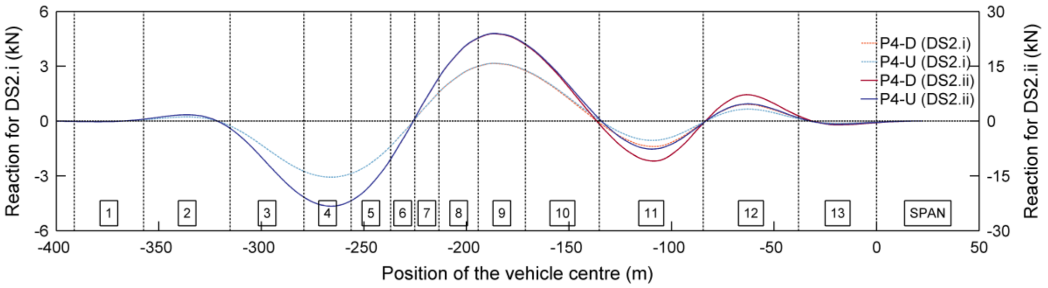

Figure 8.14 – Numerical estimates of the horizontal reactions at the supports over pillar P4 for the crossing of a 1-vehicle composition in direction 2, under the following scenarios: DS2.i (under an elastic restraint of 1960 kN/m in each support bearing installed over pillar P4) and DS2.ii (under an elastic restraint of 19600 kN/m in each support bearing installed over pillar P4).

On the assumption of linear and elastic behaviour of the structure, as simulated herein, the structural response for the crossing of a metro vehicle under these conditions results from the superposition of two effects. The first regards the vertical load of the metro vehicle, considering that the horizontal displacement at all the support bearings is allowed. The second is related with the horizontal forces that arise due to the horizontal movements of the deck induced by the structural deformation as the vehicle crosses the bridge. Therefore, the differences in the strains estimated between the baseline scenario (BS) and the damage scenario 2.ii (DS2.ii) correspond to the strains induced by the horizontal forces arising at the restrained supports.

Consider, for instance, a vehicle position in which the metro is located between pillar P2 and the arch crown. Due to the anti-symmetric loading on the arch, its deformation impels a horizontal translation of the upper deck to the right (see Figure 8.9), leading to a horizontal reaction at the support bearings over pillar P4 to the left (see Figure 8.14). Figure 8.15 depicts the deformed mesh of the structure as well as the axial forces along the elements of spans 11 to 13 under a pair of 100 kN horizontal point-loads applied to the left at the support bearings over pillar P4. It is clear that, together with the horizontal translation to the left, this pair of loads induces bending on the upper deck. Consequently, in addition to the compressive forces arising between pillar P4 and the arch crown, the strains include the effects of the deck bending.

Focusing on the vehicle path encompassing spans 3 to 6 (between pillar P2 and the arch crown), as a result of the constraint for the horizontal movement, Figure 8.13 shows that the strains estimates for cross-sections S10, S11, S13 and S14 (located in the 11th span, between pillar P4 and the arch crown) decrease, in relation with the baseline condition. As regards cross-sections S15 and S16 (located in the 12th span, away from the region comprised between the arch crown and pillar P4), the strains estimated in the former also decrease whereas in the latter increase. These changes on the strain estimates between the baseline (BS) and the damaged (DS2.ii) scenarios are in accordance with the axial forces induced at the respective bar elements by the horizontal forces at the supports (see Figure 8.15). As regards the cross-sections located at mid-span of span 12 (S17 and S18), as the induced axial forces at the bar elements are low (see Figure 8.15), the shift in the strain estimates is negligible (depicted in Figure 8.13).

In relation to the strains obtained when the vehicle crosses spans 7 to 10 (comprised between the arch crown and pillar P3), although the effects of the vertical loading are more significant and, thus, the strains related with the horizontal effects are less pronounced in the results, similar conclusions to those regarding the path comprising spans 3 to 6 may be drawn. When the vehicle traverses spans 11 and 12, due to the bending of the upper deck, horizontal reactions arise at the supports, respectively, towards the left and the right, as shown in Figure 8.14. Consequently, the strains estimated both for the baseline (BS) and the damaged (DS2.ii) scenarios are different. However, as the horizontal forces are lower than those observed when the vehicle crosses the arch, the changes are significantly smaller.

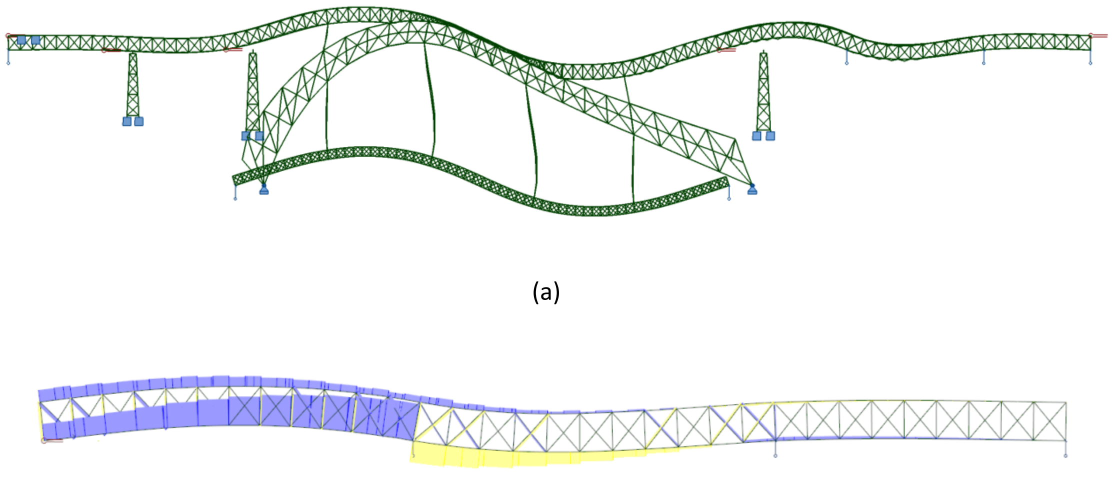

(a)

(b)

Figure 8.15 – Numerical estimates of the deformed shape and the axial forces under a pair of 100 kN horizontal point-loads applied to the left at the support bearings over pillar P4: (a) deformed mesh of the whole structure; (b) axial forces along spans 11 to 13 (blue and yellow represent, respectively, compressive and tensile forces).

It should be mentioned, however, that this qualitative analysis have taken into account the axial forces only and, thus, the elements bending, i.e., the strains resulting from bending moments along the bars, were neglected. Even though, this approach does not seem to compromise the conclusions drawn herein.

8.4. Data-driven methodologies for early damage detection

8.4.1. General remarks

This work shows the applicability of two data-driven methodologies for early damage detection based on moving-loads data. Both methods lay on the identification of changes in the pattern of the vehicle influence-lines of strains for 1-vehicle compositions of the light metro of Porto. For that purpose the vehicle influence-lines of strains for selected cross-sections are assembled in time-series and subsequently processed by using either the moving principal component analysis (MPCA) or the influence-line assurance criterion (ILAC).

Figure 8.16 depicts a set of vehicle influence-lines for the strains in selected cross-sections collected during a 3-months monitoring period of the Luiz I Bridge. Although during this period a set of about 1500 vehicle influence-lines have been collected, in order to facilitate the interpretation this figure depicts only 50 influence-lines equally distributed along the whole period of observation. The colour scheme varies between different shades of blue, green and red for, respectively, the first, intermediate and last crossings.

The plots shown in Figure 8.16 do not include the whole vehicle influence-line. On one hand, by using the B-WIM system described in chapter 7, an accurate assignment of the vehicle position to the time-instant in which a given measurement is collected cannot be assured when the vehicle is moving far from the 11th span. Consequently, the estimated vehicle influence-lines may be distorted on those regions. On the other hand, when the vehicle is traversing spans far from the one in which the cross-section under analysis is instrumented, the strains are approximately null. Consequently, these measurements lose their significance either for the characterization of the structural behaviour or for early damage detection. In this context, within this work, only the measurements regarding the span in which the cross-section is located, as well as the adjacent spans, are taken into account. As concerns the cross-sections instrumented at mid-span, such as S13 and S14, only the portion of the vehicle influence-line regarding spans 10 to 12 is considered. In relation to the cross-sections located near the supports, bearing in mind the pattern of the measurements, two spans located in each side are taken into account. Therefore, for cross-sections S10, S11 and S22, the portion of the vehicle influence-line selected comprises spans 9 to 12, whereas for S15, S16 and S24 includes spans 10 to 13.

It is noteworthy to mention, however, that, under restraints for the horizontal movement of the supports, additional strains in the instrumented cross-sections may arise particularly when the vehicle traverses the spans supported on the arch, as shown above. Even though, the portion of the vehicle influence-lines selected herein for each cross-section includes at least one span supported on the arch in which the effect of the restraints for the longitudinal movement of the support bearings is perceived. Thus, the selected portions of the vehicle influence-lines may still be used for early identification of restraints for the longitudinal displacements of the support bearings.

The length of the selected portions of the vehicle influence-lines varies for the different cross-sections included in the monitoring system. Consequently, the number of measurements included therein also varies. However, the damage detection algorithms proposed below requires an equal number of measurements in each vehicle influence-line. Therefore, prior the application of those methodologies, the portions of the vehicle influence-lines were computed for a fixed number of points (500, within this work) through an adequate interpolation of the measurements.

As noticeable in Figure 8.16, for each cross-section, although the pattern of the vehicle influence- lines collected during the monitoring period is similar, the results exhibit some variability. Note that these results are in-service field measurements, i.e., obtained under regular traffic of metro vehicle compositions on the bridge. Therefore, despite the vehicle influence-lines concern to 1-vehicle compositions, in which the geometry of the vehicle is always the same, the loading conditions may vary as regards either the total load of the vehicle or the relation between the loads in each bogie. In addition, deviations between the estimates of the position of the vehicle (to obtain the vehicle influence-line) and its actual location must be also taken into account. Finally, although the acquired signals are smoothed (see chapter 7), the effects of noise on the accuracy of the measurements should not be disregarded.

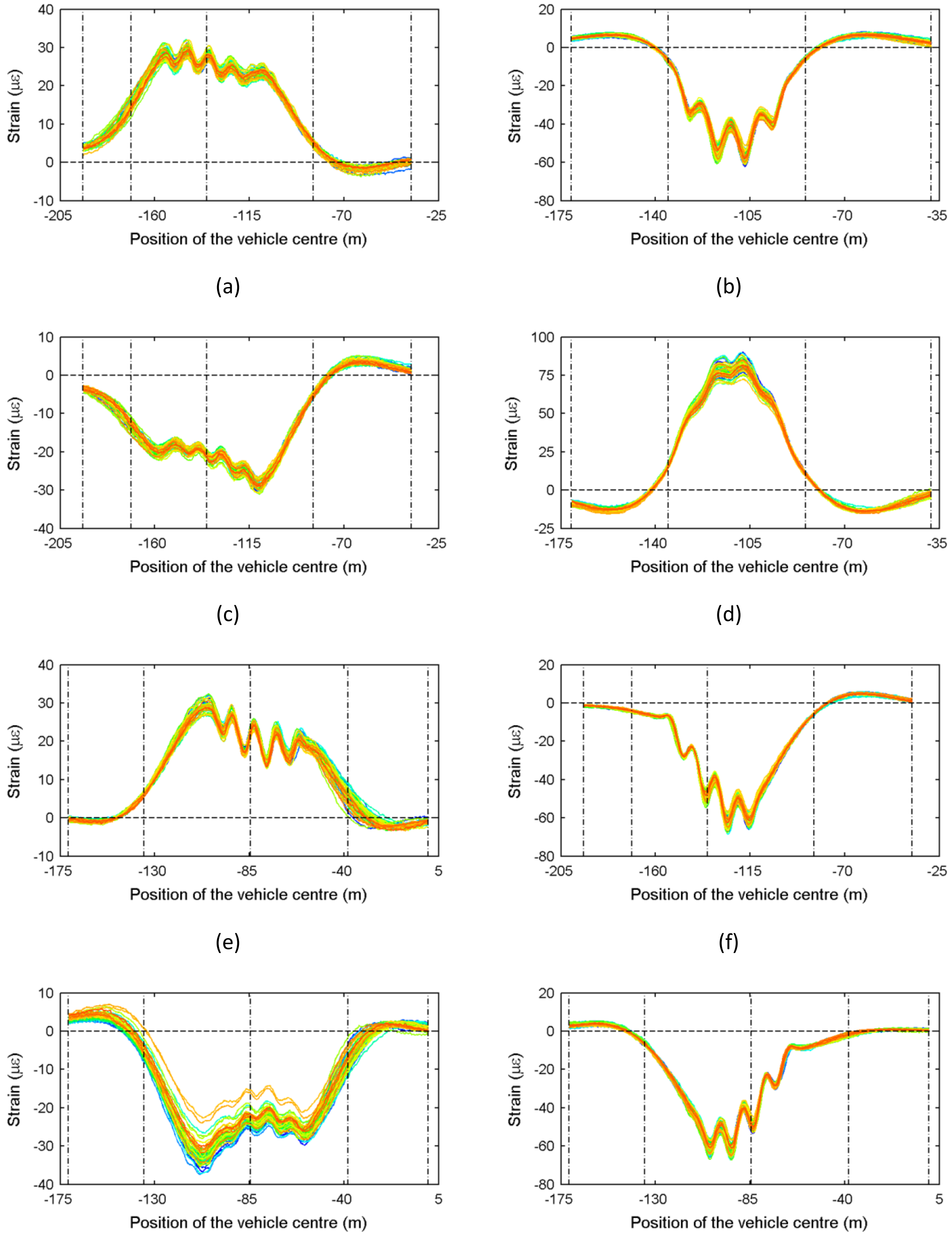

(a) (b)

(c) (d)

(e) (f)

(g) (h)

Figure 8.16 – Vehicle influence-lines of the flanges strains for selected cross-sections, for a set of crossings of 1-vehicle compositions in direction 2, collected during a 3-months monitoring period of the Luiz I Bridge. The selected cross-sections are: (a) S10; (b) S13; (c) S11; (d) S14; (e) S15; (f) S22; (g) S16; and (h) S24.

Therefore, the adoption of methodologies that allow to swiftly distinguish, on the vehicle influence-lines that are continuously collected, abnormal behaviour of the bridge from the variability of its response related with the normal operation, as described above, are needed. In this context, as referred earlier, the vehicle influence-lines collected within this work have been assembled in time-series and subsequently processed using the algorithms described below.

8.4.2. Moving principal component analysis

The principal component analysis (PCA) is one of the methods included in the proper orthogonal decomposition (POD), which is used in multivariate analysis (Liang *et al.*, 2002). The key idea of PCA is to reduce a large number of interdependent variables to a much smaller number of uncorrelated variables while retaining as much as possible of the variation present in the original dataset. This is achieved by transforming the original variables into a new set of uncorrelated variables, the principal components (PCs), which are ordered so that the first few retain most of the variation present in all of the original variables (Jolliffe, 2002). Consider a dataset matrix $X \epsilon \Re^{n\times p}$, containing n observations for p variables. The row i is a p-dimensional vector representing the i^{th} observation, whereas the column j is a n-dimensional vector representing the j^{th} variable. The dataset matrix can be written as a linear combination of a set of orthogonal vectors as follows:

$$[X] = [Z][U]^T \tag{8.1}$$

where $Z \epsilon \Re^{n\times p}$ is the scores matrix and $U \epsilon \Re^{p\times p}$ is the loadings matrix. The scores correspond to the coordinates of the original data in the new coordinate system defined by the orthogonal vectors $U_j = \left(U_{1,j},\ U_{2,j}, \dots, U_{p,j}\right)$.

As mentioned above, the first few principal components retain most of the variation present in all of the original variables. Thus, for a p-dimensional dataset, it is possible to choose only the first r principal components and obtain the original data without significant loss of information. Thus, a good approximation of the features matrix $X \epsilon \Re^{n\times p}$ can be obtained as follows:

$$[X] = [\bar{Z}][\bar{U}]^T \tag{8.2}$$

where $\bar{Z} \epsilon \Re^{n\times r}$ and $\bar{U} \epsilon \Re^{p\times r}$ are, respectively, the r-dimensional matrices of the scores and the loadings.

In the classical approach, the principal components correspond to the eigenvectors computed from the covariance matrix $S \epsilon \Re^{p \times p}$ of the dataset $X \epsilon \Re^{n \times p}$. The k^{th} principal component is the eigenvector U_k corresponding to the k^{th} largest eigenvalue (Jolliffe, 2002). It is noteworthy to mention that, in order to PCA work properly, the mean of all observations included in each feature of the dataset must be subtracted before the calculation of the covariance matrix S.

PCA has been used in numerous applications in the engineering field (a comprehensive list may be found in (Yan *et al.*, 2005a)). In the context of structural health monitoring, PCA has been widely applied in the last years with three major objectives (Figueiredo *et al.*, 2009): (i) evaluation of patterns in the data; (ii) data cleansing; and (iii) data compression.

Lanata and Del Grosso (2006) have shown that the analysis of the evolution, in terms of eigenvalues and eigenvectors, of the covariance matrix of the dataset gives a good indication of the damage initiation. However, a significant time-lag between the identification and the occurrence of damage was found. Immediately after damage occurrence, the influence of old measurements (in the undamaged state) is much higher than that of new measurements (in the damaged state), which leads that additional time is required in order to the new measurements may produce changes in the principal components. With the objective of overcoming this drawback, Posenato *et al.* (2008) proposed the moving principal component analysis (MPCA), as an extension of PCA. This approach consists in the calculation of the principal components of the data comprised in a window of constant size moving along the entire dataset. Similarly to the original approach, a change in the values of the principal components coordinates suggests the occurrence of damage. If the group of sensors considered in the analysis are correlated and if the structural conditions have not changed, the main eigenvalues, and corresponding eigenvectors, remain stable with time. However, when something occurs in the structure, the measurements collected by some sensors may vary with respect to others, which leads to changes in the eigenvectors.

8.4.3. Influence-line assurance criterion

The influence-line assurance criterion (ILAC) is a statistical indicator that yields the degree of consistency between influence-lines. This parameter is based on the modal assurance criterion (MAC), usually applied to match mode shapes (Allemang, 2003). The ILAC value between the r^{th} influence-line of a dataset A, $\Upsilon_{r,A}$, and the q^{th} influence-line of a dataset B, $\Upsilon_{q,B}$, is given as follows:

$$ILAC(r_A, q_B) = \frac{\left|\left\{\Upsilon_{r,A}\right\}^T \left\{\Upsilon_{q,B}\right\}\right|^2}{\left(\left\{\Upsilon_{r,A}\right\}^T \left\{\Upsilon_{r,A}\right\}\right)\left(\left\{\Upsilon_{q,B}\right\}^T \left\{\Upsilon_{q,B}\right\}\right)} \tag{8.3}$$

On the assumption the datasets A and B are obtained in different time-instants, the diagonal terms of the ILAC matrix may provide a good indication of the occurrence of damage in the structure. An ILAC value of one would show that the two influence-lines are perfectly correlated, or, in this case, identical. The greater the deviation from unity, the less the two modes are correlated, which suggests changes in the structural response, and, thus, the occurrence of damage.

However, preliminary tests have shown that these indicators could hardly provide a reliable damage identification due to the variability of the vehicle influence-lines, which results from the changeability of the vehicle parameters. Still, additional tests have shown that the AutoILAC, based on the AutoMAC presented by (Pastor *et al.*, 2012), allows to overcome this shortcoming. The AutoILAC quantitatively compares all the possible combinations of influence-lines pairs for only one set of mode shapes. The calculation assigns a value of one to influence-lines pairs that exactly match and a value of zero to those pairs that are completely independent or unrelated. In the context of this work, aiming at early detection of damage, instead of discovering the influence-lines included in a given dataset that exactly match, the focus lies on the surveillance of the evolution of the AutoILAC values along a monitoring period. Deviations of the AutoILAC values computed along the monitoring period suggests changes in the structural response, and, thus, the occurrence of damage.

8.4.4. Closing remarks

The application of the data-driven methodologies described above requires the definition of a training period in which the structure is assumed undamaged. The aim of this period is to estimate the variability of the control parameters, either the MPCA coordinates or the ILAC values, given by the corresponding data-processing algorithms, in order to define the thresholds for detecting anomalous behaviour in the monitoring phase. In this work the thresholds are given by $\mu_i \pm k \cdot \sigma_i$, in which μ_i and σ_i are, respectively, the mean and the standard deviation computed in the training phase, of a control parameter i. The parameter k is a constant value carefully defined in order to, on one hand, enable the detection of damage as quick as possible, and, on the other, prevent false-positive indication of damage. Still, with the objective of preventing false-positive indications of damage, an additional criterion was established: a structural change is flagged only when q consecutive points exceed the thresholds. Therefore, in the monitoring phase, during which the control values are computed for each new observation, if q consecutive points exceed the threshold bounds, an anomaly is flagged.

Within this work, for both data-processing algorithms, the training period includes 100 vehicle influence-lines. The thresholds are computed on the assumption of $k = 4$ and the number of consecutive points exceeding the thresholds that are required to flagg an anomaly are 10 ($q = 10$). The window size, an additional parameter required in the MPCA, was assumed to include a vehicle influence-line only. Therefore, both methods monitor the evolution of the respective control values computed for datasets comprising measurements regarding a single crossing only.

8.5. Application to numerically-simulated data

8.5.1. General remarks

This section shows the applicability of the methodologies for early damage detection presented above by using numerically-simulated data of the bridge structural response for the in-service traffic of the light metro of Porto. The objective of the analysis presented herein is to attain sound results aiming at the application of these methodologies on field data. Therefore, the characteristics of the numerically-simulated data analysed herein should be as similar as possible with those of the field measurements. Thus, the factors that lead to the variability of the field results (as shown and described in section 8.4.1) were taken into account within the numerical simulation of data, whose procedure is thoroughly detailed in this section.

The applicability of the methodologies for damage detection presented above is assessed through the analysis of three different situations as regards the vehicle influence-lines included in the numerically-simulated time-series. The objective of the first one is to verify the stability of the approach under undamaged conditions. The second and the third situations aim at the assessment of the ability of the methods for early detection of restraints for the longitudinal displacements of the support bearings installed at, respectively, pillars P3 and P4. The details concerning the simulation of each situation as well as the results provided by both algorithms are carefully described in this section.

8.5.2. Numerically-simulated time-series

8.5.2.1. Introductory remarks

The approach proposed herein for early damage detection is based on the structural response under moving-loads. It consists in applying suitable data-processing algorithms to detect changes in time-series of vehicle influence-lines collected under regular traffic of metro vehicle compositions on the bridge. Consequently, even with no modification on the structural conditions, the vehicle influence-lines regarding different crossings may vary as a result of: (i) the variability of the vehicles loads; (ii) uncertainty about the vehicle position; and (iii) noise in the measurements. Therefore, with the aim of reproducing the experimental conditions, these factors that lead to the variability of the field measurements must be taken into account in the development of the numerically-simulated time-series.

In a structure whose behaviour is linear and elastic, the response of a vehicle comprising a set of axles may be obtained by the superimposition of the effects of each load computed separately. The contribution of each axle is obtained by multiplying the axle load by the ordinate value of the unit influence-line at the axle position (Ghali *et al.*, 2009). Therefore, in order to obtain time-series of 1-vehicle compositions influence-lines reproducing the variability of the in-service traffic conditions, the following procedure was followed. Firstly, by using the numerical model, the structural conditions in both the baseline and the damaged scenarios are simulated and the unit influence-lines for the strains in the instrumented cross-sections are collected. Secondly, for a set of vehicle parameters such as the total weight of the vehicle, the axles loads, and varying speed, the vehicle influence-line is computed taking advantage of the superposition principle. Then, in order to simulate a measured signal, these numerical estimates are contaminated with white noise. Thirdly, the second step is repeated for different vehicle parameters, which are randomly determined in order to reproduce the variability along the time-series referred above. Note that as in the case under study the geometry of the crossing vehicles is known beforehand, both the number and the axles distances remain invariable. Finally, the set of vehicle influence-lines obtained previously are assembled in time-series for later application of data-processing algorithms in order to assess their performance for early damage detection.

It is noteworthy to mention that the aim of this procedure is not to accurately replicate the measurements collected in the monitoring period shown in section 8.4.1. The purpose of this simulation is to obtain a similar pattern in terms of variability of the structural response for a given set of vehicle influence-lines. Therefore, for the sake of simplicity, the variability and uncertainty of the vehicle features were modelled on the basis of a Gaussian distribution, whose parameters values were determined through a sensitivity analysis. Consider a Gaussian distribution with null mean and unit standard deviation $Z(0,1)$. A Gaussian distribution with mean μ and standard deviation σ, $X(\mu,\sigma)$, may be obtained as follows (Montgomery and Runger, 2003):

$$X = \mu + Z \cdot \sigma \tag{8.4}$$

The mean, μ, and the standard deviation, σ, of the Gaussian distributions adopted for each variable in order to reproduce the variability of the vehicle influence-lines in the numerically-simulated time-series are summarized in Table 8.1. It should be noted that about 95% of the values lie within two standard deviations away from the mean. For instance, for the noise in the measurements, 95% of the values lie within the range [-1, 1] $\mu\varepsilon$.

A summary of the procedure for modelling each variable is presented below. The description refers to one crossing. In order to build a complete time-series, this procedure must be repeated as many times as the number of vehicle influence-lines required.

Table 8.1 – Parameters of the Gaussian distributions adopted for each variable.

Variable	Mean, μ	Standard-deviation, σ
Total load of the vehicle	397.4 kN (in accordance with the total load of the vehicle depicted in Figure 8.3)	29.8 kN (7.5% of the total load of the vehicle)
Axles loads (ratios)	1 for the axle loads ratios (axles loads obtained in relation to the vehicle depicted in Figure 8.3)	0.075 (7.5% of the axle load ratio)
Vehicle position (distances)	4.29 m (Distance travelled during 1 out of 100 time-intervals, under constant speed)	0.15 m (3.5% of the mean)
Noise in the measurements	0 (on the assumption of white noise)	0.5 με

8.5.2.2. Variability of the vehicles loads

The vehicles loads may vary either on the total load of the vehicle, due to different number of transported passengers, or on the relation between the loads over the vehicle axles, as a result of a distinct distribution of the passengers along the composition. The total load of a given vehicle i, denoted as $F_{T,i}$, is given by:

$$\mathrm{F}_{T,i} = F_{T,0} + z_i \cdot \sigma_{F_T} \tag{8.5}$$

where $F_{T,0}$ is the total load of the reference vehicle (397.4 kN in accordance with the loads summarized in Figure 8.3), σ_{F_T} is the standard deviation of the total load (29.8 kN, given by 7.5% of the total load of the vehicle) and z_i is a random value drawn from a Gaussian distribution with null mean and unit standard deviation.

As an example, Figure 8.17 depicts the numerical estimates of the strains of the cross-section S15 flange for the crossing of two 1-vehicle compositions, weighing, respectively, 397.4 kN (the reference vehicle) and 358.4 kN (vehicle *i* with a total load of 0.90 times that of the reference vehicle), under normal operating conditions. As the total load variation results from a change of the axles loads in equal proportion, the structural responses for both vehicles are also proportional (see Figure 8.17.a). Moreover, the differences between the structural responses estimated for each case (see Figure 8.17.b) give also rise to a pattern proportional to the vehicle influence-lines.

As regards the variability of the loads over the vehicle axles, consider the axle loads ratios between a given vehicle, i, and the reference vehicle. The axle load ratio for the k^{th} axle, $r'_{k,i} = F'_{k,i}/\mathrm{F}_{k,0}$, for $k = 1, 2, \ldots, 8$, in which $F'_{k,i}$ and $\mathrm{F}_{k,0}$ are the loads of the k^{th} axle of, respectively, the former and the latter vehicles, is given by:

$$r'_{k,i} = r'_{k,0} + z_i \cdot \sigma_{r'_k} \tag{8.6}$$

where $r'_{k,0}$ is the reference axle load ratio for the k^{th} axle (assumed unitary), $\sigma_{r'_k}$ is the standard deviation of the axles loads ratios (0.075, which corresponds to 7.5% of the reference axle load ratio) and z_i is a random value drawn from a Gaussian distribution with zero mean

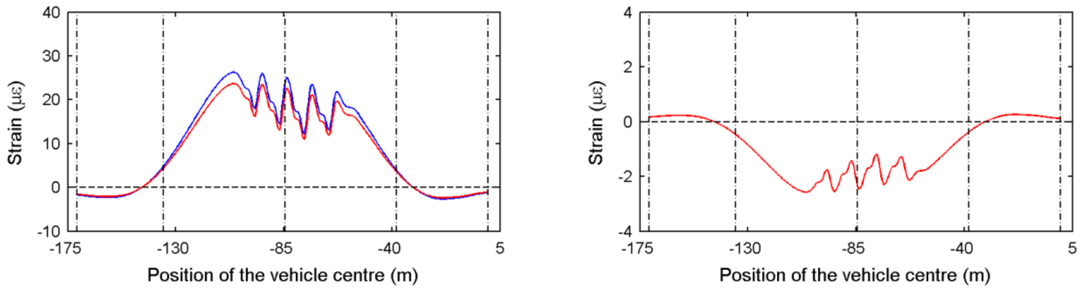

(a) (b)

Figure 8.17 – Numerical estimates of the cross-section S15 flange strains for the crossing of two 1-vehicle compositions, weighing 397.4 kN and 358.4 kN, in direction 2, under normal operating conditions: (a) comparison of the vehicle influence-lines for the reference vehicle (blue line) and a vehicle *i* (red line); and (b) differences between the latter and the former.

and unit standard deviation. Then, the k^{th} axle load for the vehicle under analysis, $F'_{k,i}$, is given by $F'_{k,i} = r'_{k,i} \cdot \mathrm{F}_{k,0}$. Finally, the axle loads expressing the variability of the axle load ratios must be normalized in order to meet the total load of the vehicle, $\mathrm{F}_{T,i}$. Thus, the normalized load, $\mathrm{F}_{k,i}$, for the k^{th} axle, for $k = 1, 2, \ldots, 8$, is given by:

$$\mathrm{F}_{k,i} = F'_{k,i} \cdot \frac{\mathrm{F}_{T,i}}{\sum F'_{k,i}} \tag{8.7}$$

Figure 8.18 depicts an example of the variability of the axles loads for a vehicle i. The axles loads depicted in Figure 8.18 (b) are normalized values so that the total load of the vehicle i equals that of the reference vehicle. The numerical estimates of the strains of the cross-section S15 flange for the crossing of this vehicle i are compared with those of the reference vehicle in Figure 8.19. Although the total load of the vehicle i equals that of the reference vehicle the structural response varies as a result of a different load distribution over the axles.

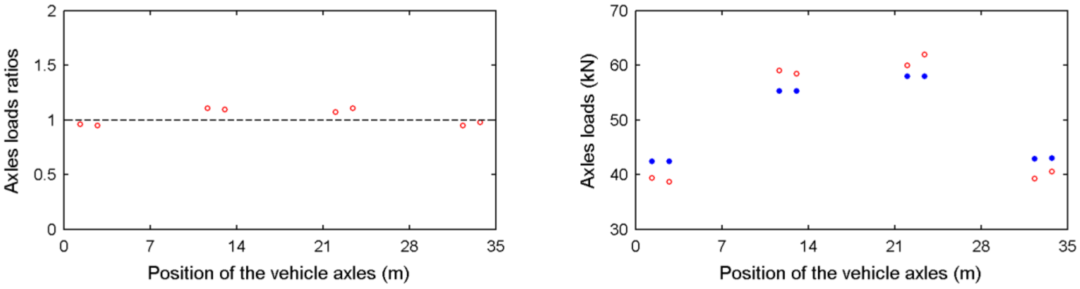

(a) (b)

Figure 8.18 – Example of the variability of the axles loads for a vehicle i: (a) axles loads ratios; and (b) comparison of the axles loads for the reference vehicle (blue dots) and a vehicle i (red dots).

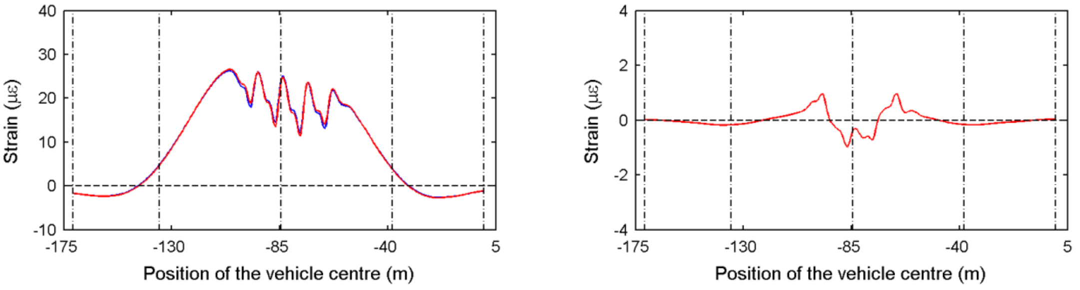

(a) (b)

Figure 8.19 – Numerical estimates of the cross-section S15 flange strains for the crossing of a vehicle i and the reference vehicle, in direction 2, under normal operating conditions: (a) comparison of the vehicle influence-lines for the reference vehicle (blue line) and a vehicle i (red line); and (b) differences between the latter and the former.

8.5.2.3. Uncertainty about the vehicle position

The experimental vehicle influence-lines were obtained using a B-WIM system, on the assumption that the vehicle speed was constant (see chapter 7). However, it was shown that it might change along the crossing of the bridge. Consequently, the estimated vehicle influence-lines may be distorted, as a result of an inappropriate assignment of the position of the vehicle to the time-instant in which a given measurement is collected.

On the assumption of constant speed, v_0, the elapsed time, Δt, for the crossing along a path of Δx in length is given by $\Delta t = \Delta x / v_0$. With the goal of estimating distorted vehicle influence-lines for the numerically-simulated time-series consider the elapsed time Δt divided into n time-intervals Δt_k, for $k = 1, 2, \dots, n$. Under constant speed, the distance travelled in the k^{th} time-interval, Δt_k, is given by $\Delta x_{k,0} = v_0 \cdot \Delta t_k$. However, under varying speed the distance travelled might be different. For the sake of simplicity, consider that the speed remains constant along a time-interval but varies from one to another. On the assumption that in the k^{th} time-interval the speed is given by $v'_k = v_0 + \delta v_{0,k}$, in which $\delta v_{0,k}$ is the speed increment in relation to the average speed v_0, the respective travelled distance is $\Delta x'_k = \Delta x_{k,0} + \delta \Delta x_{k,0}$, where $\delta \Delta x_{k,0} = \delta v_{0,k} \cdot \Delta t_k$ is the distance increment. Therefore, for a given crossing i, the distance travelled in the k^{th} time-interval, $\Delta x'_k$, may be computed as follows:

$$\Delta x'_{k,i} = \Delta x_{k,0} + z_i \cdot \sigma_{\Delta x'_k} \tag{8.8}$$

where $\Delta x_{k,0}$ is the distance travelled during the k^{th} time-interval on the assumption of constant speed for the whole path (4.29 m, dividing the whole path, 429 m long, in 100 equal parts), $\sigma_{\Delta x'_k}$ is the standard deviation of the distance travelled in the k^{th} time-interval (0.15 m, which corresponds to 3.5% of the reference distance) and z_i is a random value drawn from a Gaussian distribution with zero mean and unit standard deviation. Then, the distances travelled in the k^{th} time-interval expressing the speed changeability must be normalized so that their sum equals the length of the whole path. Thus, the normalized travelled distance for the k^{th} time-interval, for $k = 1, 2, \dots, n$, is given by:

$$\Delta x_{k,i} = \Delta x'_{k,i} \cdot \frac{\Delta x}{\sum \Delta x'_{k,i}} \tag{8.9}$$

Finally, the position $x_{j,i}$ for a given time-instant $t_{j,i}$ is obtained by the cumulative sum of the distances $\Delta x_{k,i}$ travelled until that moment.

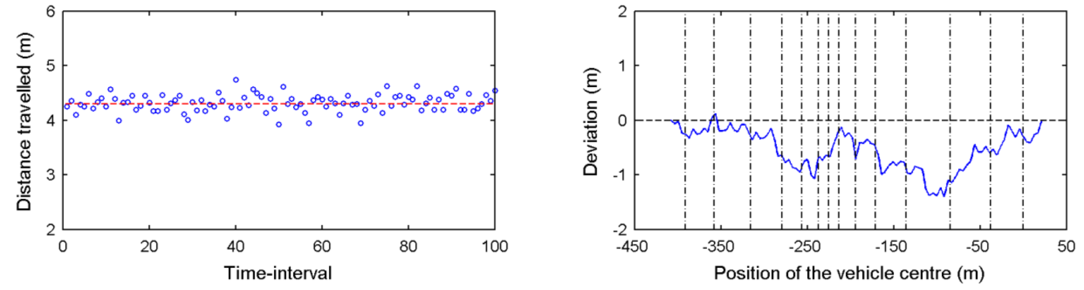

(a) (b)

Figure 8.20 – Example of the variability about the position of a vehicle *i*: (a) distances travelled in each of the 100 time-intervals in which the whole path is divided; and (b) deviation between the position of the vehicle under varying speed (computed as explained above) and the position assuming constant speed.

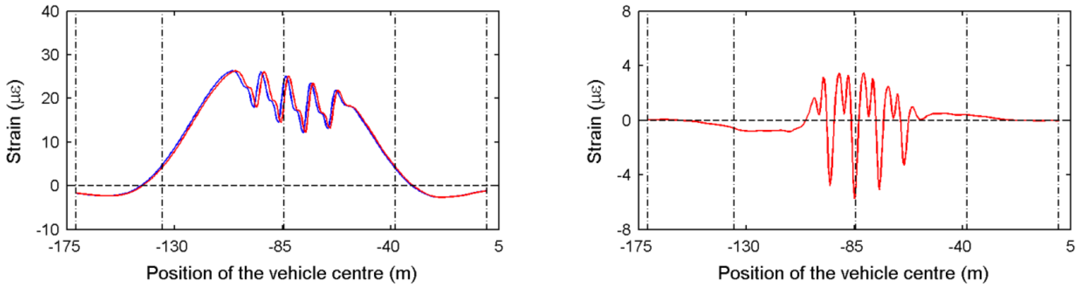

(a) (b)

Figure 8.21 – Numerical estimates of the cross-section S15 flange strains for the crossing of a vehicle i and the reference vehicle, in direction 2, under normal operating conditions: (a) comparison of the vehicle influence-lines for a vehicle under constant speed (blue line) and a vehicle i under varying speed (red line); and (b) differences between the latter and the former.

As mentioned above, the vehicle influence-lines are computed on the assumption of constant speed. Therefore, the measurements collected at a given time-instant of the crossing are assigned to a given position irrespectively of the position the vehicle might occupy under varying speed. This leads to an inappropriate matching of the measurements with the vehicle positions giving rise to distorted vehicle influence-lines. In this context, with the goal of replicating these conditions, the structural response is firstly computed based on the positions of the vehicle on the assumption of varying speed. Then, the vehicle influence-lines are built assuming constant speed, leading, thus, to the aforementioned distortion.

Figure 8.20 (a) depicts the distances travelled by a given vehicle i in each of the 100 time-intervals in which the whole path is divided. The deviations between the position of the vehicle under varying speed (computed as explained above) and the position assuming constant speed are shown in Figure 8.20 (b). The maximum deviation between the position under varying speed and the position computed on the assumption of constant speed reaches about 1.5 m (near the mid-span of the 11th span), in which for the former conditions the vehicle is behind the latter. The vehicle influence-line of the strains of the cross-section S15 flange for the crossing of this vehicle i moving under varying speed is compared with that of an equal vehicle travelling under constant speed in Figure 8.21. As in the former the speed of the vehicle is assumed constant, the structural response estimates for the actual positions of the vehicle are inappropriately assigned leading to a distorted vehicle influence-line. As shown in Figure 8.21 (a), the maximum deviation is reached near the mid-span of the 11th span, in which the structural response estimates at the actual positions are assigned to positions about 1.5 m ahead (in accordance with Figure 8.20 (b)). It is noteworthy to mention that although the vehicles loads are equal, either in terms of total load or in terms of its distribution over the axles, this distortion might lead to significant differences between the vehicle influence-lines, as depicted in Figure 8.21 (b).

8.5.2.4. Noise in the measurements

In addition to the phenomena under observation, the signals include errors which are typically described as noise. Thus, although the field results are smoothed (see chapter 7), with the objective of better simulating the experimental conditions, the numerical estimates are contaminated with white noise. This disturbance is assumed to be normally distributed with zero mean and a range of variation, given by the standard deviation, of the order of the sensors accuracy. Therefore, for a given crossing i, the error $e_{j,i}$ to be added to the simulated strain $s_{j,i}$ is given by:

$$\mathrm{e}_{j,i} = e_{j,0} + z_i \cdot \sigma_{e_j} \tag{8.10}$$

where $e_{j,0}$ is the average (null, for white noise), σ_{e_j} is the standard deviation (0.5 με) and z_i is a random value drawn from a Gaussian distribution with zero mean and unit standard deviation. Figure 8.22 depicts the comparison of noiseless and noisy vehicle influence-lines for the strains of the cross-section S15 flange.

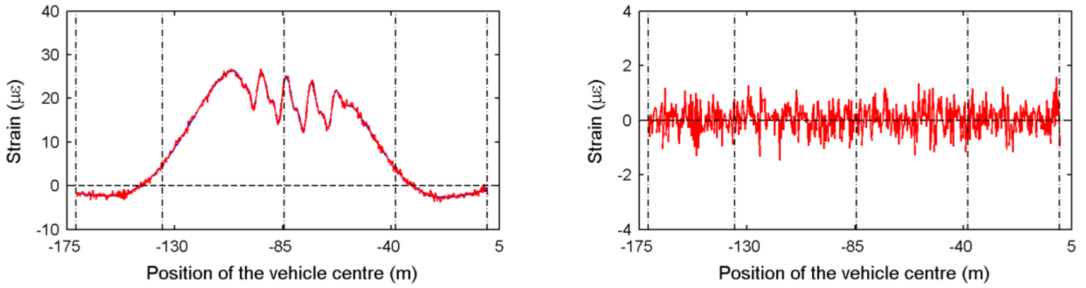

(a) (b)

Figure 8.22 – Numerical estimates of the cross-section S15 flange strains for the crossing of a vehicle i and the reference vehicle, in direction 2, under normal operating conditions: (a) comparison of noiseless (blue line) and noisy (red line) vehicle influence-lines; and (b) differences between the latter and the former.

8.5.2.5. Closing remarks

Both the simulation and the effects on the structural response of the vehicles loads variability, namely the variation as regards the axles loads ratios, the uncertainty about the vehicle position, and noise in the measurements were separately shown above. However, these issues may come together leading to differences on the vehicle influence-lines between a reference vehicle and a vehicle i that, even under the same structural conditions, might be more significant. This becomes clear in Figure 8.23, which depicts the numerical estimates of the strains of the cross-section S15 flange for the crossing of the reference vehicle, under constant speed and with noiseless measurements, and a vehicle i, whose parameters match the ones presented earlier in this section.

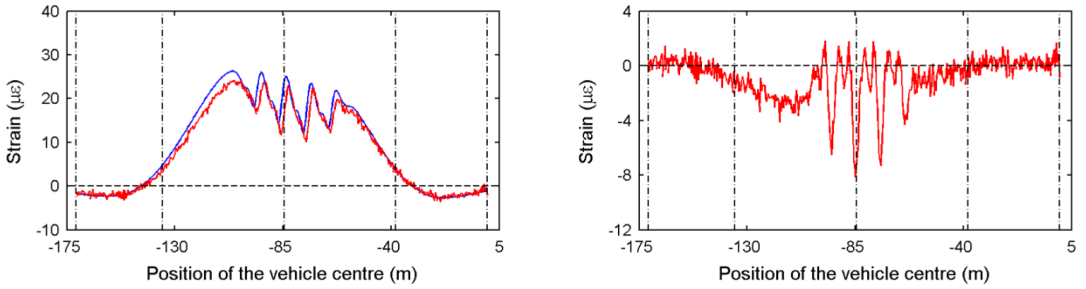

(a) (b)

Figure 8.23 – Numerical estimates of the cross-section S15 flange strains for the crossing of a vehicle i and the reference vehicle, in direction 2, under normal operating conditions: (a) comparison of the vehicle influence-lines for the reference vehicle (blue line) and a vehicle i (red line); and (b) differences between the latter and the former.

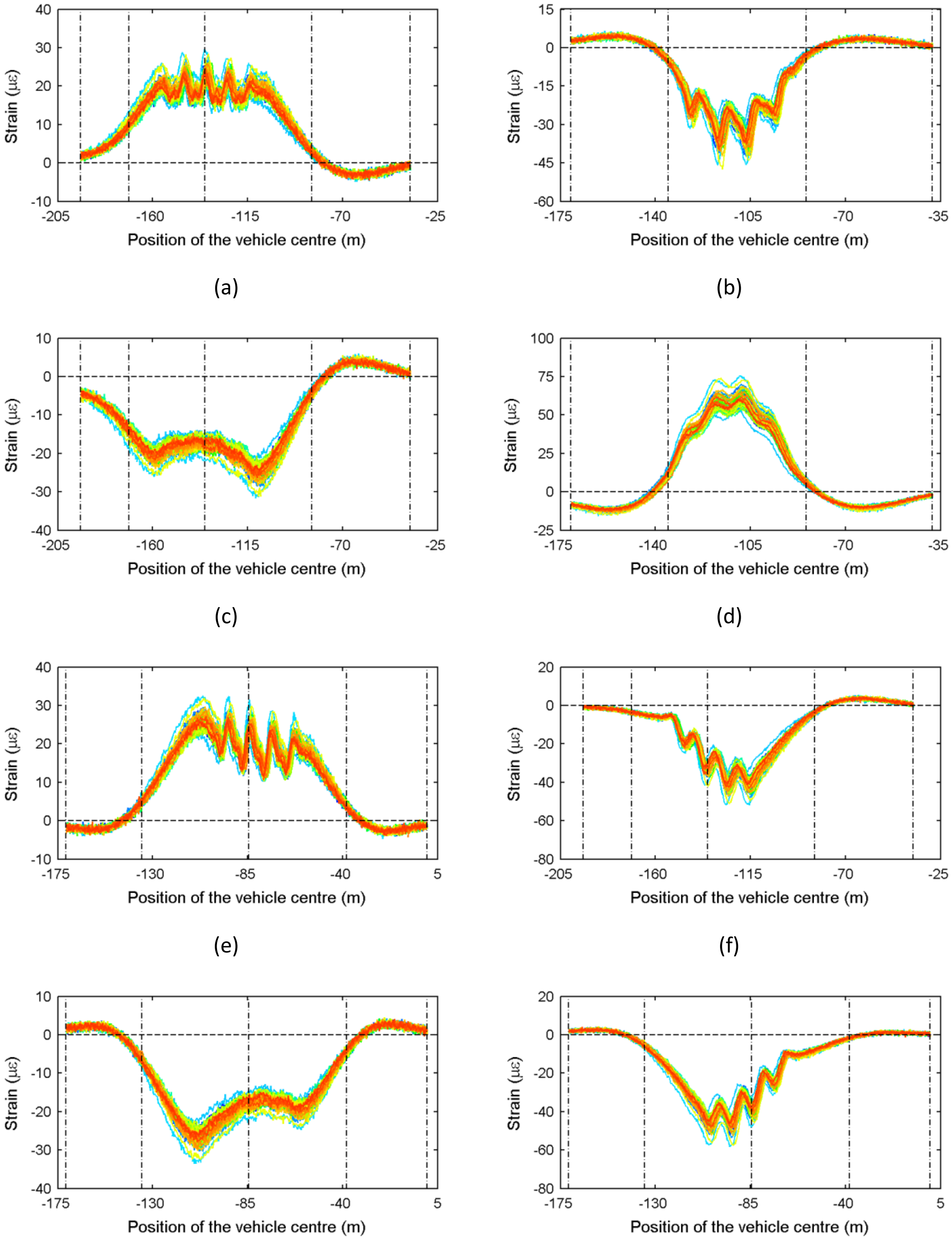

(a) (b)

(c) (d)

(e) (f)

(g) (h)

Figure 8.24 – Numerical estimates for a set of 50 vehicle influence-lines of the flanges strains for selected cross-sections, for a set of crossings of 1-vehicle compositions in direction 2, under varying conditions as regards the vehicles loads, the vehicle positions, and noise. The selected cross-sections are: (a) S10; (b) S13; (c) S11; (d) S14; (e) S15; (f) S22; (g) S16; and (h) S24.

Figure 8.24 shows the numerical estimates for a set of 50 vehicle influence-lines of the strains of the flanges for selected cross-sections, for a set of crossings of 1-vehicle compositions in direction 2, for the baseline scenario, under varying conditions as regards the vehicles loads, the vehicle positions, and noise. The colour scheme varies between different shades of blue, green and red for, respectively, the first, intermediate and last crossings. Similarly to Figure 8.16, these plots include only the numerical estimates regarding the span in which the cross-section is located as well as the adjacent spans. The numerical estimates of the vehicle influence-lines exhibit some variability, as it was intended. Despite not reproducing exactly the experimental vehicle influence-lines shown in Figure 8.16, the pattern of this set of results is analogous. In this context, the performance of the proposed approach for early damage detection applied on such numerically-simulated data may give good indications as regards its ability to be applied to field measurements.

8.5.3. Results

This section presents the results of the analyses carried out with the objective of assessing the performance of the data-processing algorithms within the approach for early damage detection presented in section 8.4. For that purpose, using numerically-simulated data, three different situations, as regards the vehicle influence-lines included in the time-series, were considered.

The objective of the first one (denoted herein as time-series 1 – TS1) is to verify the stability of the algorithms, i.e., to evaluate the possibility of occurrence of false-positive identification of damage. Therefore, the vehicle influence-lines included in the time-series (in a total of 500) regards the baseline scenario (BS) only, in which the structure is under normal operating

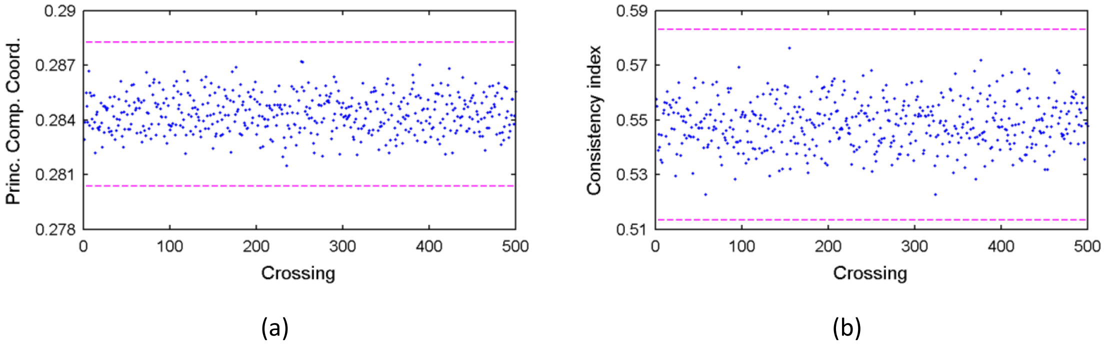

(a) (b)

Figure 8.25 – Evolution of the control values for time-series TS1: (a) MPCA coordinate related with the vehicle influence-lines for the strains estimated at the flange of cross-section S14; and (b) ILAC value for the vehicle influence-lines for the strains estimated at the flange of cross-sections S11 and S14.

conditions (as shown in Figure 8.24). As an example, Figure 8.25 depicts the evolution of the control values of either MPCA or ILAC for time-series TS1. As a result of the variability of the vehicle parameters, the control values of both algorithms vary along the time-series. Still, the threshold bounds defined in the training period (with a length of 100 vehicle influence-lines) are never exceeded, and, thus, there is no false-positive indication of damage.

The objective of the second (TS2) and the third (TS3) situations tested herein is to assess the performance of the methodologies for early detection of damage, namely to identify restraints for the longitudinal displacement of the support bearings. TS2 and TS3 regard the restraints of the support bearings installed over, respectively, pillar P3 (see section 8.3.2) and P4 (see section 8.3.3). Therefore, for each situation, the vehicle influence-lines included in the time-series regards, in the first part (with a length of 350 vehicle influence-lines), the baseline scenario, and, in the second part, the respective damage scenario (with a length of 150 vehicle influence-lines). The training period comprises the first 100 vehicle influence-lines.

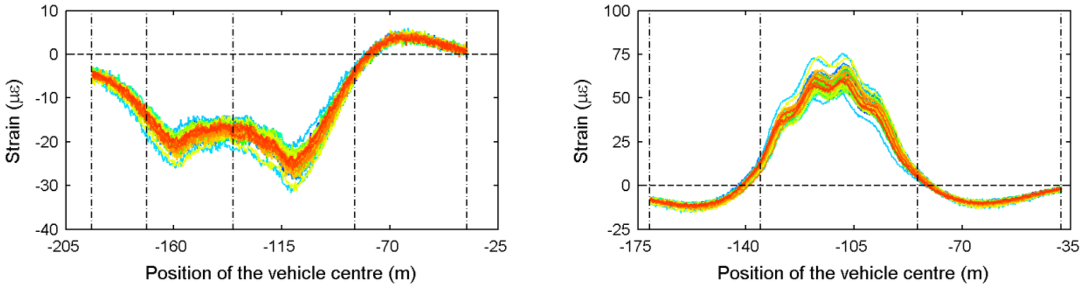

(a) (b)

Figure 8.26 – Numerical estimates for a set of 50 vehicle influence-lines of the flanges strains for selected cross-sections, for time-series TS2. The selected cross-sections are: (a) S11; and (b) S14.

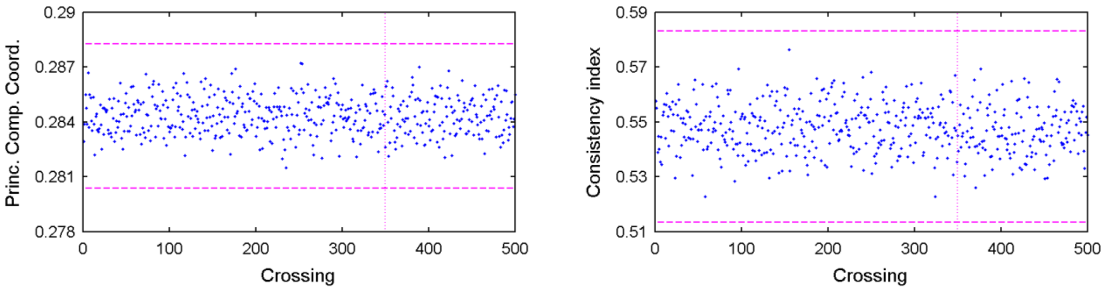

(a) (b)

Figure 8.27 – Evolution of the control values for time-series TS2: (a) MPCA coordinate related with the vehicle influence-lines for the strains estimated at the flange of cross-section S14; and (b) ILAC value for the vehicle influence-lines for the strains estimated at the flange of cross-sections S11 and S14.

As regards TS2, the restraint for the longitudinal displacement of the support bearings over pillar P3 leads to very slight changes in the strains estimated at the instrumented cross-sections included in the monitoring system (see Figure 8.12). Consequently, under in-service traffic, those differences in the vehicle influence-lines are hidden due to the variability of the characteristics of the vehicles, as shown in Figure 8.26. As depicted in Figure 8.27, the threshold bounds defined in the training period are never exceeded. Therefore, on the basis of the monitoring system constituted by the cross-sections selected for this work, the restraint for the longitudinal displacement of the support bearings is not signalized.

However, the changes in the sensors installed in the legs of pillar P3 are significant. Therefore, an additional case (TS2’) considering a monitoring system in which these sensors are included was examined. The numerical estimates for a set of 50 vehicle influence-lines, distributed along the whole time-series, of the strains for the cross-sections installed in the legs of Pillar P3 are depicted in Figure 8.28. In spite of the variability of the vehicle influence-lines, a slight

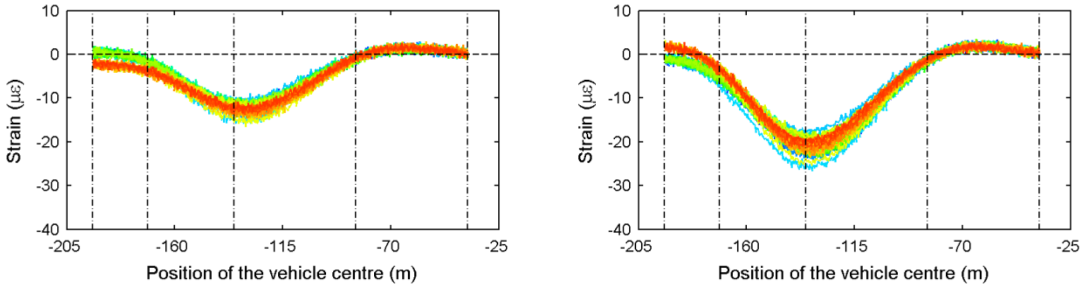

(a) (b)

Figure 8.28 – Numerical estimates for a set of 50 vehicle influence-lines of the flanges strains for selected cross-sections, for time-series TS2’. The selected cross-sections are: (a) S56; and (b) S57.

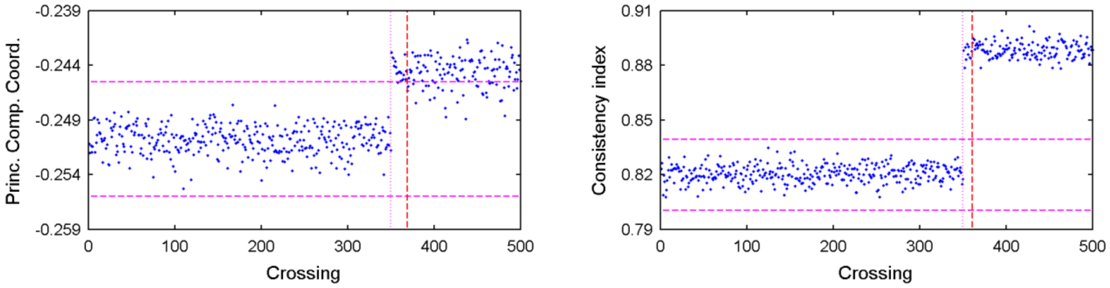

(a) (b)

Figure 8.29 – Evolution of the control values for time-series TS2’: (a) MPCA coordinate related with the vehicle influence-lines for the strains estimated at the flange of cross-section S56; and (b) ILAC value for the vehicle influence-lines for the strains estimated at the flange of cross-sections S11 and S56.

deviation in the pattern as a result of the restraint for the longitudinal movements is noticeable (note that the colour scheme varies between different shades of blue, green and red for, respectively, the first, intermediate and last crossings). Figure 8.29 depicts the evolution of the control values of either MPCA or ILAC for time-series TS2'. As shown, as soon as the structural behaviour is changed (after 350 vehicle influence-lines, signalized in the figures by a dotted pink vertical line) the control values shift. Then, when 10 consecutive points are beyond the threshold bounds damage is flagged (signalized in the figures by a dashed red vertical line). It is noteworthy to mention that, although slight deviations were observed in the pattern of the vehicle influence-lines, the data-processing algorithms used herein enabled to enhance those differences.

Regarding the restraint for the longitudinal displacement of the support bearings over pillar P4, it was shown that this structural modification leads to noticeable changes in the strains estimated at the instrumented cross-sections (see Figure 8.13). However, as depicted in Figure

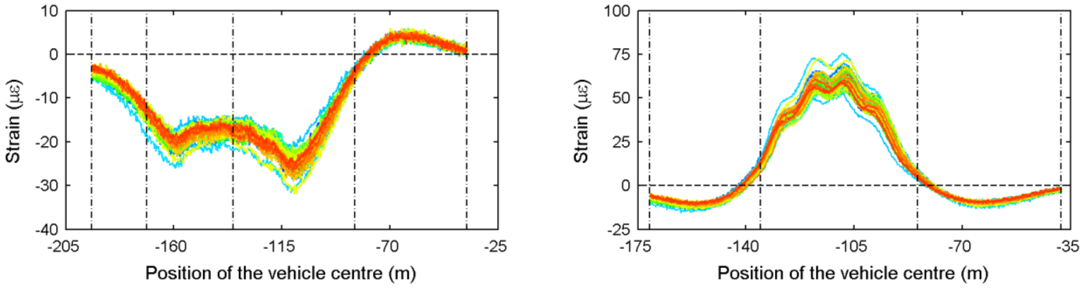

(a) (b)

Figure 8.30 – Numerical estimates for a set of 50 vehicle influence-lines of the flanges strains for selected cross-sections, for time-series TS3. The selected cross-sections are: (a) S11; and (b) S14.

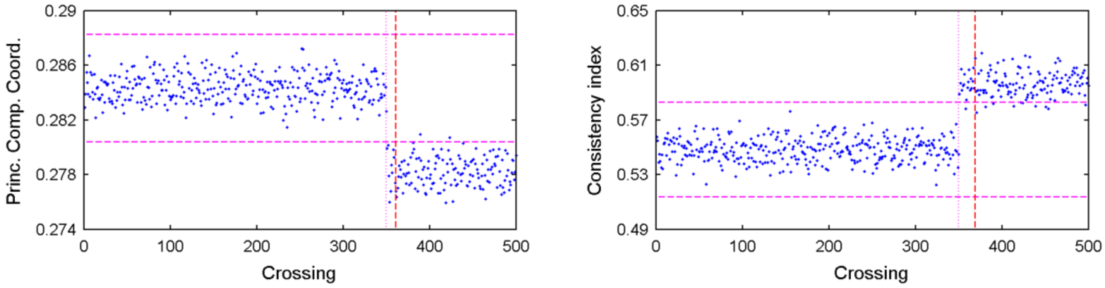

(a) (b)

Figure 8.31 – Evolution of the control values for time-series TS3: (a) MPCA coordinate related with the vehicle influence-lines for the strains estimated at the flange of cross-section S14; and (b) ILAC value for the vehicle influence-lines for the strains estimated at the flange of cross-sections S11 and S14.

8.30, as a result of the variability of the characteristics of the in-service vehicles, these changes become less clear. Even though, slight differences in the pattern of the vehicle influence-lines may be identified, and in the evolution of the control values of either MPCA or ILAC for time-series TS3 (depicted in Figure 8.31) this structural change is clearly highlighted.

The results of the analyses carried out herein are summarized in Table 8.2. Both the performance (denoted either as OK or KO) and the number of vehicle influence-lines required to detect the structural changes, designated as delay, are indicated for each situation. The proposed approach for early damage detection based on vehicle influence-lines shows good results. First, the stability of the approach under normal conditions was shown (TS1). Second, the ability of detecting damage, namely restraints for the longitudinal displacements of the support bearings, as long as that structural change produces noticeable modifications in the structural response, was demonstrated (TS2' and TS3 against TS2). Finally, both data-processing algorithms provide similar results, regarding both the ability for flagging structural changes and the time for detection.

Table 8.2 – Summary of the performance of the data-processing algorithms for early damage detection based on in-service vehicle influence-lines applied to numerically-simulated data.

	MPCA		ILAC	
	Perform	Delay	Ability	Delay
TS1	OK	-	OK	-
TS2	KO	-	KO	-
TS2'	OK	19	OK	11
TS3	OK	11	OK	11

8.6. Application to field data

This section presents the results of the application of the approach for damage detection on field data collected for a 3-months period, comprising about 1500 vehicle influence-lines of the strains for selected cross-sections.

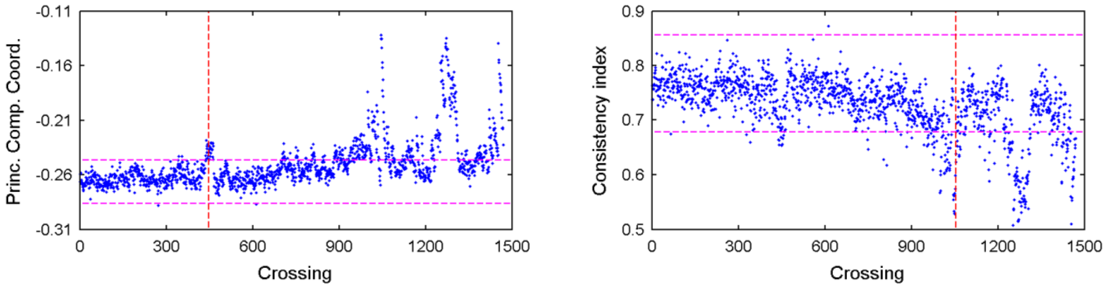

(a) (b)

Figure 8.32 – Evolution of the control values for the time-series regarding the field measurements: (a) MPCA coordinate related with the vehicle influence-lines for the strains estimated at the flange of cross-section S16; and (b) ILAC value for the vehicle influence-lines for the strains estimated at the flange of cross-sections S11 and S16.

As shown in Figure 8.32 the control values of both data-processing algorithms occasionally exceed the threshold bounds (computed for a training period of 100 vehicle influence-lines), which may indicate changes in the structural condition of the Luiz I Bridge. Given this, it should be mentioned that the vehicle influence-lines for cross-sections S14 and S16 exhibit a larger variability, mainly in terms of magnitude, than those for the remaining cross-sections (see Figure 8.16). In this respect, the comparison of the measurements of cross-sections S11 and S16, whose pattern is similar due to their location in the bridge, shows non-negligible differences.

Even though, the structural changes do not seem consistent in that the control values do not remain permanently beyond the thresholds. In this context, the monitoring of the control values of the data-processing algorithms, as well as the shape of the vehicle influence-lines, must be continued in order to assess whether these fluctuations are only circumstantial – as a result of transitional changes in the structural condition, which may require, however, careful attention – or if evolve clearly beyond the threshold bounds indicating, thus, effective anomalies on the structure. In either case the continuous surveillance of the structure is paramount.

8.7. Conclusions

This chapter presents an alternative approach for detecting damage in full-scale bridges making use of vehicle influence-lines captured under in-service traffic conditions. For this purpose, the proposed methodology firstly determines the acquisition of field data for building time-series of the structural response induced by moving-loads, and subsequently the adoption of suitable algorithms for detecting changes in the structural behaviour.

The feasibility and success of this approach was demonstrated having as case study a rehabilitated centenary steel arch double-deck bridge, in which a comprehensive fibre-optic-based monitoring system is deployed to continuously monitor its structural response. For this work only a part of this system was considered, which included the measurement of strains at selected cross-sections of diagonals and at both the top and bottom chords of the upper deck. To supplement these results, the strains of cross-sections instrumented at the legs of a steel truss pillar were also taken into account.

Given the bridge susceptibility for presenting bearings malfunctions, the identification of damage occurrence was targeted for such anomalous operating conditions. In a first stage, field results collected in periodic tests were carefully analysed by means of adequate numerical simulations provided by a suitable finite element model of the bridge. Firstly, it was demonstrated the existence of a partial restraint for the longitudinal displacement of the support bearings installed on the top of a critical steel truss pillar. This anomaly was clearly identified through the strains measured at the cross-sections instrumented at the base of the pillar legs. The results of appropriate numerical simulations have shown that, as a consequence of the large bending flexibility of this pillar, the changes in the strains estimated at the cross-sections instrumented along the upper deck are negligible, regardless the severity of the restraint at the support bearings. Therefore, the strains at the base of the pillar legs may play a major role for detecting restraints for the longitudinal displacements at the supports over this pillar whereas those of the upper deck are useless. Secondly, the numerical simulations have also shown that small magnitude restraints for the longitudinal displacements of the support bearings over a stiffer pillar produce negligible changes in the strains of the cross-sections monitored at the upper deck. However, if the severity of the restraint increases, noticeable changes are detected in these quantities.

In a second stage, numerically-simulated data regarding normal and damaged operating conditions were produced in which the variability of the measured structural response caused by the loads inconstancy of the vehicles, their varying speed, the uncertainty of their position, and the existence of noise in the measurements were taken into account through the adoption of a suitable procedure. The numerically-simulated time-series of vehicle influence-lines, as well as the field measurements continuously collected during the monitoring period, were analysed by the two selected algorithms for early damage detection: the moving principal component analysis (MPCA) and the influence-line assurance criterion (ILAC).

The applicability of these methodologies for damage detection was assessed through the analysis of reference situations, firstly to verify the stability of the approach under undamaged conditions, and then to assess the ability of the methods for early detection of restraints for the longitudinal displacements of the support bearings installed at two different pillars.

Both implemented data-processing algorithms, have shown promising results as regards the application to numerically-simulated data, regarding both the ability for flagging structural changes and the time for detection. In the case where the structure remains in normal operating conditions no indication of damage is given, whereas for the damage scenarios simulated herein the structural alteration is promptly flagged. Still, it is noteworthy to mention that damage is only detected if a suitable definition from the training period of the control parameters thresholds for detecting anomalous behaviour is made, together with the occurrence of noticeable changes in the bridge response for the quantities included in the monitoring system. Therefore, for this case study, it was shown that restraints for the longitudinal displacement at the supports installed over pillar P3 are only flagged if the strains at the pillar legs are included in the monitoring system.

With respect to the application on field data, the obtained results reveal the need of further research on the actual structural behaviour of the bridge under normal operating conditions. The control values occasionally exceeded the threshold bounds, revealing some inconsistency in time, which may point for transitional changes in the structural condition, thus requiring a continuous surveillance in order to identify unsafe trends.

Chapter 9

Conclusions and future developments

9.1. Conclusions

The scope of this thesis was the structural health monitoring (SHM) of bridges, a very comprehensive topic in the structural engineering field. In this context, this research focused on two main subjects within the SHM of bridges. The first was the condition assessment of bridges using both field-data and physics-based behavioural models. The second was the early damage identification using data-driven analysis. In order to complement the typical approaches that have been applied in the last decades, which mainly focused either on the dynamic or on the static behaviour of structures, this thesis focused on the quasi-static component of moving-loads responses in bridges. As clearly shown, this type of data gives, in addition, a valuable insight regarding the structural behaviour.

In this closing chapter, the objectives outlined at the beginning of this thesis are discussed in terms of both the success attained and the manner this research was carried out. Moreover, the main conclusions as well as the main contributions of this research are presented along the text.

General view

Framing the two main topics addressed in this thesis in the SHM of bridges

As referred above, the two subjects addressed in this thesis cannot be dissociated in that they are complementary. In this context, the first objective of this thesis was to frame the two main subjects aforementioned in the comprehensive discipline of SHM of bridges. **Chapter 2** provides a brief insight on the SHM of bridges. First, the SHM as a powerful tool in order to maintain the transport infrastructure, namely bridges, in adequate conditions, as well as the main objectives to be attained with its deployment, were addressed. Thereafter, the main components of typical SHM systems were discussed and the way these topics are integrated is described. In addition, along the separate description of each topic along the subsequent sections the advantages and shortcomings are discussed and thus, the positive outcome of the complementary use of both topics is highlighted. The main advantage of the data-driven methods is the capability of detecting damage through the statistical analysis of the monitoring data, without using physics-based numerical models. The inability of providing information regarding the structural condition is pointed out as the main shortcoming. However, currently, the state-of-the-art of automatic physics-based approaches for damage identification hardly leads to satisfactory results concerning the structural condition. In this context, the complete damage identification process should be carried out through two main steps. Firstly, drawing on the advantages of data-driven approaches, these methods should be used to flag damage. Once the damage is detected, the following steps of the damage identification process should be carried out combining field-data with physics-based analysis. Herein it is important to note that many bridges along their service-life do not suffer any damage and thus, cheap data-driven methods suffice for the surveillance and management of bridges.

Physics-based condition assessment

Within the topic concerning the condition assessment of bridges based on field-testing data and using physics-based behavioural models, the following subjects were addressed.

Field testing to obtain real data concerning the structural response

In **chapter 2** the main field-tests available aiming at the characterization of the structural response were briefly described. While field-tests enable to obtain data concerning the actual behaviour of a structure, physics-based numerical models are used to predict it. However, the actual structural response often deviates from that predicted by these models, especially those created in the design stage. Phenomena unpredicted in the numerical models arise only in the analysis of field-test results. Therefore, field-test data is crucial to assess the conformity of the numerical models. This thesis focused on load tests, especially on the quasi-static component of the response obtained during the crossing of vehicles at crawling speed. It was shown the benefits of using influence-lines for the structural characterization, in that influence- lines are complementary of measuring the deflection of a structure for a given load case. Therefore, the structural response of a given quantity is measured as a point-load moves along the structure instead of measuring the deflection curve of the structure for a given load case. In **chapters 3** and **4** field and experimental data was obtained in order to characterize the behaviour of the structures under analysis, respectively, a centenary steel truss bridge and a reinforced and prestressed concrete laboratorial model. The first comprised the observation of the structure under a locomotive and a pair of trucks. The second included the crossing of a point-load. In a preliminary analysis both structures evidenced some unexpected behaviour showing, thus, the importance of obtaining field-data as a load moves along the bridge. It was observed, in addition, that static load positions would not supply as much information as that provided by influence-lines.

Numerical modelling for the analysis and interpretation of the results

The numerical modelling based on physical behaviour is firstly addressed in **chapter 2**. Therein, the benefits of modelling, a brief description of the procedures, as well as the complexity required for the models are discussed. In this context, two different model complexities were herein addressed. The structure addressed in **chapter 3** was assumed to respond elastic and linearly. Therefore, a complying behavioural model was developed. In contrast, the reduced-scale concrete laboratorial model, in **chapter 4**, required a more complex model as regards the hysteretic structural behaviour of the cracked concrete in service. These models were crucial for analysing and interpreting the field results. In addition, numerical models are crucial for the definition of a monitoring system to be deployed in the structure, namely for choosing the quantities to be measured as well as the locations for the sensors. Furthermore, duly calibrated numerical models are useful to perform predicting analysis regarding future structural behaviour.

Combining field tests with numerical modelling for structural assessment

Field-testing and numerical modelling were addressed separately above and the main advantages and shortcomings were addressed. On one hand, field-testing is fundamental in order to obtain data concerning the actual behaviour of the structure. On the other hand, adequate numerical modelling replicating in-service conditions is useful to assist the interpretation of field results. It is noteworthy to mention, however, that sophisticated physics-based numerical models simulating structural behaviour significantly different from the real one are useless. Conversely, reliable field results that are not thoroughly understood have limited utility. As shown below, the case studies addressed both in **chapters 3** and **4** evidence the need of combining experimental data with numerical models for the assessment of the structural condition. In addition, it should be stressed that only by combining both techniques one can attain the required knowledge about the structure condition in order to move forward in the structural evaluations.

Applications

As stated along the previous paragraphs two case studies were regarded. The first, presented in **chapter 3**, was a centenary steel truss bridge, the Eiffel Bridge, comprising two superimposed decks. This structure was subjected to major rehabilitation works involving the replacement of the top concrete deck, the strengthening of the upper chords of the main truss girders and the replacement of the support bearings. In this context, a load test and an environmental test were carried out aiming at the assessment of the new structural condition and the evaluation of the effectiveness of the elements strengthening. The physics-based numerical model enabled to characterize the most relevant aspects of the structural behaviour and to support the discussion of the field results. Particular aspects concerning the main girders bending, the nature of nodes rotations, and the response under temperature changes were highlighted. The effectiveness of the top chords strengthening was verified through the analysis combining the strain measurements with the numerical results. Finally, the thorough characterization carried out enabled the establishment of a reference condition for future assessments of the structure.

A reinforced and prestressed concrete laboratorial model, as addressed in **chapter 4**, was the second case study. It consists in a reduced-scale structure resembling a typical frame bridge used for both underpasses and overpasses. The primary objective of using this laboratorial model was to obtain experimental data for validating the data-driven damage identification approach proposed in this thesis. In this context, to support the analysis of those results, the behaviour of the structure under moving-loads was carefully analysed. It was observed that although the cracks are closed, the structural behaviour was not linear. First, the experimental influence-lines depend on the direction in which the moving-load crosses the structure. With the aid of finite element analyses, it was shown that the dependency on the movement direction is due to the nonlinear behaviour of cracked concrete, and to the supports deformability. It should be emphasised that in the absence of a physics-based numerical model the usefulness of the experimental data would be very limited as its physical interpretation could hardly be attained. Secondly, it was observed that the response is not proportional to the magnitude of the moving-load, and thirdly, the response to a constant point-load crossing the structure depends on the applied prestressing force.

Data-driven damage identification

As regards the approaches for early damage identification in bridges the following topics were addressed.

Damage identification methods

In **chapter 2** the damage identification approaches were briefly reviewed. In general, the damage detection methods can be divided into two main categories: physics-based and data-driven methods. The main advantages and shortcomings of each approach, both implemented to automatically identify damage, were pointed out.

The first approach adopts a physics-based numerical model of the structure and tries to relate changes in measurements with changes in the properties of the model. Therefore, these methods require the development of a detailed and reliable analytical model of the structure. Afterwards, measurements are compared with estimates provided by the model with the aim of discovering anomalies in the structural behaviour. This analytical model is then updated through complex strategies to follow the evolution of the structure's state. In addition, physics-based models are useful for making behavioural predictions such as the reserve capacity or the ability to carry exceptional loads. However, finding an accurate behavioural model of a structure is difficult due to uncertainties in modelling and measurement, which may prevent an effective damage identification.

In the second approach, using statistical data, damage is detected by a pattern recognition algorithm, which requires, only, a reference condition. This methodology is completely data-driven and the evolution of the data is estimated without information of physical processes. These methods are generally faster than physics-based methods as they do not require the evaluation of computation-intensive numerical models. However, data-driven methods are inappropriate for estimating reserve capacity or for predicting response to functional changes.

Bearing in mind the scope of this thesis, the review of data-driven approaches based on static and quasi-static data was also emphasised in the second chapter. In addition, a set of algorithms that have been shown successful in continuous monitoring were selected and carefully described for latter application along this thesis.

Alternative approach for early damage identification

It was shown above the potentiality of moving-loads responses in order to characterize and to assess the structure condition. In this context, in **chapter 2** an alternative data-driven approach for damage identification using in-service moving-loads data was proposed. The approach consists in building time-series based on the records obtained during the passage of vehicles, and, then, using data-processing algorithms to find changes in the patterns that can signalize modifications in the structural response, and thus, in the structural condition. This approach involves three main steps: (i) data acquisition; (ii) data collection; and (iii) data-processing. The first step consists in, with the aid of an adequate acquisition system, recording the passage of every vehicle that crosses the bridge. The second step involves selecting all the vehicles that match a given vehicle-class in order to build time-series of moving-loads responses regarding a given vehicle-class. This task can be carried out by using, for instance, WIM techniques, as shown in **chapter 7** where influence-lines of in-service metro vehicles were collected by a B-WIM system especially devoted for this purpose. The final step aims at detecting changes in the structural behaviour by applying adequate data-processing algorithms. As in the structural condition assessment, herein only the quasi-static component of the structural response is taken into consideration.

Demonstrating the applicability of the proposed approach using numerically-simulated data

The proposed approach was shown to be able to identify damage at an early stage by using numerically-simulated data resembling the quasi-static response of vehicles crossing a bridge, both in **chapters 5** and **8**. In the former, the numerical model resembled the laboratorial model described in chapter 4, assuming, however, for the sake of simplicity, linear and elastic behaviour. A stiffness reduction replicating a crack was selected as the damage scenario. In the latter, the numerical simulations regarded the Luiz I Bridge, in which two damage scenarios concerning restraints for the longitudinal displacements of the support bearings were analysed. Either in chapter 5 or 8, the results demonstrated the ability of this approach for detecting changes in the structural condition.

Validating the proposed approach using experimental data

The proposed methodology for damage identification using experimental moving-loads responses was validated in **chapter 6**. The reinforced and prestressed concrete laboratorial model analysed in chapter 4 was selected as the case study. The tests were designed with the purpose of replicating as close as possible real case scenarios aiming at the application of these methodologies in full-scale bridges. In this context, two typical damage scenarios were addressed: a prestress loss and a partial restraint of the rotation of a support bearing. The results demonstrated that, in general, using either algorithm, damage may be detected by using this approach.

The results of the application of this data-driven methodology to field-measurements of the Luiz I Bridge, in **chapter 8**, gave the indication of damage. Even though, the structural changes do not seem consistent in that the control values do not remain permanently beyond the thresholds. Therefore, further analysis is required.

Final remarks

The results obtained in **chapter 8** clearly showed that physics-based and data-driven approaches are complementary methods. Firstly, the field measurements collected in periodic tests within the surveillance program of the bridge's structural integrity have indicated restraints for the longitudinal displacements of the support bearings. This hypothesis was then confirmed with the support of a physics-based model of the bridge. This chapter showed, in addition, by using numerically-simulated data, that the data-driven damage detection approach proposed herein is able to identify this structural change. Therefore, instead of performing periodical tests, if the monitoring system installed in the bridge was endowed with this algorithm, this structural change would have been promptly flagged. Then, as it was done in the sequence of the periodical tests, the results would be analysed with the aid of a physics-based model in order to identify the origin of the flagged modification.

9.2. Future developments

The work conducted within this thesis sought to contribute to the structural health monitoring of bridges. Two main subjects were addressed: the structural condition assessment combining field-results with physics-based behavioural models and the damage identification using data-driven methods. Both subjects relied on the quasi-static component of the structural response of moving-loads data. However, the research presented herein is far from being completed and, thus, further developments are needed. In the following paragraphs a few tasks that should be carried out are outlined.

As regards the Eiffel Bridge, building on the structural assessment reported in this thesis a permanent monitoring system with the objective of implementing the damage identification approach presented herein should be deployed. The research presented herein provides valuable information regarding the installation of a permanent monitoring system for the surveillance of the bridge. Although the vertical displacements are one of the most significant quantities to be monitored, as they are difficult to directly measure, alternative parameters must be sought. In general, the rotations are an adequate alternative. However, in this bridge they may be useful only to monitor the performance of the support bearings hinge.

Nonetheless, the prestressing steel bars are paramount for the safety of the structure. Thus, monitoring the strains of the prestressing steel bars, particularly at the end spans where the prestress losses are significant, should be taken into account in a surveillance system. In addition, the strains of the chords, particularly at mid-span, as they give significant information about the load distribution, should be also considered. Finally, as an adequate performance of the bearings is crucial for the bridge safety and durability, the observation of the displacements of the expansion joints cannot be ignored.

In chapter 4, the analysis of the reinforced and prestressed concrete laboratorial model focused on the structural response under moving-loads. However, additional tests, whose results were not presented in this work, were carried out in order to assess the behaviour of the structure. It is noteworthy to mention that although under a moving-load the structure undergoes a reloading/unloading cycle, traditional cyclic loading involves a loading system applied at a given position of the structure in which the cyclic loading is provided by repetitive changes on the magnitude. Conversely, in the case of a moving-load, its magnitude remains constant and, thus, the cyclic loading is provided by changes in the position. Therefore, although both tests induce reloading/unloading cycles, their nature is different. In this context, in addition to the tests carried out using moving-loads, traditional cyclic loading tests were also performed. Preliminary analyses of these results have confirmed the hysteretic behaviour described in this thesis. Moreover, tensioning and de-tensioning operations were observed through the monitoring system installed in the laboratorial model. Preliminary results have shown unexpected behaviour of the monitored quantities. Although the stiffness of the most quantities increase with the increase of the prestressing force, that of the vertical displacement at mid-span, decreases. In this context, with the objective of giving a deeper insight on the behaviour of a cracked concrete structure, the results of both tests should be further analysed and the conclusions publicized.

The analysis of the hysteretic behaviour was based on a simplified analysis which considered that bending gives rise to axial forces in a top and a bottom chord, each of which being composed by the longitudinal steel reinforcement and the surrounding concrete. In the future a more detailed analysis should be carried out, taking into account: the cyclic variation of bond stresses, τ, and corresponding slip values, s, at the interface between the longitudinal reinforcement and the surrounding concrete; and the cyclic relationship between the crack opening, w, and the concrete stress, σ_c, normal to the crack.

Furthermore, as clearly expressed above, one of the main objectives of the work presented in chapter 4 was the analysis of the in-service behaviour of concrete bridges. However, this thesis focused only on a reduced-scale laboratorial model. Therefore, a full-scale concrete bridge, that might be already cracked, as the laboratorial model was, should be selected in order to validate the conclusions drawn with the laboratorial tests.

Regarding the data-driven approach proposed herein for damage identification based on the quasi-static component of moving-loads responses, further research as regards numerically-simulated data should be carried out. First, different structural systems as well as distinct damage scenarios should be evaluated. Second, further data-processing algorithms should be tested and the performance compared with that of the algorithms applied within this thesis. Finally, a sensitivity analysis concerning different noise levels in the measurements as well as uncertainty in both the load position and the vehicles parameters must be carried out.

This data-driven methodology was implemented in a laboratorial model in order to evaluate its performance when applied to experimental data. Herein, two damage scenarios were tested: a prestress loss and a restraint for the longitudinal rotation of a support bearing. With the purpose of evaluating the ability to detect damage at its onset, different levels of severity should be analyzed, thereby enabling to define thresholds for the ability of detecting damage. Moreover, taking advantage of the versatility of the laboratorial model, different structural systems should be evaluated. Finally, within these tests, a higher number of crossings as well as wider variability of the load levels should be considered in order to better resemble real cases.

Within the context of the traffic characterization of the upper deck of the Luiz I Bridge, two primary developments should be carried out. The first is to implement an automatic data-processing in real-time preventing, thus, the storage of huge amounts of data. Secondly, as the traffic characterization presented in this thesis focused on 1-vehicle compositions only, the procedure described herein should be extended to 2-vehicles compositions.

In chapter 8, the results of the application of this data-driven methodology to field results gave the indication of damage. Even though, the structural changes do not seem consistent in that the control values do not remain permanently beyond the thresholds. In this context, the monitoring of the control values of the data-processing algorithms, as well as the shape of the vehicle influence-lines, must be continued in order to assess whether these fluctuations are only circumstantial – as a result of transitional changes in the structural condition, which may require, however, careful attention – or if they evolve clearly beyond the threshold bounds indicating, thus, effective anomalies on the structure. In either case, as the continuous surveillance of the structure is paramount, this approach should be implemented in the bridge.

References

A2P (2007). *Eiffel Bridge in Viana do Castelo - Descriptive document of the implementation project of the infrastructures strengthening and rehabilitation*.

AASHTO LRFD (2010). *AASHTO LRFD Bridge Design Specifications*Washington, DC, USA: American Association of State Highway and Transportation Officials (AASHTO).

Abdel Wahab, M. M. and De Roeck, G. (1999). *Damage detection in bridges using modal curvatures: application to a real damage scenario*. Journal of Sound and Vibration **226**(2): pp. 217-235.

Aktan, A., Catbas, F., Grimmelsman, K. and Tsikos, C. (2000). *Issues in infrastructure health monitoring for management*. Journal of Engineering Mechanics **126**(7): pp. 711-724.

Aktan, A. E., Catbas, F. N., Grimmelsman, K. A. and Pervizpour, M. (2002). *Development of a model health monitoring guide for major bridges*: Federal Highway Administration - Research and Development.

Aktan, A. E., Farhey, D. N., Brown, D. L., Dalal, V., Helmicki, A. J., Hunt, V. J. and Shelley, S. J. (1996). *Condition assessment for bridge management*. Journal of Infrastructure Systems **2**(3): pp. 108-117.

Aktan, E., Çatbaş, N., Türer, A. and Zhang, Z. (1998). *Structural Identification: Analytical Aspects*. Journal of Structural Engineering **124**(7): pp. 817-829.

Al-Ostaz, A., Cheng, A., Mullen, C. and Song, C. (2009). *Aging infrastructure: Evaluation, repair, improvement and protection*. In: Proceedings of the Stabilization of Buildings Workshop. US Army Corps of Engineers, Engineering Research and Development Center (ERDC), Vicksburg, Mississippi, USA.

Allemang, R. (2003). *The modal assurance criterion – Twenty years of use and abuse*. Sound and Vibration (August 2003): pp. 14-21.

Allen, B. J. and Rens, K. L. (2004). *Condition assessment of the Eastbound 6th Avenue Viaduct using strain gauges*. Journal of Performance of Constructed Facilities **18**(4): pp. 205-212.

Almeida, L. C. d. (2006). *Identificação de parâmetros estruturais com emprego de análise inversa [Identification of structural parameters using inverse analysis]* (in Portuguese). PhD thesis, School of Civil Engineering, Architecture and Urban Design, University of Campinas, Campinas, São Paulo, Brazil.

Andreaus, U. and Baragatti, P. (2012). *Experimental damage detection of cracked beams by using nonlinear characteristics of forced response*. Mechanical Systems and Signal Processing **31**: pp. 382-404.

Appleton, J., Saraiva, J., Moura, R. and Rodrigues, F. (2009). *The use of stainless steel in the rehabilitation of the Eiffel Bridge infrastructures, over Lima river, in Viana do Castelo - Inspection and rehabilitation (in portuguese)*. In: Proceedings of the ASCP'09 - 1.º Congresso de Segurança e Conservação de Pontes ASCP. Lisboa, Portugal.

ASCE (2011). *Structural Identification (St-Id) of Constructed Facilities - Approaches, Methods and Technologies for Effective Practice of St-Id*Reston, VA, USA: Comittee on Structural Identification of Constructed Systems - American Society of Civil Engineers (ASCE) - Structural Engineering Institute (SEI).

Azizinamini, A. (2002). *Full scale testing of old steel truss bridge*. Journal of Constructional Steel Research **58**(5-8): pp. 843-858.

Balassone, F. (2010). *Rocker bearing issues*. In: Proceedings of the Northeast Bridge Preservation Conference. Hartford, CT, USA.

Balázs, G. L. (1998). *Bond under repeated loading*. ACI Special Publication **SP180**(06): pp. 125-144.

Bandara, R. P., Chan, T. H. T. and Thambiratnam, D. P. (2014). *Frequency response function based damage identification using principal component analysis and pattern recognition technique*. Engineering Structures **66**: pp. 116-128.

Bathe, K. J. (1995). *Finite Element Method*. Springer

Bažant, Z., Yu, Q. and Li, G.-H. (2012). *Excessive long-yime deflections of prestressed box girders. I: Record-span bridge in Palau and other paradigms*. Journal of Structural Engineering **138**(6): pp. 676-686.

Bell, B. (2004). *European Railway Bridge Demography*Technical Report.

Bergmeister, K. and Santa, U. (2001). *Global monitoring concepts for bridges*. Structural Concrete **2**(1): pp. 29-39.

Biezma, M. V. and Schanack, F. (2007). *Collapse of Steel Bridges*. Journal of Performance of Constructed Facilities **21**(5): pp. 398-405.

Bisby, L. A. (2004). *An Introduction to Structural Health Monitoring.*: ISIS Canada.

Boothby, T. E. and Craig, R. J. (1997). *Experimental load rating study of a historic truss bridge*. Journal of Bridge Engineering **2**(1): pp. 18-26.

Brownjohn, J. M. W. (2007). *Structural health monitoring of civil infrastructure*. Philosophical Transactions of the Royal Society A **365**(1851): pp. 589-622.

Brownjohn, J. M. W., Moyo, P., Omenzetter, P. and Chakraborty, S. (2005). *Lessons from monitoring the performance of highway bridges*. Structural Control and Health Monitoring **12**(3-4): pp. 227-244.

Brownjohn, J. M. W., Moyo, P., Omenzetter, P. and Lu, Y. (2003). *Assessment of highway bridge upgrading by dynamic testing and finite-element model updating*. Journal of Bridge Engineering **8**(3): pp. 162-172.

BS - British Standards Institute (1983). *BS 5400-9.1:1983 - Steel, concrete and composite bridges - Bridge bearings* British Standards Institute.

Burdet, O. and Zanella, J.-L. (2000). *Automatic monitoring of bridges using electronic inclinometers*. In: Proceedings of the Structural Engineering for Meeting Urban Transportation Challenges - 16th Congress Report of IABSE. Lucerne, Switzerland.

Cantero, D. and González, A. (2014). *Bridge damage detection using weigh-in-motion technology*. Journal of Bridge Engineering: pp. 0401407801-0401407810.

Cantero, D., Karoumi, R. and González, A. (2015). *The virtual axle concept for detection of localised damage using bridge weigh-in-motion data*. Engineering Structures **89**(0): pp. 26-36.

Carden, E. P. and Fanning, P. (2004). *Vibration based condition monitoring: A review*. Structural Health Monitoring **3**(4): pp. 355-377.

Cardini, A. J. and DeWolf, J. T. (2009). *Long-term structural health monitoring of a multi-girder steel composite bridge using strain data*. Structural Health Monitoring **8**(1): pp. 47-58.

Casas, J. R. (2007). *Updated inventory on condition assessment procedures for bridges*.

Castro-Triguero, R., Murugan, S., Gallego, R. and Friswell, M. I. (2013). *Robustness of optimal sensor placement under parametric uncertainty*. Mechanical Systems and Signal Processing **41**(1–2): pp. 268-287.

Catbas, F. N., Ciloglu, K., Celebioglu, A., Popovics, J. S. and Aktan, A. E. (2001). *Fleet health monitoring of large populations: Aged concrete T-beam bridges in Pennsylvania*. In: Proceedings of the 6th Annual International Symposium on NDE for Health Monitoring and Diagnostics. S. B. Chase and A. E. Aktan (Eds.), SPIE. Newport Beach, CA, USA. Vol. 4337.

Catbas, F. N., Ciloglu, S. K., Hasancebi, O., Grimmelsman, K. and Aktan, A. E. (2007). *Limitations in structural identification of large constructed structures*. Journal of Structural Engineering **133**(8): pp. 1051-1066.

Catbas, F. N., Gul, M. and Burkett, J. L. (2008). *Conceptual damage-sensitive features for structural health monitoring: Laboratory and field demonstrations*. Mechanical Systems and Signal Processing **22**(7): pp. 1650-1669.

Cavadas, F. (2008). *Analysis and monitoring of old steel bridges behaviour - Eiffel Bridge (in portuguese)*. Master in Civil Engineering Dissertation, Faculdade de Engenharia, Universidade do Porto, Porto.

Cavadas, F., Costa, B. and Figueiras, J. (2013a). *Observação do comportamento em serviço da Ponte Luiz I - Deformações registadas durante a passagem do Metro Ligeiro do Porto [Monitoring of the in-service behaviour of the Luiz I Bridge - Strains collected during the crossing of the light metro of Porto]*Porto, Portugal: Laboratory for the Concrete

Technology and Strucutral Behaviour (LABEST) - Faculty of Engineering of the University of Porto (FEUP).

Cavadas, F. and Figueiras, J. (2014). *Detecção de dano em pontes de betão armado e pré-esforçado baseada na resposta experimental de cargas móveis [Damage detection in prestressed and reinforced concrete bridges based on experimental moving-load responses]*. In: Proceedings of the 56.º Brazilian Concrete Congress (CBC'2014). On Conference CD. A. E. Jacinto, Â. B. Masuero, L. P. V. Junior and M. P. Barbosa (Eds.), Brazilian Concrete Institute - IBRACON. Natal, Rio Grande do Norte, Brazil.

Cavadas, F., Rodrigues, C., Félix, C. and Figueiras, J. (2008). *Final load test of the Eiffel Bridge (in portuguese)*Porto: Technical Report, LABEST-FEUP.

Cavadas, F., Smith, I. F. C. and Figueiras, J. (2013b). *Damage detection using data-driven methods applied to moving-load responses*. Mechanical Systems and Signal Processing **39**(1–2): pp. 409-425.

CEN (2004). *EN1992-1-1 - European Standard Eurocode 2: Design of concrete structures - Part 1-1: General rules and rules for buildings*. Brussels: European Committee for Standardization.

Chajes, M. J., Mertz, D. R. and Commander, B. (1997). *Experimental load rating of a posted bridge*. Journal of Bridge Engineering **2**(1): pp. 1-10.

Chakraborty, S. and DeWolf, J. T. (2006). *Development and implementation of a continuous strain monitoring system on a multi-girder composite steel bridge*. Journal of Bridge Engineering **11**(6): pp. 753-762.

Chang, P. C., Flatau, A. and Liu, S. C. (2003). *Review paper: Health monitoring of civil infrastructure*. Structural Health Monitoring **2**(3): pp. 257-267.

Chang, P. C. and Liu, S. C. (2003). *Recent research in nondestructive evaluation of civil infrastructures*. Journal of Materials in Civil Engineering **15**(3): pp. 298-304.

Chase, S. B. (2001). *Smarter bridges, why and how?* Smart Materials Bulletin **2001**(10): pp. 9-13.

Chatterjee, A. (2000). *An introduction to the proper orthogonal decomposition*. Current Science **78**(7): pp. 808-817.

Chavel, B. W. and Yadlosky, J. M. (2011). *Framework for improving resilience of bridge design*Washington, D.C., USA: Federal Highway Administration (FHWA).

Choi, I.-Y., Lee, J. S., Choi, E. and Cho, H.-N. (2004). *Development of elastic damage load theorem for damage detection in a statically determinate beam*. Computers & Structures **82**(29-30): pp. 2483-2492.

Chong, C.-Y. and Kumar, S. P. (2003). *Sensor networks: evolution, opportunities, and challenges*. Proceedings of the IEEE **91**(8): pp. 1247-1256.

Chung, W., Kim, S., Kim, N.-S. and Lee, H.-u. (2008). *Deflection estimation of a full scale prestressed concrete girder using long-gauge fiber optic sensors*. Construction and Building Materials **22**(3): pp. 394-401.

Collins, M. P. and Mitchell, D. (1987). *Prestressed concrete basics*. Ottawa: CPCI, ISBN: 0-9691816-6-3.

Costa, B. J. A. (2012). *Structural identification of old steel bridges - Monitoring and rehabilitation assessment*. PhD thesis, Faculty of Engineering, University of Porto, Porto.

Costa, B. J. A. and Figueiras, J. A. (2012). *Fiber optic based monitoring system applied to a centenary metallic arch bridge: Design and installation*. Engineering Structures **44**(0): pp. 271-280.

Davis, S. L., Goldberg, D., DeGood, K., Donohue, N. and Corless, J. (2013). *The fix we're in for: The state of our nation's bridges*Washington, D.C., USA.

Del Grosso, A., Lanata, F., Inaudi, D. and Posenato, D. (2006). *Data management and damage identification for continuous static monitoring of structures*. In: Proceedings of the 4th World Conference on Structural Control and Monitoring (4WCSCM). San Diego, CA, USA.

DelGrego, M. R., Culmo, M. P. and DeWolf, J. T. (2008). *Performance Evaluation through Field Testing of Century-Old Railroad Truss Bridge*. Journal of Bridge Engineering **13**(2): pp. 132-138.

DeWolf, J. T., Lauzon, R. G. and Culmo, M. P. (2002). *Monitoring bridge performance*. Structural Health Monitoring **1**(2): pp. 129-138.

Ding, Y. and Li, A. (2011). *Assessment of bridge expansion joints using long-term displacement measurement under changing environmental conditions*. Frontiers of Architecture and Civil Engineering in China **5**(3): pp. 374-380.

Doebling, S. W., Farrar, C. R., Prime, M. B. and Shevitz, D. W. (1996). *Damage Identification and Health Monitoring of Structural and Mechanical Systems from Changes in Their Vibration Characteristics: A Literature Review*Los Alamos, NM, USA: Los Alamos National Laboratory.

Dolce, M., Cardone, D. and Croatto, F. (2005). *Frictional Behavior of Steel-PTFE Interfaces for Seismic Isolation*. Bulletin of Earthquake Engineering **3**(1): pp. 75-99.

Dong, Y., Song, R. and Liu, H. H. (2010). *Bridges structural health monitoring and deterioration detection - Synthesis of knowledge and technology*Fairbanks, AK, USA: Alaska University Transportation Center (AUTC).

Ermopoulos, J. and Spyrakos, C. C. (2006). *Validated analysis and strengthening of a 19th century railway bridge*. Engineering Structures **28**(5): pp. 783-792.

Faber, M. H., Val, D. V. and Stewart, M. G. (2000). *Proof load testing for bridge assessment and upgrading*. Engineering Structures **22**(12): pp. 1677-1689.

Farhey, D. N. (2005). *Bridge instrumentation and monitoring for structural diagnostics*. Structural Health Monitoring **4**(4): pp. 301-318.

Farhey, D. N., Naghavi, R., Levi, A., Thakur, A. M., Pickett, M. A., Nims, D. K. and Aktan, A. E. (2000). *Deterioration assessment and rehabilitation design of existing steel bridge*. Journal of Bridge Engineering **5**(1): pp. 39-48.

Farra, B. (1995). *Influence de la résistance du béton et de son adhérence avec lármature sur la fissuration [Concrete strength and reinforcement bonding influence on cracking]* (in French). PhD thesis, Civil Engineering Department, Swiss Federal Institute of Technology (EPFL), Lausanne, Switzerland.

Farrar, C. R. and Doebling, S. W. (1999). *Structural Health Monitoring at Los Alamos National Laboratory*. In: Proceedings of the Institute of Electrical Engineers Colloquium on Condition Monitoring: Machinery, External Structures and Health. Birmingham, UK.

Farrar, C. R. and Lieven, N. A. J. (2007). *Damage prognosis: the future of structural health monitoring*. Philosophical Transactions of the Royal Society A **365**(1851): pp. 623-632.

Farrar, C. R., Park, G., Allen, D. W. and Todd, M. D. (2006). *Sensor network paradigms for structural health monitoring*. Structural Control and Health Monitoring **13**(1): pp. 210-225.

Farrar, C. R. and Worden, K. (2007). *An introduction to structural health monitoring*. Philosophical Transactions of the Royal Society A **365**: pp. 303-315.

Fasheyi, A. (2012). *Bridge bearings - Merits, demerits, practical issues, maintenance and extensive surveys on bridge bearings*. MSc thesis, Department of Civil and Architectural Engineering, Royal Institute of Technology, Stockolm, Sweden.

Félix, C. (2004). *Monitorização e análise do comportamento de obras de arte [Monitoring and analysis of the structural behaviour of bridges]* (in Portuguese). PhD thesis, Faculty of Engineering, University of Porto, Porto, Portugal.

Feng, J. and Chen, H. (2000). *Bearings*. In: Bridge Engineering Handbook. W.-F. Chen and L. Duan (Eds.), Washington, D.C., USA: CRC Press, ISBN: 0-8493-7434-0.

FHWA (2009). *National Bridge Inspection Standards*Washington, DC, USA: Federal Highway Administration (FHWA) - Department of Transportation (DOT).

fib (2010). *Model Code 2010 (Final complete draft)*Lausanne, Switzerland: International Federation for Structural Concrete (fib).

Figueiras, J., Félix, C. and Costa, B. A. (2005). *Testing and monitoring of a centenary arch bridge*. Structure & Infrastructure Engineering **1**(1): pp. 63-73.

Figueiredo, E., Park, G., Figueiras, J., Farrar, C. and Worden, K. (2009). *Structural Health Monitoring Algorithm Comparisons Using Standard Data Sets*: Los Alamos National Laboratory.

FIP (2007). *Rubber bearing device - Viana do Castelo bridge rehabilitation*: FIP Industriale.

Frangopol, D. M., Ghosn, M., Hearn, G. and Nowak, A. S. (1998). *Guest Editorial: Structural Reliability in Bridge Engineering*. Journal of Bridge Engineering **3**(4): pp. 151-154.

Fraser, M., Elgamal, A., He, X. and Conte, J. (2010). *Sensor network for structural health monitoring of a highway bridge*. Journal of Computing in Civil Engineering **24**(1): pp. 11-24.

Friswell, M. I. (2007). *Damage identification using inverse methods*. Philosophical Transactions of the Royal Society A **365**(1851): pp. 393-410.

Ghali, A., Neville, A. M. and Brown, T. G. (2009). *Structural Analysis - A Unified Classical and Matrix Approach*. 6th ed. New York, NY, USA: Taylor & Francis

Glaser, S. D. and Tolman, A. (2008). *Sense of sensing: From data to informed decisions for the built environment*. Journal of Infrastructure Systems **14**(1): pp. 4-14.

González, A. and OBrien, E. J. (2008). *Calculation of the influence line of a bridge using a moving vehicle*. In: Proceedings of the IABMAS'08 - 4th International Conference on Bridge Maintenance, Safety and Management, pp. 3191-3198. H.-M. Koh and D. M. Frangopol (Eds.), Seoul, Korea.

González Silva, I. J. and Karoumi, R. (2015). *Traffic monitoring using a structural health monitoring system*. Proceedings of the ICE - Bridge Engineering **168**: pp. 13-23.

Goulet, J.-A., Kripakaran, P. and Smith, I. F. C. (2010). *Multimodel structural performance monitoring*. Journal of Structural Engineering **136**(10): pp. 1309-1318.

Hao, S. (2010). *I-35W Bridge collapse*. Journal of Bridge Engineering **15**(5): pp. 608-614.

Helmerich, R. (2007). *Guideline for inspection and condition assessment of existing european railway bridges*.

Hirachan, J. and Chajes, M. (2005). *Experimental influence lines for bridge evaluation*. Bridge Structures **1**(4): pp. 405-412.

Hjelmstad, K. D. and Shin, S. (1997). *Damage detection and assessment of structures from static response*. Journal of Engineering Mechanics **123**(6): pp. 568-576.

Hordijk, D. A. (1991). *Local approach to fatigue of concrete*. PhD thesis, Delft University of Technology, Delft, The Netherlands.

Hou, X., Yang, X. and Huang, Q. (2005). *Using Inclinometers to Measure Bridge Deflection*. Journal of Bridge Engineering **10**(5): pp. 564-569.

Housner, G. W., Bergman, L. A., Caughey, T. K., Chassiakos, A. G., Claus, R. O., Masri, S. F., Skelton, R. E., Soong, T. T., Spencer, B. F. and Yao, J. T. P. (1997). *Structural control: Past, present, and future*. Journal of Engineering Mechanics **123**(9): pp. 897-971.

Huber, P. J. (1981). *Robust Statistics*. New York, NY, USA: John Wiley & Sons, Inc., ISBN: 0-471-41805-6.

Hubert, M., Rousseeuw, P. J. and Vanden Branden, K. (2005). *ROBPCA: a new approach to robust principal component analysis*. Technometrics **47**(1): pp. 64-79.

Huth, O., Feltrin, G., Maeck, J., Kilic, N. and Motavalli, M. (2005). *Damage Identification Using Modal Data: Experiences on a Prestressed Concrete Bridge*. Journal of Structural Engineering **131**(12): pp. 1898-1910.

Jacob, B. and Feypell de La Beaumelle, V. (2010). *Improving truck safety: Potential of weigh-in-motion technology*. IATSS Research **34**(1): pp. 9-15.

Jacob, B. and Loo, H. v. (2008). *Weigh-in-motion for enforcement in Europe*. In: Proceedings of the 5th International Conference on Weigh-in-Motion (ICWIM 5) - incorporated in the International Conference on Heavy Vehicles (HVParis 2008) which integrated also the 10th International Symposium on Heavy Vehicle Transport Technology (HVTT 10), pp. 25-38. B. Jacob, E. O'Brien, A. O'Connor and M. Bouteldja (Eds.), Paris, France.

Jacob, B. and O'Brien, E. J. (2005). *Weigh-in-motion: Recent developments in Europe*. In: Proceedings of the 4th International Conference on Weigh-in-Motion (ICWIM 4). Taipei, Taiwan.

Jenkins, C. H., Kjerengtroen, L. and Oestensen, H. (1997). *Sensitivity of parameter changes in structural damage detection*. Shock and Vibration **4**(1): pp.

Jolliffe, I. T. (2002). *Principal component analysis*. 2nd ed. Springer series in statistics, New York, USA: Springer-Verlag New York, Inc., ISBN: 0-387-95442-2.

Karoumi, R., Liljencrantz, A. and Carlsson, F. (2007). *Assessment of actual traffic loads using B-WIM, site specific characteristic load from collected data & statistical evaluation of dynamic amplification factors (Background document D4.3.2)*.

Kaschner, R., Cremona, C. and Cullington, D. (1999). *Review of current procedures for assessing load carrying capacity*.

Kerschen, G., Golinval, J.-C., Vakakis, A. F. and Bergman, L. A. (2005). *The method of proper orthogonal decomposition for dynamical characterization and order reduction of mechanical systems: an overview*. Nonlinear Dynamics **41**(1): pp. 147-169.

Kim, J.-T., Ryu, Y.-S., Cho, H.-M. and Stubbs, N. (2003). *Damage identification in beam-type structures: frequency-based method vs mode-shape-based method*. Engineering Structures **25**(1): pp. 57-67.

Kim, S. and Frangopol, D. M. (2010). *Optimal planning of structural performance monitoring based on reliability importance assessment*. Probabilistic Engineering Mechanics **25**(1): pp. 86-98.

Ko, J. M. and Ni, Y. Q. (2005). *Technology developments in structural health monitoring of large-scale bridges*. Engineering Structures **27**(12): pp. 1715-1725.

Kong, D., Chang, J., Gong, P., Liu, Y., Sun, B., Liu, X., Wang, P., Wang, Z., Wang, W. and Zhang, Y. (2012). *Analysis and improvement of SNR in FBG sensing system*. Photonic Sensors **2**(2): pp. 148-157.

Kripakaran, P. and Smith, I. F. C. (2009). *Configuring and enhancing measurement systems for damage identification*. Advanced Engineering Informatics **23**(4): pp. 424-432.

Kylén, J. (2010). *2D-model of a portal frame railway bridge for dynamic analysis*. MSc thesis, Department of Civil and Architectural Engineering, Royal Institute of Technology, Stockolm, Sweden.

Lan, C., Zhou, Z. and Ou, J. (2012). *Full-Scale prestress loss monitoring of damaged RC structures using distributed optical fiber sensing technology*. Sensors (Basel, Switzerland) **12**(5): pp. 5380-5394.

Lanata, F. and Del Grosso, A. (2006). *Damage detection and localization for continuous static monitoring of structures using a proper orthogonal decomposition of signals*. Smart Materials and Structures **15**(6): pp. 1811.

Laory, I., Trinh, T., Posenato, D. and Smith, I. (2013). *Combined model-free data-interpretation methodologies for damage detection during continuous monitoring of structures*. Journal of Computing in Civil Engineering **27**(6): pp. 657-666.

Laory, I., Trinh, T. N. and Smith, I. F. C. (2011). *Evaluating two model-free data interpretation methods for measurements that are influenced by temperature*. Advanced Engineering Informatics **25**(3): pp. 495-506.

Laurencet, P., Jaccoud, J. P. and Favre, R. (1999). *Fissuration des structures en béton précontraint: Modélisation, validation et interprétation [Cracking of prestressed concrete structures: Modelisation, validation and interpretation]*. Materials and Structures **32**(5): pp. 360-369.

Lee, S.-K. (2012). *Currrent state of bridge deterioration in the US - Part 1*. Materials Performance **51**(1): pp. 62-67.

Liang, Y. C., Lee, H. P., Lim, S. P., Lin, W. Z., Lee, K. H. and Wu, C. G. (2002). *Proper Orthogonal Decomposition and its applications - Part I: Theory*. Journal of Sound and Vibration **252**(3): pp. 527-544.

Liljencrantz, A. (2007). *Monitoring railway traffic loads using Bridge Weigh-in-Motion*. Licenciate Thesis, Department of Civil and Architectural Engineering - Structural Design and Bridge Division, Royal Institute of Technology, Stockholm, Sweden.

Liljencrantz, A. and Karoumi, R. (2009). *Twim: A MATLAB toolbox for real-time evaluation and monitoring of traffic loads on railway bridges*. Structure and Infrastructure Engineering **5**(5): pp. 407-417.

Liljencrantz, A., Karoumi, R. and Olofsson, P. (2007). *Implementing bridge weigh-in-motion for railway traffic*. Computers & Structures **85**(1–2): pp. 80-88.

LisConcebe (2007). *Enlargement and rehabilitation of the road deck of Eiffel Bridge, over Lima river, in Viana do Castelo – Descriptive document of the implementation project (in portuguese)*.

Liu, C., DeWolf, J. T. and Kim, J.-H. (2009). *Development of a baseline for structural health monitoring for a curved post-tensioned concrete box–girder bridge*. Engineering Structures **31**(12): pp. 3107-3115.

Lounis, Z. (2007). *Aging highway bridges*. Canadian Consulting Engineer **48**: pp. 30-34.

Magalhães, F., Cunha, A. and Caetano, E. (2012). *Vibration based structural health monitoring of an arch bridge: From automated OMA to damage detection*. Mechanical Systems and Signal Processing **28**: pp. 212-228.

MAINLINE (2013). *Assessment methods for elderly rail infrastructure (Deliverable 1.2)*.

Masri, S. F., Sheng, L.-H., Caffrey, J. P., Nigbor, R. L., Wahbeh, M. and Abdel-Ghaffar, A. M. (2004). *Application of a web-enabled real-time structural health monitoring system for civil infrastructure systems*. Smart Materials and Structures **13**(6): pp. 1269-1283.

MatLab (2012). *MATLAB R2012.a Statistics Toolbox: Robust Regression*

Measures, R. M. (2001). *Structural Monitoring with Fiber Optic Technology*. London: Academic Press

Menn, C. (1990). *Prestressed concrete bridges*. Basel; Boston; Berlin: Birkhauser Verlag, ISBN: 3-7643-2414-7(CH); 0-8176-2414-7(US).

Meo, M. and Zumpano, G. (2005). *On the optimal sensor placement techniques for a bridge structure*. Engineering Structures **27**(10): pp. 1488-1497.

Montgomery, D. C. and Runger, G. C. (1999). *Applied Statistics and Probability for Engineers*. New York: John Wiley, ISBN: 0-471-17027-5.

Montgomery, D. C. and Runger, G. C. (2003). *Applied Statistics and Probability for Engineers*. 3rd ed. New York, NY, USA: John Wiley & Sons, Inc, ISBN: 0-471-20454-4.

Moore, M., Phares, B., Graybeal, B., Rolander, D. and Washer, G. (2001). *Reliability of visual inspection for highway bridges. Volume I: Final Report*: Federal Highway Administration - U.S. Department of Transportation.

Moses, F. (1979). *Weigh-in-motion system using instrumented bridges*. Transportation Engineering Journal **105**(3): pp. 233-249.

Moyo, P. and Brownjohn, J. M. W. (2002). *Detection of anomalous structural behaviour using wavelet analysis*. Mechanical Systems and Signal Processing **16**(2-3): pp. 429-445.

Moyo, P., Brownjohn, J. M. W., Suresh, R. and Tjin, S. C. (2005). *Development of fiber Bragg grating sensors for monitoring civil infrastructure*. Engineering Structures **27**(12): pp. 1828-1834.

Mufti, A. (2001). *Guidelines for Structural Health Monitoring - Design Manual N.º 2*: ISIS Canada.

Mufti, A. A. (2002). *Structural health monitoring of innovative Canadian civil engineering structures*. Structural Health Monitoring **1**(1): pp. 89-103.

Neild, S. A., Williams, M. S. and McFadden, P. D. (2002). *Non-linear behaviour of reinforced concrete beams under low-amplitude cyclic and vibration loads*. Engineering Structures **24**(6): pp. 707-718.

Neves, L. C. and Frangopol, D. M. (2005). *Condition, safety and cost profiles for deteriorating structures with emphasis on bridges*. Reliability Engineering & System Safety **89**(2): pp. 185-198.

Ni, Y. Q., Hua, X. G., Wong, K. Y. and Ko, J. M. (2007). *Assessment of bridge expansion joints using long-term displacement and temperature measurement*. Journal of Performance of Constructed Facilities **21**(2): pp. 143-151.

NYSDOT (2005). *Structural forensic investigation report: Partial failure of Ramp AC Dunn Memorial Bridge Interchange (BIN 109299A)*Albany, NY, USA: New York State Department of Transportation (NYSDOT).

O'Brien, E., Žnidarič, A. and Ojio, T. (2008). *Bridge weigh-in-motion: Latest developments and applications world wide*. In: Proceedings of the International Conference on Heavy Vehicles (ICWIM'5), pp. 39-56. B. Jacob, E. O'Brien, A. O'Connor and M. Bouteldja (Eds.), Paris, France.

O'Brien, E. J., Quilligan, M. J. and Karoumi, R. (2006). *Calculating an influence line from direct measurements*. Proceedings of the ICE - Bridge Engineering **159**(1): pp. 31-34.

Omenzetter, P. and Brownjohn, J. M. W. (2006). *Application of time series analysis for bridge monitoring*. Smart Materials and Structures **15**(1): pp. 129-138.

Orcesi, A. and Frangopol, D. (2010). *Inclusion of crawl tests and long-term health monitoring in bridge serviceability analysis*. Journal of Bridge Engineering **15**(3): pp. 312-326.

Orcesi, A. D. and Frangopol, D. M. (2011). *Optimization of bridge maintenance strategies based on structural health monitoring information*. Structural Safety **33**(1): pp. 26-41.

Othonos, A. (1997). *Fiber Bragg gratings*. Review of Scientific Instruments **68**(12): pp. 4309-4341.

Pastor, M., Binda, M. and Harčarik, T. (2012). *Modal assurance criterion*. Procedia Engineering **48**: pp. 543-548.

Paultre, P., Proulx, J. and Talbot, M. (1995). *Dynamic testing procedures for highway bridges using traffic loads*. Journal of Structural Engineering **121**(2): pp. 362-376.

Peeters, B., Maeck, J. and Roeck, G. D. (2001). *Vibration-based damage detection in civil engineering: excitation sources and temperature effects*. Smart Materials and Structures **10**(3): pp. 518-527.

Peterson, K., Pakzad, S., Shahidi, S., Barbachyn, S. and Kurama, Y. (2014). *Advanced sensing techniques for damage detection in reinforced concrete structures*. In: Proceedings of the Structures Congress 2014, pp. 2777-2788. G. R. Bell and M. A. Card (Eds.), American Society of Civil Engineers (ASCE). Boston, MA, USA.

Pimentel, R. M. d. C. M., Barbosa, M. C. B., Costa, N. M. S., Ribeiro, D. R. F., Ferreira, L. A. d. A., Araujo, F. M. M. and Calçada, R. A. B. (2008). *Hybrid Fiber-Optic/Electrical Measurement System for Characterization of Railway Traffic and Its Effects on a Short Span Bridge*. Sensors Journal, IEEE **8**(7): pp. 1243-1249.

Posenato, D. (2009). *Model-Free Data Interpretation for Continuous Monitoring of Complex Structures*. Ph.D. Thesis, École Polytechnique Fédérale de Lausanne,

Posenato, D., Kripakaran, P., Inaudi, D. and Smith, I. F. C. (2010). *Methodologies for model-free data interpretation of civil engineering structures*. Computers & Structures **88**(7-8): pp. 467-482.

Posenato, D., Lanata, F., Inaudi, D. and Smith, I. F. C. (2008). *Model-free data interpretation for continuous monitoring of complex structures*. Advanced Engineering Informatics **22**(1): pp. 135-144.

Quilligan, M. (2003). *Bridge Weigh-in-Motion - Development of a 2-D Multi-Vehicle Algorithm*. Licenciate Thesis, Department of Civil and Architectural Engineering - Structural Design and Bridge Division, Royal Institute of Technology, Stockholm, Sweden.

Reda Taha, M. M. and Lucero, J. (2005). *Damage identification for structural health monitoring using fuzzy pattern recognition*. Engineering Structures **27**(12): pp. 1774-1783.

Rens, K. L., Nogueira, C. L. and Transue, D. J. (2005). *Bridge management and nondestructive evaluation*. Journal of Performance of Constructed Facilities **19**(1): pp. 3-16.

Robert-Nicoud, Y., Raphael, B., Burdet, O. and Smith, I. F. C. (2005a). *Model Identification of Bridges Using Measurement Data*. Computer-Aided Civil & Infrastructure Engineering **20**(2): pp. 118-131.

Robert-Nicoud, Y., Raphael, B. and Smith, I. F. C. (2000). *Decision support through multiple models and probabilistic search*. In: Proceedings of the Construction Information Technology 2000: Taking the construction industry into the 21st century, pp. 765-779. Iceland Building Research Institute. Reykjavik, Iceland.

Robert-Nicoud, Y., Raphael, B. and Smith, I. F. C. (2005b). *Configuration of measurement systems using Shannon's entropy function*. Computers & Structures **83**(8-9): pp. 599-612.

Rodrigues, C., Cavadas, F., Félix, C. and Figueiras, J. (2012). *FBG based strain monitoring in the rehabilitation of a centenary metallic bridge*. Engineering Structures **44**: pp. 281-290.

Rotilio, J.-D. (1998). *Contribuition des actions variables aux déformations à long terme des ponts en béton [Live loads contribution to the long-term deformations of concrete bridges]* (in French). PhD thesis, Civil Engineering Department, Swiss Federal Institute of Technology (EPFL), Lausanne, Switzerland.

Rucka, M. and Wilde, K. (2006). *Crack identification using wavelets on experimental static deflection profiles*. Engineering Structures **28**(2): pp. 279-288.

Rucker, W., Hille, F. and Rohrmann, R. (2006). *Guideline for Structural Health Monitoring (F08b SAMCO Final Report)*: Structural Assessment, Monitoring and Control (SAMCO).

Ryan, T. W., Hartle, R. A., Mann, J. E. and Danovich, L. J. (2006). *Bridge Inspector’s Reference Manual*Arlington, VA, USA: Federal Highway Administration (FHWA) / National Highway Institute (HNHI-10).

Rytter, A. (1993). *Vibration based inspection of civil engineering structures*. PhD Thesis, Department of Building Technology and Structural Engineering, University of Aalborg, Aalborg, Denmark.

Salgado, R. (2008). *Damage detection methods in bridges through vibration monitoring - evaluation and application*. PhD Thesis, Department of Civil Engineering, University of Minho, Guimarães, Portugal.

Santos, J. P., Crémona, C., Orcesi, A. D. and Silveira, P. (2013). *Multivariate statistical analysis for early damage detection*. Engineering Structures **56**(0): pp. 273-285.

Saraf, V. and Nowak, A. S. (1998). *Proof load testing of deteriorated steel girder bridges*. Journal of Bridge Engineering **3**(2): pp. 82-89.

Sartor, R. R., Culmo, M. P. and DeWolf, J. T. (1999). *Short-term strain monitoring of bridge structures*. Journal of Bridge Engineering **4**(3): pp. 157-164.

Savitzky, A. and Golay, M. J. E. (1964). *Smoothing and differentiation of data by simplified least squares procedures*. Analytical Chemistry **36**(8): pp. 1627-1639.

Sedlaccek, G., Hechler, O., Losche, A. and Kuhn, B. (2007). *Guidelines for monitoring of steel railway bridges*.

Shlens, J. (2009). *A tutorial on principal component analysis*. Available from: www.snl.salk.edu/~shlens/pca.pdf (Accessed.

Silkorsky, C. (1999). *Development of a health monitoring system for civil structures using a level IV non-destructive damage evaluation method*. In: Proceedings of the 2nd International Workshop on Structural Health Monitoring, pp. 68-81. F. K. Chang (Ed.), Stanford, CA, USA.

Sohn, H. and Farrar, C. (2000). *Statistical process control and projection techniques for damage detection*. In: Proceedings of the European COST F3 Conference on System Identification & Structural Health Monitoring, pp. 105-114. Madrid, Spain.

Sohn, H. and Farrar, C. R. (2001). *Damage diagnosis using time series analysis of vibration signals*. Smart Materials and Structures **10**(3): pp. 446-451.

Sohn, H., Farrar, C. R., Hemez, F. M., Shunk, D. D., Stinemates, D. W., Nadler, B. R. and Czarnecki, J. J. (2004). *A Review of Structural Health Monitoring Literature: 1996–2001*: Los Alamos National Laboratory.

Sohn, H., Farrar, C. R., Hunter, N. F. and Worden, K. (2001). *Structural health monitoring using statistical pattern recognition techniques*. Journal of Dynamic Systems, Measurement, and Control **123**(4): pp. 706-711.

Sousa, C., Calçada, R. and Neves, A. (2015). *Numerical evaluation of the non-linear behaviour of cracked RC members under variable-amplitude cyclic loading*. Materials and Structures **48**(9): pp. 2815-2838.

Sousa, H., Félix, C., Bento, J. and Figueiras, J. (2011). *Design and implementation of a monitoring system applied to a long-span prestressed concrete bridge*. Structural Concrete **12**(2): pp. 82-93.

Splitstone, D. E., Stonecheck, S. A., Dodson, R. L. and Fuller, J. A. (2010). *Birmingham bridge emergency repairs: micropile foundation retrofit*. In: Proceedings of the GeoFlorida 2010: Advances in analysis, Modeling and Design, pp. 1479-1487. D. O. Fratta, A. J. Puppala and B. Muhunthan (Eds.), ASCE. Orlando, FL, USA.

Spyrakos, C. C., Raftoyiannis, I. G. and Ermopoulos, J. C. (2004). *Condition assessment and retrofit of a historic steel-truss railway bridge*. Journal of Constructional Steel Research **60**(8): pp. 1213-1225.

Srinivasan, M. and Kot, C. (1992). *Effects of damage on the modal parameters of a cylinder shell*. In: Proceedings of the 10th International Modal Analysis Conference, pp. 529–535. Kissimmee, Florida, USA.

Štimac Grandić, I., Grandić, D. and Bjelanović, A. (2011). *Comparison of techniques for damage identification based on influence line approach*. In: Proceedings of the VIII International Congres: Machines, Technologies, Materials, pp. 53-57. Varna, Bulgaria.

Stohr, S., Link, M., Rohrmann, R. and Rucker, W. (2006). *Damage detection based on static measurements on bridge structures*. In: Proceedings of the IMAC XXIV - 24th Conference and Exposition on Structural Dynamics, pp. 12 pages. St. Louis, Missouri, USA.

Strauss, A., Wendner, R., Frangopol, D. M. and Bergmeister, K. (2012). *Influence line- model correction approach for the assessment of engineering structures using novel monitoring techniques*. Smart Structures and Systems **9**(1): pp. 1-20.

Sun, M., Staszewski, W. J. and Swamy, R. N. (2010). *Smart sensing technologies for structural health monitoring of civil engineering structures*. Advances in Civil Engineering **2010**: pp. 1-13.

Sustainable Bridges (2007). *Guideline for Load and Resistance Assessment of Existing European Railway Bridges*.

Taylor, J. and Stanton, J. (2010). *Friction Coefficients for Stainless Steel (PTFE) Teflon Bearings*: Wisconsin Department of Transportation.

TNO DIANA BV (2011). *DIANA User's Manual - Release 9.4.4*Delft, The Netherlands.

Treacy, M. and Brühwiler, E. (2011). *Fatigue loading estimation for road bridges using long term WIM monitoring*. In: Proceedings of the European Safety and Reliability Annual Conference (ESREL 2011): Advances in Safety, Reliability and Risk Management, pp. 1870-1875. C. Berenguer, A. Grall and C. G. Soares (Eds.), Troyes, France.

Udd, E. (1995). *An overview of fiber-optic sensors*. Review of Scientific Instruments **66**(8): pp. 4015-4030.

Van der Auweraer, H. and Peeters, B. (2003). *International research projects on structural health monitoring: An overview*. Structural Health Monitoring **2**(4): pp. 341-358.

Viet Hà, N. and Golinval, J.-C. (2010). *Localization and quantification of damage in beam-like structures using sensitivities of principal component analysis results*. Mechanical Systems and Signal Processing **24**(6): pp. 1831-1843.

Vurpillot, S., Krueger, G., Benouaich, D., Clement, D. and Inaudi, D. (1998). *Vertical deflection of a pre-stressed concrete bridge obtained using deformation sensors and inclinometer measurements*. ACI Structural Journal **95**(5): pp. 518-526.

Wang, X., Hu, N., Fukunaga, H. and Yao, Z. H. (2001). *Structural damage identification using static test data and changes in frequencies*. Engineering Structures **23**(6): pp. 610-621.

WAVE (2001a). *Weigh-in-motion of Axles and Vehicles for Europe (WAVE)*General Report, Paris, France: Laboratoire Central des Ponts et Chaussées.

WAVE (2001b). *Weigh-in-motion of Axles and Vehicles for Europe (WAVE): Bridge WIM systems*Report of Work Package 1.2, Dublin, Ireland: University College Dublin.

Wong, K. Y. (2007). *Design of a structural health monitoring system for long-span bridges*. Structure and Infrastructure Engineering **3**(2): pp. 169-185.

Worden, K. and Dulieu-Barton, J. M. (2004). *An overview of intelligent fault detection in systems and structures*. Structural Health Monitoring **3**(1): pp. 85-98.

Worden, K., Manson, G. and Rippengill, S. (2009). *10 - Statistical pattern recognition and damage detection in structural health monitoring of civil infrastructure systems*. In: Structural Health Monitoring of Civil Infrastructure Systems, pp. 305-335. V. M. Karbhari and F. Ansari (Eds.): Woodhead Publishing, ISBN: 978-1-84569-392-3.

Worden, K., Sohn, H. and Farrar, C. R. (2002). *Novelty detection in a changing environment - Regression and interpolation approaches*. Journal of Sound and Vibration **258**(4): pp. 741-761.

Xu, H. and Humar, J. (2006). *Damage detection in a girder bridge by artificial neural network technique*. Computer-Aided Civil and Infrastructure Engineering **21**(6): pp. 450-464.

Yan, A. M., Kerschen, G., De Boe, P. and Golinval, J. C. (2005a). *Structural damage diagnosis under varying environmental conditions - Part I: A linear analysis*. Mechanical Systems and Signal Processing **19**(4): pp. 847-864.

Yan, A. M., Kerschen, G., De Boe, P. and Golinval, J. C. (2005b). *Structural damage diagnosis under varying environmental conditions - Part II: Local PCA for non-linear cases*. Mechanical Systems and Signal Processing **19**(4): pp. 865-880.

Yanaka, Y. and Kitagawa, M. (2002). *Maintenance of steel bridges on Honshu-Shikoku crossing*. Journal of Constructional Steel Research **58**(1): pp. 131-150.

Yang, S.-I., Frangopol, D. M. and Neves, L. C. (2004). *Service life prediction of structural systems using lifetime functions with emphasis on bridges*. Reliability Engineering & System Safety **86**(1): pp. 39-51.

Yao, R. and Pakzad, S. (2014). *Multisensor aggregation algorithms for structural damage diagnosis based on a substructure concept*. Journal of Engineering Mechanics **141**(6): pp. 0401416401-0401416416.

Yao, R. and Pakzad, S. N. (2012). *Autoregressive statistical pattern recognition algorithms for damage detection in civil structures*. Mechanical Systems and Signal Processing **31**(0): pp. 355-368.

Yeung, W. T. and Smith, J. W. (2005). *Damage detection in bridges using neural networks for pattern recognition of vibration signatures*. Engineering Structures **27**(5): pp. 685-698.

Yokoyama, K. and Rafiquzzaman, A. K. M. (2005). *Sensors and condition evaluation for bridge health monitoring using operating vehicle loading*. In: Sensing Issues in Civil Structural Health Monitoring, pp. 383-392: Springer Netherlands

Zabel, V. and Brehm, M. (2009). *Model updating methods - A comparative study*. In: Proceedings of the 27th Conference and Exposition on Structural Dynamics 2009 (IMAC XXVII). Society for Experimental Mechanics (SEM). Orlando, FL, USA.

Zanuy, C., Albajar, L. and de la Fuente, P. (2010). *On the cracking behaviour of the reinforced concrete tension chord under repeated loading*. Materials and Structures **43**(5): pp. 611-632.

Zaurin, R. and Catbas, F. N. (2011). *Structural health monitoring using video stream, influence lines, and statistical analysis*. Structural Health Monitoring **10**(3): pp. 309-332.

Zhang, Q. and Zhou, Y. (2007). *Investigation of the applicability of current bridge health monitoring technology*. Structure and Infrastructure Engineering **3**(2): pp. 159-168.

Zhao, H. and Uddin, N. (2010). *Algorithm to identify axle weights for an innovative BWIM system - Part I*. In: Proceedings of the IABSE-JSCE Joint Conference on Advances in Bridge Engineering - II, pp. 527-536. A. Amin, Y. Okui and A. Bhuiyan (Eds.), Dhaka, Bangladesh.

Zhou, Z. (2006). *Vibration-based damage detection of simple bridge structures*. PhD Thesis, Department of Civil and Geological Engineering, University of Saskatchewan, Saskatoon, Saskatchewan, Canada.

Zhu, J. and Xiao, R. (2007). *Damage identification of a large-span concrete cable-stayed bridge based on genetic algorithm* Frontiers of Architecture and Civil Engineering in China **1**(2): pp. 170-175.

Zhu, S., Levinson, D., Liu, H. X. and Harder, K. (2010). *The traffic and behavioral effects of the I-35W Mississippi River bridge collapse*. Transportation Research Part A: Policy and Practice **44**(10): pp. 771-784.